Systematic study on membrane filtration and characterization of silica stabilized water-in-oil Pickering emulsions for the application in continuous multiphase processes – experimental and modeling approach

vorgelegt von
Master of Science (M.Sc.)
Maresa Vivien Kempin

VON DER FAKULTÄT III – PROZESSWISSENSCHAFTEN
DER TECHNISCHEN UNIVERSITÄT BERLIN
ZUR ERLANGUNG DES AKADEMISCHEN GRADES

DOKTORIN DER INGENIEURWISSENSCHAFTEN
– DR.-ING. –

GENEHMIGTE DISSERTATION

Promotionsausschuss:
Vorsitzender: Prof. Dr.-Ing. habil. Jens-Uwe Repke
Gutachter: Prof. Dr.-Ing. Matthias Kraume
Gutachterin: Prof. Dr.-Ing. habil. Anja Drews
Gutachter: Prof. Dr.-Ing. Mirko Skiborowski

Tag der wissenschaftlichen Aussprache: 29. April 2022

Berlin 2022

Acknowledgements

A dissertation is not a sprint, but a marathon – with ups and downs – that does not necessarily get easier with a pandemic on the way to the finish line. But with the help of others, one can make it farther than one might think. At this point I would like to thank all those who have supported me professionally as well as personally on this journey.

This thesis is the result of my work as a research scientist in the group of Prof. Dr.-Ing. habil. Anja Drews at the University of Applied Sciences (HTW Berlin) from 2018 to 2022. I would like to thank you for giving me the opportunity to work in your group, for the trust and freedom you gave me to develop my research, for the possibility to attend international conferences, for the many fruitful discussions as well as for the always fast and very detailed feedback on, e.g., presentations and publications. Secondly, I would like to thank Prof. Dr.-Ing. Matthias Kraume for your co-supervision within the InPROMPT project (CRC/TR 63), for the continuous assistance (starting in my times as a student at TU Berlin) and the many ideas to improve my work further. Thirdly, I want to thank Prof. Dr.-Ing. Mirko Skiborowski for accepting to review my thesis as an external referee. I would also like to thank Prof. Dr.-Ing. habil. Jens-Uwe Repke for leading the examination board.

I thank all my colleagues from HTW Berlin, especially Tobias Fries, Frank Stoll, Kristina Wiltner and Tim Kreißler for their help in lab matters and with equipment, ordering chemicals, administrative stuff and the nice working atmosphere. Many thanks to Dr.-Ing. Anja Heyse for the nice welcome at HTW Berlin, for helping me find my way around our labs, for the many discussions and for always sharing ideas. Thanks also to Tina Skale and Nina Xander – my temporary office colleagues.

I would like to thank the DFG (Deutsche Forschungsgemeinschaft) for the financial support and all the colleagues from the CRC/TR 63. It was a pleasure and a great experience to be part of this major project. Special thanks to our "Pickering team" – Dr.-Ing. Lena Hohl, Susanne Röhl, Marc Petzold, Sebastian Stock and Prof. Dr. Regine von Klitzing – for the great meetings in Berlin, Darmstadt or later via Zoom, for the scientific discussions, for sharing all project results and ideas and for the support and constructive reviews. Many thanks also to Lena and Sebastian for the proofreading of this thesis.

Furthermore, I would like to thank Prof. Volodymyr V. Tarabara and Assoc. Prof. Jia-Wei Chew for the establishment of a joint international cooperation on the microfiltration of o/w emulsions and for the opportunity to visit Michigan State University and Nanyang Technological University Singapore. Special thanks to Dr. Charifa Hejase for showing me around campus, introducing me into the world of DOTM and all the fun we had. I hope that you can come and visit Berlin sometime soon.

I would like to thank all the students who made this thesis possible (thesis or research assistants): Marie Zemanek, Jonathan Pioch, Steven Pulla, Melanie Kaiser, Sonja Bläsing, Vanessa Vater (twice ☺), Aykut Özlü, Tim Tigor Hermann, Katja Osman, Graciele Oliveira de Moura et Silva (greetings to Brazil), Hendrik Schroeder, Miriam Assi and Mustafa Masoud. Thank you for trusting me as a supervisor and for the numerous hours of lab work. Thanks to Prof. Dr. Dr. Dietmar Lerche and Sebastian Boldt for giving Miriam the opportunity to investigate our Pickering emulsions at LUM GmbH.

Finally, I want to express my deepest gratitude to my family and friends!!! You were always there for me, always had an open ear and you were a great help when sometimes everything seemed to go wrong. Many thanks to Martin for the love you give and the million ways you find to cheer me up and make me laugh. Special thanks also to my parents Elke & Thomas for always believing in me (especially when I did not) and supporting me – be it through delicious food, encouraging sayings, your experience and so much more. Thank you for being who you are and helping me to get where I am today. I love you!

Abstract

Pickering emulsions consisting of water and 1-dodecene and stabilized by different solid silica nanoparticles are suitable innovative multiphase systems for, e.g., catalytic hydroformylation reactions. These enable not only high reaction rates but also an efficient and suitable phase separation to recycle the (expensive) catalyst and to achieve economically feasible continuous processes. Due to their high stability against coalescence, membrane filtration is a promising procedure: the catalyst containing water drops are retained by the membrane while the organic product containing phase is obtained as permeate. This thesis systematically addresses the membrane filtration of Pickering emulsions using selected membrane types. For a fundamental understanding of their filtration behavior, a detailed physico-chemical analysis is performed (stability, drop size distribution, rheological behavior). The homogenization conditions during Pickering emulsion preparation, the emulsion composition and the process conditions were varied and the main influencing parameters on water-in-oil Pickering emulsion filtration were determined. The tendency of nanoparticles to form three-dimensional network structures between emulsion drops and/or nanoparticles significantly influenced the filtration behavior. The filtration performance was dependent on the membrane type. This was explained by distinct nanoparticle-solvent-membrane interactions. Especially an organic solvent nanofiltration membrane showed a great reproducibility of the filtration behavior and the type of organic solvent as well as the temperature were identified as the only significant influencing parameters. Using this membrane type, Pickering emulsion filtration was – for the first time – successfully modeled via a combination of the solution-diffusion and the resistance in series model. Overall, the mechanical phase and catalyst separation of Pickering emulsions via membrane filtration is a very robust operation allowing broad operation windows. Pickering emulsions are thus suitable candidates for the application in continuous catalytic multiphase reactions.

Zusammenfassung

Pickering Emulsionen bestehend aus Wasser und 1-Dodecen und stabilisiert durch verschiedene Silika-Nanopartikel sind innovative Reaktionsumgebungen für z.B. die katalysierte Hydroformylierung langkettiger Olefine. Sie ermöglichen nicht nur hohe Reaktionsraten, sondern auch eine effiziente und geeignete Phasenseparation, um den (teuren) Katalysator zu recyceln und damit wirtschaftliche, kontinuierliche Prozesse zu etablieren. Aufgrund der hohen Stabilität der Emulsionen gegenüber Koaleszenz stellt die Membranfiltration von Pickering Emulsionen eine vielversprechende Möglichkeit dar: Die katalysatorhaltigen Wassertropfen werden durch eine Membran zurückgehalten, während die produkthaltige organische Phase als Permeat gewonnen wird. In dieser Arbeit wird die Membranfiltration von Pickering Emulsionen mit ausgewählten Membranen systematisch untersucht. Für ein grundlegendes Verständnis des Filtrationsverhaltens ist dabei auch eine detaillierte Untersuchung der physikalisch-chemischen Eigenschaften (Stabilität, Tropfengrößenverteilung, Rheologie) erforderlich. Durch die Variation der Dispergierbedingungen bei der Herstellung von Pickering Emulsionen, der Emulsions-zusammensetzung sowie der Betriebsparameter wurden die wesentlichen Einflussfaktoren auf das Filtrationsverhalten von Wasser-in-Öl Pickering Emulsionen ermittelt. Es wurde gezeigt, dass die Fähigkeit der Nanopartikel, dreidimensionale Netzwerkstrukturen zwischen Emulsionstropfen und/oder Partikeln zu formen, einen signifikanten Einfluss auf das Filtrationsverhalten hat. Das Filtrationsverhalten war abhängig von dem verwendeten Membrantyp und dem Membranmaterial. Dies wurde über die unterschiedlichen Wechselwirkungen zwischen Nanopartikeln, Lösemittel und Membran erklärt. Unter Verwendung einer Membran aus dem Bereich der organophilen Nanofiltration wurden das organische Lösemittel sowie die Temperatur als Haupteinflussparameter identifiziert. Für diese Membran wurde die Filtration von Pickering Emulsionen erstmals mathematisch modelliert. Es wurde eine Kombination aus dem Lösungs-Diffusions- und dem Widerstand-in-Reihe-Modell verwendet. Insgesamt ergibt sich, dass die einstufige (mechanische) Trennung von Pickering Emulsionen mittels Membranfiltration sehr robust ist und ein großes Optimierungspotenzial aufweist. Pickering Emulsionen sind somit geeignete Kandidaten für die Anwendung in kontinuierlichen katalysierten Reaktionen in Mehrphasensystemen.

Contents

Nomenclature

Abbreviations

AFM	atomic force microscopy
BET	Brunauer-Emmett-Teller
C	number of carbon atoms
CPME	cyclopentyl methyl ether
CTAB	cetrimonium bromide
DMF	N,N'-dimethylformamide
DOTM	direct observation through the membrane
DSD	drop size distribution
HNT	Halloysite nanotube
InPROMPT	Integrated chemical processes in liquid multiphase systems
L/L	liquid/liquid
LVE	linear-viscoelastic
MES	microemulsion system
MF	microfiltration
MWCO	molecular weight cut-off
NF	nanofiltration
NP	nanoparticle
ONF	organophilic nanofiltration
OSN	organic solvent nanofiltration
o/w	oil-in-water
PAN	polyacrylonitrile
PDMS	polydimethylsiloxane
PE	Pickering emulsion
PES	polyethersulfone
PFM	pore flow model
PI	polyimide
PP	polypropylene
PVDF	polyvinylidene fluoride
RMS	root mean square
RO	reverse osmosis
SDM	solution-diffusion model
SDMWI	solution-diffusion model with imperfections
SEM	scanning electron microscopy
SRNF	solvent resistant nanofiltration
TEM	transmission electron microscopy
TMS	thermomorphic multi-component solvent system
UF	ultrafiltration
UT	ULTRA-TURRAX®
w/o	water-in-oil

Latin letters

A	[m^2]	area
A_i	[var.]	coefficient
b_i	[var.]	coefficient
c	[mol m^{-3}]	concentration
c_p	[J kg^{-1} K^{-1}]	specific heat capacity
D	[m^2 s^{-1}]	diffusion coefficient
D_0	[m s^{-1}]	diffusion coefficient factor
d_{10}	[m]	arithmetic mean diameter
d_{32}	[m]	Sauter mean diameter

d_h	[m]	hydraulic diameter
d_i	[m]	drop diameter
d_gap	[m]	gap width
d_rotor	[m]	rotor diameter
d_stator	[m]	stator diameter
E	[J]	energy
E_A	[J mol^{-1}]	activation energy
G	[kT]	energy
G'	[Pa]	storage modulus
G''	[Pa]	loss modulus
h_gel	[m]	gel layer height
H	[m]	height
J	[L m^{-2} h^{-1}]	flux
k	[kg (m s^{2-n})$^{-1}$]	flow consistency index
m	[kg]	mass
$\widetilde{M}$	[g mol^{-1}]	molar mass
n	[-]	flow behavior index
n	[min^{-1}]	dispersing/stirrer speed
n	[mol]	amount of substance
$\dot{n}$	[mol m^{-2} s^{-1}]	molar flux
N	[-]	number
p	[Pa]	pressure
P	[L m^{-2} h^{-1} bar^{-1}]	permeability
P	[W]	power
P	[-]	n-octanol-water partition coefficient
Po	[-]	power number
q_r	[µm^{-1}]	density distribution function
Q_r	[-]	cumulative distribution function
r	[m]	radius
R	[m^{-1}]	resistance
R^2	[-]	coefficient of determination
$\Re$	[J mol^{-1} K^{-1}]	universal gas constant
Re	[-]	Reynolds number
S	[-]	swelling degree
t	[s]	time
T	[K]	temperature
v	[m s^{-1}]	superficial velocity
V	[m^3]	volume
$\dot{V}$	[m^3 s^{-1}]	flow rate
$\tilde{V}$	[m^3 mol^{-1}]	molar volume
$\overline{w}$	[m s^{-1}]	mean flow velocity
w_tip	[m s^{-1}]	tip speed
X	[var.]	variable/parameter

Greek letters

γ	[N m^{-1}]	interfacial tension
γ	[%]	deformation
$\dot{\gamma}$	[s^{-1}]	shear rate
δ	[m]	thickness
ε	[-]	porosity

ε	[W kg^{-1}]	energy dissipation rate
ζ	[-]	resistance coefficient
η	[Pa s]	dynamic viscosity
θ	[°]	contact angle
κ	[S cm^{-1}]	conductivity
ξ	[wt.%]	particle mass fraction
π	[Pa]	osmotic pressure
ρ	[kg m^{-3}]	density
σ	[N m^{-1}]	surface tension
σ_0	[var.]	standard deviation
τ	[Pa]	shear stress
φ	[vol.%]	dispersed phase fraction
ω	[rad s^{-1}]	angular frequency

Subscripts

0	dry
af	after filtration
bf	before filtration
c	cake
cP	continuous phase
dP	dispersed phase
eff	effective
fV	free volume
hso	half swept out
i	solvent
j	resistance type
k	nanoparticle type
M	membrane
min	minimum
max	maximum
o	oil
p	particle
P	permeate
s	solid
S	sediment
T	temperature
w	water
wash	washing

1 Introduction

With respect to the future scarcity of fossil fuels, the chemical industry is facing the challenge of expanding its raw material basis for chemicals production to include sustainable resources, which, in the best case, can even substitute the common organic chemicals based on fossil resources. Furthermore, the twelve principles of "Green chemistry" become more and more important. These include – in addition to the use of renewable feedstocks – e.g., energy efficiency, little need for auxiliaries, use of safer solvents, highly efficient catalysts and the prevention of waste [9, 10].

Long-chained olefins form a possible new raw material basis as they can be obtained from renewable feedstocks. To utilize these sustainable resources in an efficient and economical way, suited process concepts need to be found or developed [79]. To achieve high yields and selectivities under mild reaction conditions, homogeneous catalysis is often desirable [194]. An example is the hydroformylation of olefins. However, the established Ruhrchemie/Rhône-Poulenc process for the hydroformylation of short-chained olefins [120] fails for olefins with $C > 5$ due to their poor water-solubility and low reaction rates [92].

Here, novel innovative phase systems are suitable candidates as reaction media to realize, e.g., the rhodium-catalyzed hydroformylation of long-chained olefins such as 1-dodecene [116]. An effective and efficient recycling of the expensive catalyst-ligand complex is inevitable to achieve economically feasible processes. To establish such innovative phase systems industrially, physico-chemical as well as process engineering fundamentals must be understood. Within the collaborative research center InPROMPT ("Integrated Chemical Processes in Liquid Multiphase Systems") thermomorphic multi-component solvent systems (TMS), microemulsion systems (MES) and Pickering emulsions (PEs) were investigated (**Figure 1**).

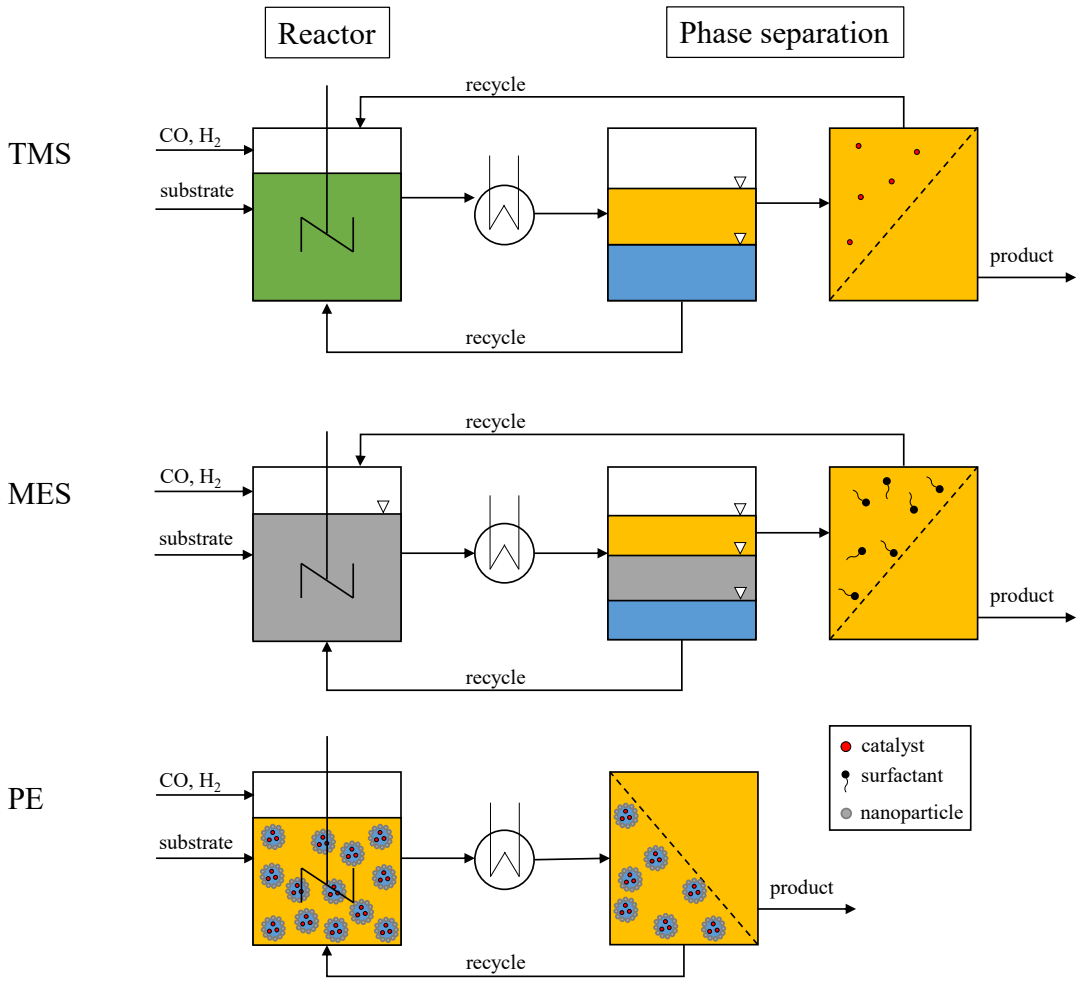

Figure 1. Schematic representation of reaction and phase separation in three different innovative phase systems. **(Top)** TMS – thermomorphic multi-component solvent systems, **(middle)** MES – microemulsion systems, and **(bottom)** PE – Pickering emulsions. Adapted from [66, 99, 167].

All these innovative phase systems have their advantages and drawbacks concerning the reaction and energy efficiency, sustainability and separation performance. These three phase systems will briefly be described in the following, with PEs being discussed in more detail, as they are examined in this thesis.

TMS are mixtures of multiple components of different polarities with a temperature dependent phase behavior. The reactions are performed under homogeneous conditions in a single liquid phase – leading to high reaction rates – while a change in temperature is used to create a two-phase system for catalyst recovery [51, 66, 256] (**Figure 1** top). A subsequent organic solvent nanofiltration (OSN) is necessary to reduce the catalyst loss to an acceptable level [66]. For product purification, a further, elaborate down-stream process is required for recycling of the non-polar solvent and unconverted alkenes [25, 51, 66]. Another disadvantage is the current need for hazardous solvents like DMF (N,N'-dimethylformamide) to adjust the sensitive phase behavior [66, 169]. Research on the (computer-aided) selection of more benign solvents is conducted in, e.g., [144, 264].

To achieve higher reaction rates, surfactants are used in MES to create a large interfacial area between the aqueous and the organic phase. Depending on the temperature and the surfactant concentration, different phase conditions exist [244]. In general, the reaction, e.g., hydroformylation of 1-dodecene, can be performed under all phase conditions [168]. By way of example, the bicontinuous microemulsion phase is shown in grey in **Figure 1** (middle). The expensive rhodium-catalyst is located in the polar phase during reaction and separation [167]. Tuning the temperature in a decanter allows phase separation and catalyst recovery, e.g., [167, 193]. As the amount of residual surfactants in the organic product phase might be too high, a subsequent OSN is necessary to retain the surfactant and to obtain a pure product [257] (**Figure 1** middle).

Nanoparticle stabilized water-in-oil (w/o) PEs constitute a promising alternative. As PEs show superior stability [26], they are suited for industrial processes where the sample is exposed to mechanical stress in form of pumping or stirring. Due to their large interfacial area (but smaller than in MES), thus enhanced mass transport and higher reaction rates, PEs have recently become of increasing interest for their use in (bio-)catalytic reactions in liquid/liquid (L/L) multiphase systems. In 2011, the first biocatalytic esterification in PEs, using hydrophobic silica particles for PE stabilization and enzymes as biological catalysts, was reported [246]. The latter one was immobilized within the aqueous phase drops, while the reactants and products were predominantly in the organic phase [246]. Since then, the feasibility of enzymatic reactions in PEs has been proven by other authors (e.g., [95, 148, 238, 261]) but also chemo-catalytic reactions, e.g., acetalization, hydrogenation, reduction, oxidation or hydroformylation have been performed in PEs [18].

For economically feasible industrial processes not only the reaction but the overall process needs to be optimized. An efficient and continuous PE separation to retain the active catalyst remained a challenge until recently [163]. Different attempts have been described in literature of which most separations were typically based on demulsification. This might cause a damage to sensitive catalysts and only allows cyclic processes. Among these approaches were the use of stimuli-responsive PEs, in which an external trigger (e.g., temperature, pH, CO_2 concentration, light intensity, ionic strength or magnetic field) led to a demulsification or inversion of the emulsion, e.g., [209, 242, 255]. Another common technique is centrifugation – having the disadvantage of multiple energy input (re-emulsification for the next reaction cycle) and possible catalyst damage, e.g., [238]. The same disadvantages apply for shear-induced coalescence [240]. An alternative ("Flow Pickering emulsion") was reported in, e.g., [261, 263], where a PE was packed into a column reactor and gravity driven flow of the organic phase through the interstices between the drops was used [261]. Flow rates were low and consequently residence times were high, leading to an economically inefficient process. Another disadvantage of this technique is that drops cannot be easily exchanged when catalyst activity decreases.

A very promising but rather new alternative to enable continuous processes is the mechanical separation of PEs via membrane filtration (**Figure 1** bottom). The catalyst-containing aqueous phase drops are retained in the retentate, while the organic product-containing phase is obtained as permeate. Compared to, e.g., TMS and MES, where the gravity driven decanter reacts sensitively to changes in, e.g., temperature or concentration and is not sufficient for phase separation and additives recycle, the use of PEs allows a simplified process flow diagram with only a single-stage separation (cf. **Figure 1**). Cooling between the reactor and the filtration might be required to meet the temperature compatibility of the membrane material.

Due to the novelty of this application, publications about the filtration of PEs are still scarce [95, 96, 199, 200] and a fundamental understanding of the underlying processes is missing. The aim of this thesis is to investigate the impact of various influencing parameters, such as PE composition and operating

conditions, on characteristic emulsion properties and on the filtration behavior. In most investigations, the model system composed of oil, water and solid nanoparticles is used (without the metal catalyst and reaction (by-)products). As the production of PEs with tailor-made characteristics is essential for robust and optimal process design, special attention is given to the drop size distribution (DSD) and empirical correlations with the preparation conditions are developed. Knowledge about the DSD and possibly freely suspended residual particles is required as they constitute the filter cake. The exact knowledge of the rheological behavior is essential for mixing, pumping and filtration. The filtration of various PEs using different membranes (membrane-solvent-particle interactions) constitutes the main part of this thesis. For the first time, a permeability model to describe the filtration of PEs is developed which can be used for process optimization.

2 Scope and Outline of this thesis

The aim of this cumulative thesis is the systematic characterization of w/o Pickering emulsions as well as the investigation and prediction of their filtration behavior under various process conditions. In this chapter the general structure as well as the own relevant journal articles used for the thesis are presented. Their chronology and place in the process flow sheet are schematically shown in **Figure 2**.

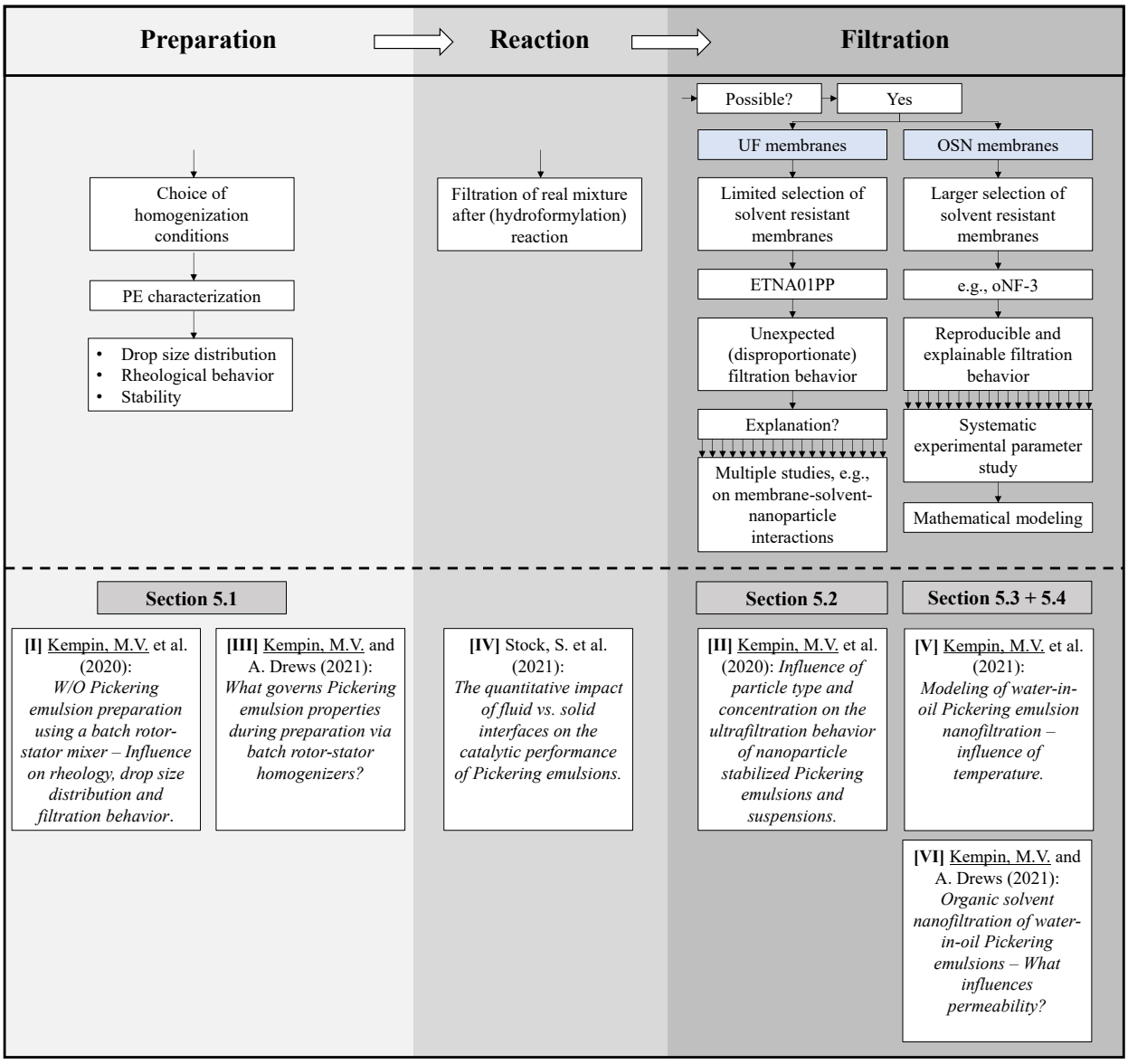

Figure 2. Schematic structure of this thesis and publications on which this thesis is based.

The basis for reaction and filtration is the preparation of PEs with tailor-made characteristics. While the impact of different PE compositions on PE properties has intensively been studied in literature (cf. **Section 3.1.3)**, the preparation process as another leverage has mostly been neglected so far. The impact of different homogenization conditions – e.g., homogenization device, time and (tip) speed – on drop size distribution, stability, rheology and filtration behavior was investigated in detail in publications [I] and [III] and is described in **Section 5.1**. These examinations were performed for a "standard" w/o PE of the same composition. The aim was to develop correlations between Sauter mean diameters or dynamic viscosity, respectively, with homogenization conditions for targeted PE preparation.

The next step to apply w/o PEs in continuous catalytic L/L multiphase systems is the reaction (e.g., hydroformylation) which was published in [IV] but is not the focus of this thesis.

For economically feasible processes, a subsequent catalyst recovery and a separation of the dispersed phase drops and the organic product containing phase is essential. The feasibility of w/o PE ultrafiltration (UF) was shown in literature [199, 200] (cf. **Section 3.2.2**). Up to date, there is no thorough understanding

for the reported unexpected, disproportionate filtration behavior. Therefore, further studies with the same UF membrane were conducted in publication [II] and are described in **Section 5.2**. Focus was laid on the impact of particle type, membrane-solvent-nanoparticle interactions as well as membrane pre-treatment. Additional to w/o and oil-in-water (o/w) PEs, nanoparticle/oil suspensions – as the extreme form of no dispersed phase fraction – were investigated.

Furthermore, an OSN membrane with a similar molecular weight cut-off but made of different material was investigated in publications [V] and [VI] and is described in **Section 5.3**. Filtration of w/o PEs using OSN membranes has never been published before. The membrane showed a very good reproducibility of the filtration performance and allowed a systematic experimental parameter study (publication [VI]). The aim was to identify the most important influencing parameters (among PE composition and process conditions) on w/o PE filtration (cf. **Section 5.3**). So far, only experimental studies concerning the filtration of PEs have been published. Therefore, publication [V] and [VI] also focused on the development of a first modeling approach to describe the observed filtration behavior, which can then be used for process design and optimization (cf. **Section 5.4**).

To summarize, this cumulative thesis seeks to answer the following questions:

- How do preparation conditions and Pickering emulsion composition influence the characteristic PE properties (especially DSD and rheological behavior)?
- What are the main influencing parameters on w/o PE filtration using ultrafiltration and organic solvent nanofiltration membranes?
- Which modeling approaches are suited to describe the filtration of w/o PEs?

In the following, the detailed references of the own relevant publications used in this thesis are listed in chronological order. Throughout all chapters of the thesis, these publications will be referred to by their Roman numerals.

[I] Kempin, M.V.; Kraume, M.; Drews, A. (2020): *W/O Pickering emulsion preparation using a batch rotor-stator mixer – Influence on rheology, drop size distribution and filtration behavior*. J. Colloid Interf. Sci., 573, 135-149, DOI: 10.1016/j.jcis.2020.03.103.

[II] Kempin, M.V.; Stock, S.; von Klitzing, R.; Kraume, M.; Drews, A. (2020): *Influence of particle type and concentration on the ultrafiltration behavior of nanoparticle stabilized Pickering emulsions and suspensions*. Sep. Purif. Technol., 252, 117457, DOI: 10.1016/j.seppur.2020.117457.

[III] Kempin, M.V.; Drews, A. (2021): *What governs Pickering emulsion properties during preparation via batch rotor-stator homogenizers?* Chem. Ing. Tech., 93, 311-317, DOI: 10.1002/cite.202000130.

[IV] Stock, S.; Schlander, A.; Kempin, M.; Geisler, R.; Stehl, D.; Spanheimer, K.; Hondow, N.; Micklethwaite, S.; Weber, A.; Schomäcker, R.; Drews, A.; Gallei, M.; von Klitzing, R. (2021): *The quantitative impact of fluid vs. solid interfaces on the catalytic performance of Pickering emulsions.* Phys. Chem. Chem. Phys., 23, 2355-2367, DOI: 10.1039/D0CP06030E.

[V] Kempin, M.V.; Schroeder, H.; Hohl, L.; Kraume, M.; Drews, A. (2021): *Modeling of water-in-oil Pickering emulsion nanofiltration – influence of temperature.* J. Membr. Sci, 636, 119547, DOI: 10.1016/j.memsci.2021.119547.

[VI] Kempin, M.V.; Drews, A. (2021): *Organic solvent nanofiltration of water-in-oil Pickering emulsions – What influences permeability?* Membranes, 11, 864, DOI: 10.3390/membranes11110864.

[VII] Stock, S.; Kempin, M.V.; Hohl, L.; Petzold, M.; Hecht, K.; von Klitzing, R.; Drews. A.: *Pickering Emulsions.* (Kraume M, ed.). Integrated chemical processes in liquid multiphase systems – from chemical reaction to process design. De Gruyter. (submitted).

3 State of the Art

This chapter provides an overview of the present state of the art concerning the field of Pickering emulsion characterization and filtration. After a brief general description of this emulsion type and emulsion stabilization mechanisms, key parameters governing their properties, possible PE preparation methods and characteristic properties such as drop size distribution and rheology are reviewed. To apply PEs in catalytic processes in L/L multiphase systems, not only the knowledge of their properties is of great importance, but an efficient catalyst recovery is essential. As the filtration of PEs is a promising procedure, its current state of the art and general aspects, as well as modeling approaches for membrane filtration, are described.

3.1 Pickering emulsions

3.1.1 Background

Emulsions are colloidal dispersions in which a liquid phase is dispersed in the form of drops into a second liquid (continuous) phase. Possible types of simple emulsions are o/w and w/o. Double or multiple emulsions also exist but were not observed in this thesis and will therefore not be further dealt with [192]. Emulsions are thermodynamically unstable systems which seek to reduce the total surface energy by coalescence, leading to a complete separation of the emulsion into two phases. Hence, an emulsifying agent, often also referred to as a stabilizer, is required to either prevent coalescence or to facilitate emulsion formation. Possible emulsifiers are, e.g., ions, surfactants, polymers, polyelectrolytes or solid particles [192, 208]. Possible physical destabilization processes of emulsions are discussed in more detail in **Section 3.1.2**.

Emulsions stabilized by solid particles, so called Pickering emulsions, have recently received increasing attention. The growing interest in PEs becomes obvious in the increasing number of publications within the last two decades. **Figure 3** displays data obtained from *Web of Science* showing that the proportion of "Pickering emulsions" among "emulsions" has increased from 0% in 2000 to 11.1% in 2020.

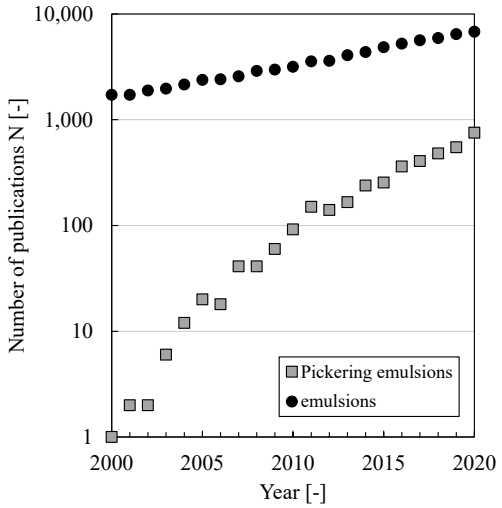

Figure 3. Number of publications with keywords "Pickering emulsions" or "emulsions" only. Source: *Web of Science*. Retrieved: October 20, 2021.

Named after S.U. Pickering, these emulsions have been first described in the early years of the 20th century [166, 174]. In contrast to conventional, e.g., surfactant stabilized emulsions, PEs have some significant advantages: a high stability against coalescence, the possibility of fine-tuning and stimuli-responsiveness, often lower toxicity and better biocompatibility [5, 247, 252]. PEs are used in numerous fields of application, which have been reviewed in recent years by a number of authors [5, 24, 57, 86, 247, 252]. Possible fields of application include biomaterials, biomedicine, (bio-)catalytic processes, cosmetics, drug delivery, food, material sciences, oil recovery, pharmaceutics and many more.

In 2002, Binks published a review about the differences and similarities of emulsion stabilization via surfactants or nanoparticles [26]. Surfactant molecules adsorb and desorb from the L/L interface on a quite fast timescale, reaching a dynamic equilibrium. In contrast, the adsorption of nanoparticles, which are typically bigger compared to surfactant molecules, to the interface is expected to be slower [26]. Once adsorbed, the nanoparticles are kept almost irreversibly at the interface between the dispersed and the continuous phase preventing coalescence through static hindrance via a mechanical barrier [26, 30, 49] (cf. **Section 3.1.2**).

The high stability of PEs is caused by the high adsorption energy of the stabilizing particles at the L/L interface. **Eq. (1)** describes the energy of detachment ($\Delta G_{\text{attachment}} = -\Delta G_{\text{detachment}}$) for a single spherical particle. A necessary condition for the application of this equation is that the particle is small enough so that the deformation of the interface due to gravity can be neglected [30, 49].

$$\Delta G_{\text{detachment}} = \pi r^2 \gamma_{\text{ow}} (1 \pm \cos\theta)^2 \quad \textbf{(1)}$$

The energy of detachment depends on particle properties such as the particle radius r and the three-phase contact angle θ measured through the more polar liquid (here water) as well as on properties of the involved liquids, e.g., the interfacial tension γ_{ow} between the organic and the aqueous phase. The impact of these three parameters on the energy of detachment decreases in the following order: contact angle > particle radius > interfacial tension. The sign within the brackets becomes positive when the particle is detached into the organic phase while it becomes negative when the particle is moved from the interface into the aqueous phase [30].

The three-phase contact angle describes the particle wettability and plays a major role in PE stabilization (**Figure 4)**.

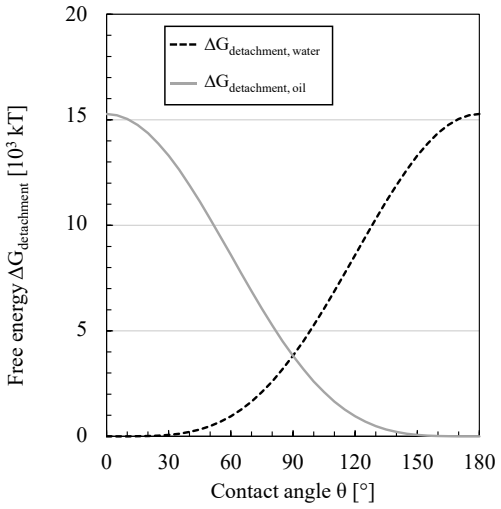

Figure 4. Free energy of detachment (given as multiples of the thermal energy kT) of a spherical particle from an oil-water interface against the contact angle (dashed line represents the detachment of the particle into the aqueous phase, solid line represents the detachment of the particle into the oil phase). Calculated by **Eq. (1)** with r = 10 nm (typical value for (primary) particle size) and γ_{ow} = 50 mN m^{-1} (typical value for water-hydrocarbon systems). Adapted from [30].

In [27], contact angles were calculated from the components of the surface energies of all phases – using the Young equation (**Eq. (2)**) – for particles of different hydrophobicity and oils of different polarity.

$$\gamma_{\text{so}} - \gamma_{\text{sw}} = \gamma_{\text{ow}} \cos\theta \quad \textbf{(2)}$$

Calculated values were in good agreement with experimental data and the approach could be successfully used to predict the preferentially formed emulsion type [27]. More hydrophilic particles can be dispersed in water and tend to stabilize o/w PEs while more hydrophobic particles can be dispersed in the organic phase and favor the formation of w/o PEs [14, 32, 33, 38]. However, neither very hydrophilic particles with contact angles much smaller than 90° nor very hydrophobic particles with contact angles much greater than 90° can efficiently stabilize PEs. For particles of intermediate hydrophobicity with contact angles close to 90° partial wetting conditions are fulfilled and the energy of detachment is several

orders of magnitude greater than the thermal energy kT causing a nearly irreversible attachment of the particles to the L/L interface [14, 26, 27, 30]. Particles of intermediate hydrophobicity can stabilize both o/w and w/o PEs [26].

The impact of the contact angle on PE stabilization and PE type is also shown in **Figure 5**. Similar to the Bancroft rule for surfactants, typically the better wetting phase becomes the continuous phase, and the more poorly wetting phase becomes the dispersed phase. It has to be considered that the initial position of the particles and the dispersed phase ratio have an influence [26]. Typically, for particles of intermediate hydrophobicity and a dispersed phase fraction of 0.5, the phase in which the particles are dispersed first becomes the continuous phase [26]. This is not necessarily the case for surfactant stabilized emulsions as surfactant molecules distribute much faster between the different phases [34]. The impact of the initial stirrer position in stirred tanks on the resulting emulsion type for surfactant stabilized emulsions was reported in, e.g., [182].

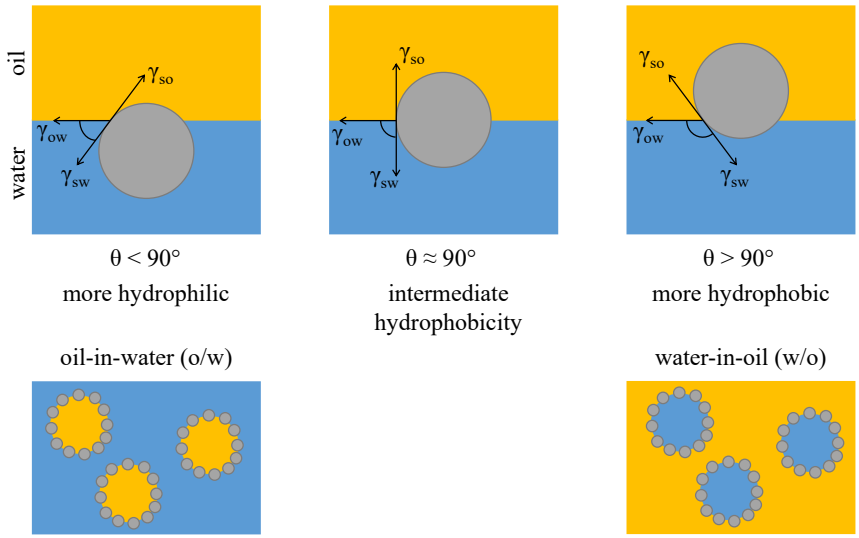

Figure 5. (Top) Schematic representation of a spherical particle at an oil-water interface for different (aqueous) contact angles. Particle-oil (γ_{so}), particle-water (γ_{sw}) and oil-water (γ_{ow}) interfacial tensions are also shown. **(Bottom)** Preferentially formed emulsion type: o/w for $\theta < 90°$ and w/o for $\theta > 90°$. Adapted from [26, 27].

3.1.2 Stability of (Pickering) emulsions

Different destabilization mechanisms can lead to a breakdown of an emulsion (**Figure 6**) [192, 208]. Depending on the differences in the dispersed and continuous phase densities, creaming (o/w) or sedimentation (w/o) of (larger) drops occurs as a result of external (gravitational or centrifugal) forces. Creaming or sedimentation does not lead to a change in the drop size and can be reversed by gentle shaking or stirring of the emulsion. For PEs, Binks [26] reported that upon an increase in particle hydrophobicity, the drop size passes through a minimum and consequently the stability against creaming or sedimentation passes through a maximum. Another destabilization process is flocculation, where multiple drops aggregate and form larger units, while the individual drop sizes remain the same. The extent of flocculation depends on the degree of attractive and repulsive forces. Ostwald ripening describes the process where molecules contained within smaller drops, having a greater solubility due to curvature effects, diffuse through the continuous phase and become deposited on larger drops. The drop size distribution is shifted towards larger drops with time [208]. For PEs, Ostwald ripening is supposed to be stopped when the particle layer adsorbed at the interface starts to buckle as a result of the reduction of the surface area. For larger, swelling drops, freely suspended particles may adsorb to enhance drop stability [26]. Upon phase inversion (often accompanied by transitional stages such as multiple emulsions) the continuous and dispersed phase are exchanged (e.g., an o/w emulsion inverts to a w/o emulsion). The coalescence of drops proceeds in several steps. After the drops approach each other, they deform and the thin continuous phase film between the drops begins to flow outward. Once a critical film thickness is reached, the film finally tears, and the drops coalesce [56]. Complete separation of an emulsion in its aqueous and organic phase as a final stage is called phase separation [208].

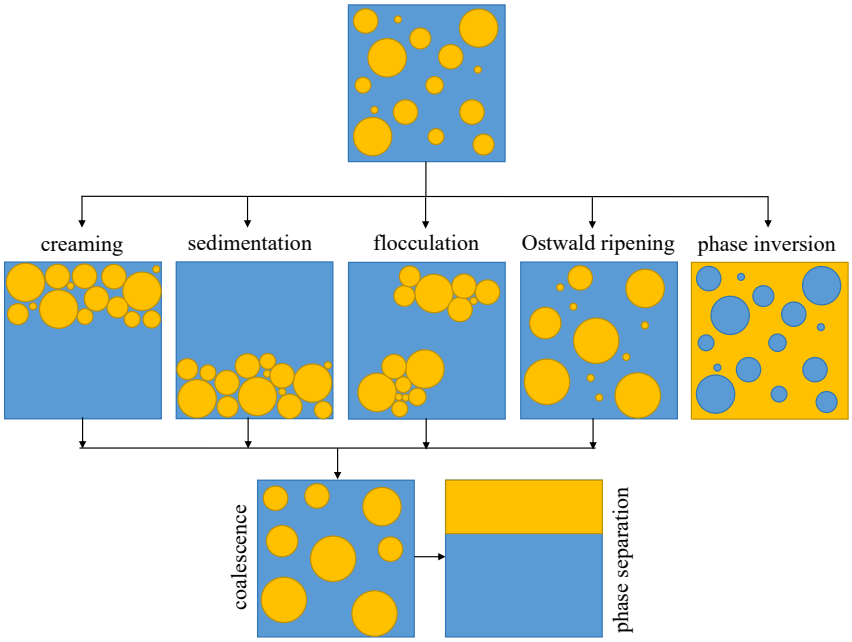

Figure 6. Schematic representation of emulsion destabilization processes. Adapted from [4, 103].

In [30], the main configurations and their underlying mechanisms for PE stabilization are summarized (**Figure 7**). For completely covered drops (**Figure 7** a)), coalescence is prevented by the two particle layers. In the case of sparsely covered drops, a bridging monolayer in the contact region forms when the particles are more wettable by the continuous phase (**Figure 7** b)). The underlying mechanisms in both configurations are the following [30]. As the particles are kept almost irreversibly at the interface, the adhesion energy prevents their displacement from the interface. There, they are in close proximity and steric hindrance prevents the lateral movement and displacement of particles. The stability of the thin continuous phase film between two approaching drops is influenced by the capillary pressure preventing film thinning and film rupture as well as the interfacial rheological properties causing a decrease in film drainage rate. Further stabilizing configurations in PEs are shown in **Figure 7** c)-e), where particles aggregate and form a two-dimensional network on the drop surface (c), where domains of particles at the interface form in the case of sparse coverage (d) or where a three-dimensional network structure of particles between drops is formed, improving the emulsion stability as contact between drops is hindered (e) [30].

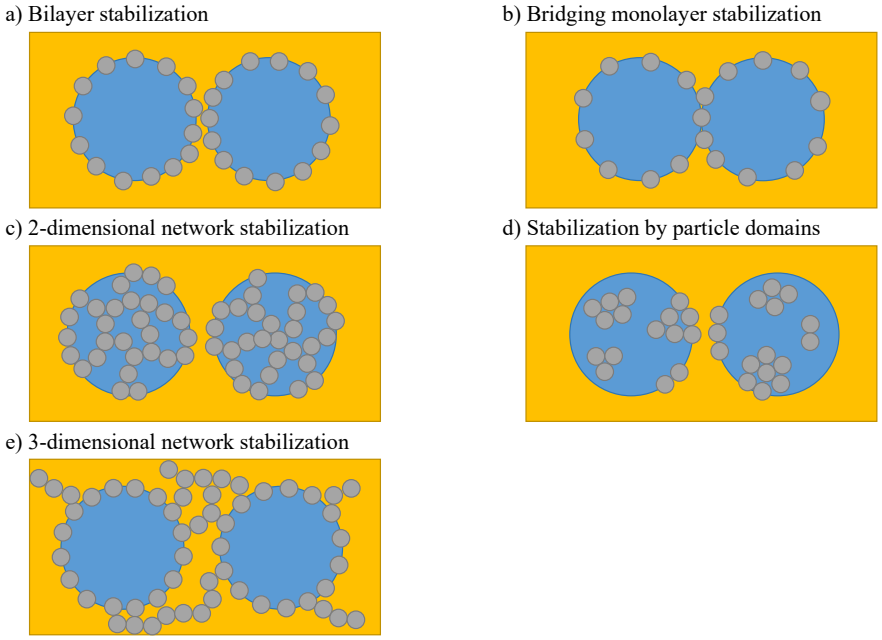

Figure 7. Schematic representation of stabilization configurations in PEs. Adapted from [30].

PE stability can be examined in different ways, e.g., via the shift of the oil-emulsion or emulsion-water boundary over time [35, 37], via the amount of released oil and emulsion after a centrifugation process [203], via the volume of separated dispersed phase after storage at higher temperatures [156] or via the comparison of drop size distributions of fresh PEs and after certain time intervals [68]. In general, small drop sizes and the presence of network structures between particles and drops are assumed to lead to higher PE stability [247].

3.1.3 Key parameters governing PE properties

The exact knowledge and control of PE properties is of great importance for design and modeling of product properties as well as reaction and separation processes. Numerous parameters can be used to tune the characteristic PE properties (such as emulsion type, stability, DSD, rheology or filtration behavior) [5, 30]. Among these are particle and oil properties, dispersed phase fraction or properties of the aqueous phase (**Figure 8**). These parameters will briefly be discussed in the following. Another leverage – that has mostly been neglected in literature so far – is the preparation process of PEs which is more intensively discussed in **Section 3.1.4**.

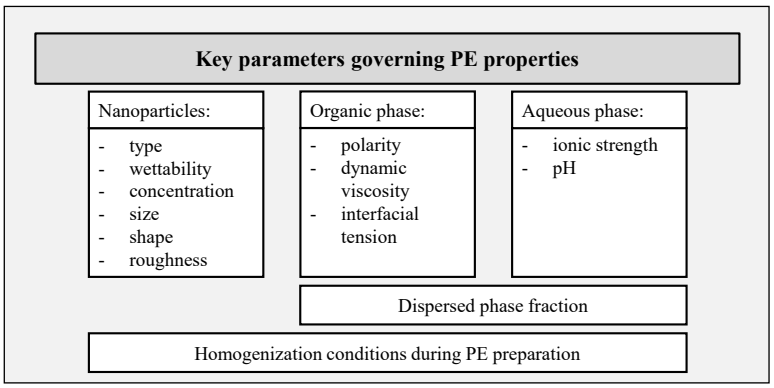

Figure 8. Schematic representation of the key parameters determining the characteristic PE properties. Adapted from [5, 30].

Particle type and wettability
Numerous types of solid particles typically used for PE stabilization have been reviewed in [252]. Among these are

- silica (e.g., [32, 77]),
- clay (e.g., [13, 241]),
- magnetic particles (e.g., [147]),
- natural emulsifiers such as starch, soy or whey protein (e.g., [145]),
- carbon nanotubes (e.g., [55]),
- polymeric particles (e.g., [36]) or
- cellulose (e.g., [68]).

Within the last years, some researchers have shifted their focus from inorganic particles to particles of biological origin or particles suited for food applications [24, 118]. However, so far, most research has been conducted with inorganic silica particles. Pure silica particles have a hydrophilic surface but can easily be modified by grafting with non-polar organic groups such as silanes to tune the particle hydrophobicity [30, 77]. In this thesis, various commercially available fumed silica particles of different hydrophobicity were used as received. A more detailed description of their preparation and modification is given in **Section 4.1**.

Particle concentration
A sufficient number of particles is necessary to achieve high drop coverage [30]. Excess particles in the continuous bulk phase can enhance emulsion stability by the formation of a three-dimensional network structure between adjacent particles and/or dispersed phase drops [3, 26, 213] (cf. **Sections 3.1.2** and **3.1.6**). Typically, an increase in particle concentration leads to an increase in emulsion volume fraction and a decrease in drop size [14]. The impact of particle concentration on the drop size distribution will be discussed in more detail in **Section 3.1.5**. However, successful emulsion stabilization can also be achieved

without full drop coverage [62, 86, 226] (cf. **Section 3.1.2**). In the case of low or only partial coverage, a reallocation and redistribution of particles at the drop surface – especially in near droplet-droplet contact areas – and a hindering of drop coalescence has been observed [226]. The possibility to induce a phase inversion by a change of particle concentration was reported in [37]. PEs with a dispersed phase fraction of 0.5 could be inverted from o/w to w/o by simply increasing the particle concentration, when particles of intermediate hydrophobicity were initially dispersed in oil. The authors explained this behavior via a change in particle hydrophobicity with increasing particle concentration due to a decrease of the effective silanol content (silanol-silanol hydrogen bonds between particles) [37].

Particle size
For successful PE stabilization, the particles should be substantially smaller than the emulsion micro-sized drops (e.g., 0.01 - 10 µm particle diameters in [36]) [5]. An increase in particle size influences the drop-particle collision force, the film drainage and the adsorption time of a particle to the interface [220]. More monodisperse particles are favorable in terms of high emulsion stability [210]. Particles that are too large become too heavy, so that gravity can no longer be neglected. However, as can be derived from **Eq. (1)**, the energy of detachment for very small particles with diameters comparable to surfactant molecules is in the order of a few kT only and hence particles might be easily detached from the interface and not too effective in PE stabilization [26].

Particle shape
For theoretical studies, model systems with well-defined spherical particles are often used [30]. Successful PE stabilization can also be achieved with non-spherical particles of irregular shape, e.g., fumed silica [31]. In this case, different particle orientations at the L/L interface are possible, making the determination of the contact angle more difficult. Hence, particle detachment energies cannot be calculated via **Eq. (1)** but the equation should be extended by the particle orientation and at least two characteristic particle sizes [5]. In recent years, particles of various shapes were investigated, e.g., spherical particles, rods, cylinders, ellipsoidal particles, flakes, fibers, cubes, peanuts and many more [5, 85, 86, 252]. Emulsion stability was found to strongly depend on the aspect ratio of the particles. For dense interfacial packing, high viscoelastic moduli and emulsion stability, a sufficiently high particle aspect ratio was necessary [69, 139]. In addition to rigid particles, soft and deformable particles, such as microgels, can also be used (e.g., [61, 63]).

Particle surface roughness
Particle wettability and emulsion stability can significantly be influenced by the particle surface roughness [249]. Whether an increased particle roughness is beneficial [183] or detrimental [226] to PE stability is subject to contradiction in literature.

Oil type and dispersed phase fraction
In contrast to surfactants, the presence of particles does not significantly change the interfacial tension between the aqueous and the organic phase [178, 226]. However, the type of oil influences the interfacial tension as well as the three-phase contact angle and the energy of particle detachment from the interface (cf. **Eq. (1)** and **(2)**). In [34], silica particles of intermediate hydrophobicity (residual silanol content of 67%) preferred the formation of o/w emulsions with non-polar oils while w/o emulsions were preferentially stabilized with polar oils. The impact of dispersed phase fraction on the drop size distribution will be discussed in **Section 3.1.5**.

Salt concentration and pH
The wettability and zeta potential (particle surface charge, respectively) of the particles and hence the electrostatic interactions can be tuned via a change of pH or salt concentration (e.g., [31, 39]). Strong repulsive electrostatic interactions between particles can hinder particle adsorption to the interface and lead to poor PE stability [176]. Attractive interparticle interactions can promote particle aggregation, which also has an influence on PE stability [5].

3.1.4 PE preparation

Regardless of the intended application, PE preparation is always the first step and is very important as it – in addition to the PE composition (cf. **Section 3.1.3**) – determines the characteristic properties of the final emulsion.

Methods known to prepare surfactant stabilized emulsions can be adopted for PE preparation [5, 57, 247]. Among these – with decreasing resulting average drop diameters – are hand shaking (e.g., [12, 82, 100]), stirrers (e.g., [220, 221]), rotor-stator devices (e.g., [29, 96, 153]), high-pressure homogenizers (e.g., [11, 87, 114]) or ultrasonication (e.g., [78, 99, 185]). Membrane emulsification (e.g., [141, 206, 215]) or microfluidic devices (e.g., [91, 154, 170]) can be applied to produce PEs with narrow drop size distributions. With regard to an intended industrial application of PEs, high-pressure homogenization and rotor-stator systems are suited best [5]. Some advantages and disadvantages of PE preparation using rotor-stator devices are listed in **Table 1**.

Table 1. Advantages and disadvantages of rotor-stator devices. Adapted from [5].

advantages	disadvantages
- low operating costs	- possibly more polydisperse emulsions
- ease of setting up	- limited energy input
- rapidity of process	- risk of temperature increase
- small amount of liquid required	- high shear rates (might deform fragile particles or shear sensitive additives, e.g., enzymes)
- available from lab to industrial scales	

Rotor-stator systems in different geometric configurations and different scales are commercially available and can be operated in batch, semi-batch or continuous mode [160]. A schematic representation of the (batch) rotor-stator devices used in this thesis (ULTRA-TURRAX® (UT)) is given in **Figure 9**. Such a device consists of a high speed rotor, which is housed concentrically inside and in close proximity to the fixed stationary stator [134, 160]. Liquid circulation through multiple channels is realized via rotors of two or more blades and openings or slots in the stator [134]. Two major forces cause the size reduction of emulsion drops: fluid acceleration and hence mechanical impingement of drops against the wall and high shear forces occurring in the gap between the rotor and the stator [134].

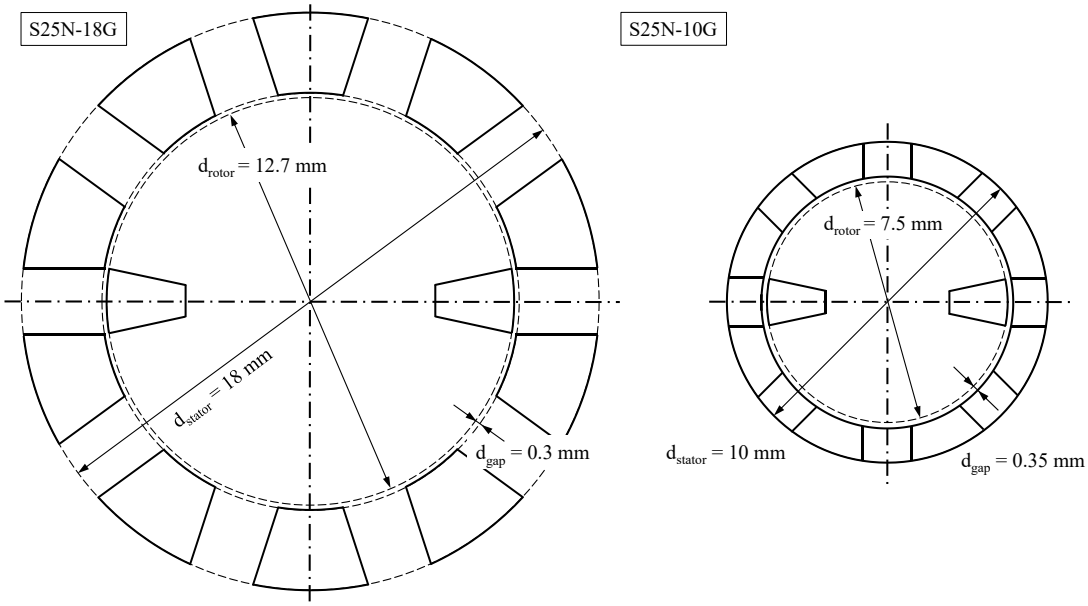

Figure 9. Schematic representation of the **(left)** S25N-18G and **(right)** S25N-10G dispersing head (IKA T 25 digital UT) with geometric dimensions of the rotor, the stator and the gap width. Adapted from [III].

Homogenization speeds and times are the two main parameters to control the resulting drop size. In contrast to conventional mechanically stirred systems, shear rates (20,000 to 100,000 s^{-1}) and energy dissipation rates (1,000 to 100,000 W kg^{-1}) are much higher in rotor-stator devices typically leading to drop sizes in the lower micrometer range (0.5 to 100 µm) [160].

Rotor-stator devices are frequently applied in literature (**Table 2**). However, the settings (as well as the geometric dimensions of the tool) used to produce o/w or w/o PEs vary greatly (dispersing speeds: 5,000 to 30,000 min^{-1} / dispersing times: 30 s to a few minutes) [5]. Typically, one fixed preparation protocol is used without any explanation why these homogenization conditions were chosen and often one or the other information concerning the specifications of the dispersing device is missing. The excerpt of a literature comparison in **Table 2** illustrates that previous work on characteristic PE properties – such as stability (cf. **Section 3.1.2**), drop size distribution (cf. **Section 3.1.5**), rheological behavior (cf. **Section 3.1.6**) or membrane filtration (cf. **Section 3.2.2**) – focused on the influence of emulsion composition at fixed homogenization conditions, but not on the PE preparation process itself. Focus was typically laid on the emulsion stability and average drop diameters. Detailed investigations of drop size distributions or the rheological behavior were only carried out in a limited number of publications. Hence, studies about the influence of PE dispersing conditions are surprisingly scarce and the differences in applied settings do not allow a direct comparison of different studies or general conclusions. The latter is indispensable for a targeted adjustment of desired PE properties.

3.1.5 Drop size distribution

The drop size distribution is one of the main characteristic emulsion properties. E.g., it determines the interfacial area available in chemical reactions and influences the rheological behavior or the speed of sedimentation or creaming.

Mean values – such as the Sauter mean diameter d_{32} (**Eq. (3)**) or the arithmetic mean diameter d_{10} (**Eq. (4)**) – and distribution functions (**Eq. (5)**) are used to describe the drop size. Here, d_i is the drop diameter and N is the number of counted drops [205].

$$d_{32} = \sum_{i=1}^{N} d_\mathrm{i}^3 \,/ \sum_{i=1}^{N} d_\mathrm{i}^2 \tag{3}$$

$$d_{10} = \sum_{i=1}^{N} \frac{d_\mathrm{i}}{N} \tag{4}$$

$$Q_0(d_\mathrm{i}) = \frac{N_{\mathrm{d<d_i}}}{N_\mathrm{total}} = \int_{d_\mathrm{min}}^{d_\mathrm{i}} q_0(d)\, dd \tag{5}$$

The Sauter mean diameter is frequently used for processes, where the interfacial area is an important factor (e.g., mass transfer and chemical reactions). It describes the average drop size of a polydisperse system, which has the same total volume as well as the same surface area as the corresponding monodisperse system [205]. Distribution functions give more detailed information about classes of drop sizes as well as polydispersity and can be given as cumulative distribution functions Q_r or density distribution functions q_r (e.g., $r = 0$: distribution function of number; $r = 3$: distribution function of volume). This is often necessary as emulsions with the same mean drop size can exhibit differences in the distribution functions.

In the case of PEs, numerous parameters have an influence on the drop size distribution (cf. **Figure 8**). A decrease in particle size (smaller adsorption times) leads to a decrease in drop diameters and an increase in emulsion stability [5, 36, 220]. For w/o PEs, more hydrophobic particles lead to larger Sauter mean diameters [99, 148]. The impact of particle wettability on emulsion stability was discussed in **Section 3.1.1**.

The influence of particle concentration on PE stability and drop size distribution was intensively studied among others by [37, 78, 200, 220]. An increase in particle concentration favors the formation of smaller drop sizes as a larger interfacial area can be stabilized and the distance between particles and the oil-water interface is reduced leading to enhanced particle-interface interactions [5].

Table 2. Preparation and characterization of PEs – overview of UT settings, investigated PE properties and varied parameters. Part of this table was adapted from [I].

type	settings		device		investigated properties					varied parameters	ref.
	n [min^{-1}]	t [min]		d_{stator} [mm]	drop diameter	DSD	η	stability	filterability		
o/w	/	/	T25	/	yes	yes	-	(yes)	-	manual shaking vs. UT vs. jet homogenizer, particle type + conc., viscosity of oil	[12]
w/o	8,000	1	T25	10	-	-	-	-	-	model enzyme reactions in microgel-stabilized PEs	[242]
o/w	8,000	2	T25	18	yes	-	-	yes	-	pH, electrolytes, type of salt	[31]
o/w	8,000	2	T18	10	yes	-	-	yes	-	hydrolysis in CO_2 / N_2 switchable PEs	[255]
o/w	10,000	5	T25	10	yes	-	-	yes	-	hydroformylation of long chained olefins, sonication vs. UT, particle type + conc.	[203]
o/w	11,000	2	T25	10	yes	-	yes	yes	-	particle conc., dispersed phase fraction, ionic strength	[248]
o/w	13,000	2	/	8	yes	-	-	yes	-	in situ hydrophobization of particles by dissolved oils, oil chain length, particle type	[42]
o/w	13,000	2	/	18	yes	yes	-	yes	-	type + composition of oil and aqueous phase (pH, electrolytes, addition of surfactant), silica particle size	[41]
o/w, w/o	13,000	2	/	/	yes	-	yes	yes	-	particle conc. + hydrophobicity + initial location	[37]
o/w, w/o	13,000	2	T25	18	yes	yes	-	-	-	particle conc. + wettability	[29]
w/o	13,000	2	/	18	yes	-	yes	yes	-	oil type, dispersed phase fraction, particle conc.	[28]
o/w, w/o	13,500	2	T25	18	yes	-	-	yes	-	oil + non-aqueous phase type, dispersed phase fraction, pH, initial particle location	[34]
o/w, w/o	13,500	2	T25	18	yes	yes	-	yes	-	particle wettability + size, dispersed phase fraction, addition of salt	[32, 36]
o/w, w/o	13,500	3	/	18	yes	yes	-	yes	-	particle conc., dispersed phase fraction, emulsification time, batch vs. continuous preparation	[40]
w/o	17,500	2	T25	/	yes	-	yes	-	-	impact of different lipases	[94]
w/o	17,500	2	T25	/	yes	yes	-	yes	yes	biocatalysis in PEs, enzyme properties, particle conc.	[96]
o/w	20,000	3	/	8	-	-	-	yes	-	particle surface roughness	[226]
o/w	20,000	5	T25	10	yes	-	-	yes	yes	particle conc.	[204]
w/o	20,000	5	T25	/	yes	yes	-	yes	yes	particle conc., UT vs. ultrasonic homogenizer	[200]
o/w	24,000	2	T25	10	yes	(yes)	-	yes	-	charged particles, pH, dispersed phase fraction, particle conc.	[176]
o/w, w/o	24,000	2	T25	18	yes	yes	-	yes	-	particle wettability, dispersed phase fraction	[32]
w/o	24,000	3	T25	10	yes	yes	yes	yes	-	synergistic interactions between hydrophobic silica particles + non-ionic surfactant	[153]
o/w, w/o	var.	2	T25	18	yes	yes	yes	yes	-	particle type + conc., dispersed phase fraction	[35]
o/w	var.	10	/	/	yes	-	yes	-	-	particles + CTAB + NaCl	[218]

Three regimes for the Sauter mean diameter – according to the particle mass fraction – were reported [78]. At low concentrations, there is a lack of particles to efficiently stabilize the emulsion drops resulting in drop coalescence and instability. At intermediate concentrations, limited coalescence – as reported in [12] – occurs as the amount of particles is not high enough to stabilize the whole interfacial area created during emulsification. At high particle mass fractions, the drop size is limited by the emulsification process (typical energy dissipation rates for rotor-stator devices were given in **Section 3.1.4**). Hence, a further increase of particle concentration does not lead to reduced drop sizes, the interface is assumed to be fully occupied by particles and excess particles in the continuous phase – possibly leading to the formation of three-dimensional network structures – might occur [57, 78].

Upon an increase of the dispersed phase fraction, an increase in Sauter mean diameters and a change in the emulsion type due to phase inversion has frequently been reported (e.g., [34, 93, 99, 141, 248]). At a constant particle concentration (and constant energy input), emulsions with smaller dispersed phase fractions develop smaller Sauter mean diameters than emulsions with higher dispersed phase fractions. The surface coverage and the number of particles per dispersed volume available for PE stabilization have an important influence [5, 99]. Furthermore, a change of the oil/water ratio has an impact on the sample viscosity and density and thus on the coalescence and break-up effects during emulsification [99]. High oil viscosities act as a damping factor, as particle diffusion and the adsorption rate to the interface are hindered [76, 220].

A synergistic effect of particles and catalyst-ligand complexes (needed for chemical reactions) on o/w PE drop size distributions was reported in [203]. The catalyst-ligand/water mixture had a lower interfacial tension than pure water and caused significantly smaller Sauter mean diameters. Also w/o PEs stabilized by silica particles and containing lipases showed smaller Sauter mean diameters compared to the emulsions without enzymes [94].

3.1.6 Rheological behavior

The rheological behavior of suspensions and (Pickering) emulsions can be investigated via, e.g., rotational and oscillatory measurements. The former give information about the magnitude of the dynamic viscosity η as well as Newtonian ($n = 1$ in **Eq. (6)** and $k = \eta$) or non-Newtonian flow behavior. **Eq. (6)** is the Ostwald-de Waele relationship with the shear stress τ, the flow consistency index k, the shear rate $\dot{\gamma}$ and the flow behavior index n. Fluids showing a decrease in viscosity with increasing shear rate exhibit shear thinning rheological behavior ($n < 1$ in **Eq. (6)**), while those showing an increase in dynamic viscosity with shear are called shear thickening ($n > 1$ in **Eq. (6)**) [115].

$$\tau = k\,\dot{\gamma}^{n} \qquad \textbf{(6)}$$

Oscillatory measurements give insights into the viscoelastic behavior of the sample. For unknown samples, an amplitude sweep needs to be conducted first to determine the sample deformation behavior in the reversible range. The deformation is changed in a stepwise manner while keeping the angular frequency constant. As a result, the linear-viscoelastic (LVE) area – where storage and loss modulus are constant and independent of the deformation – is obtained. Above the LVE area, irreversible structural changes occur within the sample [122]. The subsequent frequency sweeps are performed with a constant deformation from the LVE area. The frequency is varied to investigate the time-dependent behavior and stability of the sample [122]. Principally, the results for storage (G') and loss (G'') moduli as a function of frequency are used to indicate the presence and strength of network structures. In the case of viscous or liquid-like behavior the storage modulus is smaller than the loss modulus ($G' < G''$). In the case of elastic or solid-like behavior the storage modulus exceeds the loss modulus ($G' > G''$) [149, 156]. Emulsions are considered kinetically stable, when both moduli are almost independent of the angular frequency and when the storage modulus is greater than the loss modulus [153, 180, 207]. In [207], the application of rheological measurements to assess and predict the emulsion destabilization mechanisms described in **Section 3.1.2** are reviewed.

In recent years, many results concerning the rheological behavior of PEs have been published. Similar to the DSD, the rheology is influenced by the parameters listed in **Figure 8**. Numerous authors have reported shear thinning behavior for o/w and w/o PEs (e.g., [14, 21, 54, 94, 99, 112, 153, 156, 217, 248]). This is most often explained via the formation of a three-dimensional, elastic gel network between excess

particles in the continuous phase and/or densely packed emulsion drops (cf. **Figure 7** e)). With increasing shear, particle agglomerates and drops may undergo reorientation, alignment or partial break-up leading to a decrease in viscosity [99, 112, 158]. A three-dimensional network increases the dynamic viscosity of the emulsion and enhances the overall PE stability as drop motion is attenuated [57, 78, 100, 207].

The formation of such a network arises from hydrogen bonds of residual silanol groups on the particle surface. Therefore, the choice of particle type and hydrophobicity is important. Particles of increasing hydrophobicity (and hence smaller residual silanol contents) led to smaller dynamic viscosities and lower kinetic stabilities whereas the specific particle surface area did not show a significant influence on the rheological behavior of w/o PEs [99].

With increasing particle mass fractions, the drop size decreased, the dynamic viscosity of PEs and the amount of possibly freely suspended excess particles increased causing a thickening of the continuous phase and reducing all possible destabilization phenomena [57, 78, 156] (cf. **Section 3.1.2**). The shear thinning effect was enhanced at higher particle mass fractions and the emulsions showed elastic or solid-like behavior as the storage modulus was higher than the loss modulus ($G' > G''$) [99, 156, 248]. Both moduli increased with particle mass fraction and showed little dependency on the angular frequency indicating the formation of more stable network structures [99, 248].

In [112], the impact of particle shape (while maintaining the hydrodynamic particle size) and interparticle interactions (tuned from attractive to repulsive via a change in the salt concentration) was investigated. Fumed silica particles stabilized PE drops better than spherical ones, as they attached in densely packed layers on the drop surface while forming a three-dimensional network in the continuous phase at the same time. Due to the fractal structure of fumed silica, these particles had more contact points and multiple particles could interlock [112].

An increase in dispersed phase fraction led to an increase in Sauter mean diameters (cf. **Section 3.1.5**). The emulsion dynamic viscosity as well as storage and loss moduli ($G' > G''$) increased, the dependency of the moduli on the angular frequency became smaller and the shear thinning behavior was more pronounced [99, 248]. This is attributed to the reduced separation distance between emulsion drops at higher dispersed phase fractions, resulting in more closely packed drops which can interact and increase the resistance to flow (emulsion viscosity, respectively) [156].

From surfactant stabilized emulsions it is known that higher dynamic viscosities, more pronounced shear thinning behavior and higher storage and loss moduli are obtained in monodisperse emulsions with small drop sizes compared to more polydisperse emulsions [157, 181]. The impact of drop sizes on the rheological behavior via a change in PE composition (tuned via the particle mass and dispersed phase fraction) has been studied in literature, while the impact of homogenization conditions during PE preparation (PEs of constant composition) has not been investigated in detail yet. For o/w PEs stabilized by bentonite particles and a cationic surfactant in the presence of salt, it was found that a variation of homogenization conditions only had an influence on the viscosity at infinite shear but not on the zero shear viscosity [218].

3.2 Membrane filtration

3.2.1 Fundamentals

Filtration is the (mechanical) separation of dispersed components from a liquid or gas using a filter medium or membranes, respectively, under application of a driving force. Membranes are semi-permeable systems which form a barrier between two fluids and are permeable for certain species but impermeable for other components allowing a separation of mixtures on a molecular level (**Figure 10**) [115, 146]. The incoming feed is separated into the retentate and permeate. The retentate describes the phase that is retained by the membrane while the permeate describes the phase that passes through the membrane.

Important factors related to membrane filtration are explained in more detail in the following. Since this thesis will focus on the separation of w/o PEs, special attention is given to the organic solvent nanofiltration.

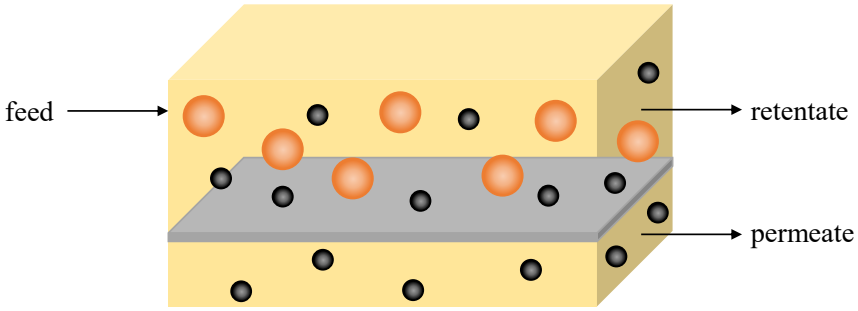

Figure 10. Schematic representation of a membrane process. Species 1 (orange) is retained by the membrane (grey) while species 2 (black) can pass the membrane. Adapted from [45, 146].

Classification of membranes

Pressure-driven membrane processes can be classified into microfiltration (MF), UF, nanofiltration (NF) or reverse osmosis (RO), based on the size of the retained species (**Figure 11**). In UF and NF applications, often the molecular weight cut-off (MWCO), which is defined as the smallest molecular weight of a molecule that is retained up to 90% by the membrane, is used to characterize and differentiate membranes [115].

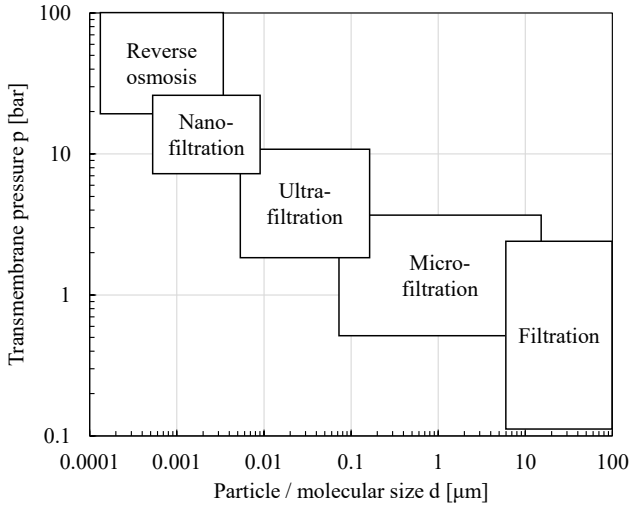

Figure 11. Overview of pressure-driven membrane processes. Adapted from [115].

Membranes with microscopically visible pores are called porous membranes, otherwise they are called dense membranes [146]. NF membranes are in the transition region as there are both porous and dense membranes [45].

Based on the membrane material, a distinction is made between inorganic (e.g., ceramic) and organic (polymeric) membranes [142], of which only the latter are used in this thesis and will therefore be described in more detail. Such membranes are often made to have an asymmetric structure and consist of a thin active layer (responsible for the separation task) and a porous support structure (responsible for mechanical membrane stabilization). Depending on the membrane preparation procedure and the materials used for the two layers, integrally skinned and thin film composite membranes are distinguished [142, 224]. While in the former case active and support layer are of the same composition, layers of thin film composite membranes consist of different materials. Typical polymers suited for membranes used in organic solvents are high performance polymers such as polydimethylsiloxane (PDMS) (e.g., [259]), polyimide (PI) (e.g., [108]) or polyacrylonitrile (PAN) (e.g., [164]). As OSN is a rather young technology, many publications focused on the development and preparation of solvent resistant membranes, but the number of commercially available membranes is still limited [224].

Operating mode

The principle of a membrane process is schematically shown in **Figure 10**. The pressure difference between feed and permeate side, called transmembrane pressure, is the driving force of the separation. The

permeate flux J, defined by **Eq. (7)**, is used to characterize membrane processes. Here, V_P is the permeate volume, t is the time and A_M is the effective membrane area. The flux and the transmembrane pressure are linked via the permeability P (**Eq. (8)**).

$$J = \frac{\dot{V}_P}{A_M} = \frac{\Delta V_P}{\Delta t\, A_M} \tag{7}$$

$$J = P\, \Delta p \tag{8}$$

Two flow configurations are used in membrane technology (**Figure 12**). In dead-end filtrations (**Figure 12** a)), the feed is orthogonal to the membrane surface. Operation can be either at constant transmembrane pressure difference or at constant flux. The retained species (e.g., particles, molecules, drops) form a filter cake on the membrane surface. The filter cake height increases with filtration time, leading to an increase of the filtration resistance and a decline in flux. To maintain a constant flux, the transmembrane pressure needs to be increased or, in extreme cases, the filtration needs to be stopped and the membrane must be cleaned or replaced [115]. In crossflow filtrations (**Figure 12** b)), the feed flow is parallel to the membrane surface. As the crossflow creates shear and lift forces, part of the retained species is convectively returned into the bulk flow leading to a constant filter cake height with filtration time [115].

Dead-end filtration is often used in lab scale feasibility studies due to the ease of setting up and as pressurization via an inert gas is possible. Stirred dead-end cells can be regarded as a mixed form, as stirring within the filtration cell creates a crossflow leading to a constant filter cake height. Crossflow filtration requires higher feed volumes and higher energy input to realize the feed circulation and high crossflow velocities [115].

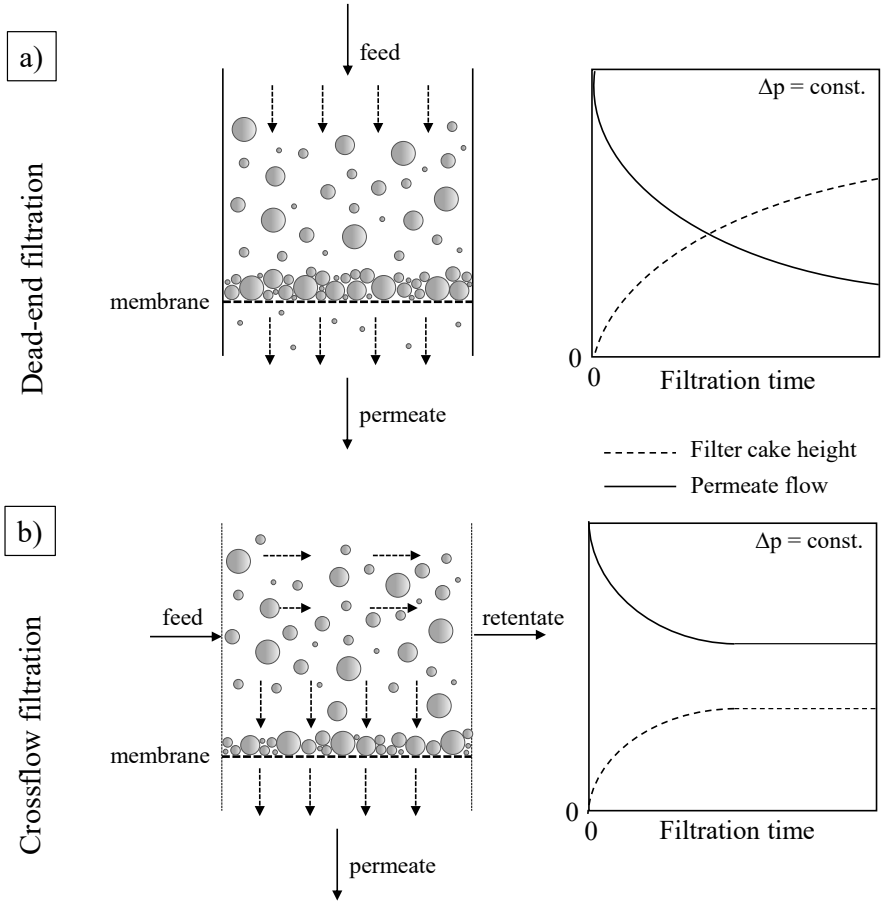

Figure 12. Schematic representation of flow configurations and general course of filter cake height and permeate flow under constant pressure conditions for **(a)** dead-end and **(b)** crossflow filtration. Adapted from [115].

Driving force reducing effects

The performance of a membrane (module) is negatively influenced by different effects, e.g., fouling, concentration polarization or membrane aging [146]. Due to a contamination, fouling increases the

transport resistance and reduces the membrane performance. This results in a flux decline during constant pressure operation or a pressure increase during constant flux operation. In the case of porous membranes, different potential fouling mechanisms or phenomena exist: adsorption, pore blocking, pore constriction, irreversible cake layer formation or gel formation [146, 196]. For attractive interactions between the solute or particles and the membrane, solute/particle adsorption and a change in membrane hydrophobicity or charge are possible. Pore blocking or pore closure on the membrane surface can be complete or partial. The adsorption of solutes/particles inside the membrane pores is also possible, narrowing or even closing the pore. The deposition of multiple layers of, e.g., particles on the membrane is called cake formation and the morphology of the cake determines the flux decline [196]. Concentration polarization – as a natural consequence of the membrane selectivity – describes the formation of concentration gradients in a boundary layer adjacent to the membrane surface caused by the accumulation of (retained) particles or molecules compared to the bulk solution [146, 196]. This causes a diffusive back transport to the bulk, a hindrance of the flux through the membrane and an osmotic back pressure reducing the transmembrane pressure [196]. The extent of the different fouling mechanisms depends on the feed composition, the hydrodynamic conditions as well as the membrane properties [196].

Organic solvent nanofiltration

OSN, also referred to as solvent resistant nanofiltration (SRNF) or organophilic nanofiltration (ONF), has emerged over the last two decades with the development of solvent resistant NF membranes [45, 190, 259]. This technology allows the separation of organic mixtures down to a molecular level (molecular range between 200 and 1,000 g mol^{-1}) [133, 259]. Research in the field of OSN includes development, preparation and characterization of new membranes and membrane materials, their application in new processes as well as the development of predictive methods for membrane selection and performance [133]. E.g., OSN has been studied in food, (bio-)catalytic, petrochemical and pharmaceutical applications, such as for the concentration and purification of products from reaction mixtures, the separation of homogeneous catalysts [172] or the recycle or exchange of solvents [45, 171, 224, 258]. OSN has several advantages over conventional separation technologies, such as distillation, extraction, crystallization or adsorption (e.g., [45, 224, 259]):

- typically, no thermal energy requirement → gentle process conditions (e.g., for sensitive products) and less energy consumption,
- reduction of process times via adjustment of the installed membrane area,
- no necessity for additives (e.g., solvents or adsorbents),
- increase of product quality,
- waste-efficiency and
- ease of installation as continuous process and combination with existing processes.

As the technology is still at an early stage of market development, open questions regarding the process design exist [45]. In contrast to aqueous systems, mutual interactions between the membrane, the solvent and the solute have to be considered in OSN [65, 214, 224, 259]. In literature, different combinations of these three parameters have been investigated but results were rather specific for certain applications. The conditions for membrane characterization as well as the actual filtration process differed strongly, making a comparison of different studies difficult [165]. This also complicates the membrane selection for a given separation task and is further complicated when commercially available membranes are used, as the composition and properties of these membranes are mostly unknown. Often extensive membrane screenings are necessary [165]. These can include solvent resistant membranes especially designed for OSN applications, but also membranes originally designed for aqueous applications might show good stability and performance in (some) organic solvents. Furthermore, appropriate conditions for membrane storage and rinsing need to be defined [224]. Effects reducing the driving force in a membrane process, as described in the previous paragraph, also exist in OSN applications but have yet been less intensively investigated compared to aqueous applications [224].

Emulsion filtration

Membrane filtration to treat the huge amounts of liquid waste emulsions produced every year by, e.g., the petrochemical, food, textile, cosmetic, steel, metallurgical or transportation industries, has intensively been studied in literature [72, 131, 222, 262]. The separation of w/o emulsions is important for the recovery of solvents or the purification of oil [72, 195]. Oily wastewaters (o/w emulsions) cannot directly be discharged as these would bring harm to people's health and the environment [72, 236, 262]. Here, membrane filtration

is superior to other o/w treatment techniques (such as chemical destabilization, centrifugation, coalescence, gravity separation, etc.) since even tiny oil drops (< 10 µm) can be rejected, which is necessary to meet the stringent standards for discharge [131, 143, 222]. For both emulsion types, the impact of emulsion composition (e.g., type of oil and surfactant, surfactant concentration), operating conditions (e.g., pressure, crossflow velocity) and membrane type (e.g., polymeric or ceramic membranes, membrane modification, design of superwetting membrane materials [262]) on the filtration performance and the fouling stages as well as fouling mechanisms have been published [52, 72, 253, 262, 80, 101, 102, 131, 143, 195, 222, 236]. As surfactant stabilized emulsions will not be further dealt with in this thesis, the reader is referred to the indicated literature for detailed information.

The treatment of nanoparticle stabilized oily wastewaters (oil drop sizes < 30 µm) via filtration of o/w PEs using either stainless steel strainers or different underwater superoleophobic polymeric membranes was reported in [67, 179]. Both approaches investigated a subsequent downstream process of nanoparticle recovery (centrifugation or magnetic separator, respectively). The current state of the art of w/o PE filtration is described in the following section.

3.2.2 Filtration of w/o Pickering emulsions

The filtration of w/o PEs is a new emerging field of interest and only a limited number of studies has been published so far. As described in **Chapter 1**, it is a promising alternative for continuous catalyst recycling in L/L multiphase reactions, where catalyst containing water drops are rejected by a membrane, while the organic product containing phase is continuously filtered through the membrane (cf. **Figure 1** and **Figure 13**).

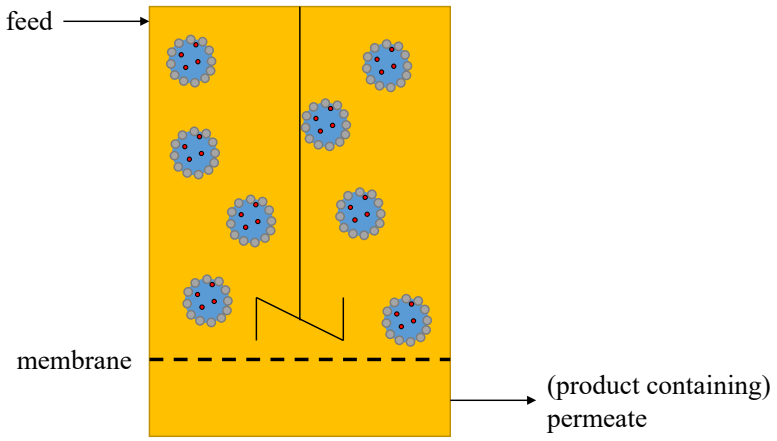

Figure 13. Schematic representation of the separation of w/o PEs via membrane filtration. Adapted from [199].

To our knowledge, the feasibility of w/o PE ultrafiltration – using the ETNA01PP membrane with a MWCO of 1,000 Da – was shown for the first time in 2016 [200]. Silica particle (HDK®H20) stabilized PEs were stable against coalescence despite the applied shear and pressure during the filtration. The water drops could successfully be retained 100% by the membrane and permeabilities of 3 - 10 L m^{-2} h^{-1} bar^{-1} were achieved [199]. However, an unexpected – but reproducible – filtration behavior was observed as the PE flux increased disproportionately with pressure and flux levels of the pure organic solvent were lower than PE fluxes. As scanning electron microscopy (SEM) images of fresh and used membranes showed an unharmed membrane surface, abrasion of the membrane surface by (residual) particles during the filtration could be ruled out. Using different organic solvents as the continuous phase, a disproportionate behavior was observed in all cases but to varying extents. The significant increase of PE fluxes seemed to be specific for 1-dodecene [199]. The impact of drop size distribution was investigated by filtration of PEs prepared with different energy input (via ultrasonication or UT, respectively) and/or with different particle mass fractions [200]. No significant impact of the drop size distribution on the flux was observed. Furthermore it was shown, that PEs can be concentrated up to a dispersed phase fraction of 80% [199].

The filtration of biocatalytically active water-in-CPME (cyclopentyl methyl ether) PEs was investigated in [95, 96] using a polyethersulfone (PES) UF membrane with a MWCO of 10 kDa. The impact of particle type, shape and size (spherical vs. fractal-like fumed silica particles), particle

concentration, dispersed phase fraction and enzyme properties on the filterability was studied. The addition of different lipases did not provide a clear effect on the filtration behavior of PEs – both an improvement and a deterioration of the filtration performance was observed [96]. In the case of spherical silica particles, an increase in particle concentration led to decreased fluxes as residual, freely suspended particles formed a filter cake [96]. The use of fumed silica particles led to smaller drop sizes, better reproducibility and higher flux levels [95]. An increase in dispersed phase fraction led to a decrease in flux. However, even at 50% water phase fraction, industrially relevant fluxes were achieved [95]. In contrast to the work by Skale et al. [199, 200], a disproportionate increase of flux with pressure for PEs was not observed and flux levels of the PEs were smaller than the pure CPME flux. Furthermore, a continuous biocatalytic transesterification in a membrane reactor was successfully carried out in long-term operation (30 hours, 8 residence times) with constant permeability [95].

3.2.3 Membrane filtration modeling approaches

For optimal filtration process design, the underlying transport mechanisms must be understood to predict the membrane performance. For both aqueous systems as well as OSN, some models have widely been accepted [115, 177, 189, 224, 259]:

- models based on irreversible thermodynamics, which consider the membrane as a black box,
- pore flow model,
- solution-diffusion model,
- solution-diffusion model with imperfections.

Up to date, there is no general agreement whether the transport through OSN membranes is mainly convective or diffusive [142, 198, 214, 259]. Successful description of experimental data based on the pore flow model (e.g., [138, 177]), the solution-diffusion model (e.g., [258]) as well as the solution-diffusion model with imperfections (e.g., [58, 75]) was reported. Different parameters, e.g., the viscosity or the molar volume of the organic liquid, the swelling degree of the membrane polymer or solvent solubility parameters were identified to influence the flow of the solvent through OSN membranes [189].

Pore flow model (PFM)

In the case of porous membranes, a laminar and convective transport through the membrane driven by a pressure gradient is assumed. The pressure difference Δp between feed and permeate side is described via **Eq. (9)** with the resistance coefficient ζ (depending on the Reynolds number Re: $\zeta \sim Re^{-1}$ and $\zeta \sim \overline{w}^{-1}$ for laminar flow conditions), the density ρ of the liquid i permeating through the porous layer, the mean flow velocity $\overline{w}$ in the porous layer and the height H as well as the hydraulic diameter d_h of the porous layer [115].

$$\Delta p = \zeta \, \frac{\rho_\mathrm{i}}{2} \, \overline{w}^2 \, \frac{H}{d_\mathrm{h}} \tag{9}$$

Depending on the assumptions made for the membrane structure, different equations for the flux can be derived (e.g., **Eq. (10)** and **(11)**), but all having in common that the pressure drop across the membrane is proportional to the superficial velocity v ($v = \overline{w}\,\varepsilon$) (flux, respectively). Assuming the membrane pores as continuous round channels of equal hydraulic diameter (Hagen-Poiseuille equation), the following equation can be derived (**Eq. (10)**). Here, the subscripts M and i denote the membrane and the solvent, respectively, ε is the membrane porosity and η is the dynamic viscosity of the permeate.

$$J_i = \frac{\varepsilon \, d_\mathrm{h}^2}{32 \, H_\mathrm{M} \, \eta_\mathrm{i}} \, \Delta p \tag{10}$$

Assuming the membrane as a porous layer comparable to a bed of particles, **Eq. (11)** can be applied (with d_{32} being the Sauter mean diameter) [115].

$$J_\mathrm{i} = \frac{1}{150} \, \frac{\varepsilon^3}{(1-\varepsilon)^2} \, d_{32}^2 \, \frac{1}{\eta_\mathrm{i}} \, \frac{\Delta p}{H} \tag{11}$$

In these models, specific membrane properties – that are seldomly provided by the membrane manufacturers – are required [214]. In Darcy's law (**Eq. (12)**), these unknown parameters are combined into one numerical value, the membrane resistance R_M, which is a material-dependent parameter [115].

$$J_\mathrm{i} = \frac{\Delta p}{\eta_\mathrm{i}\, R_\mathrm{M}} \tag{12}$$

In the resistance in series model (**Eq. (13)**), the membrane as well as each non-ideality – caused by, e.g., fouling, pore blocking or adsorption of species inside of the membrane pores – is assigned its own resistance R_j [115].

$$J_\mathrm{i} = \frac{\Delta p}{\eta_\mathrm{i}\, \sum R_\mathrm{j}} \tag{13}$$

Solution-diffusion model (SDM)

The SDM was first developed in [129] and later reviewed in [243]. The diffusive transport of a molecule through a non-porous, dense and defect-free membrane is driven by a difference of the chemical potential and constitutes of three steps: the dissolution of the molecule in the membrane, its diffusive transport through the membrane and the desorption of the molecule on the permeate side of the membrane. The pressure inside the membrane is assumed to be equal to the feed pressure [189]. Typically, only the transport through the active membrane layer is considered [115, 146], since the support layer is much more porous and its resistance is much smaller. The transport equation according to the SDM describes the flux as the product of concentration, mobility of a molecule in the polymer phase (depending on the membrane and molecule properties) and the driving force (process variable) [146], leading to **Eq. (14)**.

$$\dot{n}_\mathrm{i} = \frac{D_\mathrm{iM}\, c_\mathrm{iM}\, \tilde{V}_\mathrm{i}}{\Re\, T\, \delta_\mathrm{eff}}\, (\Delta p - \Delta\pi) \tag{14}$$

Here, D_iM is the diffusion coefficient of the solvent i in the membrane, c_iM is the concentration, $\tilde{V}_\mathrm{i}$ is the molar volume, $\Re$ is the universal gas constant, T is the temperature, δ_eff is the thickness of the active membrane layer and Δp and $\Delta\pi$ are the pressure and the osmotic pressure differences, respectively. The latter one equals zero for pure solvents [258].

Solution-diffusion model with imperfections (SDMWI)

Imperfections within the dense membrane material or an increased free volume due to different swelling degrees might lead to an additional viscous flow. The solution-diffusion model with imperfections combines diffusive and convective transport through the membrane [45] (**Eq. (15)**).

$$J_\mathrm{i} = J_\mathrm{i,SDM} + J_\mathrm{i,PFM} \tag{15}$$

4 Materials and Methods

This chapter gives an overview of the materials, experimental measurement techniques and ranges of test parameters used to investigate the characteristic properties and the filtration behavior of PEs. Further details about the exact PE composition and the specific measurements are provided in the publications [I]-[VI] and at the beginning of each result section in this thesis (**Chapter 5** – "working program").

4.1 Chemical and physical properties of used materials

Liquid components

Deionized water (Sirion Mini 10 - 15 EP system, Veolia Water Technologies Deutschland GmbH, κ = 5 µS cm^{-1}) was used as the aqueous phase for all investigated PEs. 1-dodecene (Merck KGaA), dodecane and octene (Thermo Fisher GmbH), decene (Sigma-Aldrich Chemie GmbH), and heptane (Th. Geyer GmbH & Co. KG) were used as organic liquids (**Table 3**). All organic components were used as received. 1-dodecene was chosen as the "standard" organic liquid as it is suited as a model long-chained olefin for, e.g., hydroformylation reactions, and enables comparison with previous studies, e.g., [200, 202, 203]. Decene and octene were selected from the homologous series of alkenes. Dodecane was used as it has the same chain length as 1-dodecene but no double bond. Heptane was selected based on a previous study [178].

The impact of temperature on the dynamic viscosity and density of 1-dodecene was investigated by the group of Prof. Dr.-Ing. Matthias Kraume (Technische Universität Berlin). An exponential correlation (R^2 = 0.995) was found to describe the temperature dependency of the dynamic viscosity (**Eq. (16)**). A linear correlation (R^2 = 0.987) was found for the temperature dependency of the density (**Eq. (17)**).

$$\eta_{1-\mathrm{dodecene}}(T) = 0.0403\ Pas \cdot exp\left(-0.012\frac{T}{K}\right) \tag{16}$$

$$\rho_{1-\mathrm{dodecene}}(T) = \left(775.28 - 0.7395\frac{T}{^{\circ}C}\right) kg\ m^{-3} \tag{17}$$

Table 3. Characteristics of the liquid components used in this thesis. Further properties are given in **Table 15** (appendix).

component		CAS-nr.[1]	purity	$\widetilde{M}$[1]	ρ[1] (20 °C)	η[2] (20 °C)	σ[3] (20 °C)
		[-]	[%]	[g mol^{-1}]	[kg m^{-3}]	[mPa s]	[mN m^{-1}]
water	H_2O	7732-18-5	/	18.02	998.0	1.002	72.7
1-dodecene	$C_{12}H_{24}$	112-41-4	for synthesis	168.32	758.4	1.25	25.6
dodecane	$C_{12}H_{26}$	112-40-3	> 99.0	170.33	749.5	1.44	25.4
decene	$C_{10}H_{20}$	872-05-9	> 97.0	140.27	740.8	0.71	25.0
octene	C_8H_{16}	111-66-0	> 99.0	112.21	714.9	0.29	21.8
heptane	C_7H_{16}	142-82-5	> 99.2	100.20	680.0	0.36	20.3

[1] Data taken from PubChem Database (online) https://pubchem.ncbi.nlm.nih.gov (retrieved: January 14, 2021).
[2] Own measurements: The dynamic viscosities of the pure solvents were measured using a cone and plate rheometer. Details can be found in **Section 4.3.3**.
[3] Values taken from [225] for heptane, octene, dodecane and water, [152] for decene and [161] for 1-dodecene.

Nanoparticles

Various particles differing in their specific surface area and hydrophobicity were used to prepare w/o or o/w PEs and nanoparticle/oil suspensions. Commercially available fumed silica particles (HDK series) listed in **Table 4** were kindly donated by Wacker Chemie AG [234] and used as received. Use of these particles enables comparison with previous studies, e.g., [95, 99, 178, 199].

Hydrophilic HDK is produced by flame hydrolysis of volatile chlorosilanes in a hydrogen-oxygen flame at temperatures > 1,000 °C (**Figure 14**). During the production process, individual primary particles (5 - 50 nm) fuse with each other and form aggregates and finally agglomerates leading to fractal-like particles of irregular shape [227].

Table 4. Characteristics of fractal-like silica particles received from Wacker Chemie AG.

particle type	density	residual silanol content	specific particle surface area BET	tamped density	surface modification	ref.
	[kg m^{-3}]	[%]	[m^2 g^{-1}]	[g L^{-1}]		
HDK®H15	2,200	50	130 - 170	40	dimethylsiloxy	[228]
HDK®H18	2,200	25	170 - 230	50	polydimethylsiloxy	[229]
HDK®H20	2,200	50	170 - 230	40	dimethylsiloxy	[230]
HDK®H30	2,200	50	270 - 330	40	dimethylsiloxy	[231]
HDK®H2000	2,200	25	200	100 - 250	trimethylsiloxy	[232]

While the particle aggregates do not break up under high applied shear stresses, the agglomerates are able to break up but also to reform, e.g., [15, 109, 188]. By chemical reaction of hydrophilic silica with reactive silanes, e.g., dichlorosilane, particles of various degrees of hydrophobicity – expressed via the residual silanol content – are obtained [227]. By definition, the residual silanol content is the relative silanol content in relation to the hydrophilic silica (approximately 2 SiOH nm^{-2}) [227, 233]. Particle hydrophobicity increases with decreasing residual silanol content.

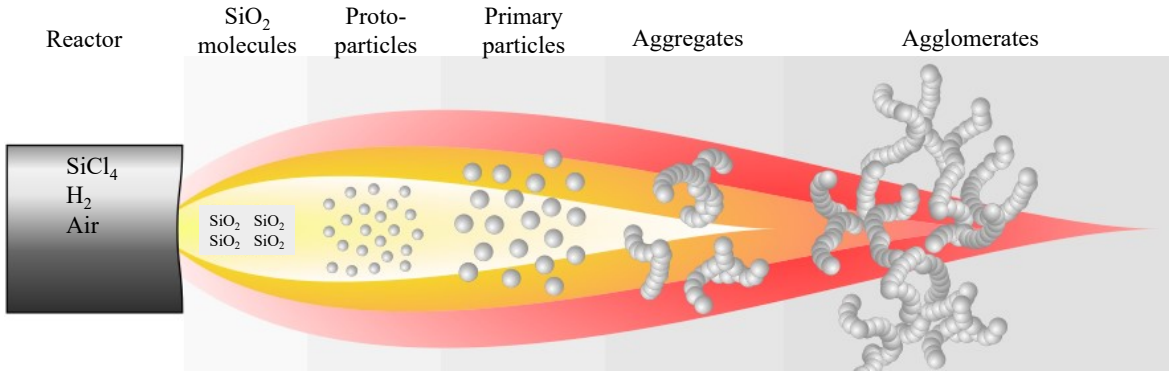

Figure 14. Schematic representation of the production of hydrophilic silica via flame hydrolysis. Adapted from [227].

The contact angle a water drop forms with the different silica particles was measured by the group of Prof. Dr. Regine von Klitzing (Technische Universität Darmstadt) (**Figure 15**). Dispersions of particles and ethanol were dried on silicon wafers. The surface topography of these particle layers was investigated by atomic force microscopy (AFM) since surface wettability is influenced by its roughness. From the AFM images, no individual particles could be seen but it was confirmed that the wafer is densely covered with a layer of particles. The root mean square (RMS) roughness was determined from the height distribution. The related contact angles of a deposited water drop on the prepared particle surfaces show that particle hydrophobicity decreases in the following order: HDK®H18 > HDK®H2000 > HDK®H15 ≥ HDK®H30 ≥ HDK®H20.

For visualization of particle size and shape, SEM images of partially hydrophobized HDK particles were published in, e.g., [57, 99, 202]. HDK®H20 particles were found to be approximately 150 nm in length and 10 - 50 nm in width [202]. HDK®H18 particles were reported to show the same structure as HDK®H20 particles [201]. The attachment of HDK®H20 to the w/o interface was visualized via confocal laser scanning microscopy in [202].

Spherical hydrophobic silica particles of different sizes and charge were prepared by the group of Prof. Dr. Regine von Klitzing (Technische Universität Darmstadt) and used for selected w/o PE filtration experiments. The procedure of particle preparation as well as particle properties were published in [IV].

For o/w PE stabilization, hydrophilic Halloysite nanotubes (HNTs) from Henan Province in China were used. These are natural clay particles consisting of rolled aluminosilicate sheets. The hollow, tubular particles have a silica layer on the (negatively charged) outside and an alumina oxide layer on the (positively charged) inner surface [2]. From transmission electron microscopy (TEM) and SEM images the following geometric dimensions of HNT particles were derived: 800 ± 200 nm mean length; 50 ± 5 nm mean outer diameter and 15 ± 2 nm mean inner diameter [203].

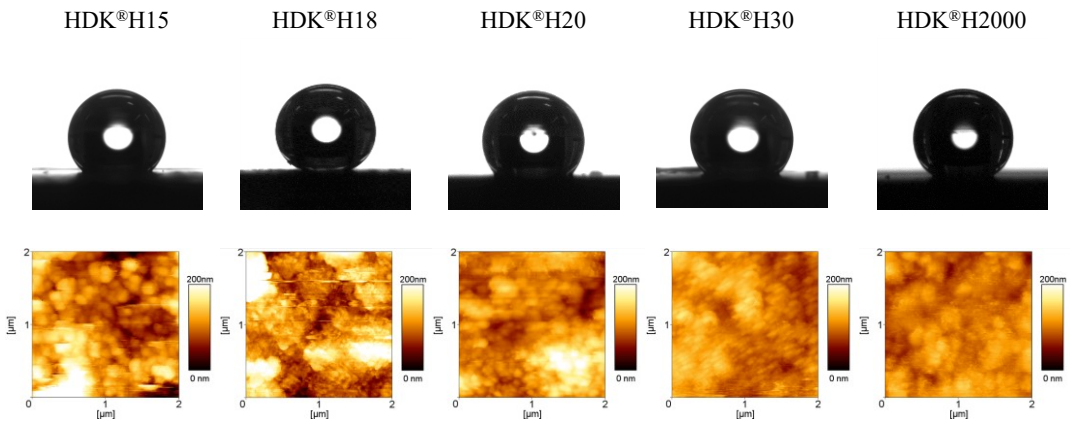

	HDK®H15	HDK®H18	HDK®H20	HDK®H30	HDK®H2000
Contact angle [°]	137 ± 3	156 ± 4	131 ± 4	132 ± 6	142 ± 5
RMS roughness [nm]	41 ± 7	36 ± 5	25 ± 5	27 ± 5	21 ± 6

Figure 15. Water drops on top of a wafer spin coated with different silica particles and corresponding AFM images of the particle layers used for contact angle measurements. Adapted from [II].

Membranes

To investigate the filtration of w/o PEs, solvent resistant membranes were needed. Both, emulsion drops as well as possibly freely suspended residual particles needed to be reliably retained. Based on these requirements and due to the novelty of this PE application, different commercially available UF flat sheet membranes were investigated (**Table 5**) and tested with 1-dodecene.

Table 5. Characteristics of membranes tested within this thesis ["/" denotes no information given by the manufacturer]. [1]Own measurements: pure 1-dodecene flux, room temperature, pressure of 4 bar, either no stirring or at 500 min^{-1}. The experimental dead-end filtration set-up is described in detail in **Section 4.4**. The membranes investigated in detail in this thesis are highlighted in dark grey and those used for selected PE filtration experiments are highlighted in light grey. Adapted from [VII].

membrane type	company	MWCO	recommended operating conditions			type	material	pure 1-dodecene flux[1]	ref.
			pH	p	T				
		[Da]	[-]	[bar]	[°C]			[L m^{-2} h^{-1}]	
ETNA01PP	Alfa Laval	1,000	1 - 11	1 - 10	5 - 60	UF	PVDF (on PP)	17.5	[6]
ETNA10PP		10,000						58.1	
GR81PP		10,000	1 - 13	1 - 10	5 - 75	UF	PES (on PP)	0.0	[7]
GR90PP		5,000						0.0	
GR95PP		2,000						0.0	
PMUC	Microdyn Nadir	30,000	2 - 11	/	< 55	UF	cellulose	93.7	[150]
PuraMemFlux	Evonik	/	7	20 - 40	< 50	OSN	silicone coated PAN	6.3	[70]
DuraMem900		900	7	< 20	< 50	OSN	modified polyimide	0.0	[71]
oNF-1	Borsig	600	/	15 - 35	< 60	OSN	silicone polymer-based composite type	20.2	[47]
oNF-2		350	/			OSN		12.0	[48]
oNF-3		900	/			OSN		14.4	[46]
HZG PDMS	Helmholtz Zentrum Geesthacht	2 µm	/	/	/	OSN	PDMS (on PAN)	8.2	[214]
HZG PIM		/	/	/	/	OSN	PIM (on PAN)	0.0	-

Since most commercial UF membranes are designed for aqueous applications, the choice was limited. While UF membranes with an active PES layer did not show any 1-dodecene fluxes, the high MWCO

membranes ETNA10PP and PMUC – despite the highest UF flux levels – were discarded to ensure complete particle retention. Reasonable 1-dodecene fluxes were obtained using the ETNA01PP membrane with a MWCO of 1,000 Da from Alfa Laval. This surface-modified membrane is of composite type with a polyvinylidene fluoride (PVDF) based active layer [237] on a polypropylene (PP) support structure [6].

To describe the filtration behavior of PEs more fundamentally, further flat sheet membranes from the field of OSN were sought for comparison (cf. **Table 5**). Although recommended operating conditions are between 15 - 35 bar, relevant 1-dodecene fluxes were obtained using the oNF-1, oNF-2 and oNF-3 membrane from Borsig Membrane Technology GmbH at the applied test conditions of 4 bar. Due to the highest MWCO, the oNF-3 membrane was used in most investigations while the oNF-1 and oNF-2 membranes were only used for selected experiments (cf. **Figure 91** and **Figure 92** (appendix)). While the MWCO of the oNF-3 membrane is comparable to that of the UF membrane ETNA01PP, the membrane material is different. Membranes PuraMemFlux from Evonik Resource Efficiency GmbH and HZG PDMS from Helmholtz Zentrum Geesthacht also worked with 1-dodecene but were used for selected experiments only due to their lower flux levels (cf. **Figure 93** and **Figure 94** (appendix)). DuraMem900 and HZG PIM membranes did not show any 1-dodecene flux at the applied test conditions.

4.2 Preparation of Pickering emulsions and suspensions

The amount of particles needed to reach a certain desired particle mass fraction ξ (defined with respect to the total mass of the emulsion, **Eq. (18)**) was weighed into a 50 mL centrifuge tube or a 100 mL glass bottle, depending on the total PE batch volume. The subscripts in **Eq. (18)** denote particle (p), organic phase (o) and aqueous/water phase (w) and m is the mass.

$$\xi = \frac{m_\mathrm{p}}{m_\mathrm{p} + m_\mathrm{o} + m_\mathrm{w}} \tag{18}$$

The particles were then completely wetted with the continuous phase and finally, the required volume of dispersed phase was added with a pipette. The dispersed phase fraction φ is defined from the volumes V of the dispersed (dP) and continuous (cP) phase (**Eq. (19)**).

$$\varphi_\mathrm{dP} = \frac{V_\mathrm{dP}}{V_\mathrm{dP} + V_\mathrm{cP}} \tag{19}$$

If not stated otherwise, both liquid phases and the particles were directly homogenized using a batch rotor-stator system (IKA T 25 digital ULTRA-TURRAX®, P_max = 500 W [104]) equipped with either a S25N-10G or a S25N-18G dispersing head (cf. **Figure 9** in **Section 3.1.4)**. Some manufacturers' specifications of these two dispersing heads are given in **Table 6**. For better comparability, the position of the tip of the UT was always kept at the level of the interface between the organic and the aqueous phase.

To determine the energy density during PE preparation, the emulsion temperature was measured right before and after homogenization (high-precision Pt100 thermometer – GMH 3700 series, GMH Messtechnik GmbH).

Table 6. Manufacturers' specifications of the dispersing tools [105, 106].

specification		S25N-10G	S25N-18G
working volume	[mL]	1 - 100	10 - 1,500
(outer) stator diameter	[mm]	10	18
(outer) rotor diameter	[mm]	7.5	12.7
gap width between rotor and stator	[mm]	0.35	0.3
max. dispersing speed	[$\mathrm{min^{-1}}$]	25,000	25,000
max. tip speed	[$\mathrm{m\ s^{-1}}$]	9.8	16.6
pH range	[-]	2 - 13	2 - 13
temperature range	[°C]	< 180	< 180
solvent resistivity	[-]	yes	yes
final emulsion fineness	[µm]	1 - 10	1 - 10

Various compositions of w/o PEs were investigated (**Table 7**). The varied parameters include the type of organic solvent, the dispersed phase fraction, the nanoparticle (NP) type and mass fraction, the PE

volume and the homogenization conditions during PE preparation. Highlighted in grey are the parameters used to prepare a "standard" w/o PE. If not stated otherwise, all experiments were conducted with individually prepared emulsions.

Table 7. Parameters used for w/o PE preparation.

investigated parameter	solvent type	φ	NP type	ξ	PE volume	homogenization conditions
		[-]		[wt.%]	[mL]	[min^{-1}] / [min]
solvent type	1-dodecene dodecane decene octene heptane	0.25	HDK®H20 HDK®H2000	0.5	100	17,500 / 2 (S25N-18G)
φ	1-dodecene	0.1 0.25 0.4 0.5	HDK®H20 HDK®H2000	0.5 (1.0)	100	17,500 / 2 (S25N-18G)
NP type	1-dodecene	0.25	HDK®H15 HDK®H18 HDK®H20 HDK®H30 HDK®H2000	0.5	100	17,500 / 2 (S25N-18G)
ξ	1-dodecene	0.25	HDK®H20 HDK®H2000	0.25 0.5 1.0	(20) 100	17,500 / 2 (S25N-10G + S25N-18G)
PE volume	1-dodecene	0.25	HDK®H20	0.5	20 50 100	var. (S25N-18G)
homogenization conditions	1-dodecene	0.25	HDK®H20	0.5	20	var. (S25N-10G + S25N-18G)

In the case of nanoparticle/oil suspensions, the desired amount of particles was weighed into a glass bottle first. The mass of particles was equal to the mass used for w/o PEs prepared with a dispersed phase fraction of 0.25 and a particle mass fraction of either 0.5 or 1.0 wt.%. The particles were then dispersed in 100 mL of the pure organic solvent using the S25N-18G dispersing head at dispersing conditions of 17,500 min^{-1} / 2 min. An overview of the varied suspension compositions is given in **Table 8**. Highlighted in grey are the parameters used for the preparation of a "standard" suspension.

Table 8. Parameters used for nanoparticle/oil suspension preparation.

investigated parameter	solvent type	NP type	ξ
			[wt.%]
solvent type	1-dodecene dodecane decene octene heptane	HDK®H20 HDK®H2000	0.5
NP type	1-dodecene	HDK®H18 HDK®H20 HDK®H2000	0.5 1.0
ξ	1-dodecene	HDK®H18 HDK®H20 HDK®H2000	0.5 1.0 (1.25)

For selected experiments, o/w PEs were used. Consistent with studies of the project partners – group of Prof. Dr. Regine von Klitzing (Technische Universität Darmstadt) [203, 204] – 16 g emulsion batches consisting of 13 g of deionized water and 3 g of 1-dodecene with particle mass fractions of either 0.5 or 1.0 wt.% were prepared. The o/w PEs were homogenized using the same UT (S25N-18G) as used for w/o PE preparation but at dispersing conditions of 20,000 min^{-1} / 5 min. Either HDK®H20 particles, which are of intermediate hydrophobicity and able to stabilize both w/o and o/w PEs, or HNTs were used as PE stabilizers.

4.3 Characterization of Pickering emulsions

PEs were characterized in terms of DSD, stability and rheological behavior. Characterization experiments were conducted before and after the filtration process to identify the impact of pressure, drag and shear forces during the filtration on the PE properties.

4.3.1 Drop size distribution

Drop size distributions were determined via optical microscopy. To minimize overlapping and clustering of drops on the microscopic images, PEs were diluted with the continuous phase which was proven not to change the DSD in [35]. PE samples were inverted 10-fold by hand prior to application onto a glass slide to avoid sedimentation or creaming of emulsion drops within the sample tube. As reported in [202], shaking does not affect the DSD of w/o PEs stabilized by silica particles. Right after application onto the glass slide, the sample was covered with a 0.13 mm thick coverslip. At least 25 microscopic images were taken with a 10- or 20-fold magnification (Carl Zeiss AG, Axio Scope.A1, equipped with BRESSER MikroCam SP 5.1). To get statistically sound results, a minimum of 500 drops per distribution were found to be sufficient as the Sauter mean diameters then remained constant despite further counted drops (cf. **Figure 59** (appendix)).

An automated image analysis software was used to analyze the pictures and to evaluate the data (SOPAT GmbH) [135]. The user has to define representative sample drops to receive appropriate search patterns needed for the analysis algorithm. Only spherical drops can be considered, which was not a restriction, as the number of non-spherical drops was low (estimated less than 5%). Comparability between mean diameters from microscopic images taken with different foci was guaranteed by always using the center of the observed rim as the drop size. By way of example, this is shown in **Figure 16** by circular green markings on selected drops. If necessary, the automated drop detection was corrected (e.g., faulty drops were deleted) or image series were analyzed manually. Two factors – the definition of the sample drops and the manual correction – might have introduced a subjective factor into the drop size evaluation. According to [97, 135], where images obtained via an endoscope technique were investigated, this subjective assessment led to deviations of 4 - 7% in the Sauter mean diameters. The error was in a similar range, when one set of images was automatically analyzed by different persons, by using different sample drops and different search patterns or when automated and manual image analysis were compared [97, 99, 135, 199].

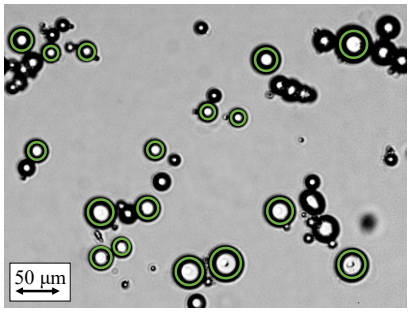

Figure 16. Example microscopic image of a w/o PE to illustrate the drop profiles. Adapted from [I].

4.3.2 Stability

In this thesis the stability of PEs against coalescence was evaluated in two different ways. For selected experiments, the drop size distributions of freshly prepared w/o PEs and after a storage time of two and ten weeks, respectively, were compared. Occurring drop sedimentation during storage was not considered as instability as the drops could be re-dispersed by gentle hand shaking. Furthermore, the stability against the applied pressure and shear during the filtration process was evaluated by comparison of drop size distributions before and after the filtration.

4.3.3 Rheological behavior

The rheological behavior of PEs was analyzed using a cone and plate rheometer with temperature control (Anton Paar GmbH, MCR 302, measurement system CP50-1: cone diameter 49.969 mm, angle 0.997°, gap size 0.102 µm). All measurements were performed at $T = 20.0 \pm 0.1$ °C. Prior to application of PE samples onto the plate, PEs were manually inverted 10-fold to avoid differences in applied phase fractions resulting from drop sedimentation or creaming within the sample tube. The rheological measurement parameters were adapted from [99] and are summarized in **Table 9**.

In rotational measurements, the PE sample was pre-sheared at a constant shear rate of 400 s^{-1} for 5 min to eliminate effects that might occur from non-uniform shearing histories [112]. The sample rheology was then determined by increasing the shear rate from 1 to 1,000 s^{-1} followed by a decrease of the shear rate from 1,000 to 1 s^{-1} to identify potential hysteresis effects.

Oscillatory measurements were conducted to investigate the linear-viscoelastic behavior. Amplitude sweeps at a constant angular frequency were performed first to determine the LVE area. Based on these results, frequency sweeps at a constant deformation from the LVE area were conducted (a deformation of 0.1% was found to be suited for all PEs). Shear rate, deformation and angular frequency were increased in a logarithmic ramp.

Table 9. Rheological measurement parameters applied in this thesis.

measurement	shear rate $\dot{\gamma}$	deformation γ	angular frequency ω
	[s^{-1}]	[%]	[rad s^{-1}]
flow curve	1 - 1,000 / 1,000 - 1	/	/
amplitude sweep	/	0.01 - 100	10
frequency sweep	/	0.1	100 - 0.1

4.4 Dead-end filtration of pure solvents, suspensions and Pickering emulsions

The experimental set-up is shown in **Figure 17**. Dead-end filtration experiments were conducted in batch-mode in a solvent resistant, magnetically stirred cell (4) designed for 47 mm membrane discs (XFUF0471, Merck KGaA, working volume $V = 91.5$ mL, effective membrane area $A_{\text{eff}} = 13.2$ cm^2). Except for the experiments to study the influence of temperature on the filtration behavior, all experiments were conducted at room temperature ($T = 22.1 \pm 1.3$ °C). If not stated otherwise, a new membrane sample was used for each experiment. At least duplicates were performed with each type of pure solvent, suspension or PE.

Transmembrane pressure differences were applied using nitrogen (1). As pipe length and permeate flow rates were small, pressure drops were regarded as negligibly small, and the applied pressure equaled the transmembrane pressure. The pressure was controlled by a pressure valve (VPPM-6, Festo GmbH) (2). A feed tank (17530, Sartorius AG) (3) was connected to the stirred cell (4). Experiments were conducted with or without stirring. Stehl et al. [202] observed drop coalescence and PE break up when emulsion drops got caught between a stir bar and a vessel bottom (experiments conducted in a beaker with the stir bar on the bottom). In the stirred cell the distance between the membrane surface and the hanging stir bar (octahedral, length 38 mm, width 10 mm, VWR International GmbH) was approximately 1.5 mm and hence much larger than the expected drop size (range of micrometers, e.g., [200, 202]). The permeate was collected in a beaker (7) and weighed on an electronic balance (weighing range 720 g, accuracy 0.001 g,

VWR International GmbH) (8) (measurement every 5 seconds). For the experiments to investigate the impact of temperature on the filtration behavior, the stirred cell was positioned in a water bath (5) whose temperature was controlled via a thermostat (Alpha A12, Lauda Dr. R. Wobser GmbH & Co. KG) (6). Data was recorded using LabVIEW (Laboratory Virtual Instrumentation Engineering Workbench) software, version 12.0, and used to calculate the flow rate $\dot{V}$ and the flux J (cf. **Eq. (7)**).

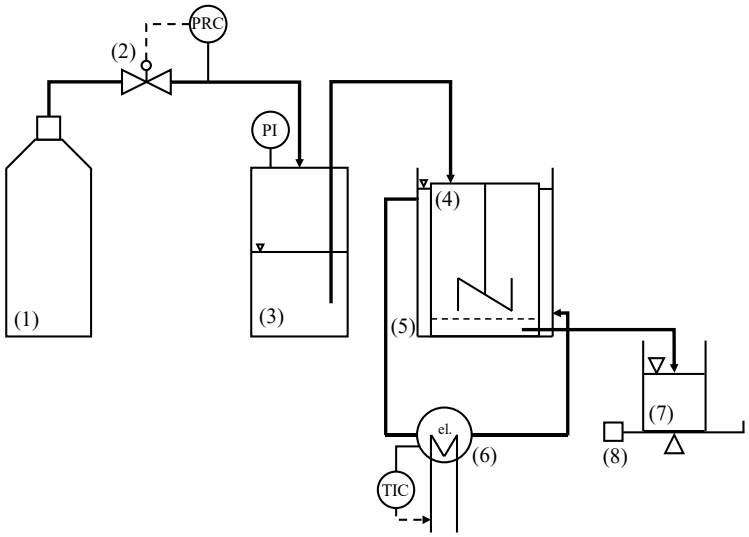

Figure 17. Schematic representation of the experimental dead-end filtration set-up: nitrogen gas cylinder (1), pressure valve (2), feed tank (3), stirred cell (4), water bath (5), thermostat (6), permeate beaker (7) on an electronic balance (8). Adapted from [199].

Following the membrane pre-treatment (**Section 4.4.1**), three different types of filtration experiments were performed: (mainly) pressure stepping experiments at constant phase ratio (**Section 4.4.2**), long-term filtration experiments at constant pressure and constant phase ratio (**Section 4.4.3**) as well as concentration experiments at constant pressure (**Section 4.4.4**).

4.4.1 Membrane pre-treatment

Two different membrane pre-treatment procedures, hereinafter referred to as “normal” or “specialized” pre-treatment, respectively, were investigated to achieve wetting, swelling and pre-compaction of the membrane samples before the actual experiment and to avoid overlapping effects from these time dependent phenomena. The stirrer speed during the pre-treatment was adjusted according to the speed during the actual filtration test.

The “normal” pre-treatment was adapted from [199, 200]. The membrane samples were soaked in the pure continuous phase solvent at least one day prior to use and then flushed with the pure solvent at a constant pressure of 4 bar for 90 min. Longer pre-treatment times did not help to reach steady state fluxes faster [199].

For selected experiments with the UF membrane ETNA01PP, an additional “specialized” pre-treatment procedure was investigated. The effect of a gradual solvent exchange on the membrane performance, inspired by [84, 197], was studied. The membrane samples were first immersed in pure deionized water for 3 hours, then immersed in a mixture of 50:50 vol.% of either isopropanol/1-dodecene or ethanol/1-dodecene, respectively, for 3 hours and finally immersed in pure 1-dodecene overnight. According to the “normal” pre-treatment, the membranes were then washed with pure 1-dodecene at a constant pressure of 4 bar for 90 min.

4.4.2 Pressure stepping experiments

To investigate the influence of pressure on the filtration performance, pressure stepping experiments were conducted. When 100 mL of PE or suspension were prepared, the stirred cell was completely filled with the emulsion or suspension, respectively. This was also the case for the pure solvents. For lower PE volumes additional pure solvent was added to obtain a completely filled cell. The pressure stepping

experiment was conducted at a constant phase ratio within the stirred cell as fresh solvent was continuously transported from the feed tank to the stirred cell when pressure was applied. To pre-condition the membrane and to reach steady states faster, pressure was first increased in a stepwise manner from 1 to 4 bar (in steps of 1 bar). The pressure was then decreased in steps of 1 bar. Each pressure step was kept for 30 min. The results presented in this thesis always represent the steady state fluxes received during pressure descent (cf. **Figure 60** (appendix)). For data evaluation, the average of 100 flux values at the end of each pressure step was used (measurement every five seconds).

4.4.3 Long-term filtration experiments

Some selected experiments were conducted at a constant pressure of 4 bar for 5 hours at constant dispersed phase fraction within the stirred cell as the organic phase was continuously transported from a feed tank to the stirred cell when pressure was applied. The stirrer speed was set to either 0 or 500 min^{-1}, respectively. All long-term filtration experiments were conducted at room temperature.

4.4.4 Concentration experiments

Concentration experiments were conducted to investigate up to which dispersed phase ratio the PEs could be concentrated. Since no pure solvent was continuously transported from the feed tank to the stirred cell throughout the concentration experiments, the dispersed phase fraction in the stirred cell increased with filtration time. The dispersed phase fraction at certain times was calculated from a mass balance (**Eq. (20)**) [199].

$$\varphi_{\mathrm{dP}}(t) = \frac{V_{\mathrm{dP}}}{\left(V_{\mathrm{dP}} + V_{\mathrm{cP,t=0}} - V_{cP}(t)\right)} \qquad \textbf{(20)}$$

The pressure and stirrer speed were set to 4 bar and either 0 or 500 min^{-1}, respectively. All concentration experiments were conducted at room temperature.

5 Results and Discussion

In this chapter, the results concerning the characteristic properties of w/o PEs and their filtration behavior are presented. In **Section 5.1**, the impact of homogenization conditions during PE preparation on stability, DSD, rheology and filtration using an UF and an OSN membrane are discussed. Since the UF membrane showed a qualitatively and quantitatively different behavior compared to the OSN membrane, further results for these two membranes – along with the accompanying investigations on PE characterization – are separately discussed in **Sections 5.2** and **5.3**. Furthermore, a mathematical model to describe the filtration of w/o PEs using the OSN membrane is developed and discussed in **Section 5.4**.

5.1 Choice of Pickering emulsion preparation conditions[1]

The exact knowledge and the adjustment of PE properties are crucial in terms of process design including the catalytic L/L reaction as well as the filtration for catalyst recovery. While a high interfacial area (small drops) is required for high reaction rates, supposedly larger drops are favorable for the filtration step to achieve high fluxes. Previous studies on PEs focused on the impact of PE composition on characteristic emulsion properties while the actual preparation procedure as another leverage for targeted PE design was mostly neglected (cf. **Table 2** in **Section 3.1.4)**.

5.1.1 Working program

The impact of homogenization conditions on w/o PE properties was investigated for a "standard" emulsion of the same composition prepared using 1-dodecene, 0.5 wt.% HDK®H20 and a dispersed phase fraction of 0.25. The preparation procedure via an UT and the two dispersing heads were already described in **Section 4.2**. **Table 10** summarizes the varied parameters. Experiments with identical dispersing speeds were conducted in [I] while identical tip speeds were compared in [III] to create a larger database (highlighted in grey in **Table 10**). The membranes ETNA01PP and oNF-3 introduced in **Section 4.1** were used.

Table 10. Parameters used for the investigation on the impact of homogenization conditions on PE properties.

n	w_{tip}		t	V_{PE}
	S25N-10G	S25N-18G		
[min^{-1}]	[m s^{-1}]	[m s^{-1}]	[min]	[mL]
9,000	-	6	2	20
10,000	3.9	6.6	2 / 5	20
10,500	-	7	2	20
12,000	-	8	2	20
12,500	4.9	8.3	2 / 5	20
13,500	-	9	2	20
15,000	5.9	10	2	20
15,300	6	-	2	20
17,500	6.9	11.6	0.5 / 1 / 2 / 3 / 5	20 / 50 / 100*
17,800	7	-	2	20
20,000	7.9	13.3	2 / 5	20
20,400	8	-	2	20
22,900	9	-	2	20
25,000	10	-	2	20

*Variation of PE volume only for the S25N-18G head and dispersing conditions of 17,500 min^{-1} / 2 min.

[1] The content of this section was partially published in [I] Kempin, M.V.; Kraume, M.; Drews, A. (2020): *W/O Pickering emulsion preparation using a batch rotor-stator mixer – Influence on rheology, drop size distribution and filtration behavior.* J. Colloid. Interf. Sci., 573, 135-149, DOI: 10.1016/j.jcis.2020.03.103 and [III] Kempin, M.V.; Drews, A. (2021): *What governs Pickering emulsion properties during preparation via batch rotor-stator homogenizers?* Chem. Ing. Tech., 93, 311-317, DOI: 10.1002/cite.202000130.

5.1.2 Impact on drop size distribution and PE stability

Impact of dispersing head and dispersing speed

By way of example, **Figure 18** shows microscopic images and corresponding Sauter mean diameters of PEs prepared at a dispersing time of 2 min but different dispersing speeds. At identical dispersing speeds, Sauter mean diameters obtained with the S25N-18G head were always smaller than those obtained with the S25N-10G head

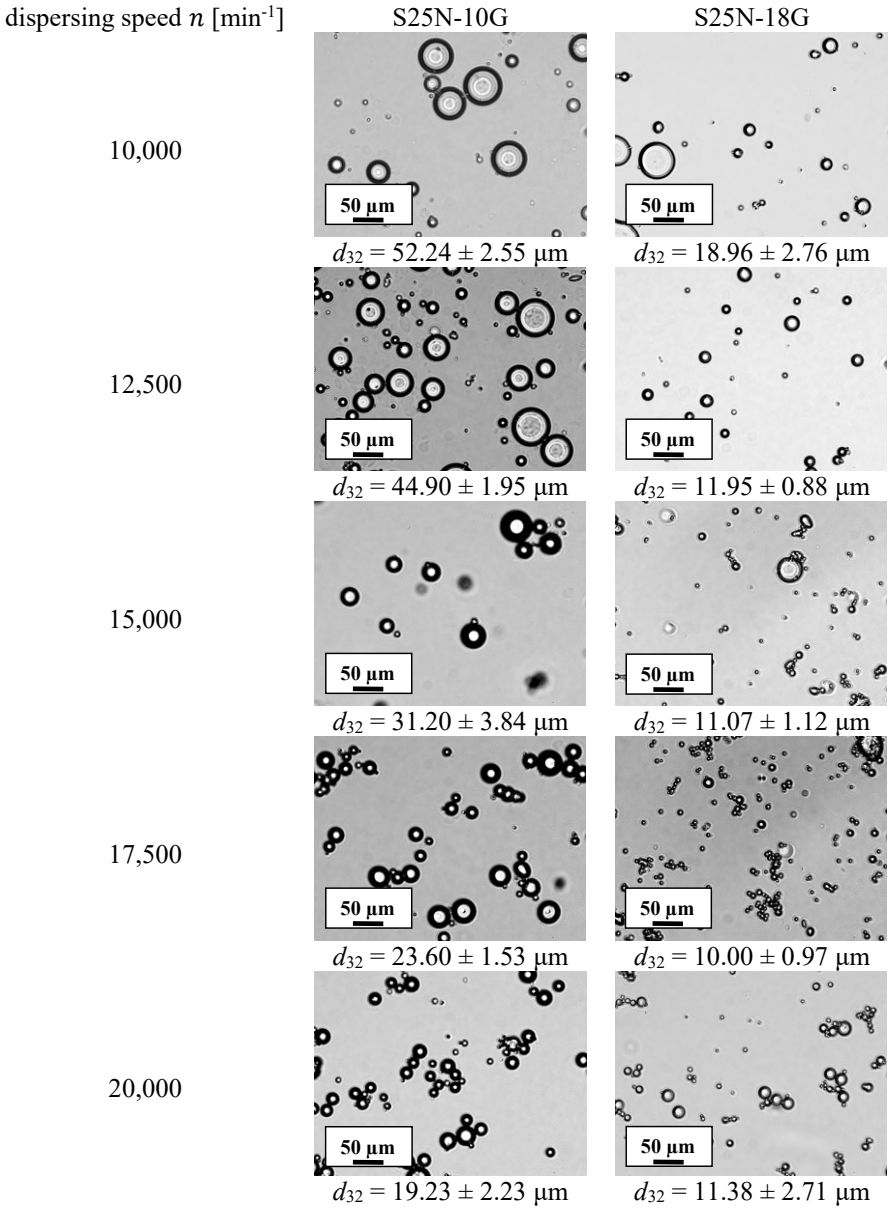

Figure 18. Optical microscopy images of "standard" w/o PEs prepared at different dispersing speeds (dispersing time of 2 min) for visualization of drop size distributions and corresponding Sauter mean diameters. Different dilutions led to different numbers of drops per picture. All experiments were conducted at least in triplicate. For the Sauter mean diameters, mean values and standard deviations are given. Images for 17,500 min^{-1} were adapted from [I].

In general, breakage of the dispersed phase into drops generates new interfacial area during a homogenization process. In the case of PEs, particles adsorb at the interface and thus might not only reduce coalescence rates but also influence breakage phenomena due to the rigid particle layer. Two factors determine the resulting drop size distribution of PEs [220]:

- the "interface generation capacity" – depending on the homogenization conditions and the dispersing device – when the particle mass fraction is sufficient to completely cover the interfacial area,

- the "coverage capacity" – depending on the particle type and concentration – when the particle mass fraction is too low to completely cover the freshly generated interfacial area and limited coalescence [12] occurs.

Comparable to surfactant stabilized systems [235] or dilute o/w dispersions [60], increasing dispersing speeds led to a steady decrease of the average drop size for the S25N-10G head. The "interface generation capacity" was the determining factor as the energy input was not sufficient to generate as much interfacial area as could be stabilized by the used particle concentration (cf. **Figure 18**, right column). In contrast, for the S25N-18G head, only an increase of the dispersing speed to 12,500 min^{-1} led to a significant decrease of the drop size. A limiting minimum Sauter mean diameter of ≈ 10 µm exists, which could not further be reduced by higher energy input for the investigated particle mass fraction here. The "coverage capacity" was crucial as with a higher particle mass fraction using the same dispersing conditions, smaller Sauter mean diameters were obtained (**Figure 19**). Since a quadrupling of the particle mass fraction did not result in a quadrupling of the stabilized interfacial area (factor of 2.8 ± 0.3 was calculated), excess silica particles must be present in the continuous phase.

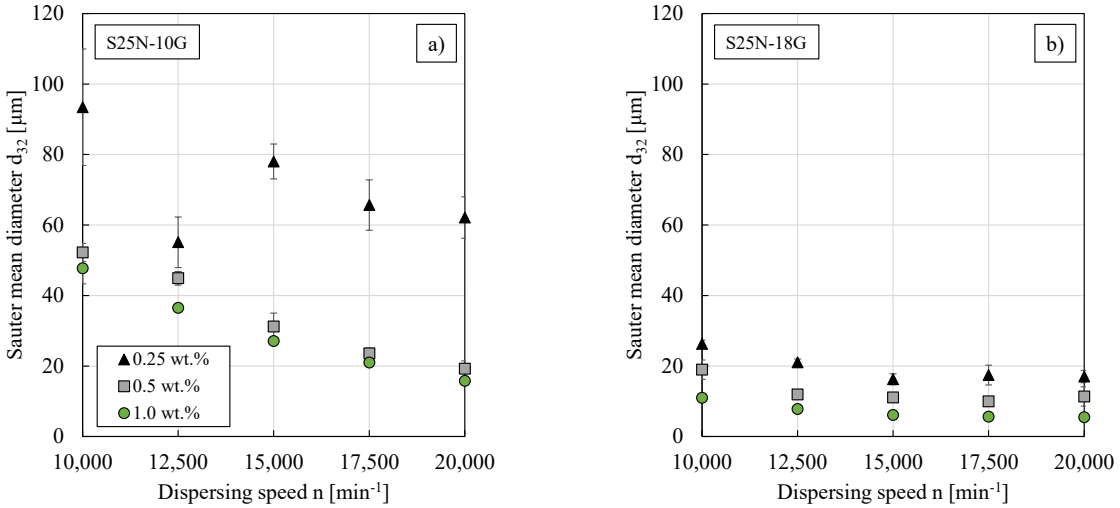

Figure 19. Sauter mean diameter against dispersing speed (dispersing time of 2 min) of PEs stabilized by different particle mass fractions of HDK®H20 and prepared with the two dispersing heads: **(a)** S25N-10G and **(b)** S25N-18G. All experiments were conducted at least in triplicate and mean values are shown. Error bars represent the standard deviation. Where not visible, error bars are smaller than the symbol size. Adapted from [I].

In [35], no significant influence of the dispersing speed (n = 8,000 - 24,000 min^{-1}, t = 2 min, UT T25 with an 18 mm head) on the average drop size ($d_{v,50}$ = 0.6 µm) was observed. A minimum drop diameter was also found for their system (water-in-toluene PEs, φ = 0.1, 2 wt.% HDK®H30). The difference in the average drop sizes can possibly be explained by the differences in the PE compositions. The authors in [35] used a higher particle mass fraction and a lower dispersed phase fraction compared to the PEs studied here (the impact of these parameters on the resulting drop size distribution was discussed in **Section 3.1.5**). Furthermore, another organic solvent differing in its physical properties compared to the one studied in this thesis was used (e.g., interfacial tension water/toluene: 37.6 mN m^{-1} (25 °C) [95]; water/1-dodecene: 50 mN m^{-1} [161]). In [43], o/w PEs stabilized by silica particles with different surface modifications were prepared using an IKA Magic Lab with the module UTC. A decrease of the median drop diameter from 10.2 to 3.6 µm was observed for dispersing speeds varied between 10,000 and 20,000 min^{-1}.

PE stability

The adsorption of particles to L/L interfaces and their effective stabilization mechanisms were described in **Sections 3.1.1** and **3.1.2**. The stability against coalescence of w/o PEs prepared using the S25N-10G head at three distinct dispersing speeds (t = 2 min) was investigated by comparison of drop size distributions of freshly prepared PEs and after a storage time of two or ten weeks, respectively.

Within the experimental error, no significant change in the cumulative number distributions or the corresponding Sauter mean diameters was observed (**Figure 20**), proving the long-term stability of PEs stabilized by 0.5 wt.% HDK®H20 particles.

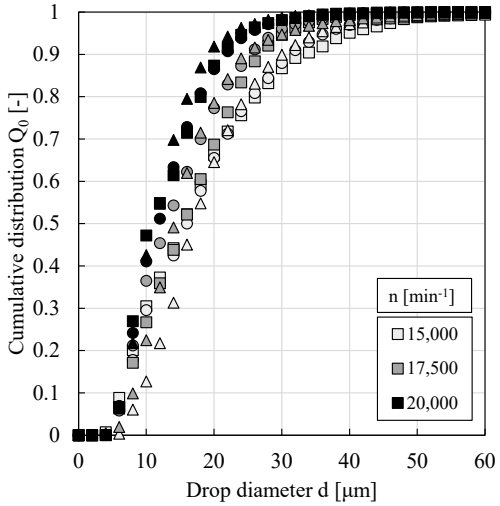

dispersing speed n [min^{-1}]	Sauter mean diameter d_{32} [µm]		
	fresh PE	after 2 weeks	after 10 weeks
	□	○	△
15,000	31.20 ± 3.84	29.04 ± 1.38	28.07 ± 2.03
17,500	23.60 ± 1.53	23.36 ± 3.60	24.49 ± 4.08
20,000	19.23 ± 2.23	19.64 ± 1.56	18.94 ± 0.77

Figure 20. Cumulative number distribution and Sauter mean diameter of "standard" w/o PEs prepared using the S25N-10G head at three dispersing speeds (dispersing time of 2 min). To check the PE stability, drop sizes of freshly prepared PEs and after a storage time of two and ten weeks, respectively, were compared. All experiments were conducted in triplicate and mean values are shown. For better graph clarity, error bars are not shown in the left diagram. For the Sauter mean diameters, standard deviations are given. Cumulative number distributions for fresh PEs and all Sauter mean diameters were adapted from [I].

As PEs of the same composition and dispersing conditions but prepared using the S25N-18G head showed even smaller Sauter mean diameters (cf. **Figure 18**), their long-term stability was assumed without any further experimental proof.

In literature, long-term stability against coalescence of both o/w as well as w/o PEs prepared with various particle types (e.g., starch granules, differently modified colloidal silica particles or latex particles) was reported. Sauter mean diameters, ranging from a few microns up to even 270 µm, did not change over storage times of several months or up to two years, e.g., [36, 43, 216].

Impact of dispersing time and PE volume

Increasing the dispersing time (at a fixed dispersing speed) and thus the energy input led to a decrease of the Sauter mean diameters (**Figure 21** a)). Different limiting dispersing times for the two UT heads existed above which no further reduction of the average drop diameter was obtained (S25N-10G: 3 min; S25N-18G: 2 min). From a certain dispersing time, either drop formation or breakage were no further promoted ("interface generation capacity" – S25N-10G) or partial coalescence occurred until the "coverage capacity" of the system was reached when the particle mass fraction was too small to stabilize a larger interfacial area (S25N-18G). Similar results were published for water/chlorobenzene dispersions prepared via mechanical agitation using a Rushton turbine [19], for surfactant stabilized emulsions prepared using an UT or ultrasound [4], or for o/w PEs prepared using an UT [40] or ultrasonication [113].

So far, 20 mL PE samples were prepared and investigated. The dispersing head S25N-18G is suited for the treatment of larger volumes (cf. **Table 6**). **Figure 21** b) shows that within the investigated range (up to 100 mL), no significant impact of the emulsion volume on the resulting Sauter mean diameter was observed. This is consistent with [134], where the average drop size of either 12, 120, 600 or 1,100 mL of w/o emulsions stabilized by polyvinyl alcohol and prepared using a rotor-stator system at a constant dispersing speed were compared. Since a maximum PE volume of 100 mL was sufficient for the experimental studies of this thesis (working volume of the stirred filtration cell, compare **Section 4.4**), larger volumes were not investigated. For the application described in **Chapter 1** in an industrial scale, an investigation on the preparation of larger PE volumes would be required. At the end of this section, the results will therefore be expressed in a manner which is independent of the explicit equipment and conditions.

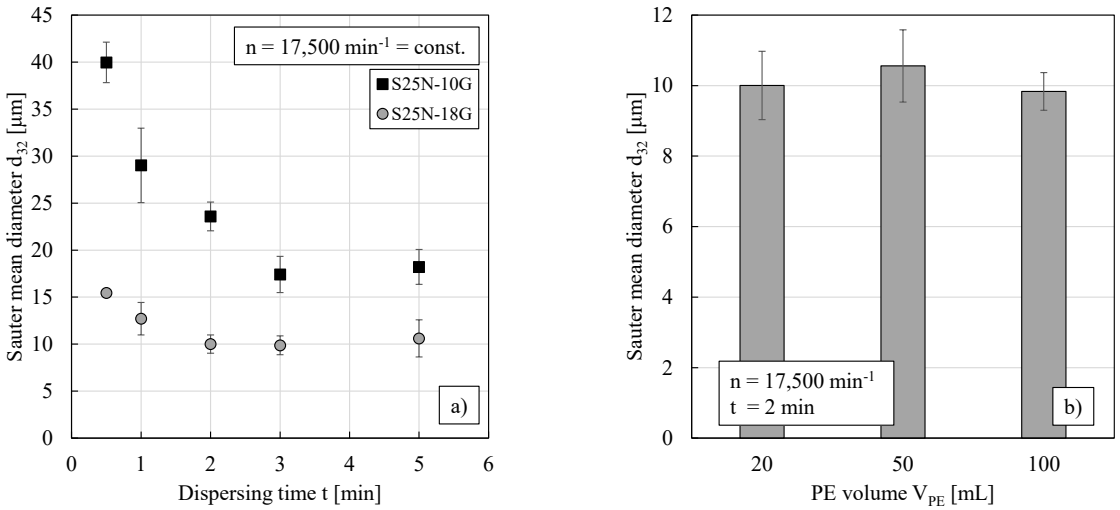

Figure 21. Sauter mean diameter against **(a)** dispersing time (for both dispersing heads) and **(b)** PE volume (for the S25N-18G head). All measurements were conducted in triplicate and mean values are shown. Error bars represent the standard deviation. Where not visible, error bars are smaller than the symbol size. Data for the S25N-18G head was adapted from [I].

Impact of nanoparticle pre-dispersion using a sonication bath

So far, the particles, the continuous and the dispersed phase were directly dispersed via an UT for PE preparation. In some literature studies, PEs were prepared by initially pre-dispersing the particles in the continuous phase (e.g., via ultrasonication) prior to the actual PE preparation (via rotor-stator systems), e.g., [28, 29, 77, 81, 141, 148]. Pre-dispersion via ultrasonication or a sonication bath can promote deagglomeration of particle clusters [15, 20, 109, 186, 188]. Particle powders incorporated into the continuous liquid phase can exist as primary particles, aggregates or agglomerates (cf. **Section 4.1**). While the more weakly-aggregated larger agglomerates (van-der-Waals forces and hydrogen bonds) can be broken into finer structures in a processing environment, aggregates are held together by strong sintering bridges and thus determine the resulting dispersion fineness [15, 29, 109].

The following procedure was investigated: the particles were dispersed in the organic phase 1-dodecene three times for 10 min each in a sonication bath (Bandelin Sonorex Super RK 1028 BH) with brief manual shaking of the sample tube between each run. Then, water was added, and the PE was prepared with the UT (S25N-10G or S25N-18G, respectively) at homogenization conditions of 17,500 min^{-1} / 2 min. Results for the S25N-10G head with homogenization conditions of 10,000 min^{-1} or 25,000 min^{-1} / 2 min, respectively, after particle pre-dispersion are shown in **Figure 63** (appendix).

Figure 22 shows that for PE preparation using the S25N-10G head, the cumulative distribution of number was shifted towards smaller drop sizes when the particles were pre-dispersed in the continuous phase. In contrast, the drop size distributions of PEs prepared with the S25N-18G head – within the experimental error – did not show any significant differences. At identical dispersing conditions, the power input was smaller for the S25N-10G head compared to the S25N-18G head. It is assumed that particle deagglomeration using the S25N-18G head only was possible while for the S25N-10G head (and the here applied homogenization conditions) a particle pre-dispersion in the continuous phase via a sonication bath prior to PE preparation was necessary to obtain smaller drop sizes.

In [29], the “dispersed particle method” (with particle pre-dispersion) and the “powder particle method” (without particle pre-dispersion) during PE preparation were compared. No significant impact on the resulting Sauter mean diameters was observed but the results obtained without particle pre-dispersion showed slightly higher scatter. As the authors used an IKA UT T25 equipped with an 18 mm head, these findings are consistent with the results shown in **Figure 22** b).

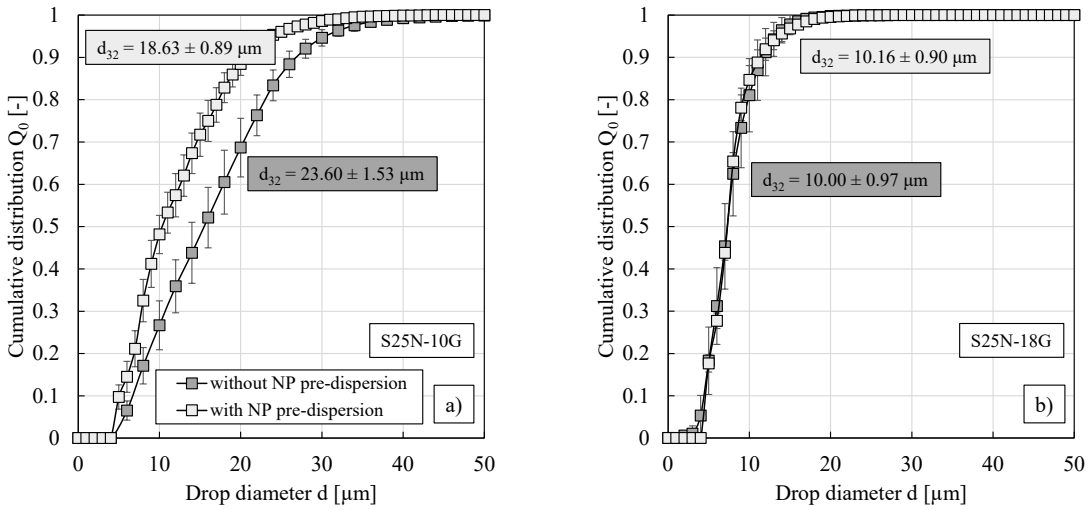

Figure 22. Cumulative number distribution against drop diameter without or with pre-dispersion of the silica particles in 1-dodecene in a sonication bath prior to PE preparation via the UT (20 mL, 17,500 min^{-1} / 2 min). **(a)** S25N-10G and **(b)** S25N-18G head. All experiments were conducted in triplicate and mean values are shown. Error bars represent the standard deviation. Where not visible, error bars are smaller than the symbol size.

Development of correlations

The previously shown results are summarized in **Figure 23**, where Sauter mean diameters were correlated via power laws with different parameters (X) in order to express the results in a manner which is independent of the explicit equipment and conditions (**Eq. (21)**).

$$d_{32} = A_{\mathrm{i}}(X)^{b_{\mathrm{i}}} \tag{21}$$

The energy density (calculated in two ways), energy dissipation rate and tip speed were chosen as these variables are often used to correlate drop sizes of different dispersing processes or as scaling parameters [44, 88, 260].

In **Figure 23** a), Sauter mean diameters were correlated with the energy density which was defined as the dissipated amount of energy per unit of emulsion volume and was calculated – according to [23] – using the experimentally detected rise of temperature (± 0.6 °C) during PE preparation (**Eq. (22)**).

$$\left(\frac{E}{V_{PE}}\right)_T = \left[\varphi\, \rho_{dP}\, c_{p,dP} + (1-\varphi)\, \rho_{cP}\, c_{p,cP}\right]\Delta T \tag{22}$$

A decrease of Sauter mean diameters with increasing energy densities was observed, even if the obtained results scattered a lot (exponent of -0.61 and coefficient of determination of 0.65; not all data points were considered for the power law since a minimum Sauter mean diameter of approximately 10 µm was obtained). Nevertheless, these first results were reasonable since typical energy densities were reported as 1 - 100 J cm^{-3} for w/o or o/w emulsions and different dispersing devices [23, 89, 111]. Detecting the temperature rise as a function of time and insulation of both, the sample tube and the dispersing device, might lead to more precise results [111, 155].

In **Figure 23** b), the power consumption in the rotor-stator system was correlated with the Reynolds (Re) and power (Po) number as known from stirred tanks [88, 89, 155, 187, 191, 250]. The power numbers for the dispersing heads S25N-10G and S25N-18G were unknown but were assumed to be constant in the turbulent flow regime. The Sauter mean diameters were correlated with an energy density normalized with the power number and half of the swept-out volume (subscript hso) of the dispersing tool (instead of the total PE volume) [60]. A decrease of Sauter mean diameters with increasing energy densities was observed with a little less scatter than in **Figure 23** a) (again, not all data points were considered for the power law since a minimum Sauter mean diameter of approximately 10 µm was obtained). The exponent was -0.47 with a coefficient of determination of 0.81. More details on the exact calculation of the energy density (cf. **Figure 23** a) and b)) can be found in publication [I].

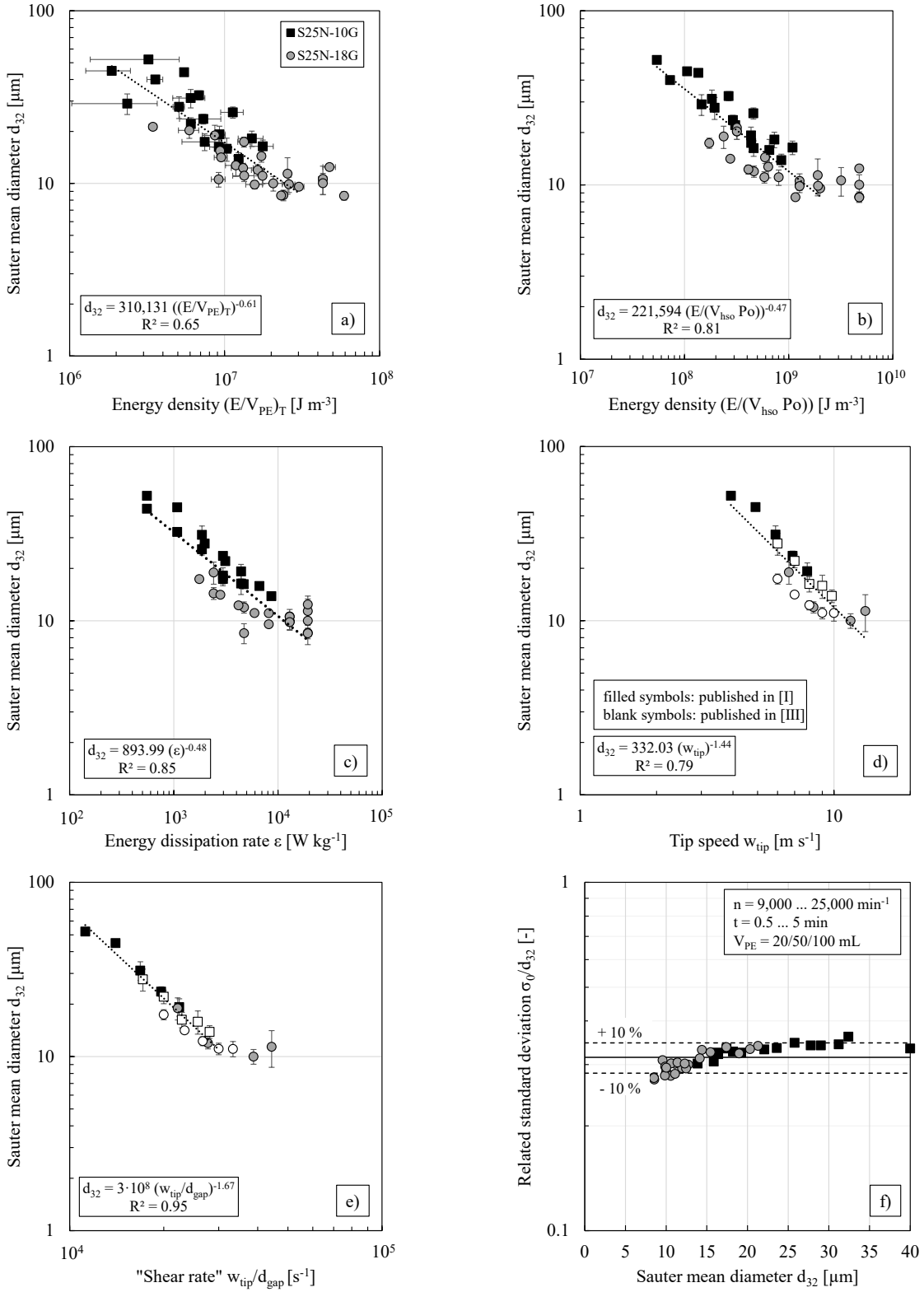

Figure 23. Sauter mean diameter against **(a, b)** energy density, **(c)** energy dissipation rate, **(d)** tip speed and **(e)** "shear rate". **(f)** Related standard deviation against Sauter mean diameter. All experiments were conducted at least in triplicate and mean values are shown. Error bars represent the standard deviation. Where not visible, error bars are smaller than the symbol size. Adapted from [I] and [III].

In **Figure 23** c), Sauter mean diameters are shown as a function of the energy dissipation rate. As the dispersing time is not included in its calculation, data points are stacked on top of one another. To minimize this, values for dispersing times < 2 min were not included (and again, not all data points were considered for the power law since a minimum Sauter mean diameter of approximately 10 µm was obtained). In

accordance with energy dissipation rates published in literature [160], values for both dispersing heads lie mostly within 1,000 - 10,000 W kg^{-1}. The exponent of -0.48 (coefficient of determination of 0.85) was slightly higher than exponents reported in literature (exponents between -1/3 (dissipation range) and -0.4 (inertial range) [245]).

In **Figure 23** d) and e), Sauter mean diameters were correlated with the tip speed or the "shear rate", respectively, with the latter being defined as the ratio of the tip speed and the respective gap width between rotor and stator. As the definition of these two parameters only contains the dispersing speed and the geometric dimensions of the rotor, no distinction between different PE volumes or homogenization times could be made. Therefore, only results obtained with a dispersing time of 2 min are presented (PE volume of 20 mL) to minimize stacking of data points on top of each other. In **Figure 23** d), the exponent was -1.44 with a coefficient of determination of 0.79. In literature, an exponent of -1.4 for surfactant dispersions prepared using an in-line Silverson rotor-stator mixer in multiple pass mode was reported [89]. For surfactant stabilized o/w emulsions prepared using a batch rotor-stator homogenizer, exponents between -0.77 and -1.09 were reported (depending on the dispersed phase ratio and the viscosity) [126]. Different results were published for PEs. For w/o PEs no significant impact of the rotor speed or tip speed, respectively, on the average drop diameter was observed in [35]. These differences from the behavior observed in this thesis might be explained by the different organic phase, particle properties and dispersed phase fractions and the resulting much smaller drop sizes in [35] ($d_{v,50}$ = 0.6 µm). In [64], a decrease of Sauter mean diameters with increasing dispersing speeds was reported for o/w PEs. The corresponding drop size distributions were multimodal with drop sizes ranging from 1 to 60 µm (comparable to the drop sizes shown in **Figure 23**). The peak drop diameters of the multimodal distributions as a function of homogenization speed were correlated using an exponential correlation but the data could just as well be described using power laws. For the different peaks, exponents between -1.02 and -1.54 could be obtained and were thus comparable to the exponent determined in this thesis.

According to [134], the drop size is mainly affected by the shear forces and therefore shear rates within the gap between the rotor and the stator (cf. **Figure 23** e)). The results for the two dispersing heads yielded a coherent course of the curve with an exponent of -1.67 and a much higher coefficient of determination of 0.95 (data points for tip speeds > 10 m s^{-1} were neglected since Sauter mean diameters stayed constant).

Figure 23 f) shows the related standard deviation as a function of the Sauter mean diameter. A constant value of 0.31 ± 10% was found which is consistent with values reported in literature for stirred model systems or w/o dispersions under the addition of surfactants or particles [44, 98, 117, 178].

To summarize, Sauter mean diameters – obtained for PEs of the same composition but prepared using various homogenization conditions and different dispersing heads – shown in **Figure 23** could be best correlated with the "shear rate" during emulsification. The developed correlations allow a direct comparison of different dispersing tools and the preparation of PEs with targeted average drop sizes.

5.1.3 Impact on rheological behavior

Knowledge about the rheological behavior is crucial for process design (e.g., fluid dynamic design of equipment and choice of operating conditions). Therefore, the impact of dispersing head, dispersing speed and particle pre-dispersion will be discussed in the following (20 mL; 0.5 wt.% HDK®H20; dispersing time of 2 min). The impact of particle concentration, dispersing time or PE volume on the dynamic viscosity is shown in **Figure 62**, **Figure 65** and **Figure 66** (appendix).

During the increase and decrease of shear rates, slight differences in the dynamic viscosity were only observed for PEs prepared using the S25N-10G head and shear rates < 10 s^{-1} (e.g., **Figure 61** (appendix)). For better graph clarity, only the increase of shear rate is shown in the following.

Impact of dispersing head and dispersing speed

All investigated PEs showed shear thinning rheological behavior and much higher dynamic viscosities compared with the pure organic solvent 1-dodecene. By way of example, **Figure 24** shows viscosity curves of PEs prepared at dispersing conditions of 17,500 min^{-1} / 2 min with the two dispersing heads. A local maximum of the dynamic viscosity (between shear rates of approximately 5 - 20 s^{-1}) indicating shear thickening behavior appeared for the small dispersing head (cf. **Figure 24**). The occurrence of such local maxima was also observed for other PEs, e.g., [94, 99], and disappeared for PEs with more pronounced shear thinning behavior. This is consistent with the results observed in **Figure 24**.

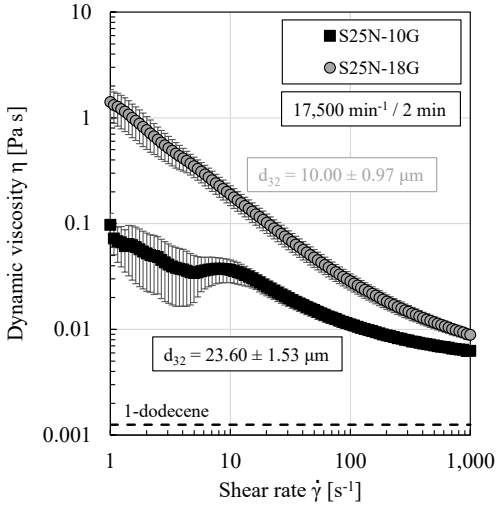

Figure 24. Emulsion viscosity against shear rate of "standard" w/o PEs prepared using the two different dispersing heads (17,500 min^{-1} / 2 min). All experiments were conducted in triplicate and mean values are shown. Error bars represent the standard deviation. Where not visible, error bars are smaller than the symbol size. Adapted from [I].

Fumed silica particles of irregular shape – such as HDK®H20 – can form highly interlocked agglomerates and often show the ability to form hydrogen bonds between silanol groups on the particle surface and are thus able to form three-dimensional network structures between adjacent drops or particles [94, 99]. Depending on the capability of the solvent to form hydrogen bonds, liquid molecules can build a solvation layer on the silica particle surface and thus avoid particle contact [173]. For weakly hydrogen bonding liquids, such as 1-dodecene [99], the interactions between the silanol groups of the particles dominate.

Shear thinning behavior of PEs was frequently reported in literature and is explained via a reorientation of drops within the bulk phase or a (partial) break-up of particle agglomerates or network structures under the applied shear [57, 112, 153, 157, 173].

The results of rotational measurements for PEs prepared using different dispersing speeds or tip speeds, respectively, are summarized in **Figure 25**. Dynamic viscosities at three distinct shear rates are plotted versus the "shear rate" during PE preparation (**Figure 25** a)) or versus the Sauter mean diameter (**Figure 25** b)). The shear thinning rheological behavior of all investigated PEs becomes clear, since an increase in applied shear rates (10, 100 or 1,000 s^{-1}) led to a decrease of the dynamic viscosity. The results in **Figure 25** a) and b) are reversed since the Sauter mean diameter depends on tip speed or "shear rate", respectively (cf. **Figure 23**).

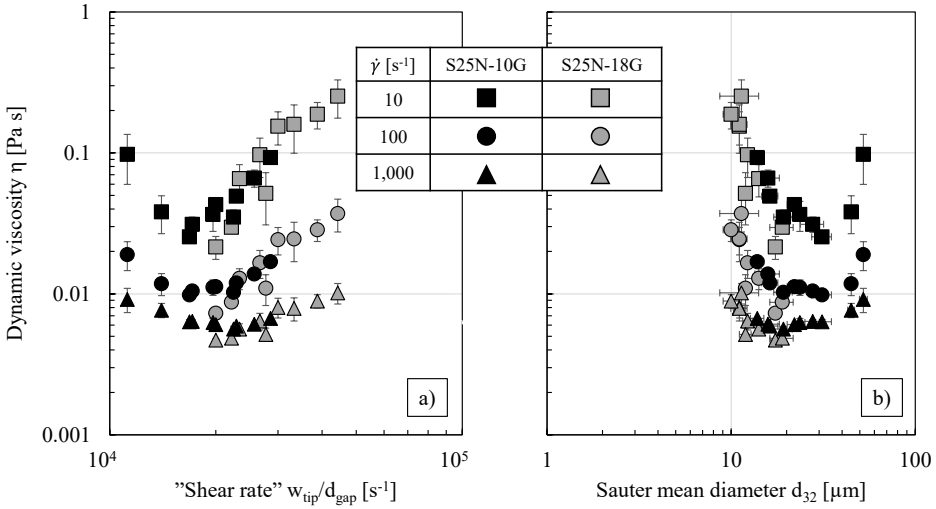

Figure 25. Emulsion viscosity at three distinct shear rates of "standard" w/o PEs prepared using various dispersing conditions of the S25N-10G and S25N-18G head against **(a)** "shear rate" or **(b)** Sauter mean diameter. All experiments were conducted at least in triplicate and mean values are shown. Error bars represent the standard deviation. Where not visible, error bars are smaller than the symbol size. Adapted from [I] and [III].

Despite some scatter, clear tendencies could be observed and the results for the two different dispersing heads overlapped resulting in a coherent course of the curve. For Sauter mean diameters between approximately 15 and 40 µm and a given applied shear rate, an almost constant (minimum) dynamic viscosity was observed. When the Sauter mean diameter exceeded or fell below this range, an increase of the dynamic viscosity was observed.

In literature, an increase of the dynamic viscosity and a more pronounced shear thinning rheological behavior with decreasing drop sizes is generally reported, e.g., [157, 181]. This was attributed to a decrease in polydispersity, increased hydrodynamic interactions between drops due to shorter distances and increased flocculation of smaller drops [157].

It was hypothesized that the dynamic viscosity of PEs depends on both, the average drop size as well as the amount of residual particles in the continuous phase. For emulsions of the same composition, bigger Sauter mean diameters (and consequently a smaller total interfacial area) lead to a higher amount of freely suspended particles which in turn can form a three-dimensional network. For the S25N-10G head, a decrease of the Sauter mean diameter reduced the amount of residual particles and thus – similar to the rheological behavior of nanoparticle/oil suspensions, e.g., [99] – smaller dynamic viscosities were observed. It was further assumed that at a certain drop size (corresponding to an optimum particle coverage), a shift from the "unbound silica nanoparticle amount" dominated regime to a "drop size" dominated regime occurred as an increase of the dynamic viscosity with increasing "shear rates" was observed. The applied particle mass fraction might now be too small to cover the whole interfacial area and drops might share particles. Drops would thus be attached to each other which could cause the increase in viscosity and lead to a strong network structure. For the S25N-18G head and "shear rates" larger than 30,000 s^{-1}, the minimum Sauter mean diameter of ≈ 10 µm was obtained and the increase of the dynamic viscosity was then less pronounced. The hypothesis is illustrated schematically in **Figure 26**.

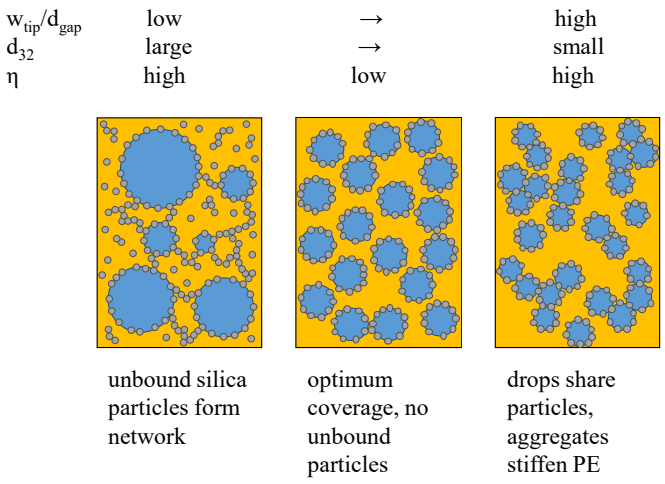

Figure 26. Schematic representation of the impact of the amount of residual particles and drop size distribution on the dynamic viscosity of PEs of otherwise the same composition. Clustering of drops due to network formation using the HDK®H20 particles can also be seen in **Figure 33** in **Section 5.2**.

By way of example, **Figure 27** shows the results of two amplitude sweep measurements as these are essential to conduct frequency sweep measurements at a constant deformation from the LVE area (cf. **Section 3.1.6)**. The LVE area (parallel course of G' and G'') is highlighted in **Figure 27**. A deformation of 0.1% was used for all subsequent frequency sweep measurements. First conclusions concerning the strength of the formed network structure can also be drawn from amplitude sweeps [122]: The intersection of the storage and loss modulus is an indicator for the break-up of the three-dimensional network structure. The PEs prepared using the S25N-18G head constituted a stronger network as the cross-over appeared at a higher deformation.

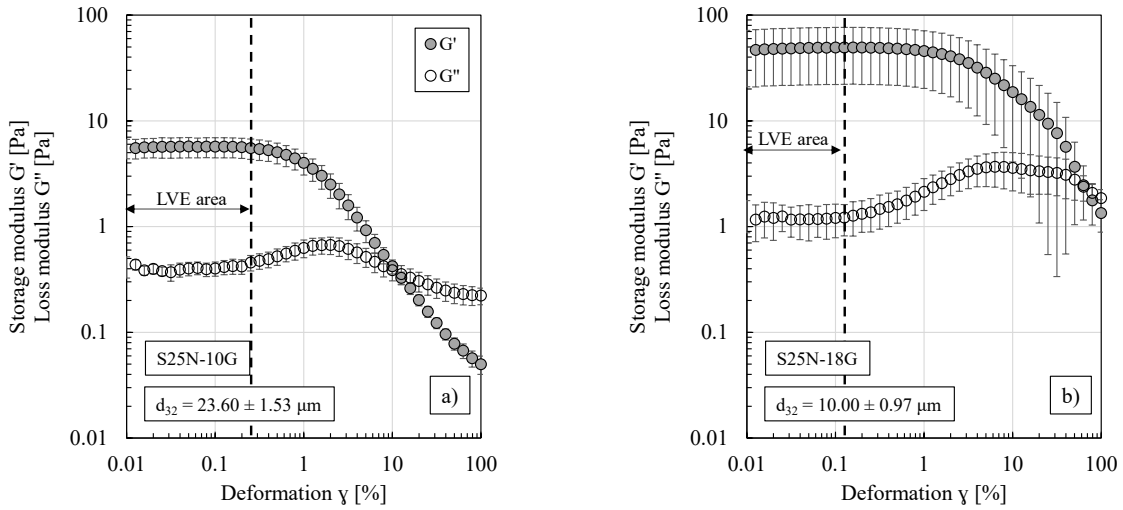

Figure 27. Exemplary amplitude sweeps of "standard" w/o PEs prepared using the two dispersing heads (17,500 min^{-1} / 2 min) to determine the LVE area at a fixed angular frequency of 10 rad s^{-1}. **(a)** S25N-10G and **(b)** S25N-18G head. All experiments were conducted in triplicate and mean values are shown. Error bars represent the standard deviation. Where not visible, error bars are smaller than the symbol size.

Figure 28 summarizes all results from oscillatory frequency sweep measurements. Storage and loss moduli at an angular frequency of 10 rad s^{-1} are plotted versus the "shear rate" (**Figure 28** a)) and the Sauter mean diameter (**Figure 28** b)). Storage moduli were always larger than loss moduli indicating the viscoelastic behavior of the PEs. The higher the storage and loss moduli, the stronger was the three-dimensional particle/drop network. The results support the above-mentioned hypothesis (of an "unbound silica nanoparticle amount" and "drop size" dominated regime, cf. **Figure 26**) as within a certain region of the "shear rate" a minimum in storage and loss moduli was observed.

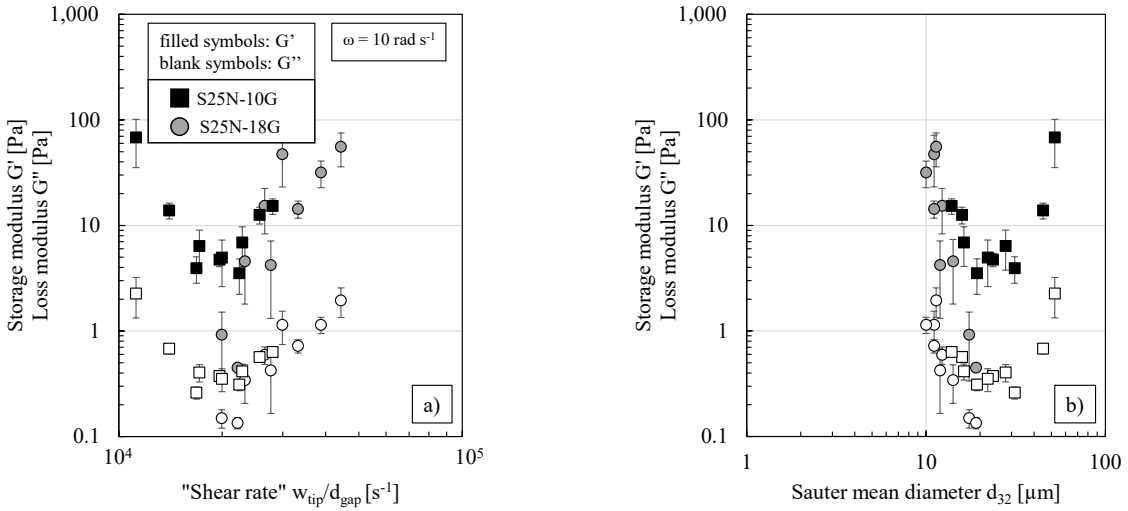

Figure 28. Storage and loss modulus of "standard" w/o PEs prepared using various dispersing conditions of the S25N-10G and S25N-18G head against **(a)** "shear rate" and **(b)** Sauter mean diameter. Experiments were performed at a deformation of 0.1%. All experiments were conducted at least in triplicate and mean values are shown. Error bars represent the standard deviation. Where not visible, error bars are smaller than the symbol size.

Impact of nanoparticle pre-dispersion using a sonication bath

The impact of particle pre-dispersion in the organic phase via a sonication bath prior to the actual PE preparation using the UT on the rheological behavior was investigated. From **Figure 29** a), one can conclude that – under the here applied UT settings (17,500 min^{-1} / 2 min) – a particle pre-dispersion in the continuous phase did not have a significant impact on the viscosity curves. Consistent with the previously shown results (cf. **Figure 24**), PEs prepared using the S25N-18G head showed larger dynamic viscosities.

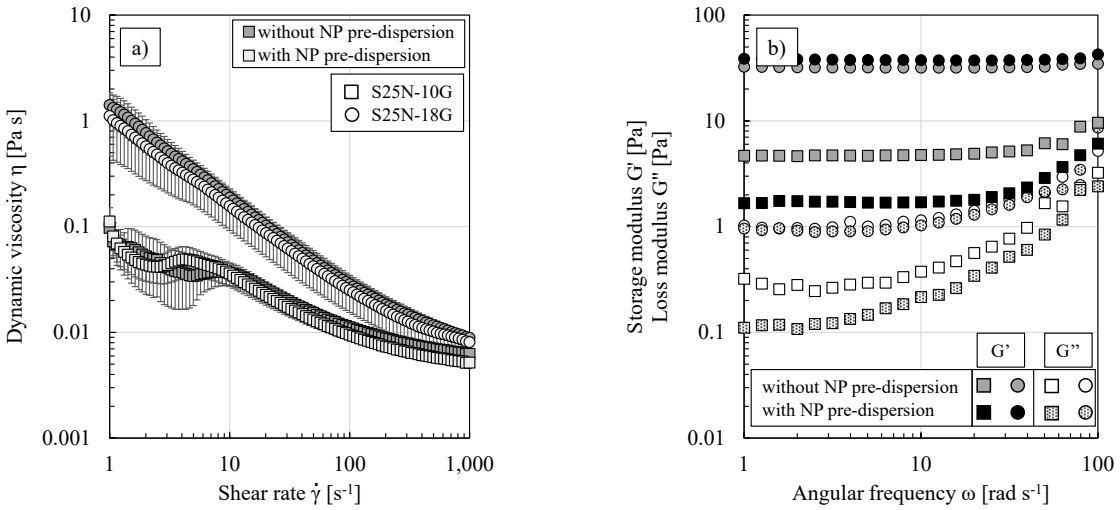

Figure 29. (a) Emulsion viscosity against shear rate and **(b)** frequency sweep measurements of "standard" w/o PEs prepared without or with silica pre-dispersion in 1-dodecene in a sonication bath prior to PE preparation using the UT (17,500 min^{-1} / 2 min) for the two dispersing heads. All experiments were conducted at least in triplicate and mean values are shown. Error bars in (a) represent the standard deviation. For better graph clarity, error bars are not shown in (b).

For the S25N-18G head, drop size distributions (cf. **Figure 22** b), reaching the minimum Sauter mean diameter of ≈ 10 µm), dynamic viscosities (cf. **Figure 29** a)) but also storage and loss moduli (cf. **Figure 29** b)) did not change when particles were pre-dispersed in the organic phase or not. The power input of this dispersing tool was high enough to promote particle cluster deagglomeration (cf. **Section 5.1.2**).

A significant impact of particle pre-dispersion on the storage and loss moduli was observed for PEs prepared using the S25N-10G head (cf. **Figure 29** b)). Despite the smaller obtained Sauter mean diameters, both moduli decreased when the particles were pre-dispersed in the continuous phase. Using the S25N-10G head only, the particles kept their fractal like structure and consequently provided several contact points and particle interlocking [112] leading to the formation of strong network structures. It is assumed that particle pre-dispersion using the sonication bath, destroyed (part of) the fractal particle agglomerates into smaller particle fractions. These were not too efficient in network formation and consequently lower storage and loss moduli were measured.

This is similar to findings reported in literature, where an impact of particle shape on PE stabilization and rheology was observed, e.g., [69, 112, 139]. It was reported that non-spherical particles with higher aspect ratios are more likely to form three-dimensional networks. The results presented in **Figure 64** (appendix) confirm this hypothesis (PEs prepared using the S25N-10G head at dispersing conditions of either 10,000 min^{-1} or 25,000 min^{-1} / 2 min, with or without particle pre-dispersion, respectively). Thus, when applying particle pre-dispersion prior to the actual PE preparation, the observed increase of the dynamic viscosity (cf. **Figure 25**) and the storage or loss modulus (cf. **Figure 28**) at very low ratios of tip speed and gap width might vanish. As the drop size distribution was barely affected (cf. **Figure 63** a) (appendix)), maybe not only the size of drops and the amount of residual particle traces, as proposed in our hypothesis schematically shown in **Figure 26**, might be relevant parameters but also the tendency of particles to interlock.

5.1.4 Impact on filtration behavior

The filtration performance of PEs prepared using different homogenization conditions will be discussed in the following. In all filtration experiments, a stirrer speed of 500 min^{-1} was applied within the stirred cell.

Impact of PE volume

In [199, 200], the same material system as used in this thesis was investigated. There, small amounts of PEs (16 g or 30 mL, respectively) were prepared and then diluted in the stirred cell to get a completely filled cell and to conduct pressure stepping experiments at constant phase ratio. Hence, the dispersed phase ratio during PE preparation did not correspond to that in the stirred cell. **Figure 30** shows the impact of PE

volume (during PE preparation) or the corresponding dispersed phase fraction within the stirred cell on the filtration behavior using two different membrane types. As shown in **Figure 21** b) and **Figure 66** (appendix), neither the drop size distribution nor the rheology changed when different PE volumes were prepared. The dilution of the PEs with the pure solvent in the stirred cell did not change the average drop size (as reported in [35]) but reduced the dynamic viscosity of the PEs (cf. **Figure 68** (appendix)).

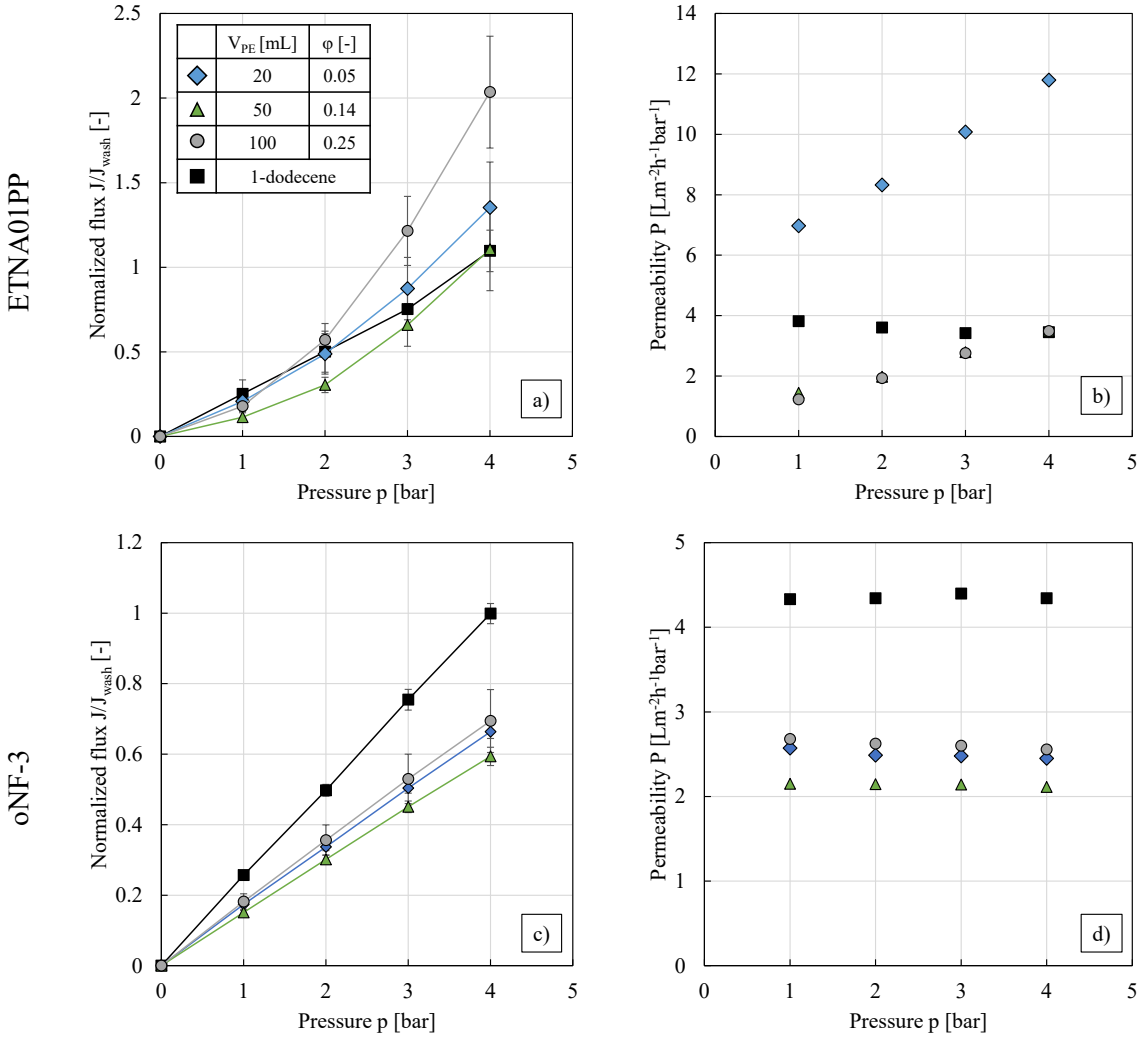

Figure 30. Influence of dispersed phase fraction on the filtration behavior of w/o PEs (17,500 min^{-1} / 2 min, S25N-18G) using the **(a, b)** ETNA01PP and **(c, d)** oNF-3 membrane. The indicated volumes refer to the PE volume during homogenization while the dispersed phase fractions correspond to those after dilution in the stirred cell to obtain a completely filled cell. **(a, c)** Normalized flux against pressure. All experiments were conducted in triplicate and mean values are shown. Error bars represent the standard deviation. Where not visible, error bars are smaller than the symbol size. Adapted from [I]. **(b, d)** Permeability (calculated from the average flux at each pressure step) against pressure.

For the UF membrane ETNA01PP, considerable differences in pure 1-dodecene fluxes during the pre-treatment occurred ($J_{wash}(p = 4\ bar) = 17.5 \pm 12.3\ L\ m^{-2}\ h^{-1}$, cf. **Figure 67** a) (appendix)). These might be explained by the non-homogeneity of the small membrane samples ($A_{eff} = 13.2\ cm^2$, cf. **Section 4.4**) [137]. To eliminate these strong deviations, the flux from the pressure stepping experiment was normalized with respect to the flux from the membrane pre-treatment. Even though the results obtained with the oNF-3 membrane showed much better reproducibility ($J_{wash}(p = 4\ bar) = 14.4 \pm 2.4\ L\ m^{-2}\ h^{-1}$, cf. **Figure 67** b) (appendix)), fluxes are also shown in the normalized manner for better comparability.

As stated in **Section 4.4.2**, the results presented in this thesis always represent the steady state fluxes received during pressure descent. Using the oNF-3 membrane, no hysteresis of flux between pressure increase and descent occurred, indicating the incompressibility of this membrane and the filter cake within the investigated pressure range. For the ETNA01PP membrane, fluxes during pressure descent were slightly smaller than those during pressure increase (data not shown). In all PE filtration experiments, particle and drop retention were 100%.

For the UF membrane (cf. **Figure 30** a)), within the experimental error, no distinct impact of the dispersed phase fraction on the filterability of w/o PEs could be observed. PE fluxes were (mostly) higher than the 1-dodecene flux and a disproportionate filtration behavior was observed (consistent with [199, 200]). **Figure 30** b) illustrates the increase in permeability with pressure for PEs.

A qualitatively different result was obtained with the oNF-3 membrane, where the permeability remained constant with pressure for 1-dodecene and slightly decreased for the PEs (cf. **Figure 30** c) and d)), and PE fluxes were significantly smaller than the pure solvent flux. Within the experimental error, also no significant impact of the PE volume on the filtration behavior could be observed, allowing the filtration of highly concentrated PEs without any loss in filtration performance.

Impact of Sauter mean diameter

The impact of the drop size distribution on the filtration behavior of w/o PEs was – due to the better reproducibility – only investigated for the oNF-3 membrane. Different dispersing speeds for the two dispersing heads were used to obtain PEs with a wide range of Sauter mean diameters. Results on the self-similarity and width of different drop size distributions are shown in **Figure 69** (appendix).

An increase in flux with the Sauter mean diameter squared – as one might expect from theoretical considerations (cf. **Eq. (11)**) – was not observed here (**Figure 31**). Within the experimental error no significant impact of the Sauter mean diameter on the flux was observed. The three measurement points deviating from this showed the largest error bars. **Eq. (11)** only applies under the following assumptions: constant filter cake porosity, constant dynamic viscosity of the permeating liquid, constant filter cake height and constant transmembrane pressure difference. For a constant particle mass fraction, bigger Sauter mean diameters mean a higher amount of freely suspended residual particles. The results for the rheological behavior obtained in **Section 5.1.3** showed that all investigated PEs form three-dimensional network structures. Hence, possibly freely suspended HDK®H20 particles are part of this network instead of accumulating on the membrane surface in the form of a dense filter cake.

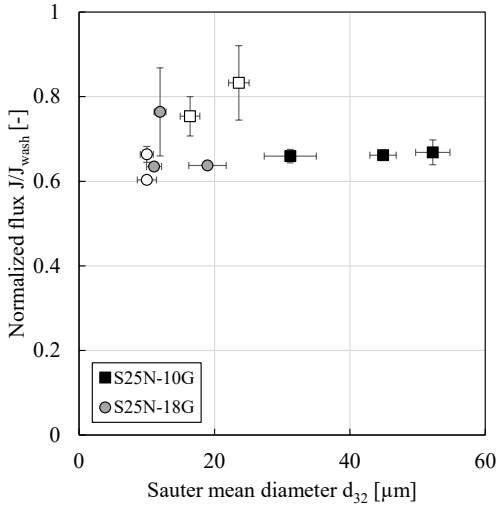

Figure 31. Normalized flux at a pressure of 4 bar against Sauter mean diameter of w/o PEs prepared with the two dispersing heads. 20 mL of PEs were prepared using various dispersing speeds. All experiments were conducted at least in duplicate and mean values are shown. Error bars represent the standard deviation. Where not visible, error bars are smaller than the symbol size. Blank symbols were adapted from [I].

In [199], a slight influence of the drop size distribution on flux was only observed for PEs with many larger drops. The authors also investigated water-in-1-dodecene emulsions stabilized by HDK®H20 particles but conducted their experiments using the ETNA01PP membrane. Therefore, their observed differences in flux might also result from the differences in membrane samples (cf. **Figure 67** a) (appendix)) instead of differences in the drop size distributions. For bioactive w/o PEs, no clear correlation between permeability and drop size could be found [96].

In collaboration with LUM GmbH, investigations of filter cake properties were performed. Four different PEs were investigated with regard to the packing density, sediment height and compressibility. The results – together with the corresponding Sauter mean diameters – are shown in **Figure 32**.

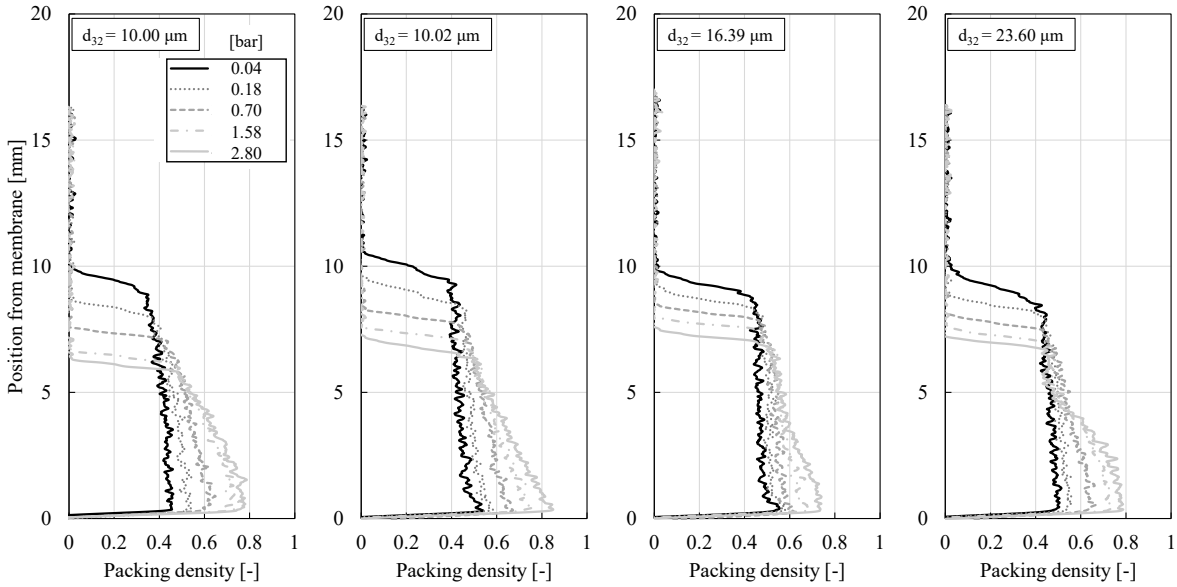

Figure 32. Packing density of four different w/o PEs prepared using different homogenization conditions and resulting in different Sauter mean diameters against the position from the membrane surface (bottom of the sample tube, respectively). All experiments were conducted in duplicate and mean values are shown. For better graph clarity, error bars are not shown.

The analytical centrifugation experiments were conducted using a LUMiSizer® and a LUMiReader X-Ray® at a constant dispersed phase fraction. The experimental procedure is described in more detail in, e.g., [123, 130]. During centrifugation, all drops participated in the sedimentation process and formed the filter cake. In contrast, in the stirred filtration cell, stirring caused a crossflow and thus led to an almost constant (much smaller) filter cake height (cf. **Section 3.2.1** and **4.4**) while all other drops were kept in motion and did not settle. Consequently, the operating conditions in the LUMiSizer® and the stirred filtration cell cannot be directly compared, but still give an important first insight into the properties of the sediment.

Within the LUMiSizer® different rotational speeds, and consequently different centrifugal forces or pressures, respectively, were applied. The transmembrane pressure in centrifugal filtration depends on the centrifugal rotation speed and the height of the sample column (for details, e.g., [128]). The sediment volume decreased with increasing pressures, indicating the presence of compressible particle network structures between adjacent drops. The tendency to compression was pronounced in the range of low pressures but decreased with higher applied pressures (comparable to those studied in the stirred filtration cell ≥ 1 bar). The resulting sediment height (6 - 7 mm) as well as the maximum packing density (≈ 0.8 at the bottom of the sample tube) at the highest applied pressure were – within the experimental error – very similar for the different w/o PEs. The packing density of a cubic close packing of 0.74 could be exceeded due to the polydispersity of the PEs or potential drop deformation. Further results on the relative sediment volume under different applied pressures are shown in **Figure 70** (appendix).

To summarize, the investigated PEs with different Sauter mean diameters or drop size distributions, respectively, showed very similar filter cake properties and hence no significant influence of the drop size distribution on flux was observed.

5.1.5 Conclusions

To apply PEs in, e.g., hydroformylation processes (cf. **Figure 1**), PE preparation can be used as a leverage to design PEs with tailored characteristics. In this section, the impact of homogenization conditions during PE preparation on characteristic emulsion properties as well as on their filtration behavior was systematically investigated for the first time. All emulsions were stable against coalescence for at least 10 weeks.

Suitable parameters for comparison of different dispersing tools were identified by harmonizing the preparation conditions in a manner which is independent of the explicit volume and equipment and correlations for, e.g., Sauter mean diameters and dispersion process characteristics were developed (cf.

Figure 23). Such correlations allow the preparation of PEs with tailored drop sizes suited for the desired application and allow better comparison of different studies but were not yet available for PEs. The "shear rate" during PE preparation – defined as the ratio of tip speed and the respective rotor-stator gap width – was suited best to correlate the obtained results (power law model with an exponent of -1.67 and a coefficient of determination of 0.95). For the S25N-10G head the "interface generation capacity" was the determining factor and a particle pre-dispersion in the continuous phase via a sonication bath was required to obtain smaller drop sizes. For the S25N-18G head, a limiting minimum Sauter mean diameter (depending on the used particle mass fraction and consequently the "coverage capacity"; approximately 10 µm for 0.5 wt.% HDK®H20 particles) existed which could not be reduced by further increase of the energy input. Since small drop sizes are required for a high interfacial area and high reaction rates, and the energy demand for PE preparation should be as low as possible, the following homogenization conditions were selected for all further studies on w/o PEs: S25N-18G, 17,500 min^{-1} / 2 min, no particle pre-dispersion via a sonication bath.

The dynamic viscosity of the PEs first decreased with increasing tip speeds, then passed through a plateau value and finally increased again. The dynamic viscosity was lowest for Sauter mean diameters between approximately 15 and 40 µm. The higher the shear rate applied in rheological measurements, the lower was the increase of the dynamic viscosity when this range of Sauter mean diameters was exceeded. It was hypothesized that freely suspended residual particles and their formed networks dominate at low tip speeds (large Sauter mean diameters) while a stiffening of the emulsion drops takes place at high tip speeds (small Sauter mean diameters). This hypothesis was supported by additional oscillatory measurements. For process design, the shear rates applied during mixing, pumping or filtration need to be estimated and compared with the findings presented in this section.

Two membranes – the ultrafiltration membrane ETNA01PP and the organic solvent nanofiltration membrane oNF-3 – were studied and a qualitatively different behavior was observed. The UF membrane showed a disproportionate increase of flux with pressure, while the oNF-3 membrane showed a constant permeability and significantly lower fluxes during PE filtration compared to the pure solvent flux. To explain the observed differences and membrane-particle-solvent interactions, the two membranes will be separately investigated and discussed in the following sections. No significant impact of drop size distribution or PE volume within the stirred cell on the filtration performance could be detected. This is beneficial for the application of PEs in catalytic L/L multiphase reactions, as it allows the filtration of concentrated PEs and an adjustment of the drop size distribution to meet the needs for the actual reaction step.

5.2 Pickering emulsion filtration using the ultrafiltration membrane ETNA01PP[2]

The feasibility of w/o PE filtration using the UF membrane ETNA01PP has been shown for the first time in 2016 [200]. So far, the impact of DSD [199, 200] (**Section 5.1.4**), organic solvent type [199] or dispersed phase fraction (**Section 5.1.4**) was investigated and in all cases an unexpected disproportionate increase of flux with pressure was observed. In all of the mentioned investigations, PEs were stabilized by HDK®H20 particles. A more fundamental investigation on the influence of particle type as well as on the interactions between membrane, solvent and particles is still missing. These interactions have to be considered and understood for a safe and robust process design.

5.2.1 Working program

The impact of different particle types on characteristic PE properties as well as on their filtration behavior was investigated. For selected experiments, nanoparticle/oil suspensions – as an extreme form of no dispersed aqueous phase fraction – were studied to get a better understanding of the interactions between the particles and the membrane without any additional interactions between emulsion drops.

1-dodecene was used as the organic phase. For suspensions and w/o PEs, 100 mL samples were prepared using the S25N-18G dispersing head at dispersing conditions of 17,500 min^{-1} / 2 min (cf. **Section 5.1**). w/o PEs were prepared at a volumetric dispersed phase fraction of 0.25. For o/w PEs, the following preparation procedure was used (according to [204]): 20,000 min^{-1} / 5 min (S25N-18G). **Table 11** summarizes the varied parameters. As the particle hydrophobicity determines the emulsion type (cf. **Section 3.1.1**), o/w PEs could only be stabilized by HDK®H20 or HNTs. The impact of particle concentration on the filterability of w/o PEs will be discussed for the oNF-3 membrane in **Section 5.3.3**. More detailed information about the different particle types was introduced in **Section 4.1**.

All suspensions were filtered without stirring to allow particle sedimentation onto the membrane surface with time and thus not to disturb the deposit layer. While this is obviously undesirable for practical applications, the influence of the different particle types on the shape of the filter cake should be investigated here. All PEs were filtered at a stirrer speed of 500 min^{-1}. If not stated otherwise, a new membrane sample was used for each experiment. Due to the considerable differences in pure 1-dodecene fluxes during the membrane pre-treatment (cf. **Figure 67** a) (appendix)), the filtration results will be presented in a normalized manner (flux from pressure stepping experiments divided by flux from membrane pre-treatment).

Table 11. Parameters used for the investigation of suspension and PE filtration using the UF membrane ETNA01PP.

particle type	particle mass fraction ξ* [wt.%]	investigated samples
HDK®H15	0.5	w/o PE
HDK®H18	0.5 / 1.0	suspension
HDK®H20	0.5 / 1.0	suspension, w/o PE, o/w PE
HDK®H30	0.5	w/o PE
HDK®H2000	0.5 / 1.0	suspension, w/o PE
HNT	0.5	o/w PE

* The higher particle mass fraction of 1.0 wt.% was only investigated for the nanoparticle/oil suspensions.

5.2.2 Properties of w/o PEs under variation of particle type

The characteristic properties of PEs stabilized by different particle types are presented first. Then, the results on the UF of PEs using the ETNA01PP membrane are discussed.

[2] The content of this section was partially published in [II] Kempin, M.V.; Stock, S.; von Klitzing, R.; Kraume, M.; Drews, A. (2020): *Influence of particle type and concentration on the ultrafiltration behavior of nanoparticle stabilized Pickering emulsions and suspensions.* Sep. Purif. Technol., 252, 117457, DOI: 10.1016/j.seppur.2020.117457.

5.2.2.1 Drop size distribution

Figure 33 shows microscopic images of w/o PEs stabilized by different particle types and their corresponding Sauter mean diameters. Drop size distributions were measured and compared before and after the filtration process to evaluate the stability of the PEs against the applied pressure and shear during the filtration. The corresponding cumulative distribution functions of number are shown in **Figure 71** (appendix). As PEs prepared with HDK®H18 particles under the here applied UT settings were not stable, no results are shown for this particle type.

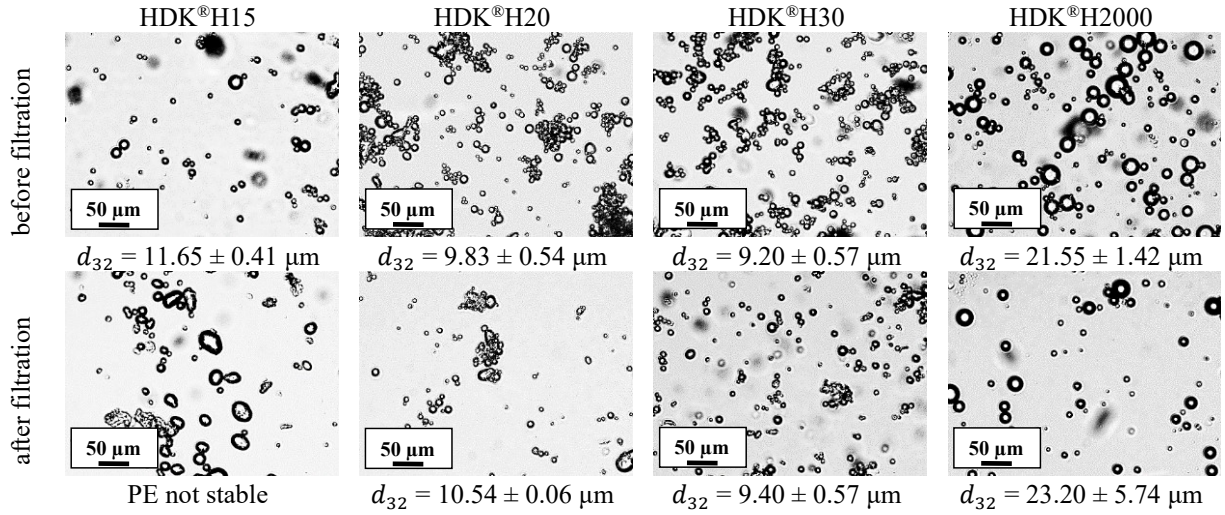

Figure 33. Optical microscopy images of "standard" w/o PEs prepared with different types of particles for visualization of drop size distributions and corresponding Sauter mean diameters. Different dilutions led to different numbers of drops per picture. All experiments were conducted at least in triplicate. For the Sauter mean diameters, mean values and standard deviations are given. **(Top)** Before filtration, **(bottom)** after filtration. Adapted from [II].

PEs stabilized by HDK®H15, H20 and H30 particles showed very similar Sauter mean diameters before the filtration (cf. **Figure 33** top) although they differ in their specific particle surface area while having the same residual silanol content of 50% (cf. **Table 4**). Clusters of drops were observed which can be explained via the stabilizing mechanism described in **Section 3.1.2** (particle bridging and/or the formation of three-dimensional network structures). For HDK®H20 and H30 particles, within the experimental error, Sauter mean diameters remained the same after the filtration indicating their great stability. HDK®H15 stabilized PEs showed larger and more deformed drops after the filtration and partial coalescence occurred. Results of contact angle and corresponding AFM measurements indicated that HDK®H15 particles form a different superstructure compared to HDK®H20 and H30 (indicated by the RMS roughness, cf. **Figure 15**). It can be assumed that the roughness of the drop surface after particle adsorption to the interface is significantly changed for HDK®H15 particles resulting in a lower stability under pressure and shear.

For HDK®H2000 particles, having a smaller residual silanol content and consequently fewer hydrogen bonds between particles can be built, no cluster formation but individually distributed emulsion drops and much bigger Sauter mean diameters were observed (cf. **Figure 33**). Within the experimental error, the Sauter mean diameters before and after the filtration stayed the same.

Binks et al. [29, 32] investigated the impact of particle hydrophobicity on PE type, drop size and transitional phase inversion. PEs were prepared with a dispersed phase fraction of 0.5 and a fixed concentration of silica particles of different hydrophobization (varied between 14 and 100% SiOH). They found smallest drop sizes for emulsions stabilized by particles of intermediate hydrophobicity with a residual silanol content corresponding to a contact angle of ≈ 90°. Particles with higher (o/w emulsions) or smaller (w/o emulsions) residual silanol contents yielded larger Sauter mean diameters. For o/w PEs prepared in a stirred tank, an increase of the particle contact angle from 48° to 93° decreased the Sauter mean diameter by approximately 20% [220]. Hohl et al. [99] found a strong impact of particle hydrophobicity on the resulting drop size distribution but not of the specific particle surface area. The results presented here concerning the impact of particle hydrophobicity and specific surface area are in line with findings reported in literature, e.g., [29, 99].

Concerning the impact of pressure or shear on w/o PE drop size distributions and stability, different results were reported. In [200], a slight increase in Sauter mean diameters (11 to 14 µm) and polydispersity

after the filtration was observed for HDK®H20 stabilized water-in-1-dodecene PEs prepared with an ultrasonic homogenizer. The impact of shear stress in a stirred tank under reaction conditions on the drop size distribution of the same PEs was investigated in [202]. The authors observed a slight increase of Sauter mean diameters compared to an unstirred system. In [96], PEs prepared with CPME as the continuous phase, spherical in-house silica particles and shear-sensitive enzymes in the aqueous phase as biocatalysts showed a decrease in Sauter mean diameters after the filtration. This might be attributed to the different material system, different homogenization conditions and the resulting larger Sauter mean diameters of freshly prepared PEs ($d_{32} \approx 30$ µm).

5.2.2.2 Rheological behavior

Before the filtration, PEs stabilized by HDK®H15, H20 and H30 particles did not only show very similar drop size distributions (cf. **Figure 33** top, **Figure 71** and **Figure 72** (appendix)) but the same shear thinning rheological behavior and similar storage and loss moduli (**Figure 34**). An explanation for the shear thinning behavior of PEs was already given in **Section 5.1.3**. The storage moduli exceeded the loss moduli indicating a viscoelastic gel-like behavior. Both moduli were almost independent of the angular frequency (for G'' for angular frequencies < 10 rad s^{-1}) indicating the emulsion stability within the investigated range (cf. **Section 3.1.6**). The different specific particle surface areas of HDK®H15, H20 and H30 did not significantly influence the rheological behavior of w/o PEs which is in line with [99].

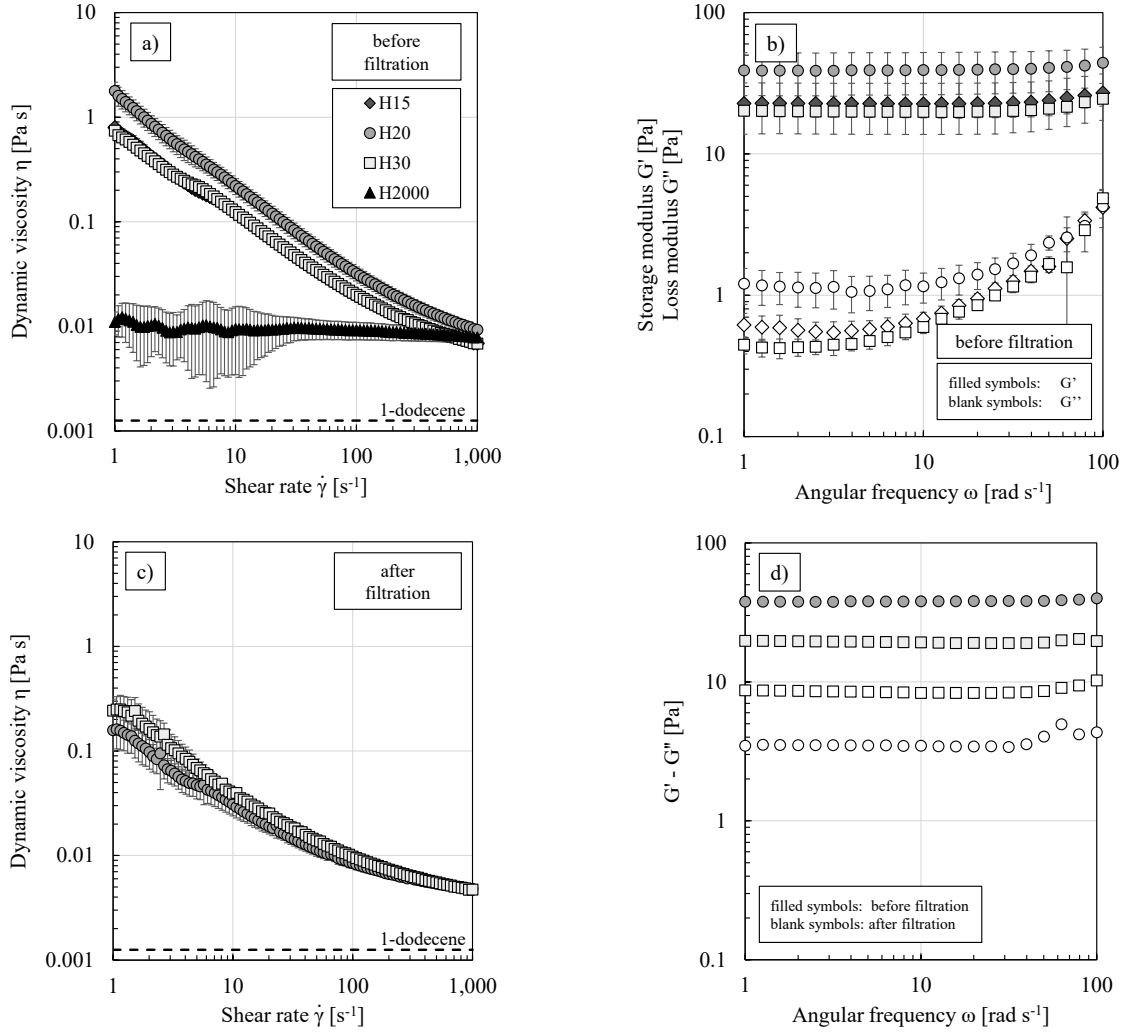

Figure 34. (a, c) Emulsion viscosity against shear rate and **(b, d)** frequency sweep measurements of "standard" w/o PEs prepared with different particle types before and after the filtration. All experiments were conducted at least in triplicate and mean values are shown. Error bars represent the standard deviation. Where not visible, error bars are smaller than the symbol size. Adapted from [II].

For PEs stabilized by HDK®H2000 particles, a Newtonian flow behavior was observed and no LVE area was determined in amplitude sweep measurements (cf. **Section 3.1.6**). Consequently, HDK®H2000 particles do not form three-dimensional network structures between residual particles and/or emulsion drops. This is in line with the microscopic images shown in **Figure 33**, where only for HDK®H2000 particles, drops were individually distributed within the bulk phase without cluster (network) formation. These results are consistent with [99], where more hydrophobic silica particles led to smaller dynamic viscosities and a less pronounced shear thinning behavior.

Not only the residual silanol content (particle hydrophobicity, respectively) but also the type of surface modification has an influence. In [22], it was reported that particles with a dimethylsiloxy surface modification (such as HDK®H15, H20 and H30, cf. **Table 4**) allow a stronger thickening effect than particles with a trimethylsiloxy surface modification (such as HDK®H2000, cf. **Table 4**). This is consistent with the information provided by the manufacturer, that all particles – except for HDK®H2000 – can be applied as thickeners [228, 230–232].

To the best of our knowledge, no experimental results regarding the rheological behavior of PEs after a filtration process have been published so far. As PEs stabilized by HDK®H15 particles did not remain stable throughout the filtration (cf. **Section 5.2.2.1**) and HDK®H2000 stabilized PEs showed strong fluctuations in the viscosity curves (cf. **Figure 73** (appendix); standard deviations for Sauter mean diameters after the filtration were also highest for this particle type), dynamic viscosities as well as differences between storage and loss moduli after the filtration are only shown for HDK®H20 and H30 particles in **Figure 34** c) and d).

The qualitative shear thinning behavior was maintained after the filtration, but dynamic viscosities were smaller. The change in the rheological behavior cannot be traced back to changes in the drop size distributions, as these remained the same for the two particle types (cf. **Figure 33** and **Figure 71** (appendix)). From constant drop size distributions one can assume that also the amount of residual particles remained the same, leaving the particle and droplet clusters as the only possible explanation.

A deeper understanding is possible when looking at the results of the frequency tests. For both particle types, the difference ($G' - G''$) decreased after the filtration indicating a (partial) break-up of the three-dimensional network structures. As this decrease was more pronounced for the HDK®H20 particles, it can be assumed that PEs stabilized by HDK®H30 particles are more stable against the applied shear and pressure during the filtration.

Furthermore, rotational measurements on the structure reconstruction after shear stress were carried out via a time-dependent shear rate profile. The sample was first exposed to a very low shear rate to simulate the resting behavior, then to a high shear rate to simulate the structure degradation and finally to the same low shear rate as from the first section to simulate the structure reconstruction [149]. The results for the different w/o PEs are shown in **Figure 35**.

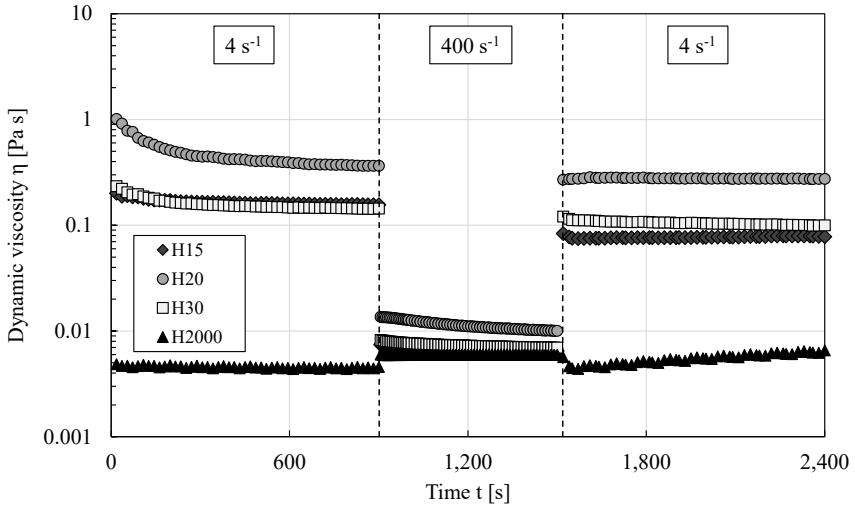

Figure 35. Emulsion viscosity as a function of time of "standard" w/o PEs stabilized by different particle types. A shear rate profile was applied to simulate the rheological behavior at rest, structure degradation and structure reconstruction. All experiments were repeated in triplicate and mean values are shown. For better graph clarity, error bars are not shown.

As PEs stabilized by HDK®H2000 particles showed a Newtonian flow behavior, the change of shear rates does not significantly influence the dynamic viscosity. For emulsions stabilized by particle types with gelling properties, the high shear rate led to a significant decrease of the dynamic viscosity indicating the (partial) break-up of the network structures. Reducing the shear rate to a low value in the third section led to an almost instantaneous increase of the dynamic viscosity. The absolute value of the dynamic viscosity was lower than in the first section for all emulsions. The percentage regeneration for HDK®H20, H30 and H15 was approximately 75%, 70% and 50%, respectively. This supports the other observations made that HDK®H15 stabilized PEs show the lowest stability against external forces.

5.2.3 Ultrafiltration of w/o PEs

Filtration of nanoparticle/oil suspensions

As an extreme form of no dispersed phase fraction, nanoparticle/oil suspensions were filtered to identify particle-membrane interactions without any additional interactions between emulsion drops. In order not to disturb the deposition of particles onto the membrane surface (superimposition of sedimentation, applied pressure and drag created by the flux), all suspension filtrations were conducted without stirring. HDK®H20 was selected representatively from the group of HDK®H15, H20 and H30 due to the largest data base (preliminary works, e.g., [99, 199, 200, 202]). Suspensions of more hydrophobic HDK®H18 and H2000 particles were also investigated. Since HDK®H18 particles did not successfully stabilize w/o PEs, the experimental results for these suspensions are shown in the appendix (cf. **Figure 74**). The dependency of the normalized flux on pressure for HDK®H20 and H2000 suspensions using a particle mass fraction of either 0.5 or 1.0 wt.%, respectively, is shown in **Figure 36**.

Against expectations, suspensions with HDK®H20 particles yielded higher fluxes than pure 1-dodecene (**Figure 36** a)). In contrast to previous PE filtrations (cf. [199, 200] and **Section 5.1.4**), within the experimental error a linear increase of flux with pressure was observed (except for the lower particle mass fraction).

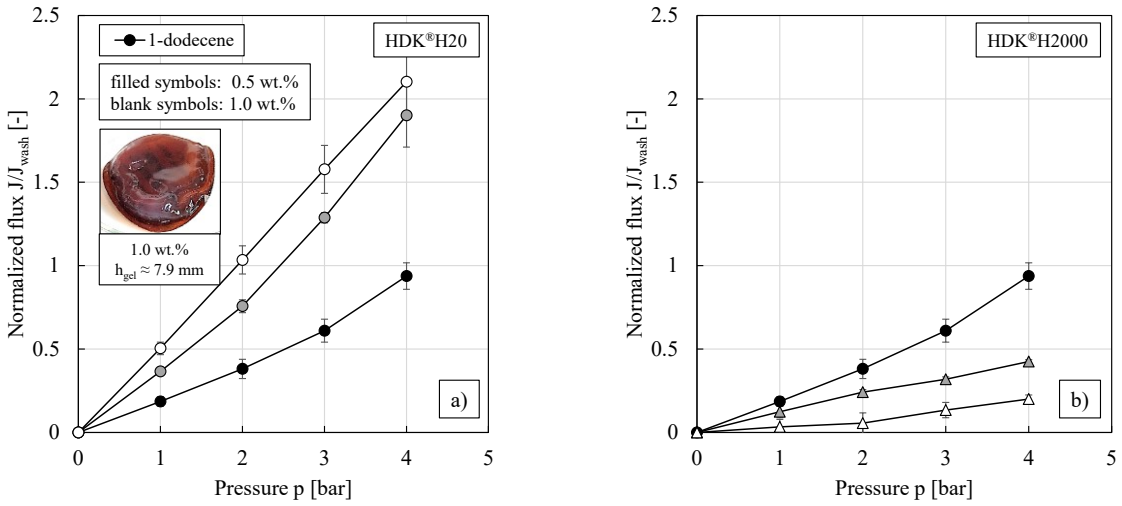

Figure 36. Normalized flux against pressure of suspensions using different particle mass fractions and different particle types: **(a)** HDK®H20 and **(b)** HDK®H2000. All filtration experiments were conducted in triplicate and mean values are shown. Error bars represent the standard deviation. Where not visible, error bars are smaller than the symbol size. Adapted from [II].

By way of example, the inset in **Figure 36** a) shows the several millimeter thick gel layer formed on the membrane surface after the filtration of a 1.0 wt.% suspension. The gel layer height increased with increasing particle mass fraction (measured at different points of the membrane surface using a caliper gauge; 5.7 ± 0.8 mm for 0.5 wt.% and 7.9 ± 0.9 mm for 1.0 wt.% suspensions, respectively). The porosity ε of the gel layer was calculated using the volumes V of the gel and the particles (expressed via the effective membrane area A_{eff} and the gel layer height h_{gel} or the particle mass m_{p} and density ρ_p, respectively) (**Eq. (23)**) and was found to be larger than 99%. Thus, the gel is highly permeable for the pure organic solvent.

$$\varepsilon_{\mathrm{gel}} = \frac{V_{\mathrm{gel}} - V_{\mathrm{p}}}{V_{\mathrm{gel}}} = \frac{A_{\mathrm{eff}} h_{\mathrm{gel}} - \frac{m_{\mathrm{p}}}{\rho_{\mathrm{p}}}}{A_{\mathrm{eff}} h_{\mathrm{gel}}} \quad \textbf{(23)}$$

A completely different behavior was observed when suspensions with HDK®H2000 particles were filtered. As expected from theory, these particles deposited on the membrane surface, formed a (dense) filter cake and increased the overall filtration resistance (cf. **Eq. (13)**). Compared to the pure solvent flux, these suspensions showed decreasing flux levels with increasing particle mass fraction (cf. **Figure 36** b)) and no gel layer formation on the membrane surface was observed.

To better interpret the different results depending on the particle type, additional contact angle measurements of water or 1-dodecene drops on fresh and used membranes were performed (**Figure 37**). A more detailed description of the experimental procedure is described in [II]. A 1-dodecene drop showed a contact angle of approximately 20° on a fresh ETNA01PP membrane. A quantitative determination of 1-dodecene contact angles on used membranes (after silica particle contact) was impossible as the liquid was sucked immediately into the membrane. These results show that the particles changed the membrane wettability, turning it more hydrophobic. This effect seemed to be even more pronounced for HDK®H20 compared to HDK®H2000 (**Figure 37** bottom). For the HDK®H20 particles, the formation of a porous gel layer together with the increase in membrane wettability caused a significant increase in flux compared to the pure solvent 1-dodecene. In contrast, for HDK®H2000 particles the change in membrane wettability was exceeded by the formation of the filter cake and thus a decrease in flux compared to the pure solvent was observed. Considering the differences in the particles tamped densities, these results are plausible since HDK®H2000 particles can be much more densely packed (cf. **Table 4**, 40 g L^{-1} for HDK®H20 and 100 - 250 g L^{-1} for HDK®H2000, respectively).

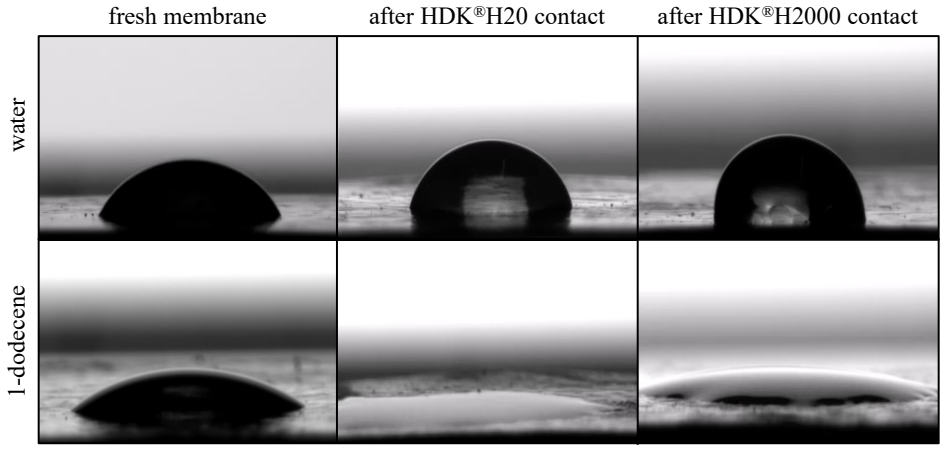

Figure 37. Images of **(top)** water or **(bottom)** 1-dodecene drops on different ETNA01PP membrane samples. **(Left)** fresh membrane, **(middle)** after filtration of a HDK®H20 suspension and **(right)** after filtration of a HDK®H2000 suspension. Adapted from [II].

Among others, a change of wettability of different solid surfaces after particle deposition was reported in [125, 140, 223, 254]. Many publications about the modification (e.g., hydrophilicity/ hydrophobicity) of membranes in order to reduce fouling and to enhance the permeability and the rejection were published in literature (e.g., [110]). This intentional modification of membranes with nanoparticles – either via the incorporation of particles into the membrane structure or via self-assembly – was reported to improve the membrane performance [16, 17, 53, 124, 127, 132]. In [219], similar findings were reported for the adsorption of different surfactants onto membrane surfaces. Thus, the qualitative enhancement of flux after silica particle contact observed here is plausible.

To further test the hypothesis of an increased membrane wettability for 1-dodecene, by way of example, pure solvent fluxes (at a pressure of 4 bar) through a single membrane sample before and after the filtration of 1.0 wt.% HDK®H20 suspensions were compared. The experiments were conducted in duplicate with relatively high standard deviations which can be explained by different amounts of particle traces on the membrane surface after the careful removal of the gel layer as well as the inherently strong deviations in different membrane samples (cf. **Figure 67** a) (appendix)). The pure solvent flux increased from approximately 9 L m^{-2} h^{-1} (fresh membrane) to 120 L m^{-2} h^{-1} (used membrane after suspension filtration). As this increase in flux was significantly higher than the increase during the filtration of the

suspension (cf. **Figure 36** a)), the gel layer contributes to the filtration resistance to some extent (despite its high porosity).

Filtration of w/o Pickering emulsions

Filtration results of w/o PEs stabilized by different silica particles are shown in **Figure 38**. For all emulsions, a disproportionate increase of flux with pressure was observed (even for HDK®H2000 where – due to flatter curves – the deviation from linearity was less obvious). Hence, the unexpected filtration behavior using the ETNA01PP membrane is not restricted to HDK®H20 particles. Comparable to the results of suspension filtrations, HDK®H2000 stabilized PEs showed lower flux levels than the pure solvent while HDK®H15, H20 and H30 stabilized PEs showed an increase in flux (cf. **Figure 36** and **Figure 38**).

The latter three particle types showed a shear thinning and viscoelastic gel-like rheological behavior (cf. **Section 5.2.2.2**), and hence the ability to form network structures between adjacent particles and emulsion drops. Even if the number of possibly freely suspended particles in the continuous phase increases throughout the filtration due to a partial break-up of these network structures (cf. **Figure 34**), these do not significantly add to the filtration resistance as shown in the filtration of nanoparticle/oil suspensions (cf. **Figure 36** a)). Highest flux levels were obtained for HDK®H30 PEs which showed the highest stability throughout the filtration process (cf. **Figure 34** d)).

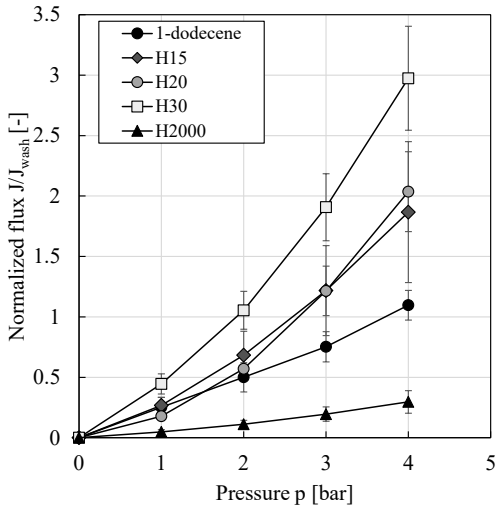

Figure 38. Normalized flux against pressure of "standard" PEs stabilized by different particle types. All filtration experiments were conducted in triplicate and mean values are shown. Error bars represent the standard deviation. Adapted from [II].

Sauter mean diameters for HDK®H2000 stabilized PEs were largest among the investigated particle types (cf. **Section 5.2.2.1**). One might expect higher fluxes due to higher hydraulic diameters (cf. **Eq. (11)**). Assuming a similar surface coverage, larger Sauter mean diameters for the same particle mass fraction mean a higher amount of freely suspended residual particles in the continuous phase. Particles without the ability to form network structures, as shown for the HDK®H2000 particles in **Section 5.2.2.2**, form a dense filter cake and/or settle in the voids between emulsion drops increasing the filtration resistance. This seems to outweigh the impact of the larger Sauter mean diameters and consequently led to a flux decline (cf. **Figure 38**).

These findings are consistent with [95] where highest flux levels were found for water-in-CPME PEs stabilized by fractal-like silica particles with gelling properties, intermediate flux levels for fractal-like particles without gelling properties and lowest flux levels for spherical in-house silica particles (PES ultrafiltration membrane with a MWCO of 10 kDa).

Impact of membrane pre-treatment

The membrane pre-treatment plays an important role as the membrane performance – both, permeability and rejection, respectively – can be significantly influenced by membrane-solvent interactions [151, 175, 184] (cf. **Section 4.4.1)**. Especially commercially available polymeric UF membranes are often designed for aqueous applications [59], such as the ETNA01PP membrane used here [8, 204], and a suitable membrane pre-treatment is inevitable to use these membranes in non-aqueous systems. Regardless of the membrane type (e.g., UF or OSN membrane), in non-aqueous systems the membrane pre-treatment should

be performed using an organic solvent. While an appropriate membrane pre-treatment is necessary to remove potential residues from the manufacturing process, further impacts of organic solvents on the filtration properties exist. Due to the exposure to organic solvents, a reorganization of the membrane material and a change of the polymeric membrane structure was observed [50, 59, 84]. These structural changes caused a change of the membrane surface hydrophobicity [50, 59, 83, 175]. Membrane swelling [184] or a change in pore size distribution [50, 83] – both affecting the membrane performance – are also possible. Furthermore, the membrane pre-treatment might prevent pore collapse during the filtration of organic solvents and allows the solvent to penetrate into and to wet all pores [107, 162, 175]. Different pre-treatment solvents and times were proposed [162, 175]. In literature, three different pre-treatment procedures are often described [59]:

1. Immersion of the membrane into the pure organic solvent.
2. Conditioning of the membrane with a gradual series of solvents with different polarities.
3. Flushing of the membrane with the pure organic solvent.

The procedures of the membrane pre-treatment used in this thesis were described in detail in **Section 4.4.1**. Typically, the normal pre-treatment was used (combination of pre-treatment procedures 1 and 3, adapted from [199]). **Figure 39** shows filtration results of pure 1-dodecene, suspensions and w/o PEs (stabilized by HDK®H20) after the normal pre-treatment in comparison to the specialized membrane pre-treatment (combination of pre-treatment procedures 2 and 3).

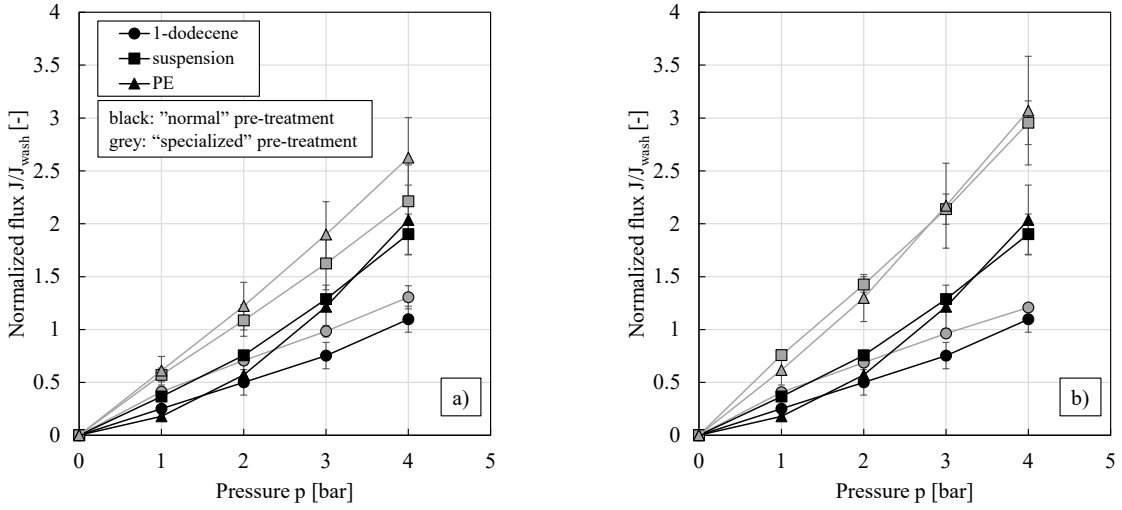

Figure 39. Normalized flux against pressure for filtration of pure 1-dodecene, nanoparticle/oil suspensions and "standard" w/o PEs after different membrane pre-treatment procedures. Specialized pre-treatment: **(a)** Immersion of membrane samples in water, isopropanol/1-dodecene, 1-dodecene. **(b)** Immersion of membrane samples in water, ethanol/1-dodecene, 1-dodecene. All experiments were conducted at least in duplicate and mean values are shown. Error bars represent the standard deviation. Where not visible, error bars are smaller than the symbol size. Data for PEs was adapted from [II].

In all cases fluxes were higher after the specialized membrane pre-treatment, where the membrane pores were first wetted with the pure polar phase, followed by a replacement of this internal aqueous phase with a mixture of solvents of decreasing polarities and finally pure 1-dodecene. This seems to have opened up further pores. Furthermore, a linear dependency between flux and pressure was now observed and the unexpected disproportionate filtration behavior for PEs was eliminated.

5.2.4 Ultrafiltration of o/w PEs

Results of filtration as well as characterization experiments for o/w PEs stabilized by either 0.5 wt.% HDK®H20 or HNTs, respectively, are shown in **Figure 40**.

o/w PEs showed a qualitatively and quantitatively different filtration behavior compared to w/o PEs (cf. **Figure 40** a) and **Figure 38**). No disproportionate increase in flux was observed and the PE fluxes were – within the experimental error – similar to the pure water flux. The average water flux from the (normal) membrane pre-treatment was $J_{\mathrm{wash}}(p = 4\ \mathrm{bar}) = 97.6 \pm 14.6\ \mathrm{L\ m^{-2}\ h^{-1}}$. In contrast to the filtration of w/o PEs using the same membrane ETNA01PP and in the case of HDK®H20 the same particle type, no

significant impact of particle covered oil drops in water or freely suspended particle traces was observed. In the case of HDK®H20, potentially residual particles are assumed to be present in the oil drops and hence particle contact with the membrane surface and a change in membrane wettability is assumed to be small. As a stirrer speed of 500 min^{-1} was applied in all PE filtration experiments and as oil drops rather tend to cream due to the density difference, filter cake formation is assumed to be small and therefore no influence on flux was observed. In [204], concentration experiments of o/w PEs stabilized by 0.5 wt.% HNTs at a pressure of 2.5 bar showed that the emulsions can be concentrated up to 90% (vol.) dispersed phase fraction.

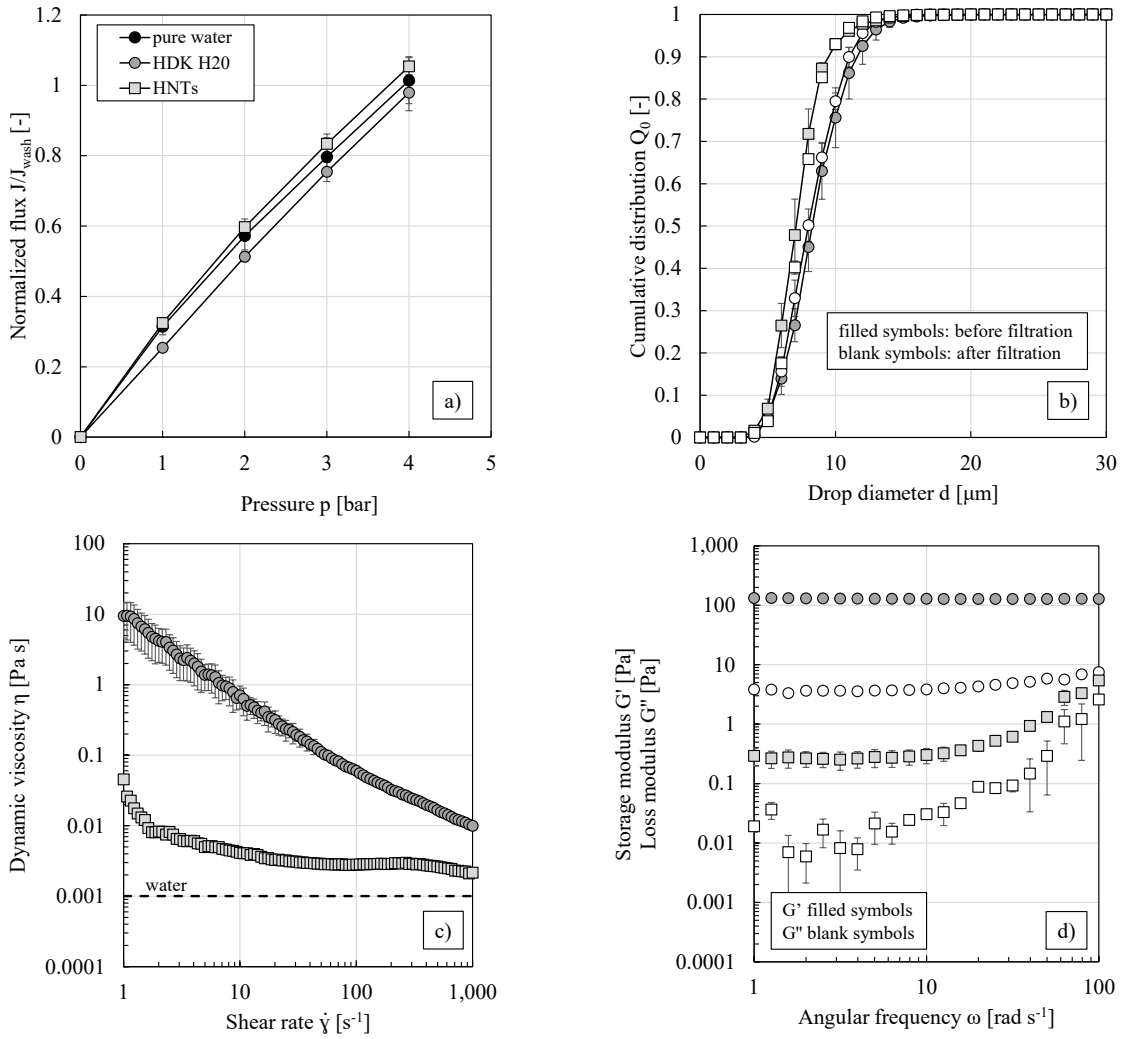

Figure 40. (a) Normalized flux against pressure, **(b)** cumulative number distribution, **(c)** viscosity curve and **(d)** frequency sweep measurement of o/w PEs stabilized by 0.5 wt.% HDK®H20 or HNTs, respectively. The characteristic properties refer to "before filtration". All experiments were conducted in triplicate and mean values are shown. Error bars represent the standard deviation. Where not visible, error bars are smaller than the symbol size. Adapted from [II].

The cumulative number distributions are shown in **Figure 40** b). The corresponding Sauter mean diameters were 9.69 ± 0.63 µm for HDK®H20 and 8.28 ± 0.14 µm for HNT stabilized PEs, respectively. HDK®H20 stabilized o/w PEs showed a more pronounced shear thinning behavior and higher dynamic viscosities as well as storage and loss moduli than HNT stabilized emulsions (**Figure 40** c) and d)). These different PE properties did not influence the overall filtration performance. The rheological behavior of o/w PEs under variation of, e.g., particle concentration or dispersed phase fraction, was investigated in, e.g., [136, 248].

5.2.5 Conclusions

The ultrafiltration membrane ETNA01PP is originally functionalized for its use in aqueous applications [8]. Pressure stepping experiments of o/w PEs showed – regardless of the particle type – the expected linear increase of flux with pressure and almost no difference to the pure water flux. Nanoparticle covered oil drops did not significantly add to a filtration resistance and no specialized membrane pre-treatment was necessary.

For the intended process described in **Chapter 1**, the filtration of w/o PEs is required. As an unexpected filtration behavior was observed for w/o PEs stabilized by HDK®H20 particles in literature [199, 200] and in **Section 5.1.4**, further investigations on the influence of particle type and interactions between membrane, solvent and particles were needed. All w/o PEs showed a more or less pronounced disproportionate increase of flux with pressure. By an adjustment of the membrane pre-treatment using a gradual change of solvents of different polarity, this disproportionate filtration behavior was eliminated, and generally higher fluxes were achieved. For the filtration of nanoparticle/oil suspensions and w/o PEs, an increase in membrane wettability (turning it more hydrophobic) after silica particle contact was observed. When particles with gelling properties were used, this increased wettability led to an increase in flux compared to the pure solvent as potential residual particles built highly porous three-dimensional network structures and did not (significantly) add to the filtration resistance. When particles without gelling properties were used, the increased membrane wettability for the organic solvent was outweighed by the residual particles which formed a dense filter cake and settled in the voids between emulsion drops.

The ability of particles to form such network structures was indicated by the shear thinning rheological behavior, the viscoelastic properties (storage moduli greater than loss moduli) and the microscopic images, where the formation of drop clusters was observed for certain particle types. While the tendency to form networks significantly influenced the filtration behavior, the impact of specific particle surface area or hydrophobicity as well as drop size distribution seemed to be negligible.

To conclude, the ultrafiltration membrane ETNA01PP can be applied for the filtration of both o/w and w/o PEs stabilized by different particles, while in the latter case an adjusted membrane pre-treatment is recommended. The interactions between solvent, membrane material and particle type are of significant importance, especially when membranes originally designed for aqueous applications are used in organic systems. Accompanying measurements regarding the fundamental characterization of PE properties (DSD and rheology) helped to better understand and explain the observed filtration results.

5.3 Pickering emulsion filtration using the organic solvent nanofiltration membrane oNF-3 – systematic experimental parameter study[3]

5.3.1 Working program

As shown in **Section 5.1.4**, the oNF-3 membrane showed a very reproducible filtration behavior allowing a systematic parameter study to identify the main influencing parameters on w/o PE membrane filtration (**Table 12**). "Standard" PEs were prepared using 1-dodecene as the continuous phase, 0.5 wt.% silica particles (HDK®H20 or HDK®H2000, respectively), a dispersed phase fraction of 0.25 and dispersing conditions of 17,500 min^{-1} / 2 min (S25N-18G) (cf. **Section 5.1**). If not stated otherwise, 100 mL of PE were prepared and investigated. Deviations from this standard composition are indicated in the respective subsections. Except for the experiments to study the impact of temperature on the filtration performance, all experiments were conducted at room temperature. If not stated otherwise, in all w/o PE filtration experiments a stirrer speed of 500 min^{-1} was applied within the stirred cell.

Table 12. Parameters used to identify the main influencing parameters on w/o PE filtration using the oNF-3 membrane.

	Impact on flux?	
PE composition		
particle type	no	**Figure 41**
particle concentration	no	**Figure 43**
dispersed phase fraction	no	**Figure 44**
catalyst / reaction (by-)products	no	**Figure 41** + **Figure 43**
solvent type	yes	**Figure 49**
PE properties		
drop size distribution	no	**Section 5.1.4**
Operating conditions		
pressure	yes	**Sections 5.1 - 5.3**
temperature	yes	**Figure 48**
shear rate / crossflow velocity	(yes)	**Figure 45**

5.3.2 Impact of particle type

The particle type has a significant impact on the drop size distribution and the rheological behavior of PEs (cf. **Section 5.2.2)**. This has also been frequently reported in literature and has been described in detail in **Sections 3.1.5** and **3.1.6**.

Filtration of w/o PEs prepared using seven different types of particles yielded – within the experimental error – a normalized flux of ≈ 0.6 at a pressure of 4 bar (**Figure 41**).

In [95], the impact of different particles on flux was evaluated for bioactive water-in-CPME PEs using a PES ultrafiltration membrane (MWCO of 10 kDa). Spherical particles, not able to form three-dimensional network structures, formed a dense filter cake and led to a decrease in flux compared to colloidal particles. The results published in [95] and this work cannot be directly compared due to the different material pairings and since in [95] long-term filtration runs at a constant pressure (instead of pressure stepping experiments) were performed. As no normalized filtration data was presented, no conclusion could be drawn about the variation of pure solvent fluxes during the membrane pre-treatment for different membrane samples and their impact on the results of PE filtration. Furthermore, detailed information about the interactions between the PES membrane, the solvent CPME and the particles was missing.

[3] The content of this section was partially published in [V] Kempin, M.V.; Schroeder, H.; Hohl, L.; Kraume, M.; Drews, A. (2021): *Modeling of water-in-oil Pickering emulsion nanofiltration – influence of temperature.* J. Membr. Sci., 636, 119547, DOI: 10.1016/j.memsci.2021.119547 and [VI] Kempin, M.V.; Drews, A.: *Organic solvent nanofiltration of water-in-oil Pickering emulsions – What influences permeability?* Membranes, 11, 864, DOI:10.3390/membranes11110864.

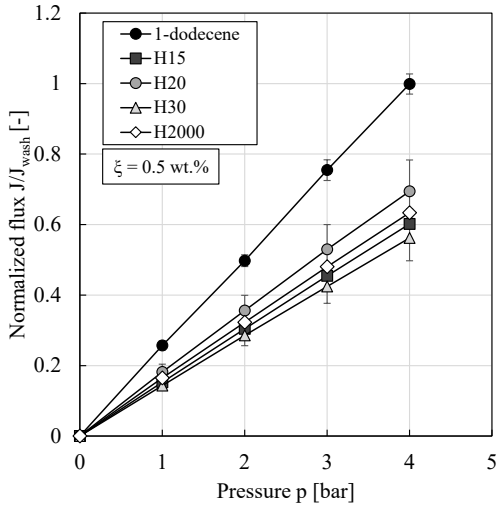

particle type	$J/J_{wash}(p=4bar)$ [-]	d_{32} [µm]
HDK®H15	0.60 ± 0.01	11.65 ± 0.41
HDK®H20	0.69 ± 0.09	9.83 ± 0.54
HDK®H30	0.56 ± 0.06	9.20 ± 0.57
HDK®H2000	0.63 ± 0.01	21.55 ± 1.42
mod. H20	0.63 ± 0.02	17.84 ± 1.07
*50 C18n-	0.66	20.13
*50 C18n+	0.52	16.84

Figure 41. Normalized flux against pressure of "standard" PEs prepared using different particle types and corresponding Sauter mean diameter of freshly prepared PEs. Except for 50 C18n- and 50 C18n+ particles, all experiments were conducted at least in duplicate and mean values are shown. Error bars represent the standard deviation. Where not visible, error bars are smaller than the symbol size. PEs highlighted with a (*) are those used for a hydroformylation reaction and contain catalyst and reaction (by-)products. Except for the mod. H20 particles, data was adapted from [VI].

In contrast to the results presented here, an impact of particle type on the filtration behavior was observed when the UF membrane ETNA01PP was used (cf. **Section 5.2.3**). Particles able to form three-dimensional networks led to an increase in flux while particles without gelling properties showed a decrease in flux compared to the pure solvent. PE compositions and preparation conditions as well as the operating conditions during filtration in **Section 5.2.3** and this section were equal. It can be assumed that the interactions of the particles with the two membranes were different. **Table 13** summarizes the percentage increase or decrease of flux compared to the pure solvent flux at a pressure of 4 bar for suspensions and PEs (prepared at a fixed particle mass fraction of 0.5 wt.% of either HDK®H20 or HDK®H2000 particles) using the two membranes. Comparing the results from suspension filtrations (cf. also **Figure 36** and **Figure 86** a) (appendix)), one can conclude that the increase in membrane wettability after particle contact and the impact of particle gelling properties was more pronounced for the ETNA01PP membrane.

Table 13. Percentage increase or decrease of flux (at a pressure of 4 bar) of suspensions and PEs compared to the pure solvent flux using the ETNA01PP or the oNF-3 membrane, respectively.

		ETNA01PP	oNF-3
suspension	HDK®H20	+90%	+16%
	HDK®H2000	-58%	-17%
PE	HDK®H20	+104%	-31%
	HDK®H2000	-70%	-37%

Filter cake properties of PEs stabilized by 0.5 wt.% HDK®H20 or HDK®H2000 particles were investigated in collaboration with LUM GmbH (as introduced in **Section 5.1.4**). **Figure 42** shows the results for the packing density, sediment height and compressibility under variation of pressure. While for HDK®H20 low packing densities and a compressive behavior were observed at low pressures, HDK®H2000 particles showed an almost incompressible behavior with the formation of a dense sediment even at the lowest applied pressures. At pressures > 1 bar (and thus the pressures applied in the pressure stepping filtration experiments), sediment heights as well as the maximum packing density were similar for both particle types. Together with the results shown in **Table 13**, this might explain why no impact of particle type on the filtration behavior using the oNF-3 membrane was observed.

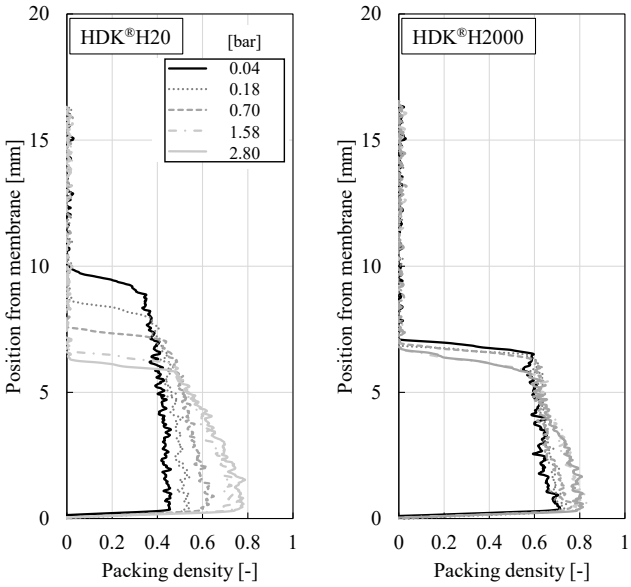

Figure 42. Packing density of "standard" w/o PEs stabilized by HDK®H20 or HDK®H2000 particles against the position from the membrane surface (bottom of the sample tube, respectively). All experiments were conducted in duplicate and mean values are shown. For better graph clarity, error bars are not shown.

5.3.3 Impact of particle concentration

The impact of particle concentration on the resulting drop size distribution and the dynamic viscosity of PEs has been described in detail in **Sections 3.1.5** and **3.1.6.** By way of example, the Sauter mean diameters are shown in **Figure 43** (right) where a decrease of the average drop size with increasing particle mass fraction is observed. The rheological behavior of PEs stabilized by 0.5 wt.% of either HDK®H20 or H2000 particles was already shown in **Figure 34**, results for the higher particle mass fraction of 1.0 wt.% are shown in **Figure 75** (appendix).

Within the experimentally investigated range, the impact of particle concentration on the filtration behavior was negligible and a normalized flux of ≈ 0.6 was obtained at a pressure of 4 bar (cf. **Figure 43**).

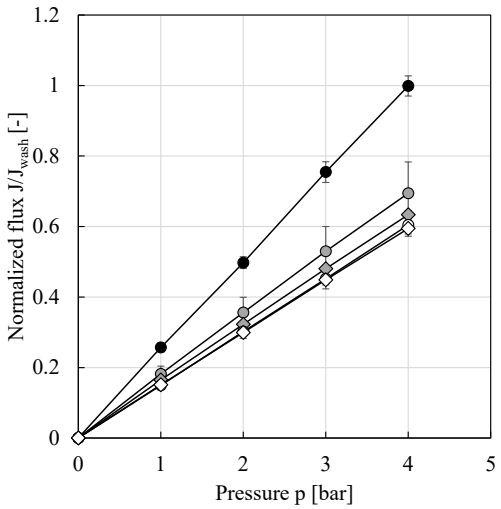

particle type	NP mass fraction [wt.%]	$J/J_{wash}(p=4bar)$ [-]	d_{32} [µm]
HDK®H20	0.5	0.69 ± 0.09	9.83 ± 0.54
	1.0	0.60 ± 0.03	6.59 ± 0.30
HDK®H2000	0.5	0.63 ± 0.01	21.55 ± 1.42
	1.0	0.59 ± 0.02	12.42 ± 1.26
*100 C18n+	0.75	0.64	12.67
	0.875	0.65	13.37
	1.0	0.64	11.78

Figure 43. Normalized flux against pressure of PEs prepared using different particle types at different particle mass fractions and corresponding Sauter mean diameter of freshly prepared PEs. Except for 100 C18n+ particles, all experiments were conducted at least in duplicate and mean values are shown. Error bars represent the standard deviation. Where not visible, error bars are smaller than the symbol size. PEs highlighted with a (*) are those used for a hydroformylation reaction and contain catalyst and reaction (by-)products. Except for 0.75 and 0.875 wt.% of 100 C18n+ particles, data was adapted from [VI].

In [200], concentration experiments using the UF membrane ETNA01PP of w/o PEs prepared using different particle mass fractions of HDK®H20 and either an UT or ultrasonication were compared. PEs of

higher particle mass fractions led to higher PE stability during the filtration and could be concentrated up to higher water contents.

Heyse et al. [96] observed a decrease in flux with higher silica particle mass fractions (15 g L_{dP}^{-1} versus 60 g L_{dP}^{-1}) and explained this via the higher amount of residual spherical (non-gelling) silica particles in the continuous CPME phase forming a denser filter cake. In [78], it was shown that the ratio of freely suspended to bound silica particles (o/w PEs, mean drop sizes of ≈ 3.5 to 5 µm) was stable up to a particle concentration of ≈ 35 g L_{dP}^{-1} while it increased rapidly for higher particle concentrations. While Heyse et al. [96] used much higher particle mass fractions, the ones used in this work correspond to a particle concentration of maximum 33 g L_{dP}^{-1} and were thus below the "limit" reported in [78].

5.3.4 Impact of dispersed phase fraction

The fraction of dispersed phase significantly influences the drop size distribution and the rheological behavior (cf. **Sections 3.1.5** and **3.1.6**). Results of characteristic properties of PEs stabilized by either 0.5 wt.% HDK®H20 or HDK®H2000 particles, respectively, are shown in **Figure 76** (appendix).

No impact of the dispersed phase fraction on the qualitative and quantitative filtration behavior was observed in pressure stepping experiments (**Figure 44**). In contrast to **Figure 30** in **Section 5.1.4**, here, 100 mL of PEs were directly prepared with different dispersed phase fractions without any further dilution within the stirred cell (leading to different drop size distributions and particle mass fractions [related to the dispersed phase] compared to **Figure 30**).

While no significant impact of the aqueous phase fraction on the filtration behavior was observed for HDK®H20 stabilized water-in-CPME PEs in long-term filtration experiments at constant pressure, increasing the dispersed phase fraction from 0.1 to 0.5 significantly decreased the filterability of HDK®H2000 PEs to almost 50% in [95]. Further discussion of their results was not possible as detailed information about the interactions between the PES membrane, the continuous phase CPME and the used particles was missing.

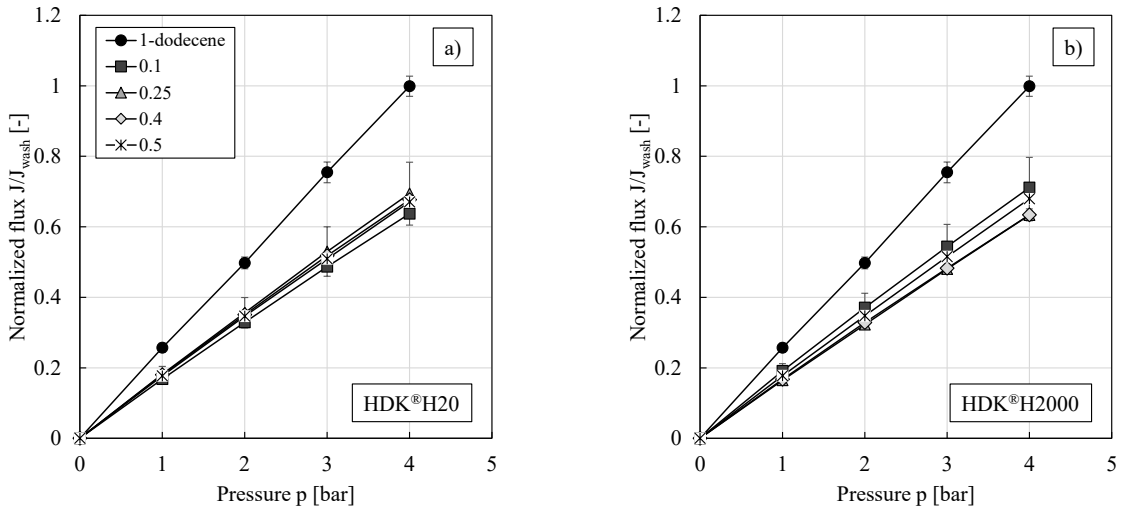

Figure 44. Normalized flux against pressure of PEs prepared using **(a)** HDK®H20 or **(b)** HDK®H2000 particles at different dispersed phase fractions. All experiments were conducted at least in duplicate and mean values are shown. Error bars represent the standard deviation. Where not visible, error bars are smaller than the symbol size. Adapted from [VI].

5.3.5 Impact of catalyst / reaction (by-)products

As the field of PE filtration for its application in continuous processes is still rarely explored, PEs were typically prepared using only water, the organic phase and the particles in this thesis. For selected experiments, PEs were prepared under addition of the catalyst-ligand complex and hydroformylation reactions were performed prior to filtration (cf. [IV]). Consequently, not only the catalyst but also reaction products and byproducts were present. These emulsions were marked with a (*) in **Figure 41** and **Figure 43**. The filtration performance was not significantly affected. Drop size distributions of freshly prepared

PEs, after the reaction and after the filtration are summarized in **Figure 77** (appendix). It was shown that Sauter mean diameters as well as drop size distributions – within the experimental error – did not change throughout the entire process indicating the great stability of the PEs.

5.3.6 Impact of shear rate / crossflow velocity

Pressure stepping experiments were also performed for "standard" w/o PEs using different stirrer speeds within the filtration cell (**Figure 45**). The stirred cell can thus be regarded as a mixed form, as the crossflow – created by the stirring – led to a presumably constant filter cake height. Under the applied test conditions, regardless of particle type, the stirrer speed did not have an impact on the resulting filtration performance (cf. **Figure 45**). **Figure 78** and **Figure 79** (appendix) show additional results for PEs prepared using different homogenization conditions resulting in larger Sauter mean diameters (cf. **Section 5.1.2**).

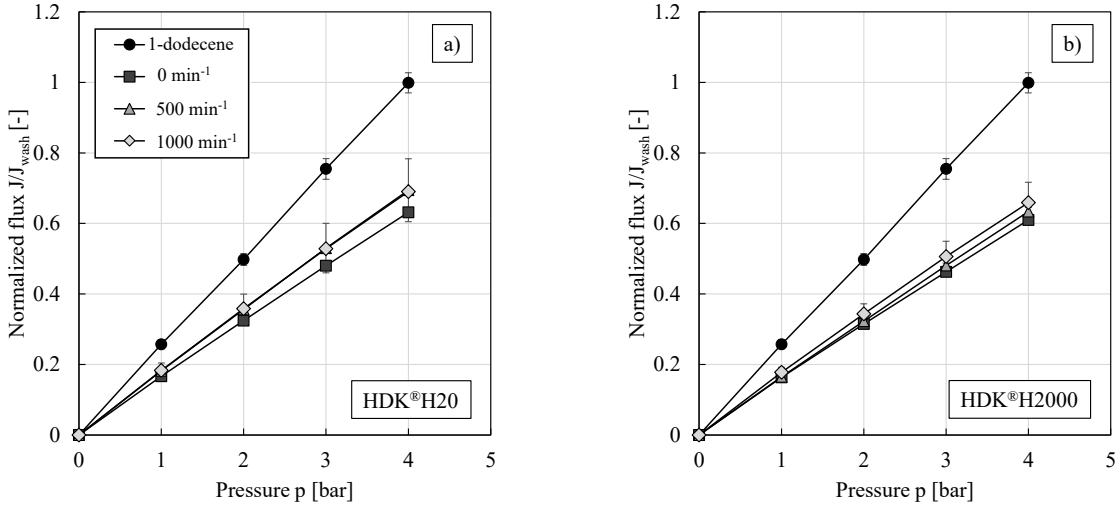

Figure 45. Normalized flux against pressure of "standard" PEs prepared using **(a)** HDK®H20 or **(b)** HDK®H2000 particles under application of different stirrer speeds within the filtration cell. All experiments were conducted at least in duplicate and mean values are shown. Error bars represent the standard deviation. Where not visible, error bars are smaller than the symbol size. Adapted from [VI].

Conducting long-term filtration experiments at a constant pressure instead of pressure stepping experiments revealed differences with regard to the impact of stirrer speed on the filtration behavior of PEs stabilized by different particle types. **Figure 46** shows the filtration results (5 h at a constant pressure of 4 bar) using HDK®H20 and HDK®H2000 particles with and without stirring in the filtration cell.

For HDK®H20 particles no impact of the stirrer speed was observed and the flux remained constant over the entire time period. The slight increase of flux with time could be traced back to an increase of temperature (~ 2 - 3 °C) in the lab throughout the day (cf. **Section 5.3.8** for the impact of temperature on the filtration behavior).

For HDK®H2000 stabilized PEs, the flux remained only constant when stirring was applied but significantly decreased after approximately 75 min in the case without stirring. The filter cake resistance then increased with time. This can possibly be traced back to the differences in sedimentations velocities of drops (µm-range) and particles (nm-range). A simple calculation of the sedimentation velocities of a single droplet or a single particle without and with superposition of the flux (at a pressure of 4 bar) was used as a first estimate. For a 20 µm big droplet, the superposition of the flux does not significantly reduce the sedimentation time. It takes a single droplet less than 5 minutes to settle from the top of the filtration cell to the membrane surface. For the nm-sized particles, the superposition of the flux significantly decreases the sedimentation time. After 75 minutes, all particles being present in an ≈ 1.3 cm thick layer above the membrane have settled to the membrane surface. It is assumed that in the beginning of the filtration experiment, the filter cake mainly consisted of drops but with time, more particle aggregates or agglomerates sedimented and settled in the voids between the emulsion drops. The non-gelling HDK®H2000 particles formed a dense filter cake instead of three-dimensional network structures

(cf. **Section 5.2.3** for PEs and suspensions using the ETNA01PP membrane and **Figure 86** a) (appendix) for suspensions using the oNF-3 membrane).

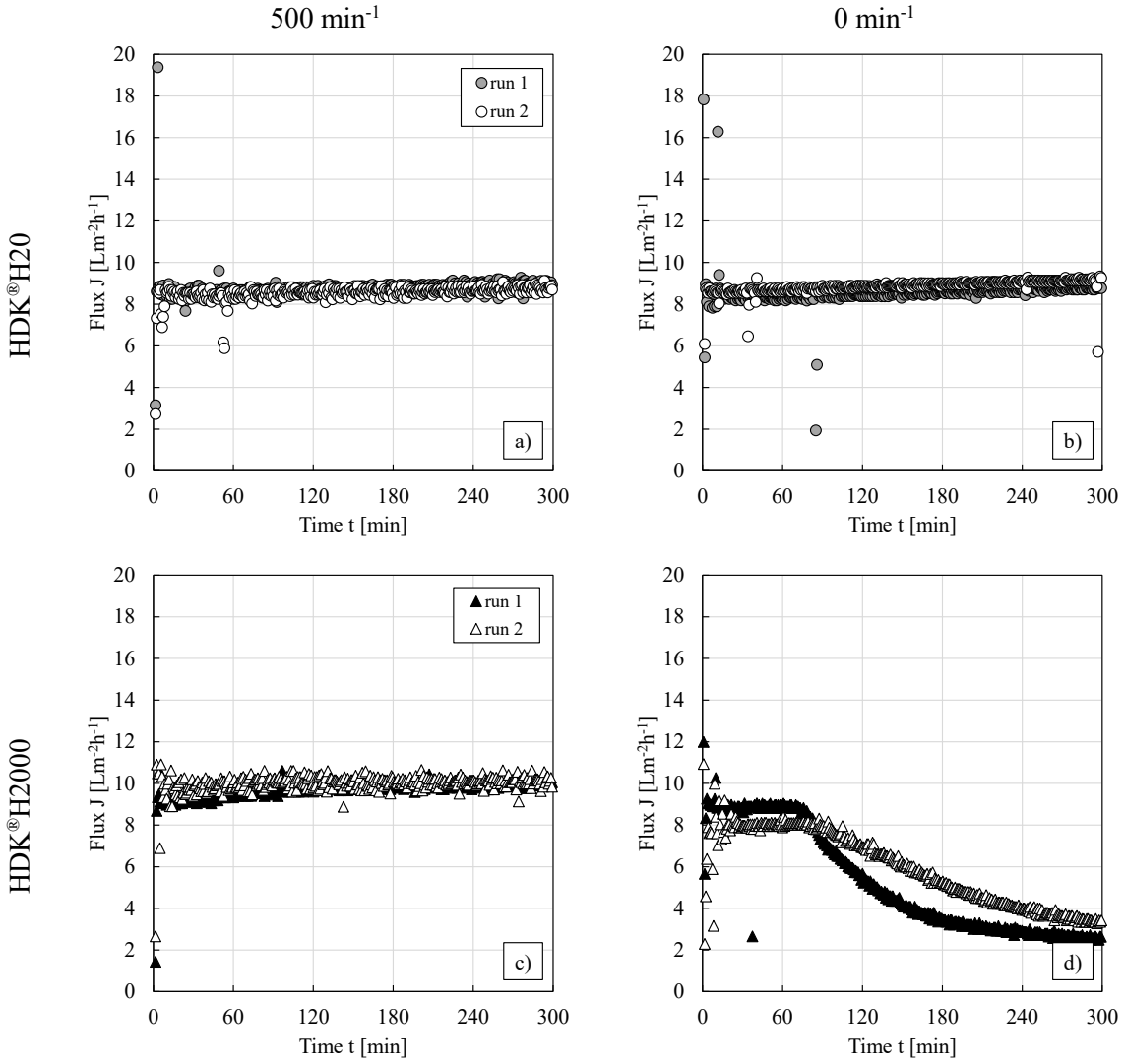

Figure 46. Flux as a function of time for long-term filtration experiments at a constant pressure of 4 bar of "standard" PEs stabilized by HDK®H20 or HDK®H2000 particles: **(a, c)** with and **(b, d)** without stirring. Duplicate experimental runs are shown. Adapted from [VI].

The corresponding cumulative number distributions Q_0 showed slight differences before and after the long-term filtration experiments although no clear tendency could be observed (cf. **Figure 80** (appendix)). For HDK®H20 stabilized emulsions, the drop size distribution and the Sauter mean diameter stayed constant when no stirring was applied during filtration ($d_{32,\mathrm{bf}}$ = 9.62 µm; $d_{32,\mathrm{af}}$ = 9.93 µm), while an increase of the Sauter mean diameter was observed when a stirrer speed of 500 min^{-1} was applied ($d_{32,\mathrm{bf}}$ = 8.66 µm; $d_{32,\mathrm{af}}$ = 13.01 µm). For HDK®H2000 stabilized emulsions, the Sauter mean diameter decreased when stirring was applied during the long-term filtration experiments ($d_{32,\mathrm{bf}}$ = 19.66 µm; $d_{32,\mathrm{af}}$ = 13.24 µm; cumulative number distribution shifted to smaller drop diameters) while it increased without stirring ($d_{32,\mathrm{bf}}$ = 22.31 µm; $d_{32,\mathrm{af}}$ = 26.07 µm; cumulative number distribution shifted to larger drop diameters).

5.3.7 Concentration experiments

In addition to the experiments at constant phase ratio within the stirred cell (as fresh organic phase was continuously transported from a feed tank to the filtration cell), some selected concentration experiments were conducted to figure out to what extent PEs can be concentrated (cf. **Section 4.4.4**). 20 mL "standard"

PEs stabilized by either 0.5 wt.% HDK®H20 or H2000 particles and an initial dispersed phase fraction of 0.25 were investigated (**Figure 47**). The x-axis starts at a dispersed phase fraction of 0.2, since an additional volume of 5 mL of 1-dodecene was used to flush the funnel used to fill the PEs into the stirred cell. The dispersed phase fraction at certain times was calculated from a mass balance (cf. **Eq. (20)**).

For all investigated PEs – within the experimental error – a constant flux was observed up to a dispersed phase fraction of approximately 60%. Concentrating the emulsions further, led to a steep decrease in flux. PEs stabilized by HDK®H20 particles could be concentrated up to a dispersed phase fraction of approximately 75% while the more polydisperse HDK®H2000 stabilized PEs could be concentrated a bit further.

The results were similar to those presented in [199], where PEs stabilized by HDK®H20 particles could be concentrated up to a dispersed phase fraction of approximately 80% using the ETNA01PP membrane. While in [199] water then passed through the membrane, a clear water-free permeate was obtained using the oNF-3 membrane.

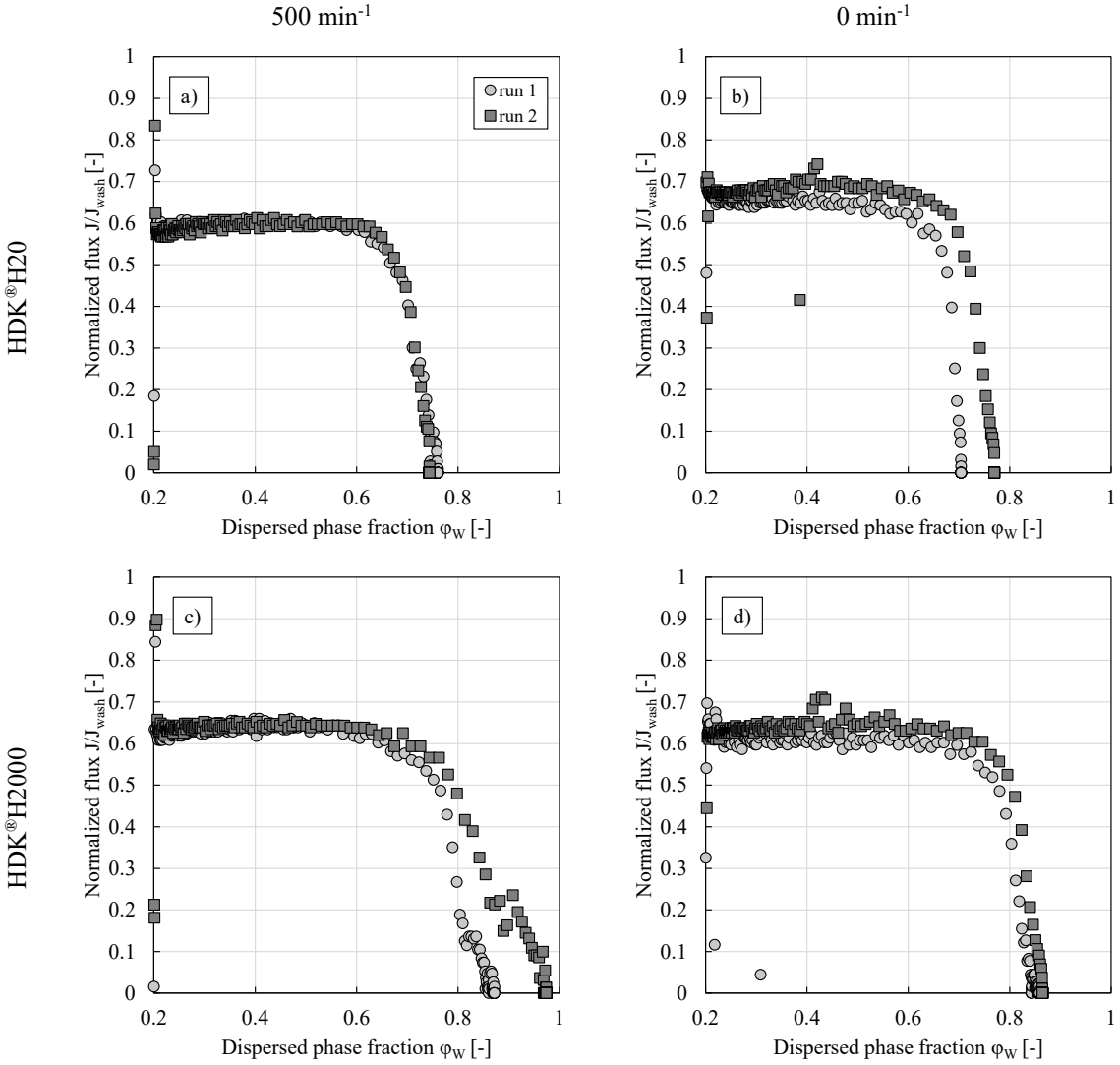

Figure 47. Normalized flux against dispersed phase fraction from concentration experiments of "standard" PEs stabilized by **(a, b)** HDK®H20 or **(c, d)** HDK®H2000 particles. PEs were filtered at a constant pressure of 4 bar either with or without stirring within the filtration cell. Duplicate experimental runs are shown.

5.3.8 Impact of temperature

The impact of temperature on the filtration behavior was investigated for the pure organic solvent 1-dodecene and for "standard" w/o PEs stabilized by either HDK®H20 or HDK®H2000 particles. According to the manufacturer, typical operating conditions of the oNF-3 membrane are temperatures up to 60 °C [46].

Figure 48 shows an increase in flux with increasing temperature for the pure organic solvent as well as for the filtration of PEs. For the investigated temperature range (25 to 50 °C), a factor in flux of 1.7 - 1.9 was observed. Consistent with the previous results, PE fluxes were lower than the pure solvent fluxes and almost no impact of particle type on the filtration behavior was observed.

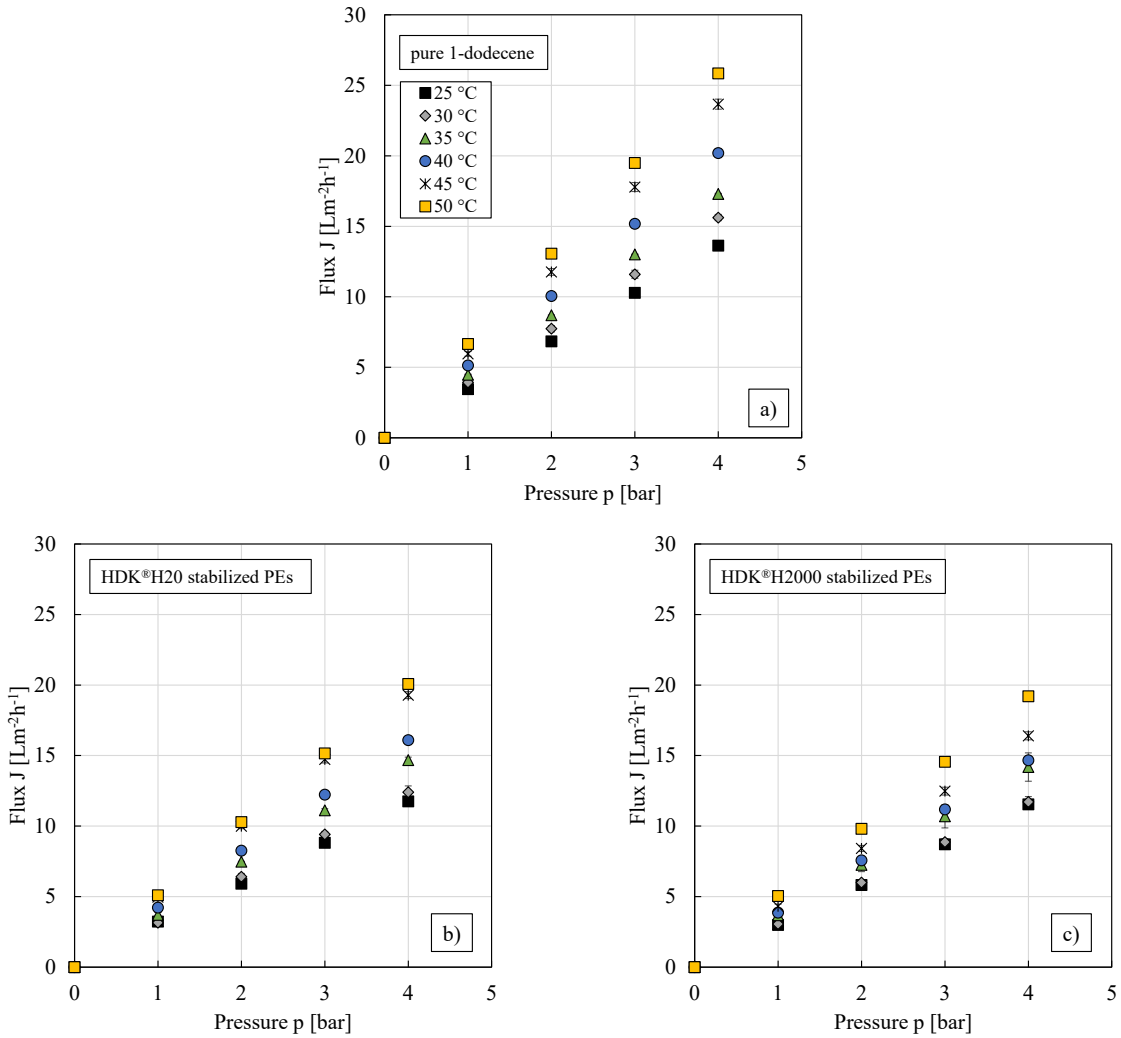

Figure 48. Flux against pressure for **(a)** pure 1-dodecene, **(b)** HDK®H20 and **(c)** HDK®H2000 stabilized "standard" PEs under variation of temperature. All experiments were conducted at least in duplicate and mean values are shown. Error bars represent the standard deviation. Where not visible, error bars are smaller than the symbol size. Adapted from [V].

For the permeation of pure solvents, a 1.5 to 3-fold increase in flux with temperature (varied between 0 and 65 °C) was also reported in, e.g., [45, 137, 257]. To the best of our knowledge, the impact of temperature on the PE filtration behavior has not been published before. However, for surfactant stabilized w/o emulsions also an increase in permeate flux with increasing temperature has been reported (e.g., [72, 101]). The authors explained this increase in flux with increasing temperature via an increase in the solvent diffusion coefficient and a decrease in the solvent viscosity.

5.3.9 Impact of organic solvent type

As the level of permeate flux can be expected to depend on the type of solvent and its interaction with the membrane, different organic solvents varying in their properties (e.g., dynamic viscosity, molar mass or interfacial tension, cf. **Table 3**) were investigated. Characteristic PE properties (DSD, viscosity curves and packing densities of the sediment) are shown in **Figure 87**, **Figure 88** and **Figure 89** (appendix), respectively.

Figure 49 shows that the type of organic solvent has a significant impact on the flux level. A decrease in chain length led to an increase in flux while the difference between 1-dodecene and dodecane (same chain length but differing in double or single bonds) was negligible. Consistent with the previous results, PE fluxes were smaller than the pure organic solvent fluxes and almost no impact of particle type on the filtration behavior was observed.

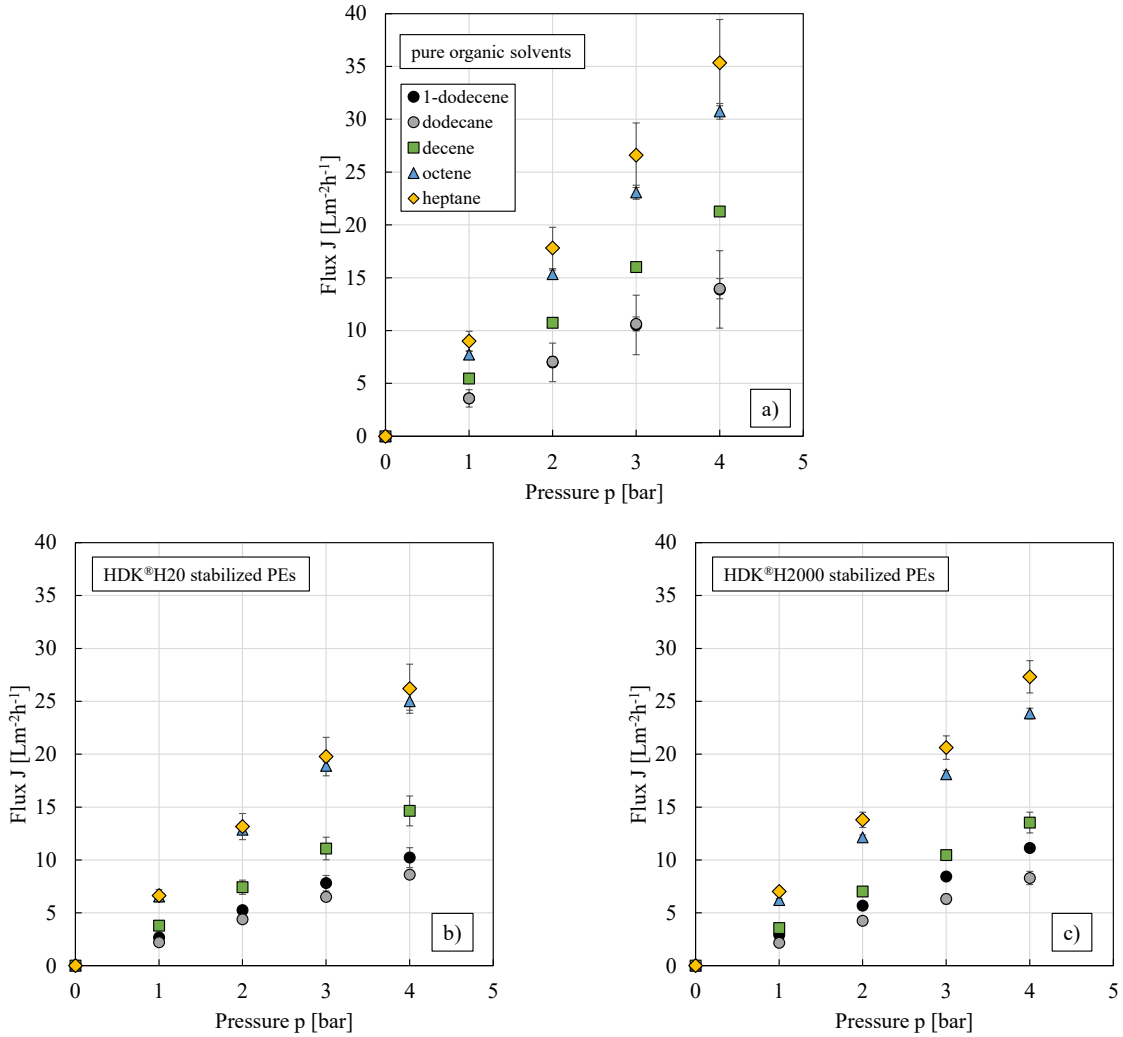

Figure 49. Flux against pressure for **(a)** pure organic solvents, **(b)** HDK®H20 and **(c)** HDK®H2000 stabilized "standard" PEs under variation of organic solvent type. All experiments were conducted at least in duplicate and mean values are shown. Error bars represent the standard deviation. Where not visible, error bars are smaller than the symbol size. Adapted from [VI].

In [137], the flux of several solvents differing in their physical properties (e.g., molecular size, polarity, dielectric constant, viscosity, …) using a MPF-50 membrane was investigated. Consistent with the results presented here, within a homologous series of solvents, the authors found an increase in flux with decreasing molecular volume. Ultrafiltration of w/o PEs prepared using different organic solvents (1-dodecene, decene, decane, toluene) as the continuous phase were investigated in [199]. Focus in [199] was on the explanation of the unexpected disproportionate PE filtration behavior using the ETNA01PP membrane (cf. **Section 5.2**) and not on the impact of specific solvent properties. However, strong differences in pure solvent as well as PE fluxes comparing the different organic solvents were observed even though solvents of similar chain length and hydrophobicity but of different purity were chosen [199].

5.3.10 Conclusions

In this section, a systematic parameter variation to identify the main influencing parameters on w/o PE filtration using the organic solvent nanofiltration membrane oNF-3 was performed.

In contrast to the UF membrane ETNA01PP (cf. **Section 5.2.3**), using the oNF-3 membrane, all PEs showed the expected linear increase of flux with pressure and fluxes were lower compared to the pure solvent flux (permeability reduced by approximately only 40%). No specialized membrane pre-treatment was required. Consistent with results published for the ETNA01PP membrane [199], PEs could be concentrated up to a dispersed phase fraction of approximately 75% without emulsion break-up. In the case of the oNF-3 membrane, the flux remained constant up to a dispersed phase fraction of about 60% and then steeply decreased. No water passed through the membrane and a clear permeate was obtained.

In terms of PE composition, only the type of organic solvent (and consequently its characteristic properties such as dynamic viscosity or diffusion coefficient) had a significant impact on the filtration behavior. In terms of process conditions, pressure and temperature played a key role. The applied stirrer speed within the filtration cell only had an impact on the filtration performance when particles without the tendency to form three-dimensional network structures were used in long-term filtration experiments. The filtration behavior of w/o PEs using the oNF-3 membrane was insensitive towards the particle type, the particle concentration, the dispersed phase fraction as well as the presence of catalyst and reaction (by-)products. These findings allow a robust operation as well as broad operation windows and an optimization of the PE composition to meet the needs of the actual reaction.

5.4 Pickering emulsion filtration using the organic solvent nanofiltration membrane oNF-3 – modeling approach[4]

The OSN membrane oNF-3 showed a great reproducibility of the filtration performance and a systematic parameter study was performed (cf. **Section 5.3**). Interestingly, only a limited number of parameters showed a significant impact on the filtration behavior of w/o PEs. The main influencing parameter – apart from the pressure – was found to be the dynamic viscosity of the continuous organic phase, varied either via the temperature (for one specific solvent type) or via the use of different organic solvents (at room temperature). The other parameters, such as the particle type and concentration, the dispersed phase fraction, the presence of catalyst or reaction (by-)products, as well as the stirrer speed within the filtration cell did not show any significant impact on the filtration behavior in pressure stepping experiments of water-in-1-dodecene PEs (cf. **Section 5.3**). Therefore, for the first time, a mathematical modeling approach to describe the temperature dependent filtration behavior (cf. **Section 5.4.2**) and the impact of the organic solvent type on membrane filtration (cf. **Section 5.4.3**) is developed and discussed in this section.

5.4.1 Working program

The impact of temperature and organic solvent type on the filtration of w/o PEs was investigated for "standard" emulsions prepared using 0.5 wt.% of either HDK®H20 or HDK®H2000 particles, respectively, a dispersed phase fraction of 0.25 and dispersing conditions of 17,500 min^{-1} / 2 min (S25N-18G). In all filtration experiments a stirrer speed of 500 min^{-1} was applied within the filtration cell.

5.4.2 Impact of temperature

Pure 1-dodecene fluxes

Since the oNF-3 membrane has a relatively high MWCO (900 Da), there may be a diffusive but also a convective flow component. Different modeling approaches (cf. **Section 3.2.3**) were followed to describe the permeation of pure 1-dodecene at different temperatures. The reader is referred to [V] for more detailed information.

The oNF-3 membrane is of silicone polymer-based composite type [133]. As oNF-1 and oNF-2 membranes were reported to have a PDMS active layer on a PAN support structure [45, 212, 239, 259], this membrane composition was also assumed for the oNF-3 membrane and the modeling approach presented here. It is likely that the main transport resistance occurs in the active PDMS layer.

The solution-diffusion model combined with an Arrhenius-type relationship to express the temperature dependency of the diffusion coefficient was found to be most appropriate (cf. [V]) and will therefore be described in detail in the following.

To obtain the volumetric instead of the molar flux in [L m^{-2} h^{-1}], an extension of **Eq. (14)** by the quotient of molar mass and density was required (**Eq. (24)**). The membrane thickness δ_{eff} was expressed via the swelling degree S and the dry (active layer) membrane thickness δ_0 [258].

$$J_{\mathrm{i}}(T) = \frac{D_{\mathrm{iM}}(T)}{\delta_0} \frac{c_{\mathrm{iM}}\, \tilde{V}_{\mathrm{i}}(T)\, \tilde{M}_{\mathrm{i}}}{\Re\, T\, \rho_{\mathrm{i}}(T)\, S}\, \Delta p \qquad \textbf{(24)}$$

The temperature T and the pressure p were defined for each experiment, the universal gas constant $\Re$ and the molar mass $\tilde{M}$ of the solvent i were taken from literature, the temperature dependent density ρ of the solvent was determined experimentally (cf. **Eq. (17)** in **Section 4.1**), leaving the swelling degree S, the concentration c of solvent inside the membrane, the dry membrane thickness δ_0 and the diffusion coefficient D as unknown parameters.

The parameter determination was based on [258], where the retention of the non-ionic surfactant Marlipal 24/70 from the organic solvent 1-dodecene using oNF-1 and oNF-2 membranes was investigated. The authors used the same organic solvent as used in this thesis and membranes of the same series as the

[4] The content of this section was partially published in [V] Kempin, M.V.; Schroeder, H.; Hohl, L.; Kraume, M.; Drews, A. (2021): *Modeling of water-in-oil Pickering emulsion nanofiltration – influence of temperature.* J. Membr. Sci., 636, 119547, DOI: 10.1016/j.memsci.2021.119547 and [VI] Kempin, M.V.; Drews, A.: *Organic solvent nanofiltration of water-in-oil Pickering emulsions – What influences permeability?* Membranes, 11, 864, DOI:10.3390/membranes11110864.

oNF-3 membrane but with smaller MWCOs (600 Da and 350 Da, respectively, cf. **Table 5**). It is thus likely that the model parameters determined in [258] can be applied for the permeation of pure 1-dodecene and the filtration of w/o PEs presented here.

The thickness of a dry and swollen PDMS layer upon contact with 1-dodecene at room temperature and atmospheric pressure was measured using a micrometer gauge in [258]. The swelling degree S was found to be 2. The extent of swelling of PDMS in different solvents can either increase, stay constant or decrease with increasing temperature [73]. For a PDMS membrane upon contact with toluene (Hildebrand solubility parameter of 18.20 $(\mathrm{J\ cm^{-3}})^{0.5}$) the swelling degree based on the length and weight increase, increased by 4.3% and 9.1%, respectively, when the temperature was increased from 8 to 42 °C [121]. In [73], it was stated that the impact of temperature on the swelling degree is smaller for "better" solvents with "good" and "poor" solvents being classified via the differences in the solubility parameters between the respective solvent and PDMS [251]. The Hildebrand solubility parameter for PDMS was reported to be 15.0 - 15.5 $(\mathrm{J\ cm^{-3}})^{0.5}$ [1, 119, 211, 259]. The one for 1-dodecene was calculated based on the molecular structure of the solvent as published in [74] and found to be 16.75 $(\mathrm{J\ cm^{-3}})^{0.5}$. 1-dodecene was assumed to be a "good" solvent (even "better" than toluene) and the impact of temperature on the swelling degree was assumed to be low. This was confirmed by experimental results in [258], where the solvent uptake by the membrane at 25 °C and 35 °C was equal. The swelling degree of the oNF-3 membrane in 1-dodecene was therefore assumed to be independent of temperature and the constant value of $S = 2$ reported in [258] was used in the modeling approach.

The concentration of 1-dodecene in the (swollen) active PDMS membrane material was calculated using **Eq. (25)** in [258].

$$c_{\mathrm{iM}} = \frac{n_{\mathrm{i}}}{V_{\mathrm{total}}} = \frac{m_{\mathrm{i}}/\widetilde{M}_{\mathrm{i}}}{V_{\mathrm{PDMS}} - V_{\mathrm{fV}} + V_{\mathrm{solvent}}} \tag{25}$$

The maximum absorbed amount of 1-dodecene m_{i} per gram PDMS was determined via gravimetric absorption and swelling experiments and was found to be 1.6 g [258]. Using the densities of 1-dodecene (cf. **Table 3**) and PDMS (970 kg $\mathrm{m^{-3}}$), the volumes V_{PDMS} and V_{solvent} were calculated to be 1.03 $\mathrm{cm^3}$ and 2.11 $\mathrm{cm^3}$, respectively, [258]. Furthermore, a free volume V_{fV} of approximately 19% (0.2 $\mathrm{cm^3}$) was assumed [258]. The calculated concentration c_{iM} of 3,240 mol $\mathrm{m^{-3}}$ was also used for the modeling approach in this thesis and a temperature dependency was neglected.

The dry active membrane layer thickness δ_0 for oNF-1 and oNF-2 membranes was reported to be 3.5 µm and 2.5 µm, respectively, in [258] but is unknown for the oNF-3 membrane. The membrane was shown to be incompressible within the experimentally investigated pressure range (cf. **Sections 5.1.4** and **5.3**) and the dry membrane thickness was assumed to be constant and lumped with the diffusion coefficient in the fitting.

A theoretical derivation of the diffusion coefficient of a solvent through a membrane is typically not possible, as it depends on, e.g., the crosslinking degree or the procedure of the membrane production [258]. For commercially available membranes, these properties are mostly unknown. In the modeling approach developed here, the diffusion coefficient was assumed to be independent of pressure but temperature dependent. According to [90, 159], the temperature dependency was expressed via an Arrhenius-type relationship (**Eq. (26)**).

$$\frac{D_{\mathrm{iM}}}{\delta_0} = D_0 \exp\left(-\frac{\mathrm{E_A}}{\Re\, T}\right) \tag{26}$$

The coefficient D_0 and the activation energy E_{A} were fitted to the experimental permeation data of pure 1-dodecene obtained at three distinct temperatures (25, 35 and 45 °C). Values for the coefficient and the activation energy were found to be 2.75 m $\mathrm{s^{-1}}$ and 22.7 kJ $\mathrm{mol^{-1}}$, respectively, with the latter being in the same order of magnitude as reported for, e.g., dodecane [90] or cyclohexane [159] and polymeric membranes.

The parity plot (**Figure 50**) shows that deviations between experimental and modeled values were smaller than 5%, indicating the great accuracy of the developed model (given in **Eq. (24)** with the ratio of diffusion coefficient and dry active membrane layer thickness expressed via **Eq. (26)** and the temperature dependent density given in **Eq. (17)**). The experimental results (flux against pressure) as well as the results from the model fit and model prediction are shown in **Figure 81** (appendix).

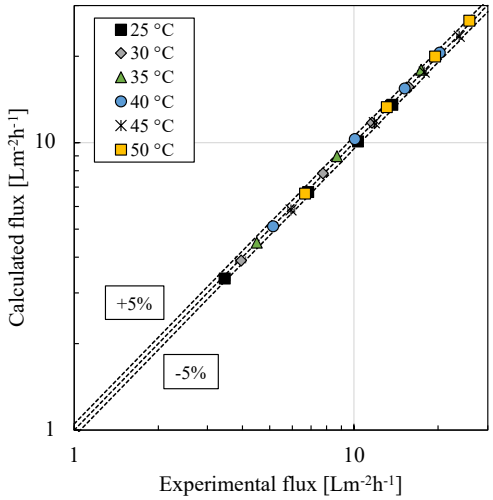

Figure 50. Parity plot for pure 1-dodecene fluxes at different temperatures with the modeled values against the experimental data. The solution-diffusion model (**Eq. (24)**) combined with an Arrhenius-type relationship to describe the temperature dependency of the diffusion coefficient (**Eq. (26)**) was used. For the model fit, the experimental results at temperatures of 25, 35 and 45 °C were used. All experiments were conducted at least in duplicate. Error bars represent the standard deviation. Where not visible, error bars are smaller than the symbol size. Adapted from [V].

In summary, the proposed model is able to successfully represent pure 1-dodecene fluxes through oNF-3 membranes at different temperatures and will therefore be used in the following. The modeling approach via the solution-diffusion model is schematically summarized in **Figure 51**.

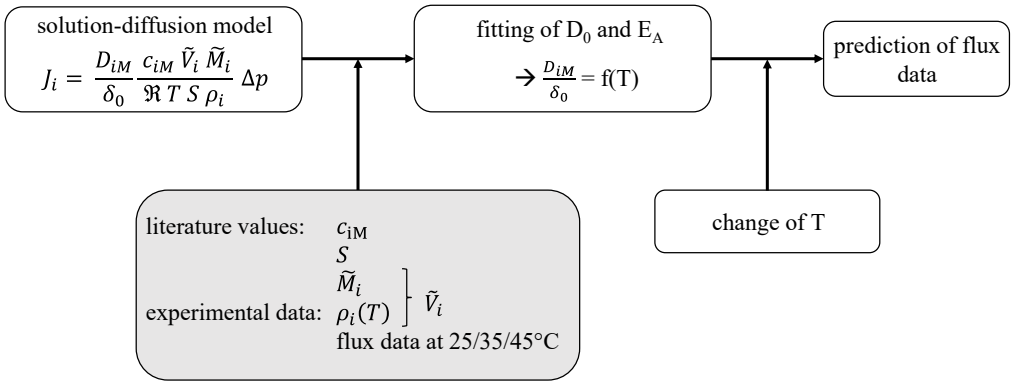

Figure 51. Schematic representation of pure 1-dodecene flux modeling. Highlighted in grey are necessary literature values and experimental data. Filtration experiments were conducted in pressure stepping mode at four different pressures as described in **Section 4.4.2**. Adapted from [V].

Filtration of w/o PEs

For the prediction of PE fluxes, a combination of the SDM (developed in the previous paragraph) and the resistance in series model was used (**Eq. (27)**).

$$\frac{1}{J_{\mathrm{PE,k}}(T)} = \frac{\eta_{\mathrm{i}}(T)\, R_{\mathrm{M}}}{\Delta p} + \frac{\eta_{\mathrm{i}}(T)\, R_{\mathrm{c,k}}(25°C)}{\Delta p} = \frac{1}{J_{\mathrm{i,SDM}}(T)} + \frac{\eta_{\mathrm{i}}(T)\, R_{\mathrm{c,k}}(25°C)}{\Delta p}$$

$$\frac{1}{J_{\mathrm{PE,k}}(T)} = \frac{\delta_0\, \Re\, T\, \rho_{\mathrm{i}}(T)\, S}{D_{\mathrm{iM}}(T)\, c_{\mathrm{iM}}\, \tilde{V}_{\mathrm{i}}(T)\, \tilde{M}_{\mathrm{i}}\, \Delta p} + \frac{\eta_{\mathrm{i}}(T)\, R_{\mathrm{c,k}}(25°C)}{\Delta p} \qquad \textbf{(27)}$$

All parameters needed for the first term are known by now. The subscript i denotes the pure solvent 1-dodecene, while the subscript k denotes the particle type (HDK®H20 or HDK®H2000, respectively). The temperature dependent dynamic viscosity of 1-dodecene was expressed via **Eq. (16)**.

Cake resistances shown in **Figure 52** were calculated from experimental filtration data at different temperatures via the resistance in series model (cf. **Eq. (13)**) with the membrane resistance R_{M} calculated from **Eq. (12)** using the results from the permeation of the pure solvent (range of $6 \cdot 10^{13}$ - $1 \cdot 10^{14}$ m^{-1}, cf. **Figure 82** (appendix)).

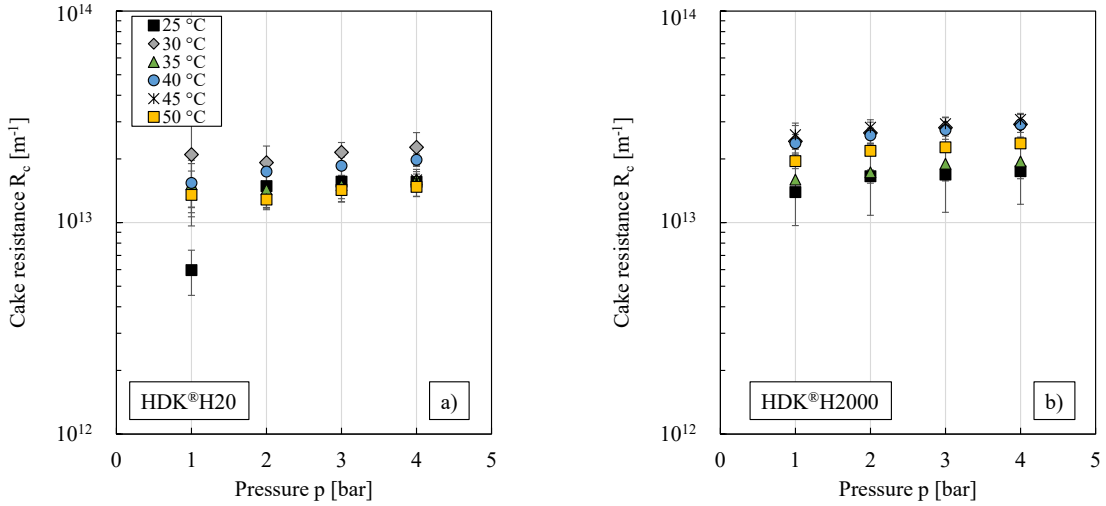

Figure 52. Cake resistance against pressure of "standard" w/o PEs stabilized by **(a)** HDK®H20 or **(b)** HDK®H2000 particles. Error bars represent the standard deviation. Where not visible, error bars are smaller than the symbol size. Adapted from [V].

All PEs were prepared at room temperature and heated to the desired temperature within the stirred cell. Consequently, all freshly prepared PEs showed – depending on the particle type – the same Sauter mean diameters and the same dynamic viscosity (cf. **Section 5.2.2**). Although the characteristic properties (DSD and rheological behavior) of the HDK®H20 and H2000 stabilized emulsions differed significantly, cake resistances were very similar for both particle types. Filter cake properties at the pressures applied here were also similar (cf. **Figure 42**). Differences in cake resistances with increasing pressure were small and were assumed to lie within or at least close to the experimental error. Cake resistances were also assumed to be independent of temperature, as – despite higher scatter – no clear tendency was observed (cf. **Figure 52**). In the following, cake resistances were fitted to the experimental data at 25 °C only (small number of experiments regarding the practical applicability of the developed model). Mean cake resistances and standard deviations were calculated to be $R_{c,H20} = (16.9 \pm 2.76)\ 10^{12}$ m^{-1} and $R_{c,H2000} = (24.1 \pm 5.38)\ 10^{12}$ m^{-1}, respectively. Being significantly smaller than the membrane resistance, the differences in cake resistances only play a minor role on the total resistance and can therefore be safely averaged.

Deviations between modeled and experimental values for emulsions stabilized by either HDK®H20 or HDK®H2000 particles were smaller than 10 or 15%, respectively (**Figure 53**).

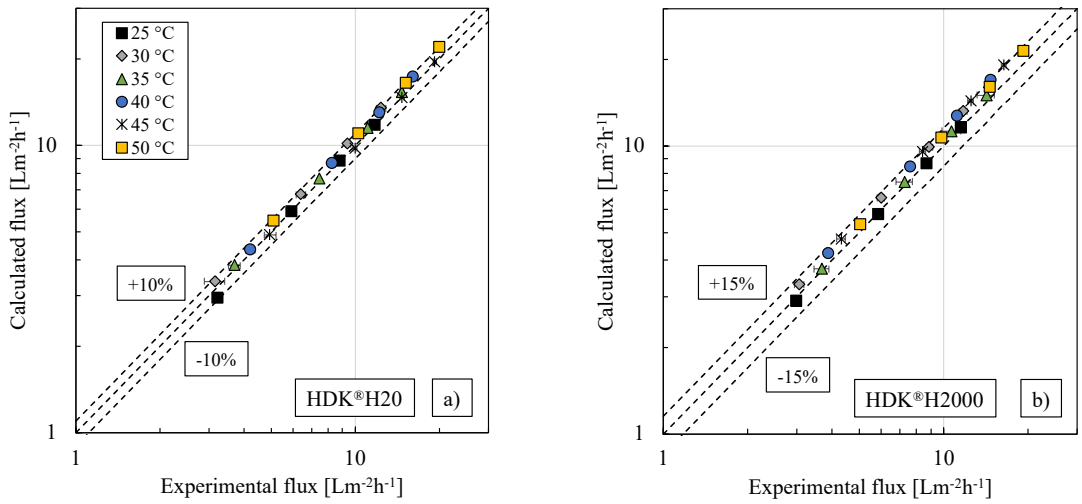

Figure 53. Parity plot for w/o PE fluxes at different temperatures with the modeled values against the experimental data. A combination of the solution-diffusion and the resistance in series model was used. For the model fit (**Eq. (27)**), the experimental results at a temperature of 25 °C were used. **(a)** HDK®H20 and **(b)** HDK®H2000 stabilized PEs. All experiments were conducted at least in duplicate. Error bars represent the standard deviation. Where not visible, error bars are smaller than the symbol size. Adapted from [V].

As the cake resistance at the lowest applied temperature was used for the model fit, a slight systematic overestimation of flux was observed. The experimental results (flux against pressure) as well as the results from the model fit and model prediction are shown in **Figure 83** (appendix).

To summarize, the proposed model successfully predicts w/o PE fluxes at different temperatures. It shows great practical applicability as model fits should be performed with the smallest experimental effort. Here, only a limited number of filtration experiments – the permeation of the pure organic solvent at three distinct temperatures and one filtration run for PEs (one for each particle type) – was necessary. The modeling approach for w/o PE filtration via the combined solution-diffusion and resistance in series model is schematically shown in **Figure 54**.

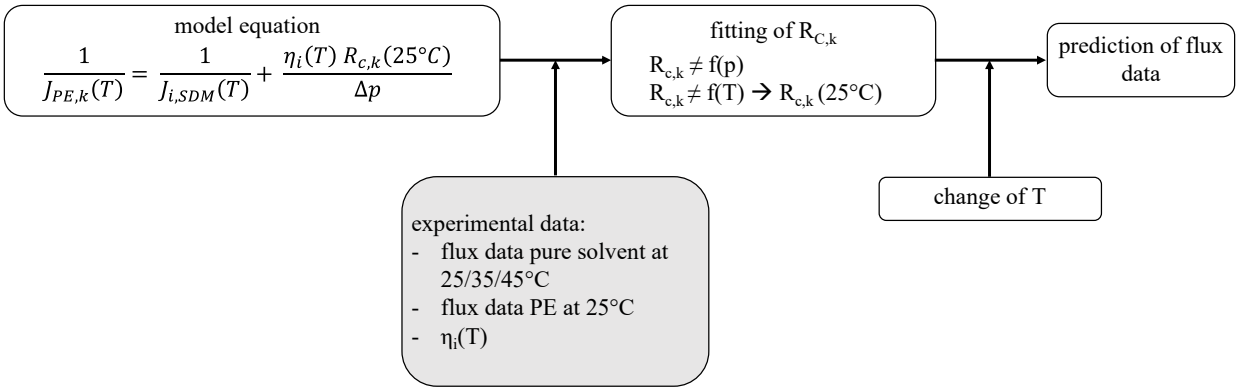

Figure 54. Schematic representation of w/o PE filtration modeling. Highlighted in grey are necessary experimental data. Filtration experiments were conducted in pressure stepping mode at four different pressures as described in **Section 4.4.2**. Adapted from [V].

5.4.3 Impact of organic solvent type

Pure organic solvent fluxes

The solution-diffusion model was well suited to describe pure 1-dodecene fluxes through the oNF-3 membrane under variation of temperature (cf. **Section 5.4.2**). Therefore, **Eq. (24)** was also used to model the permeation of different organic solvents. The concentration c of solvent inside the membrane, the swelling degree S, the dry membrane thickness δ_0 and the diffusion coefficient D were the unknown parameters which needed to be identified first.

The concentration of solvent inside the membrane was calculated using **Eq. (25)**. The free volume as well as the volume of PDMS were kept constant and the values published in [258] and described in **Section 5.4.2** were used. The parameter m_i was determined experimentally via solvent uptake measurements. The mass of dry and wet membrane samples was measured. The samples were soaked in the respective solvent for 48 hours at room temperature and carefully dried with filter paper prior to the measurement. For each solvent, the experiments were repeated with five membrane samples and mean values as well as standard deviations are given in **Table 14**. The experimentally determined values for 1-dodecene are in good agreement with the values published in [258].

Table 14. Results from solvent uptake experiments to determine the mass of solvent inside of oNF-3 membrane samples and calculated concentrations of solvent inside the membrane using **Eq. (25)**. Adapted from [VI].

	m_i [g]	c_iM [mol m^{-3}]
1-dodecene	1.58 ± 0.03	3,214.8
dodecane	1.57 ± 0.03	3,148.3
decene	1.51 ± 0.02	3,746.5
octene	1.36 ± 0.03	4,429.5
heptane	1.20 ± 0.03	4,613.5

The swelling degree of $S = 2$ used for 1-dodecene in **Section 5.4.2** and adapted from [258] was determined by experimental thickness measurements. Since we did not have access to the pure PDMS material, only the composite membrane was available and experimental thickness measurements for the

different solvents were not possible. In this first modeling approach the value of $S = 2$ was assumed to be constant for all solvents.

The (constant) dry membrane thickness was again lumped with the diffusion coefficient in the fitting. According to [90], the diffusion coefficient decreases linearly with the molar volume. A linear correlation between the ratio of diffusion coefficient and dry membrane thickness and the molar volume calculated from the experimental data of 1-dodecene and heptane was used in a first attempt (cf. **Eq. (28)** and **Figure 55**).

$$\frac{D_{\mathrm{iM}}}{\delta_0} = -1.23\ 10^{-5}\ \tilde{V}_{\mathrm{i}}\ \frac{mol}{m^2 s} + 0.003\ \frac{m}{s} \qquad \textbf{(28)}$$

Differences between experimental and modeled data were relatively high (up to 30%).

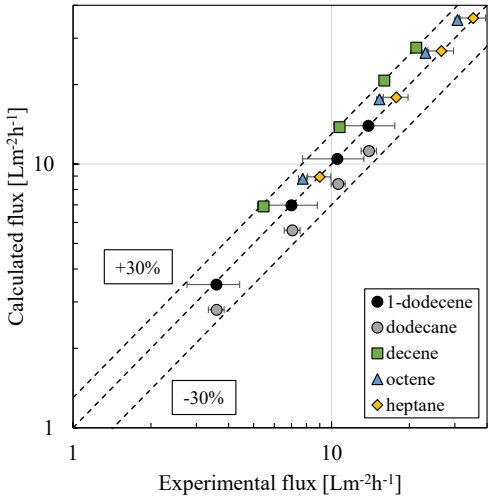

Figure 55. Parity plot for pure organic solvent fluxes with the modeled values against the experimental data. The solution-diffusion model (**Eq. (24)**) combined with a linear correlation between the ratio of diffusion coefficient and dry membrane thickness and the molar volume of the organic solvent (**Eq. (28)**) was used. For the model fit, the experimental results using 1-dodecene and heptane were used. All experiments were conducted at least in duplicate. Error bars represent the standard deviation. Where not visible, error bars are smaller than the symbol size. Adapted from [VI].

Significantly better predictions were obtained when the ratio of diffusion coefficient and dry membrane thickness was linearly correlated with the reciprocal of the molar mass of the solvents (again, the experimental data of 1-dodecene and heptane were used) (**Eq. (29)** and **Figure 56**).

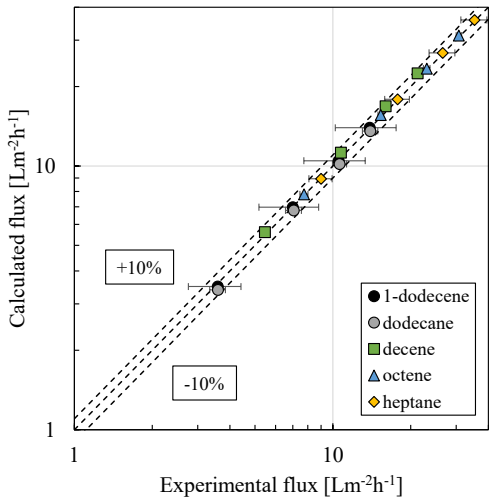

Figure 56. Parity plot for pure organic solvent fluxes with the modeled values against the experimental data. The solution-diffusion model (**Eq. (24)**) combined with a linear correlation between the ratio of diffusion coefficient and dry membrane thickness and the reciprocal of the molar mass of the organic solvent (**Eq. (29)**) was used. For the model fit, the experimental results using 1-dodecene and heptane were used. All experiments were conducted at least in duplicate. Error bars represent the standard deviation. Where not visible, error bars are smaller than the symbol size. Adapted from [VI].

Consequently, when correlating via the molar mass, the exact knowledge of the swelling degree for each solvent is not necessary and the assumption made (S = 2 for all solvents) is sufficient.

$$\frac{D_{\mathrm{iM}}}{\delta_0} = \left(0.2272\ \frac{1}{\widetilde{M}_{\mathrm{i}}}\ \frac{g}{mol} - 0.001\right)\frac{m}{s} \qquad \textbf{(29)}$$

As deviations between experimental and calculated fluxes were smaller than 10%, this modeling approach will be used in the following. The experimental results (flux against pressure) as well as the results from the model fit and model prediction are shown in **Figure 84** (appendix).

Filtration of w/o PEs

A combination of the solution-diffusion model and a resistance in series model was used to describe the filtration behavior of w/o PEs (cf. **Eq. (27)**). Cake resistances were calculated from experimental filtration data via the resistance in series model (cf. **Eq. (13)**), with the membrane resistance R_{M} calculated from **Eq. (12)** using the results from the permeation of the different pure organic solvents (range of $7.1 \cdot 10^{13}$ - $1.6 \cdot 10^{14}$ m^{-1}, cf. **Figure 90** (appendix)). The cake resistances were – within the experimental error – assumed to be independent of pressure (**Figure 57**). Scatter of cake resistances for varying organic solvents was bigger but no clear correlation of cake resistances with either the characteristics of the organic solvents or the experimentally determined Sauter mean diameters was found. In this first modeling approach (cf. **Eq. (27)** combined with **Eq. (29)**), constant mean cake resistances obtained from filtration experiments using 1-dodecene at room temperature were used for the model fit ($3.07 \cdot 10^{13}$ m^{-1} for HDK®H20 and $2.23 \cdot 10^{13}$ m^{-1} for HDK®H2000 stabilized PEs).

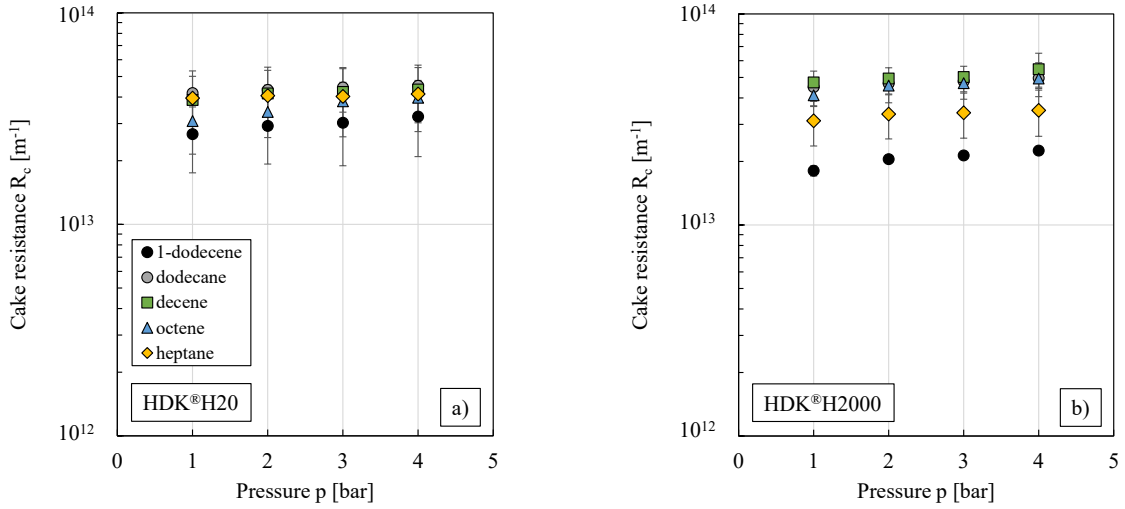

Figure 57. Cake resistance against pressure of "standard" w/o PEs prepared using different organic solvents and stabilized by **(a)** HDK®H20 or **(b)** HDK®H2000. Error bars represent the standard deviation. Where not visible, error bars are smaller than the symbol size. Adapted from [VI].

Deviations between modeled and experimental values for emulsions stabilized by either HDK®H20 or HDK®H2000 particles were smaller than 20% and a slight overestimation of flux was observed (**Figure 58**). Considering the simplified assumptions made, the results can be rated as good. The experimental results (flux against pressure) as well as the results from the model fit and model prediction are shown in **Figure 85** (appendix).

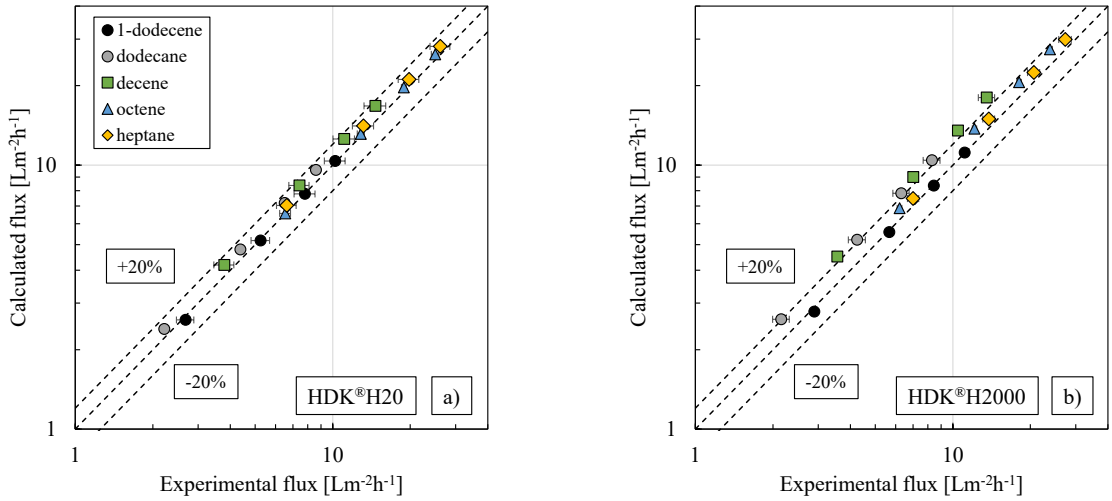

Figure 58. Parity plot for w/o PE fluxes (prepared using different organic solvents) with the modeled values against the experimental data. A combination of the solution-diffusion and the resistance in series model was used. For the model fit (**Eq. (27)** combined with **Eq. (29)**), the experimental results of 1-dodecene at room temperature were used. **(a)** HDK®H20 and **(b)** HDK®H2000 stabilized PEs. All experiments were conducted at least in duplicate and mean values are shown. Error bars represent the standard deviation. Where not visible, error bars are smaller than the symbol size. Adapted from [VI].

5.4.4 Conclusions

A mathematical model to describe the filtration of w/o PEs was developed for the first time. Cake resistances were (almost) independent of pressure, temperature and the type of organic solvent. The membrane itself was incompressible within the experimentally investigated pressure range, but the membrane resistance depended on the diffusion coefficient. Pure solvent fluxes were predicted with great accuracy using the solution-diffusion model (deviations between experimental and calculated fluxes lower than 10%). The temperature dependency of the diffusion coefficient was modeled via an Arrhenius-type relationship, while the diffusion coefficient for the different organic solvents was modeled via a linear correlation with the reciprocal of the molar mass. Combining this solution-diffusion model with a resistance in series model yielded a model for w/o PE filtration (deviations between experimental and calculated fluxes lower than 20%). Another advantage of the developed model is that it can easily be applied in practice, as only a limited number of filtration experiments is necessary – namely, filtration experiments with (two) organic solvents (at three temperatures) and only one PE filtration experiment (for each particle type).

The results obtained in this section are indispensable for a model-based optimal process design for PE application in continuous catalytic L/L multiphase systems.

6 Summary and Outlook

Pickering emulsion filtration for phase separation as well as efficient catalyst and additives recycling in the PE assisted interfacial catalysis was proven to be a promising procedure to enable economically feasible and continuous processes. It is a very robust procedure (in the investigated range) for the (single stage) mechanical separation of the catalyst containing dispersed phase drops and the continuous organic (product containing) phase with broad operation windows and a large optimization potential. For a complete understanding of the filtration process, a detailed characterization of the Pickering emulsions was essential. Knowledge about the drop size distribution and residual particles is indispensable as these constitute the filter cake. Exact knowledge about the rheological behavior is necessary in terms of, e.g., mixing, pumping or stirring. Therefore, the PE preparation procedure and physico-chemical properties (stability, DSD, rheological behavior) were investigated. The operating conditions and the emulsion composition were varied. This thesis systematically addressed the membrane filtration of PEs using selected membrane types. The main influencing factors on PE filtration were identified and, for the first time, a transport model to describe the filtration of w/o PEs was developed. The three questions elaborated in **Chapter 2**, which have been examined in detail in the context of this thesis, will be briefly answered in the following.

How do preparation conditions and PE composition influence the characteristic PE properties?
To the best of our knowledge, no empirical correlations to describe the impact of preparation process conditions on, e.g., drop size distributions, existed so far. The impact of homogenization conditions using two different heads of a rotor-stator device on the properties of w/o PEs of constant composition (stabilized by gelling particles) was systematically investigated. Depending on the dispersing head either the "interface generation capacity" (i.e., the power input) or the "coverage capacity" (i.e., the particle mass fraction) determined the drop size distribution while in the latter case a limiting minimum Sauter mean diameter was obtained. The results of the two dispersing heads could be best correlated using a power law and the "shear rate" during PE preparation (defined as the ratio of the tip speed and the respective gap width between the rotor and the stator). This correlation now allows the prediction of the "shear rate" (and thus tip speed for a given device) to prepare PEs with tailored drop sizes. For increasing "shear rates" the dynamic viscosity passed through a minimum leading to the assumption that both, the amount of unbound silica particles (i.e., network formation) and the drop size distribution (i.e., stiffening of drops) have an impact on the emulsion viscosity. Based on these investigations, the following homogenization conditions were chosen for all further studies: S25N-18G dispersing head, 17,500 min^{-1} / 2 min without particle pre-dispersion in the continuous phase in a sonication bath prior to the actual PE preparation.

The analysis of the PE composition was based on a broad knowledge from literature and was in good agreement with published results. More hydrophobic silica particles led to larger Sauter mean diameters and smaller dynamic viscosities, while the specific particle surface area only had a minor impact. Higher particle mass fractions led to smaller drop sizes and higher dynamic viscosities. An increase of the dispersed phase fraction led to an increase of the Sauter mean diameter and the dynamic viscosity. Particles of intermediate hydrophobicity showed shear thinning rheological behavior and oscillatory measurements proved their feasibility to form three-dimensional network structures. More hydrophobic silica particles (with a higher tamped density) showed a Newtonian flow behavior without gelling properties. This was also proven in analytical centrifugation experiments on the packing densities of the "filter cakes" in collaboration with LUM GmbH.

What are the main influencing parameters on w/o PE filtration using UF and OSN membranes?
Due to the novelty of Pickering emulsion filtration, suitable membranes were screened and interactions between the membrane, particles and the solvent were characterized. Significantly different results of the PE filtration behavior were observed for the ultrafiltration membrane ETNA01PP and the organic solvent nanofiltration membrane oNF-3 despite their similar MWCO.

To apply the ETNA01PP membrane in organic solvents (originally designed for its application in aqueous systems) and to diminish the unexpected disproportionate increase of flux with pressure, a specialized membrane pre-treatment by a gradual solvent exchange was elaborated. The contact of the silica particles with the membrane led to an increased membrane hydrophobicity. During filtration, particles with gelling properties were able to form a highly porous gel layer on the membrane surface. This additional resistance was outweighed by the increase in membrane wettability and fluxes of suspensions

and w/o PEs were higher than pure solvent fluxes. Particles with non-gelling properties formed a dense filter cake, leading to a flux decline. Filtration of o/w PEs was successful and PE fluxes were close to those of pure water. No specialized membrane pre-treatment was necessary and the reproducibility of the filtration performance was much better than in the case of organic solvents.

The oNF-3 membrane showed a great reproducibility of the filtration behavior, the expected linear increase of flux with pressure, lower fluxes for w/o PEs compared to the pure solvent and no specialized membrane pre-treatment was necessary. This membrane type was used to systematically investigate the impact of varying PE compositions and operating conditions on the filtration behavior. The main influencing parameters were the transmembrane pressure, the temperature and the type of organic solvent. The stirrer speed within the filtration cell only became important when particles without gelling properties were used in long-term filtration experiments. Neither the drop size distribution nor the dispersed phase fraction had a significant impact on the filtration performance allowing the filtration of concentrated PEs in small reactors which is beneficial in terms of process intensification.

Which modeling approaches are suited to describe the filtration of w/o PEs?
A suitable transport model to describe the permeation of solvent through the membrane – which is essential for process design (membrane surface area) and optimization (temperatures and pressures) – was developed for the first time. Pure solvent fluxes – either under variation of temperature or organic solvent type – were modeled via the solution-diffusion model with high accuracy (deviations between experimental and calculated fluxes < 10%). The temperature dependency of the diffusion coefficient was described via an Arrhenius-type relationship while the diffusion coefficient for the different solvents was linearly correlated with the reciprocal of the molar mass. Cake resistances were almost independent of pressure, temperature, solvent and particle type. The filtration of w/o PEs was successfully modeled by combining the solution-diffusion model with a resistance in series model (deviations between experimental and calculated fluxes < 20%). As only very few filtration experiments were necessary for the model fit, the developed model is of great practical applicability.

In future works, the interactions between the nanoparticles (silica as well as other materials), the solvent and different membrane types should be investigated in more detail by using swelling experiments, contact angle measurements or SEM and TEM of the membrane surface and the membrane cross-section. As shown in this thesis, different membranes showed significant differences in the qualitative and quantitative filtration performance, specific interactions with the particles and in some cases a specified membrane pre-treatment was necessary. Therefore, (in-house) membranes with tailored properties should be tested to promote the physical understanding of the underlying phenomena even further.

The robust filtration behavior of the oNF-3 membrane enables the optimization of the PEs to meet the needs of the reaction (e.g., particle type and concentration, catalyst). As, e.g., hydroformylation reactions are typically performed at higher temperatures and pressures and the retentate is to be returned to the reactor, cooling costs should be as low as possible. PE filtration at higher temperatures was therefore investigated and modeled in this thesis. Future work should include higher pressures and (real) crossflow filtration. A transferability of the developed model to these changed operating conditions and modes as well as different membranes must be examined. For crossflow operation, the pumpability of different PEs needs to be determined. In addition, the system is probably extendable to other (bio-)chemical reactions. If the pressure and temperature applied during the reaction are compatible with the membrane material, the filtration can even be integrated into the reactor. Focus should also be laid on long-term operation to investigate the membrane performance and the PE stability.

Furthermore, it would be interesting to track the drop size distribution and the formation of the filter cake on-line. Different in-situ monitoring techniques, e.g., DOTM (direct observation through the membrane) exist and allow the observation of, e.g., droplet attachment onto the membrane or droplet coalescence on the membrane surface. Since significantly different operating conditions are required for this type of experiment (e.g., very low dispersed phase fraction, low crossflow velocity), the transferability of these results must be verified.

In summary, this thesis has advanced the knowledge about the properties of Pickering emulsions and their influence on the filtration behavior under various process conditions and thus helps to pave the way towards a genuine continuous reaction and filtration system.

References

[1] Abdellah MH, Scholes CA, Freeman BD, Liu L, Kentish SE (2018) Transport of terpenes through composite PDMS/PAN solvent resistant nanofiltration membranes. Sep Purif Technol 207:470–476. doi: 10.1016/j.seppur.2018.06.074

[2] Abdullayev E, Lvov Y (2013) Halloysite clay nanotubes as a ceramic "skeleton" for functional biopolymer composites with sustained drug release. J Mater Chem B 1:2894–2903. doi: 10.1039/c3tb20059k

[3] Abend S, Lagaly G (2001) Bentonite and double hydroxides as emulsifying agents. Clay Miner 36:557–570. doi: 10.1180/0009855013640009

[4] Abismaïl B, Canselier JP, Wilhelm AM, Delmas H, Gourdon C (1999) Emulsification by ultrasound: droplet size distribution and stability. Ultrason Sonochem 6:75–83. doi: 10.1016/S1350-4177(98)00027-3

[5] Albert C, Beladjine M, Tsapis N, Fattal E, Agnely F, Huang N (2019) Pickering emulsions: Preparation processes, key parameters governing their properties and potential for pharmaceutical applications. J Control Release 309:302–332. doi: 10.1016/j.jconrel.2019.07.003

[6] Alfa Laval Corporate AB (2020) Alfa Laval UF flat sheet membranes. Flat sheet membranes for ultrafiltration - FS, UFX, RC and ETNA types

[7] Alfa Laval Corporate AB (2020) Alfa Laval UF-pHt flat sheet membranes. Flat sheet membranes for ultrafiltration - GR types

[8] Alfa Laval Corporate AB (2020) Flat sheet membranes. Alfa Laval ultrafiltration membranes - PP series

[9] Anastas P, Eghbali N (2010) Green chemistry: Principles and Practice. Chem Soc Rev 39:301–312. doi: 10.1039/b918763b

[10] Anastas P, Warner JC (1998) Green Chemistry: Theory and Practice. Oxford University Press

[11] Arditty S, Schmitt V, Lequeux F, Leal-Calderon F (2005) Interfacial properties in solid-stabilized emulsions. Eur Phys J B 44:381–393. doi: 10.1140/epjb/e2005-00137-0

[12] Arditty S, Whitby CP, Binks BP, Schmitt V, Leal-Calderon F (2003) Some general features of limited coalescence in solid-stabilized emulsions. Eur Phys J E 11:273–281. doi: 10.1140/epje/i2003-10018-6

[13] Ashby NP, Binks BP (2000) Pickering emulsions stabilised by Laponite clay particles. Phys Chem Chem Phys 2:5640–5646. doi: 10.1039/b007098j

[14] Aveyard R, Binks BP, Clint JH (2003) Emulsions stabilised solely by colloidal particles. Adv Colloid Interface Sci 100–102:503–546. doi: 10.1016/S0001-8686(02)00069-6

[15] Bacon J, Rielly C, Özcan-Taşkin NG (2018) Break up of silica nanoparticle clusters using ultrasonication. In: Presented at the 16th European Conference on Mixing (Mixing 16). Toulouse, France

[16] Bae T-H, Kim I-C, Tak T-M (2006) Preparation and characterization of fouling-resistant TiO_2 self-assembled nanocomposite membranes. J Membr Sci 275:1–5. doi: 10.1016/j.memsci.2006.01.023

[17] Bae T-H, Tak T-M (2005) Effect of TiO_2 nanoparticles on fouling mitigation of ultrafiltration membranes for activated sludge filtration. J Membr Sci 249:1–8. doi: 10.1016/j.memsci.2004.09.008

[18] Bago Rodriguez AM, Binks BP (2020) Catalysis in Pickering emulsions. Soft Matter 16:10221–10243. doi: 10.1039/d0sm01636e

[19] Bałdyga J, Bourne JR, Pacek AW, Amanullah A, Nienow AW (2001) Effects of agitation and scale-up on drop size in turbulent dispersions: allowance for intermittency. Chem Eng Sci 56:3377–3385. doi: 10.1016/S0009-2509(01)00027-6

[20] Bałdyga J, Makowski Ł, Orciuch W, Sauter C, Schuchmann HP (2008) Deagglomeration processes in high-shear devices. Chem Eng Res Des 86:1369–1381. doi: 10.1016/j.cherd.2008.08.016

[21] Barman S, Christopher GF (2014) Simultaneous interfacial rheology and microstructure measurement of densely aggregated particle laden interfaces using a modified double wall ring interfacial rheometer. Langmuir 30:9752–9760. doi: 10.1021/la502329s

[22] Barthel H (1995) Surface interactions of dimethylsiloxy group-modified fumed silica. Colloids Surf A Physicochem Eng Asp 101:217–226. doi: 10.1016/0927-7757(95)03179-H

[23] Behrend O, Ax K, Schubert H (2000) Influence of continuous phase viscosity on emulsification by ultrasound. Ultrason Sonochem 7:77–85. doi: 10.1016/S1350-4177(99)00029-2

[24] Berton-Carabin CC, Schroën K (2015) Pickering emulsions for food applications: background, trends, and challenges. Annu Rev Food Sci Technol 6:263–297. doi: 10.1146/annurev-food-

081114-110822
[25] Bianga J, Künnemann KU, Gaide T, Vorholt AJ, Seidensticker T, Dreimann JM, Vogt D (2019) Thermomorphic multiphase systems: switchable solvent mixtures for the recovery of homogeneous catalysts in batch and flow processes. Chem Eur J 25:11586–11608. doi: 10.1002/chem.201902154
[26] Binks BP (2002) Particles as surfactants - similarities and differences. Curr Opin Colloid Interface Sci 7:21–41. doi: 10.1016/S1359-0294(02)00008-0
[27] Binks BP, Clint JH (2002) Solid wettability from surface energy components: relevance to Pickering emulsions. Langmuir 18:1270–1273. doi: 10.1021/la011420k
[28] Binks BP, Clint JH, Whitby CP (2005) Rheological behavior of water-in-oil emulsions stabilized by hydrophobic bentonite particles. Langmuir 21:5307–5316. doi: 10.1021/la050255w
[29] Binks BP, Fletcher PDI, Holt BL, Parker J, Beaussoubre P, Wong K (2010) Drop sizes and particle coverage in emulsions stabilised solely by silica nanoparticles of irregular shape. Phys Chem Chem Phys 12:11967–11974. doi: 10.1039/c0cp00581a
[30] Binks BP, Horozov TS (2006) Colloidal particles at liquid interfaces, 1st ed. Cambridge University Press
[31] Binks BP, Lumsdon SO (1999) Stability of oil-in-water emulsions stabilised by silica particles. Phys Chem Chem Phys 1:3007–3016. doi: 10.1039/A902209K
[32] Binks BP, Lumsdon SO (2000) Influence of particle wettability on the type and stability of surfactant-free emulsions. Langmuir 16:8622–8631. doi: 10.1021/la000189s
[33] Binks BP, Lumsdon SO (2000) Transitional phase inversion of solid-stabilized emulsions using particle mixtures. Langmuir 16:3748–3756. doi: 10.1021/la991427q
[34] Binks BP, Lumsdon SO (2000) Effects of oil type and aqueous phase composition on oil-water mixtures containing particles of intermediate hydrophobicity. Phys Chem Chem Phys 2:2959–2967. doi: 10.1039/b002582h
[35] Binks BP, Lumsdon SO (2000) Catastrophic phase inversion of water-in-oil emulsions stabilized by hydrophobic silica. Langmuir 16:2539–2547. doi: 10.1021/la991081j
[36] Binks BP, Lumsdon SO (2001) Pickering emulsions stabilized by monodisperse latex: effect of particle size. Langmuir 17:4540–4547. doi: 10.1021/la0103822
[37] Binks BP, Philip J, Rodrigues JA (2005) Inversion of silica-stabilized emulsions induced by particle concentration. Langmuir 21:3296–3302. doi: 10.1021/la046915z
[38] Binks BP, Rodrigues JA (2003) Types of phase inversion of silica particle stabilized emulsions containing triglyceride oil. Langmuir 19:4905–4912. doi: 10.1021/la020960u
[39] Binks BP, Rodrigues JA (2005) Inversion of emulsions stabilized solely by ionizable nanoparticles. Angew Chemie - Int Ed 44:441–444. doi: 10.1002/anie.200461846
[40] Binks BP, Whitby CP (2004) Silica particle-stabilized emulsions of silicone oil and water: aspects of emulsification. Langmuir 20:1130–1137. doi: 10.1021/la0303557
[41] Binks BP, Whitby CP (2005) Nanoparticle silica-stabilised oil-in-water emulsions: improving emulsion stability. Colloids Surf A Physicochem Eng Asp 253:105–115. doi: 10.1016/j.colsurfa.2004.10.116
[42] Binks BP, Yin D (2016) Pickering emulsions stabilized by hydrophilic nanoparticles: in situ surface modification by oil. Soft Matter 12:6858–6867. doi: 10.1039/c6sm01214k
[43] Björkegren S, Nordstierna L, Törncrona A, Palmqvist A (2017) Hydrophilic and hydrophobic modifications of colloidal silica particles for Pickering emulsions. J Colloid Interface Sci 487:250–257. doi: 10.1016/j.jcis.2016.10.031
[44] Bliatsiou C, Malik A, Böhm L, Kraume M (2019) Influence of impeller geometry on hydromechanical stress in stirred liquid/liquid dispersions. Ind Eng Chem Res 58:2537–2550. doi: 10.1021/acs.iecr.8b03654
[45] Blumenschein S (2017) Application of organic solvent nanofiltration for multi-purpose production. Technische Universität Dortmund
[46] BORSIG Membrane Technology GmbH (2019) Liquid separation. Organic solvent nanofiltration. Membrane data sheet oNF-3
[47] BORSIG Membrane Technology GmbH (2021) Liquid separation. Organic solvent nanofiltration. Membrane data sheet oNF-1
[48] BORSIG Membrane Technology GmbH (2021) Liquid separation. Organic solvent nanofiltration. Membrane data sheet oNF-2
[49] Bresme F, Oettel M (2007) Nanoparticles at fluid interfaces. J Phys Condens Matter 19. doi: 10.1088/0953-8984/19/41/413101
[50] Van der Bruggen B, Geens J, Vandecasteele C (2002) Fluxes and rejections for nanofiltration with solvent stable polymeric membranes in water, ethanol and n-hexane. Chem Eng Sci 57:2511–2518. doi: 10.1016/S0009-2509(02)00125-2

[51] Brunsch Y, Behr A (2013) Temperature-controlled catalyst recycling in homogeneous transition-metal catalysis: minimization of catalyst leaching. Angew Chemie - Int Ed 52:1586–1589. doi: 10.1002/anie.201208667
[52] Cao G, Wang Y, Wang C, Ho SH (2019) A dually prewetted membrane for continuous filtration of water-in-light oil, oil-in-water, and water-in-heavy oil multiphase emulsion mixtures. J Mater Chem A 7:11305–11313. doi: 10.1039/c9ta01889a
[53] Cao X, Ma J, Shi X, Ren Z (2006) Effect of TiO_2 nanoparticle size on the performance of PVDF membrane. Appl Surf Sci 253:2003–2010. doi: 10.1016/j.apsusc.2006.03.090
[54] Chen J, Vogel R, Werner S, Heinrich G, Clausse D, Dutschk V (2011) Influence of the particle type on the rheological behavior of Pickering emulsions. Colloids Surf A Physicochem Eng Asp 382:238–245. doi: 10.1016/j.colsurfa.2011.02.003
[55] Chen W, Liu X, Liu Y, Bang Y, Kim H-I (2011) Preparation of O/W Pickering emulsion with oxygen plasma treated carbon nanotubes as surfactants. J Ind Eng Chem 17:455–460. doi: 10.1016/j.jiec.2010.10.027
[56] Chesters AK (1991) The modelling of coalescence processes in fluid-liquid dispersions: A review of current understanding. Chem Eng Res Des 69:259–227
[57] Chevalier Y, Bolzinger MA (2013) Emulsions stabilized with solid nanoparticles: Pickering emulsions. Colloids Surf A Physicochem Eng Asp 439:23–34. doi: 10.1016/j.colsurfa.2013.02.054
[58] Darvishmanesh S, Buekenhoudt A, Degrève J, Van der Bruggen B (2009) General model for prediction of solvent permeation through organic and inorganic solvent resistant nanofiltration membranes. J Membr Sci 334:43–49. doi: 10.1016/j.memsci.2009.02.013
[59] Darvishmanesh S, Degrè J, Bruggen B Van Der (2010) Performance of solvent-pretreated polyimide nanofiltration membranes for separation of dissolved dyes from toluene. Ind Eng Chem Res 49:9330–9338. doi: 10.1021/ie101050k
[60] Davies JT (1987) A physical interpretation of drop sizes in homogenizers and agitated tanks, including the dispersion of viscous oils. Chem Eng Sci 42:1671–1676. doi: 10.1016/0009-2509(87)80172-0
[61] Deshmukh OS, Van Den Ende D, Stuart MC, Mugele F, Duits MHG (2015) Hard and soft colloids at fluid interfaces: Adsorption, interactions, assembly & rheology. Adv Colloid Interface Sci 222:215–227. doi: 10.1016/j.cis.2014.09.003
[62] Destribats M, Gineste S, Laurichesse E, Tanner H, Leal-Calderon F, Héroguez V, Schmitt V (2014) Pickering emulsions: What are the main parameters determining the emulsion type and interfacial properties? Langmuir 30:9313–9326. doi: 10.1021/la501299u
[63] Destribats M, Lapeyre V, Wolfs M, Sellier E, Leal-Calderon F, Ravaine V, Schmitt V (2011) Soft microgels as Pickering emulsion stabilisers: Role of particle deformability. Soft Matter 7:7689–7698. doi: 10.1039/c1sm05240c
[64] Ding M, Zhang T, Zhang H, Tao N, Wang X, Zhong J (2019) Effect of preparation factors and storage temperature on fish oil-loaded crosslinked gelatin nanoparticle Pickering emulsions in liquid forms. Food Hydrocoll 95:326–335. doi: 10.1016/j.foodhyd.2019.04.052
[65] Dobrak-Van Berlo A, Vankelecom IFJ, Van der Bruggen B (2011) Parameters determining transport mechanisms through unfilled and silicalite filled PDMS-based membranes and dense PI membranes in solvent resistant nanofiltration: Comparison with pervaporation. J Membr Sci 374:138–149. doi: 10.1016/j.memsci.2011.03.027
[66] Dreimann JM, Hoffmann F, Skiborowski M, Behr A, Vorholt AJ (2017) Merging thermomorphic solvent systems and organic solvent nanofiltration for hybrid catalyst recovery in a hydroformylation process. Ind Eng Chem Res 56:1354–1359. doi: 10.1021/acs.iecr.6b04249
[67] Dudchenko AV, Rolf J, Shi L, Olivas L, Duan W, Jassby D (2015) Coupling underwater superoleophobic membranes with magnetic Pickering emulsions for fouling-free separation of crude oil/water mixtures: an experimental and theoretical study. ACS Nano 9:9930–9941. doi: 10.1021/acsnano.5b04880
[68] Duffus LJ, Norton JE, Smith P, Norton IT, Spyropoulos F (2016) A comparative study on the capacity of a range of food-grade particles to form stable O/W and W/O Pickering emulsions. J Colloid Interface Sci 473:9–21. doi: 10.1016/j.jcis.2016.03.060
[69] Dugyala VR, Daware SV, Basavaraj MG (2013) Shape anisotropic colloids: synthesis, packing behavior, evaporation driven assembly, and their application in emulsion stabilization. Soft Matter 9:6711–6725. doi: 10.1039/c3sm50404b
[70] Evonik Resource Efficiency GmbH (2017) Instruction for use PuraMem®Selective, Performance, Flux - Flat Sheet
[71] Evonik Resource Efficiency GmbH (2017) Instruction for use DuraMem®Membrane Flat Sheet
[72] Ezzati A, Gorouhi E, Mohammadi T (2005) Separation of water in oil emulsions using

microfiltration. Desalination 185:371–382. doi: 10.1016/j.desal.2005.03.086
[73] Favre E (1996) Swelling of crosslinked polydimethylsiloxane networks by pure solvents: Influence of temperature. Eur Polym J 32:1183–1188. doi: 10.1016/S0014-3057(96)00062-6
[74] Fedors RF (1974) A method for estimating both the solubility parameters and molar volumes of liquids. Polym Eng Sci 14:472–472. doi: 10.1002/pen.760140611
[75] Fierro D, Boschetti-de-Fierro A, Abetz V (2012) The solution-diffusion with imperfections model as a method to understand organic solvent nanofiltration of multicomponent systems. J Membr Sci 413–414:91–101. doi: 10.1016/j.memsci.2012.04.027
[76] Fournier C-O, Fradette L, Tanguy PA (2009) Effect of dispersed phase viscosity on solid stabilized emulsions. Chem Eng Res Des 87:499–506. doi: 10.1016/j.cherd.2008.11.008
[77] Frelichowska J, Bolzinger MA, Chevalier Y (2009) Pickering emulsions with bare silica. Colloids Surf A Physicochem Eng Asp 343:70–74. doi: 10.1016/j.colsurfa.2009.01.031
[78] Frelichowska J, Bolzinger MA, Chevalier Y (2010) Effects of solid particle content on properties of o/w Pickering emulsions. J Colloid Interface Sci 351:348–356. doi: 10.1016/j.jcis.2010.08.019
[79] Gaide T, Behr A, Arns A, Benski F, Vorholt AJ (2016) Hydroesterification of methyl 10-undecenoate in thermomorphic multicomponent solvent systems - Process development for the synthesis of sustainable polymer precursors. Chem Eng Process 99:197–204. doi: 10.1016/j.cep.2015.07.009
[80] Gao N, Fan Y, Quan X, Cai Y, Zhou D (2016) Modified ceramic membranes for low fouling separation of water-in-oil emulsions. J Mater Sci 51:6379–6388. doi: 10.1007/s10853-016-9934-3
[81] Gao Z, Zhao J, Huang Y, Yao X, Zhang K, Fang Y, Nishinari K, Phillips GO, Jiang F, Yang H (2017) Edible Pickering emulsion stabilized by protein fibrils. Part 1: Effects of pH and fibrils concentration. LWT - Food Sci Technol 76:1–8. doi: 10.1016/j.lwt.2016.10.038
[82] Gautier F, Destribats M, Perrier-Cornet R, Dechezelles J-F, Giermanska J, Heroguez V, Ravaine S, Leal-Calderon F, Schmitt V (2007) Pickering emulsions with stimulable particles: from highly- to weakly-covered interfaces. Phys Chem Chem Phys 9:6455–6462. doi: 10.1039/b710226g
[83] Geens J, Van der Bruggen B, Vandecasteele C (2004) Characterisation of the solvent stability of polymeric nanofiltration membranes by measurement of contact angles and swelling. Chem Eng Sci 59:1161–1164. doi: 10.1016/j.ces.2004.01.003
[84] Giorno L, Mazzei R, Oriolo M, De Luca G, Davoli M, Drioli E (2005) Effects of organic solvents on ultrafiltration polyamide membranes for the preparation of oil-in-water emulsions. J Colloid Interface Sci 287:612–623. doi: 10.1016/j.jcis.2005.02.015
[85] Glotzer SC, Solomon MJ (2007) Anisotropy of building blocks and their assembly into complex structures. Nat Mater 6:557–562. doi: 10.1038/nmat1949
[86] Gonzalez Ortiz D, Pochat-Bohatier C, Cambedouzou J, Bechelany M, Miele P (2020) Current trends in Pickering emulsions: particle morphology and applications. Engineering 6:468–482. doi: 10.1016/j.eng.2019.08.017
[87] Gupta R, Rousseau D (2012) Surface-active solid lipid nanoparticles as Pickering stabilizers for oil-in-water emulsions. Food Funct 3:302–311. doi: 10.1039/c2fo10203j
[88] Hall S, Cooke M, Pacek AW, Kowalski AJ, Rothman D (2011) Scaling up of silverson rotor-stator mixers. Can J Chem Eng 89:1040–1050. doi: 10.1002/cjce.20556
[89] Hall S, Pacek AW, Kowalski AJ, Cooke M, Rothman D (2013) The effect of scale and interfacial tension on liquid-liquid dispersion in in-line Silverson rotor-stator mixers. Chem Eng Res Des 91:2156–2168. doi: 10.1016/j.cherd.2013.04.021
[90] Harogoppad SB, Aminabhavi TM (1991) Diffusion and sorption of organic liquids through polymer membranes. 5. Neoprene, styrene-butadiene-rubber, ethylene-propylene-diene terpolymer, and natural rubber versus hydrocarbons (C_8-C_{16}). Macromolecules 24:2598–2605. doi: 10.1021/ma00009a070
[91] Hassan N, Stocco A, Abou-Hassan A (2015) Droplet liquid/liquid interfaces generated in a microfluidic device for assembling Janus inorganic nanohybrids. J Phys Chem C 119:10758–10765. doi: 10.1021/acs.jpcc.5b02527
[92] Haumann M, Koch H, Hugo P, Schomäcker R (2002) Hydroformylation of 1-dodecene using Rh-TPPTS in a microemulsion. Appl Catal A Gen 225:239–249. doi: 10.1016/S0926-860X(01)00869-9
[93] He Y, Wu F, Sun X, Li R, Guo Y, Li C, Zhang L, Xing F, Wang W, Gao J (2013) Factors that affect Pickering emulsions stabilized by graphene oxide. ACS Appl Mater Interfaces 5:4843–4855. doi: 10.1021/am400582n
[94] Heyse A, Kraume M, Drews A (2020) The impact of lipases on the rheological behavior of colloidal silica nanoparticle stabilized Pickering emulsions for biocatalytical applications. Colloids Surf B Biointerfaces 185:110580. doi: 10.1016/j.colsurfb.2019.110580
[95] Heyse A, Plikat C, Ansorge-Schumacher M, Drews A (2019) Continuous two-phase biocatalysis

using water-in-oil Pickering emulsions in a membrane reactor: Evaluation of different nanoparticles. Catal Today 331:60–67. doi: 10.1016/j.cattod.2017.11.032
[96] Heyse A, Plikat C, Grün M, Delaval S, Ansorge-Schumacher M, Drews A (2018) Impact of enzyme properties on drop size distribution and filtration of water-in-oil Pickering emulsions for application in continuous biocatalysis. Process Biochem 72:86–95. doi: 10.1016/j.procbio.2018.06.018
[97] Hohl L (2018) Dispersion and phase separation in liquid multiphase systems: Influence of three phase conditions on drop size distributions. Technische Universität Berlin
[98] Hohl L, Röder V, Kraume M (2019) Dispersion and phase separation of water-oil-amphiphile systems in stirred tanks. Chem Eng Technol 42:1574–1586. doi: 10.1002/ceat.201800743
[99] Hohl L, Röhl S, Stehl D, von Klitzing R, Kraume M (2016) Influence of nanoparticles and drop size distributions on the rheology of w/o Pickering emulsions. Chem Ing Tech 88:1815–1826. doi: 10.1002/cite.201600063
[100] Horozov TS, Binks BP (2006) Particle-stabilized emulsions: a bilayer or a bridging monolayer? Angew Chemie 118:787–790. doi: 10.1002/ange.200503131
[101] Hu B, Scott K (2008) Microfiltration of water in oil emulsions and evaluation of fouling mechanism. Chem Eng J 136:210–220. doi: 10.1016/j.cej.2007.04.003
[102] Hu MZ, Bischoff BL, Morales-Rodriguez ME, Gray KA, Davison BH (2019) Superhydrophobic or hydrophilic porous metallic/ceramic tubular membranes for continuous separations of biodiesel-water W/O and O/W emulsions. Ind Eng Chem Res 58:1114–1122. doi: 10.1021/acs.iecr.8b04888
[103] Hu YT, Ting Y, Hu JY, Hsieh SC (2017) Techniques and methods to study functional characteristics of emulsion systems. J Food Drug Anal 25:16–26. doi: 10.1016/j.jfda.2016.10.021
[104] IKA-Werke GmbH & Co. KG (2019) Data sheet T25 digital ULTRA-TURRAX
[105] IKA-Werke GmbH & Co. KG (2019) Data sheet dispersing element S25N-10G
[106] IKA-Werke GmbH & Co. KG (2019) Data sheet dispersing element S25N-18G
[107] Jansen JC, Darvishmanesh S, Tasselli F, Bazzarelli F, Bernardo P, Tocci E, Friess K, Randova A, Drioli E, Van der Bruggen B (2013) Influence of the blend composition on the properties and separation performance of novel solvent resistant polyphenylsulfone/polyimide nanofiltration membranes. J Membr Sci 447:107–118. doi: 10.1016/j.memsci.2013.07.009
[108] Jimenez Solomon MF, Bhole Y, Livingston AG (2012) High flux membranes for organic solvent nanofiltration (OSN) - Interfacial polymerization with solvent activation. J Membr Sci 423–424:371–382. doi: 10.1016/j.memsci.2012.08.030
[109] Kamaly SW, Tarleton AC, Özcan-Taşkın NG (2017) Dispersion of clusters of nanoscale silica particles using batch rotor-stators. Adv Powder Technol 28:2357–2365. doi: 10.1016/j.apt.2017.06.017
[110] Kang G-D, Cao Y-M (2014) Application and modification of poly(vinylidene fluoride) (PVDF) membranes - A review. J Membr Sci 463:145–165. doi: 10.1016/j.memsci.2014.03.055
[111] Karcher V, Perrechil FA, Bannwart AC (2015) Interfacial energy during the emulsification of water-in-heavy crude oil emulsions. Brazilian J Chem Eng 32:127–137. doi: 10.1590/0104-6632.20150321s00002696
[112] Katepalli H, John VT, Tripathi A, Bose A (2017) Microstructure and rheology of particle stabilized emulsions: Effects of particle shape and inter-particle interactions. J Colloid Interface Sci 485:11–17. doi: 10.1016/j.jcis.2016.09.015
[113] von Klitzing R, Stehl D, Pogrzeba T, Schomäcker R, Minullina R, Panchal A, Konnova S, Fakhrullin R, Koetz J, Möhwald H, Lvov Y (2017) Halloysites stabilized emulsions for hydroformylation of long chain olefins. Adv Mater Interfaces 4:1600435. doi: 10.1002/admi.201600435
[114] Köhler K, Santana AS, Braisch B, Preis R, Schuchmann HP (2010) High pressure emulsification with nano-particles as stabilizing agents. Chem Eng Sci 65:2957–2964. doi: 10.1016/j.ces.2010.01.020
[115] Kraume M (2012) Transportvorgänge in der Verfahrenstechnik, 2nd ed. Springer-Verlag, Berlin
[116] Kraume M (2013) Integrierte chemische Prozesse in flüssigen Mehrphasensystemen. Chem Ing Tech 85:1499–1511. doi: 10.1002/cite.201300013
[117] Kraume M, Gäbler A, Schulze K (2004) Influence of physical properties on drop size distributions of stirred liquid-liquid dispersions. Chem Eng Technol 27:330–334. doi: 10.1002/ceat.200402006
[118] Lam S, Velikov KP, Velev OD (2014) Pickering stabilization of foams and emulsions with particles of biological origin. Curr Opin Colloid Interface Sci 19:490–500. doi: 10.1016/j.cocis.2014.07.003
[119] Lee JN, Park C, Whitesides GM (2003) Solvent compatibility of poly(dimethylsiloxane)-based

microfluidic devices. Anal Chem 75:6544–6554. doi: 10.1021/ac0346712
[120] van Leeuwen PWNM, Claver C (2002) Rhodium catalyzed hydroformylation, 22nd ed. Kluwer Academic Publishers, New York
[121] Leitner L, Harscoat-Schiavo C, Kapel R, Vallieres C (2014) Organic solvent nanofiltration with a Poly(dimethylsiloxane) membrane: Parameters affecting its sieving properties. J Appl Polym Sci 131. doi: 10.1002/app.41171
[122] Lerche D, Miller R, Schäffler M (2015) Dispersionseigenschaften - 2D-Rheologie, 3D-Rheologie, Stabilität, 1st ed. Own publishing, Berlin
[123] Lerche D, Sobisch T (2007) Consolidation of concentrated dispersions of nano- and microparticles determined by analytical centrifugation. Powder Technol 174:46–49. doi: 10.1016/j.powtec.2006.10.020
[124] Li J-H, Xu Y-Y, Zhu L-P, Wang J-H, Du C-H (2009) Fabrication and characterization of a novel TiO_2 nanoparticle self-assembly membrane with improved fouling resistance. J Membr Sci 326:659–666. doi: 10.1016/j.memsci.2008.10.049
[125] Lim S, Horiuchi H, Nikolov AD, Wasan D (2015) Nanofluids alter the surface wettability of solids. Langmuir 31:5827–5835. doi: 10.1021/acs.langmuir.5b00799
[126] Liu C, Li M, Liang C, Wang W (2013) Measurement and analysis of bimodal drop size distribution in a rotor-stator homogenizer. Chem Eng Sci 102:622–631. doi: 10.1016/j.ces.2013.08.030
[127] Liu F, Hashim NA, Liu Y, Abed MRM, Li K (2011) Progress in the production and modification of PVDF membranes. J Membr Sci 375:1–27. doi: 10.1016/j.memsci.2011.03.014
[128] Loginov M, Samper F, Gésan-Guiziou G, Sobisch T, Lerche D, Vorobiev E (2017) Centrifugal ultrafiltration for determination of filter cake properties of colloids. J Membr Sci 536:59–75. doi: 10.1016/j.memsci.2017.04.064
[129] Lonsdale HK, Merten U, Riley RL (1965) Transport properties of cellulose acetate osmotic membranes. J Appl Polym Sci 9:1341–1362. doi: 10.1002/app.1965.070090413
[130] Low LE, Siva SP, Ho YK, Chan ES, Tey BT (2020) Recent advances of characterization techniques for the formation, physical properties and stability of Pickering emulsion. Adv Colloid Interface Sci 277:102117. doi: 10.1016/j.cis.2020.102117
[131] Lu D, Zhang T, Ma J (2015) Ceramic membrane fouling during ultrafiltration of oil/water emulsions: Roles played by stabilization surfactants of oil droplets. Environ Sci Technol 49:4235–4244. doi: 10.1021/es505572y
[132] Luo M-L, Zhao J-Q, Tang W, Pu C-S (2005) Hydrophilic modification of poly(ether sulfone) ultrafiltration membrane surface by self-assembly of TiO_2 nanoparticles. Appl Surf Sci 249:76–84. doi: 10.1016/j.apsusc.2004.11.054
[133] Lyko H (2013) Stand und Perspektiven der organophilen Nanofiltration. F S Filtr und Sep 27:141–146
[134] Maa Y-F, Hsu C (1996) Liquid-liquid emulsification by rotor / stator homogenization. J Control Release 38:219–228. doi: 10.1016/0168-3659(95)00123-9
[135] Maaß S, Rojahn J, Hänsch R, Kraume M (2012) Automated drop detection using image analysis for online particle size monitoring in multiphase systems. Comput Chem Eng 45:27–37. doi: 10.1016/j.compchemeng.2012.05.014
[136] Macedo Fernandes Barros F, Chassenieux C, Nicolai T, de Souza Lima MM, Benyahia L (2018) Effect of the hydrophobicity of fumed silica particles and the nature of oil on the structure and rheological behavior of Pickering emulsions. J Dispers Sci Technol 40:1169–1178. doi: 10.1080/01932691.2018.1500480
[137] Machado DR, Hasson D, Semiat R (1999) Effect of solvent properties on permeate flow through nanofiltration membranes. Part I: investigation of parameters affecting solvent flux. J Membr Sci 163:93–102. doi: 10.1016/S0376-7388(99)00158-1
[138] Machado DR, Hasson D, Semiat R (2000) Effect of solvent properties on permeate flow through nanofiltration membranes. Part II. Transport model. J Membr Sci 166:63–69. doi: 10.1016/S0376-7388(99)00251-3
[139] Madivala B, Vandebril S, Fransaer J, Vermant J (2009) Exploiting particle shape in solid stabilized emulsions. Soft Matter 5:1717–1727. doi: 10.1039/b816680c
[140] Maghzi A, Mohebbi A, Kharrat R, Ghazanfari MH (2011) Pore-scale monitoring of wettability alteration by silica nanoparticles during polymer flooding to heavy oil in a five-spot glass micromodel. Transp Porous Media 87:653–664. doi: 10.1007/s11242-010-9696-3
[141] Manga MS, York DW (2017) Production of concentrated Pickering emulsions with narrow size distributions using stirred cell membrane emulsification. Langmuir 33:9050–9056. doi: 10.1021/acs.langmuir.7b01812
[142] Marchetti P, Jimenez Solomon MF, Szekely G, Livingston AG (2014) Molecular separation with

organic solvent nanofiltration: A critical review. Chem Rev 114:10735–10806. doi: 10.1021/cr500006j
[143] Matos M, Gutiérrez G, Lobo A, Coca J, Pazos C, Benito JM (2016) Surfactant effect on the ultrafiltration of oil-in-water emulsions using ceramic membranes. J Membr Sci 520:749–759. doi: 10.1016/j.memsci.2016.08.037
[144] McBride K, Linke S, Xu S, Sundmacher K (2018) Computer aided design of green thermomorphic solvent systems for homogeneous catalyst recovery. Comput Aided Chem Eng 44:1783–1788. doi: 10.1016/B978-0-444-64241-7.50292-5
[145] McClements DJ, Gumus CE (2016) Natural emulsifiers - biosurfactants, phospholipids, biopolymers, and colloidal particles: Molecular and physicochemical basis of functional performance. Adv Colloid Interface Sci 234:3–26. doi: 10.1016/j.cis.2016.03.002
[146] Melin T, Rautenbach R (2004) Membranverfahren: Grundlagen der Modul- und Anlagenauslegung, 2nd ed. Springer-Verlag, Berlin
[147] Melle S, Lask M, Fuller GG (2005) Pickering emulsions with controllable stability. Langmuir 21:2158–2162. doi: 10.1021/la047691n
[148] Meng T, Bai R, Wang W, Yang X, Guo T, Wang Y (2019) Enzyme-loaded mesoporous silica particles with tuning wettability as a Pickering catalyst for enhancing biocatalysis. Catalysts 9. doi: 10.3390/catal9010078
[149] Mezger TG (2017) Angewandte Rheologie - Mit Joe Flow auf der Rheologie-Straße, 3rd ed. Anton Paar GmbH, Graz
[150] MICRODYN-NADIR GmbH (2007) The art to clear solutions
[151] de Morais Coutinho C, Chiu MC, Basso RC, Ribeiro APB, Gonçalves LAG, Viotto LA (2009) State of art of the application of membrane technology to vegetable oils: A review. Food Res Int 42:536–550. doi: 10.1016/j.foodres.2009.02.010
[152] National Center for Biotechnology Information PubChem Database. 1-Decene. https://pubchem.ncbi.nlm.nih.gov/compound/1-Decene. Accessed 19 May 2020
[153] Nesterenko A, Drelich A, Lu H, Clausse D, Pezron I (2014) Influence of a mixed particle/surfactant emulsifier system on water-in-oil emulsion stability. Colloids Surf A Physicochem Eng Asp 457:49–57. doi: 10.1016/j.colsurfa.2014.05.044
[154] Nie Z, Park J, Li W, Bon SAF, Kumacheva E (2008) An “inside-out” microfluidic approach to monodisperse emulsions stabilized by solid particles. J Am Chem Soc 130:16508–16509. doi: 10.1021/ja807764m
[155] Özcan-Taşkin G, Kubicki D, Padron G (2011) Power and flow characteristics of three rotor-stator heads. Can J Chem Eng 89:1005–1017. doi: 10.1002/cjce.20553
[156] Pajouhandeh A, Kavousi A, Schaffie M, Ranjbar M (2017) Experimental measurement and modeling of nanoparticle-stabilized emulsion rheological behavior. Colloids Surf A Physicochem Eng Asp 520:597–611. doi: 10.1016/j.colsurfa.2017.02.002
[157] Pal R (1996) Effect of droplet size on the rheology of emulsions. AIChE J 42:3181–3190. doi: 10.1002/aic.690421119
[158] Pal R (1997) Dynamics of flocculated emulsions. Chem Eng Sci 52:1177–1187. doi: 10.1016/S0009-2509(96)00451-4
[159] Paul DR, Ebra- Lima OM (1971) The mechanism of liquid transport through swollen polymer membranes. J Appl Polym Sci 15:2199–2210. doi: 10.1002/app.1971.070150912
[160] Paul EL, Atiemo-Obeng VA, Kresta SM (2004) Handbook of industrial mixing: science and practice, 1st ed. John Wiley & Sons, Inc., New Jersey
[161] Paul N (2014) Theoretische und experimentelle Untersuchungen von Transport- und Grenzflächenphänomenen in mizellaren Flüssig/flüssig-Systemen. Technische Universtität Berlin
[162] Penha FM, Rezzadori K, Proner MC, Zanatta V, Zin G, Tondo DW, Vladimir De Oliveira J, Petrus JCC, Di Luccio M (2015) Influence of different solvent and time of pre-treatment on commercial polymeric ultrafiltration membranes applied to non-aqueous solvent permeation. Eur Polym J 66:492–501. doi: 10.1016/j.eurpolymj.2015.03.010
[163] Pera-Titus M, Leclercq L, Clacens J-M, De Campo F, Nardello-Rataj V (2015) Pickering interfacial catalysis for biphasic systems: From emulsion design to green reactions. Angew Chemie - Int Ed 54:2006–2021. doi: 10.1002/anie.201402069
[164] Pérez-Manríquez L, Aburabi’e J, Neelakanda P, Peinemann KV (2015) Cross-linked PAN-based thin-film composite membranes for non-aqueous nanofiltration. React Funct Polym 86:243–247. doi: 10.1016/j.reactfunctpolym.2014.09.015
[165] Le Phuong HA, Blanford CF, Szekely G (2020) Reporting the unreported : the reliability and comparability of the literature on organic solvent nanofiltration. Green Chem 22:3397–3409. doi: 10.1039/d0gc00775g
[166] Pickering SU (1907) CXCVI.-Emulsions. J Chem Soc, Trans 91:2001–2021. doi:

10.1039/CT9079102001
[167] Pogrzeba T, Müller D, Illner M, Schmidt M, Kasaka Y, Weber A, Wozny G, Schomäcker R, Schwarze M (2016) Superior catalyst recycling in surfactant based multiphase systems – Quo vadis catalyst complex? Chem Eng Process 99:155–166. doi: 10.1016/j.cep.2015.09.003
[168] Pogrzeba T, Schmidt M, Milojevic N, Urban C, Illner M, Repke JU, Schomäcker R (2017) Understanding the role of nonionic surfactants during catalysis in microemulsion systems on the example of rhodium-catalyzed hydroformylation. Ind Eng Chem Res 56:9934–9941. doi: 10.1021/acs.iecr.7b02242
[169] Prat D, Hayler J, Wells A (2014) A survey of solvent selection guides. Green Chem 16:4546–4551. doi: 10.1039/c4gc01149j
[170] Priest C, Reid MD, Whitby CP (2011) Formation and stability of nanoparticle-stabilised oil-in-water emulsions in a microfluidic chip. J Colloid Interface Sci 363:301–306. doi: 10.1016/j.jcis.2011.07.060
[171] Priske M, Lazar M, Schnitzer C, Baumgarten G (2016) Recent applications of organic solvent nanofiltration. Chem Ing Tech 88:39–49. doi: 10.1002/cite.201500084
[172] Priske M, Wiese KD, Drews A, Kraume M, Baumgarten G (2010) Reaction integrated separation of homogenous catalysts in the hydroformylation of higher olefins by means of organophilic nanofiltration. J Membr Sci 360:77–83. doi: 10.1016/j.memsci.2010.05.002
[173] Raghavan SR, Walls HJ, Khan SA (2000) Rheology of silica dispersions in organic liquids: New evidence for solvation forces dictated by hydrogen bonding. Langmuir 16:7920–7930. doi: 10.1021/la991548q
[174] Ramsden W (1903) Separation of solids in the surface-layers of solutions and “suspensions” (observations on surface-membranes, bubbles, emulsions, and mechanical coagulation). Proc R Soc Lond 72:156–164. doi: 10.1098/rspl.1903.0034
[175] Rezzadori K, Marques Penha F, Proner MC, Zin G, Cunha Petrus JC, Prádanos P, Palacio L, Hernández A, Di Luccio M (2015) Evaluation of reverse osmosis and nanofiltration membranes performance in the permeation of organic solvents. J Membr Sci 492:478–489. doi: 10.1016/j.memsci.2015.06.005
[176] Ridel L, Bolzinger MA, Gilon-Delepine N, Dugas PY, Chevalier Y (2016) Pickering emulsions stabilized by charged nanoparticles. Soft Matter 12:7564–7576. doi: 10.1039/c6sm01465h
[177] Robinson JP, Tarleton ES, Millington CR, Nijmeijer A (2004) Solvent flux through dense polymeric nanofiltration membranes. J Membr Sci 230:29–37. doi: 10.1016/j.memsci.2003.10.027
[178] Röhl S, Hohl L, Kempin M, Enders F, Jurtz N, Kraume M (2019) Influence of different silica nanoparticles on drop size distributions in agitated liquid- liquid systems. Chem Ing Tech 91:1640–1655. doi: 10.1002/cite.201900049
[179] Sabri F, Berthomier K, Wang CS, Fradette L, Tavares JR, Virgilio N (2019) Tuning particle-particle interactions to control Pickering emulsions constituents separation. Green Chem 21:1065–1074. doi: 10.1039/c8gc03007c
[180] Saha D, Bhattacharya S (2010) Hydrocolloids as thickening and gelling agents in food: a critical review. J Food Sci Technol 47:587–597. doi: 10.1007/s13197-010-0162-6
[181] Salager J-L, Briceno MI, Bracho CL (2001) Heavy hydrocarbon emulsions. Making use of the state of the art in formulation engineering. In: Encyclopedic Handbook of Emulsion Technology. Marcel Dekker, New York, pp 455–495
[182] Salager SE, Tyrode EC, Celis MT, Salager JL (2001) Influence of the stirrer initial position on emulsion morphology. Making use of the local water-to-oil ratio concept for formulation engineering purpose. Ind Eng Chem Res 40:4808–4814. doi: 10.1021/ie010196r
[183] San-Miguel A, Behrens SH (2012) Influence of nanoscale particle roughness on the stability of Pickering emulsions. Langmuir 28:12038–12043. doi: 10.1021/la302224v
[184] Sani NAA, Lau WJ, Ismail AF (2015) Morphologies and separation characteristics of polyphenylsulfone-based solvent resistant nanofiltration membranes: Effect of polymer concentration in casting solution and membrane pretreatment condition. Korean J Chem Eng 32:743–752. doi: 10.1007/s11814-014-0281-2
[185] Sarker M, Tomczak N, Lim S (2017) Protein nanocage as a pH-switchable Pickering emulsifier. ACS Appl Mater Interfaces 9:11193–11201. doi: 10.1021/acsami.6b14349
[186] Sauter C, Emin MA, Schuchmann HP, Tavman S (2008) Influence of hydrostatic pressure and sound amplitude on the ultrasound induced dispersion and de-agglomeration of nanoparticles. Ultrason Sonochem 15:517–523. doi: 10.1016/j.ultsonch.2007.08.010
[187] Schäfer M (2015) Herstellung und Charakterisierung submikroner Ionenaustauscherpartikel – Vergleich von Miniemulsionspolymerisation und Feinstmahlung. Technische Universität Bergakademie Freiberg

[188] Schilde C, Mages-Sauter C, Kwade A, Schuchmann HP (2011) Efficiency of different dispersing devices for dispersing nanosized silica and alumina. Powder Technol 207:353–361. doi: 10.1016/j.powtec.2010.11.019
[189] Schmidt P, Lutze P (2013) Characterisation of organic solvent nanofiltration membranes in multi-component mixtures: Phenomena-based modelling and membrane modelling maps. J Membr Sci 445:183–199. doi: 10.1016/j.memsci.2013.05.062
[190] Schmidt P, Micovic J, Lutze P, Gõrak A (2014) Organophile Nanofiltration - Herausforderungen und Lösungsansätze zur Anwendung eines innovativen Membrantrennverfahrens. Chem Ing Tech 86:602–610. doi: 10.1002/cite.201300153
[191] Schönstedt B (2012) Dispergierung pyrogener Nanopartikeln und deren Anwendung in dünnen Sol-Gel Schichten. Technische Universität Carolo-Wilhelmina zu Braunschweig
[192] Schramm LL (2005) Introduction. In: Emulsions, Foams, and Suspensions. WILEY-VCH Verlag GmbH & Co KGaA, Weinheim, pp 1–12
[193] Schwarze M, Pogrzeba T, Seifert K, Hamerla T, Schomäcker R (2015) Recent developments in hydrogenation and hydroformylation in surfactant systems. Catal Today 247:55–63. doi: 10.1016/j.cattod.2014.06.026
[194] Schwarze M, Pogrzeba T, Volovych I, Schomäcker R (2015) Microemulsion systems for catalytic reactions and processes. Catal Sci Technol 5:24–33. doi: 10.1039/c4cy01121j
[195] Scott K, Mahmood AJ, Jachuck RJ, Hu B (2000) Intensified membrane filtration with corrugated membranes. J Membr Sci 173:1–16. doi: 10.1016/S0376-7388(00)00327-6
[196] Shi X, Tal G, Hankins NP, Gitis V (2014) Fouling and cleaning of ultrafiltration membranes : A review. J Water Process Eng 1:121–138. doi: 10.1016/j.jwpe.2014.04.003
[197] Shukla R, Cheryan M (2002) Performance of ultrafiltration membranes in ethanol-water solutions: Effect of membrane conditioning. J Membr Sci 198:75–85. doi: 10.1016/S0376-7388(01)00638-X
[198] Silva P, Livingston AG (2006) Effect of solute concentration and mass transfer limitations on transport in organic solvent nanofiltration - partially rejected solute. J Membr Sci 280:889–898. doi: 10.1016/j.memsci.2006.03.008
[199] Skale T, Hohl L, Kraume M, Drews A (2017) Feasibility of w/o Pickering emulsion ultrafiltration. J Membr Sci 535:1–9. doi: 10.1016/j.memsci.2017.04.006
[200] Skale T, Stehl D, Hohl L, Kraume M, von Klitzing R, Drews A (2016) Tuning Pickering emulsions for optimal reaction and filtration conditions. Chem Ing Tech 88:1827–1832. doi: 10.1002/cite.201600099
[201] Stehl D (2019) Physico-chemical properties of Pickering emulsions stabilized by different nanoparticles for hydroformylation of long-chain olefins. Technische Universität Darmstadt
[202] Stehl D, Hohl L, Schmidt M, Hübner J, Lehmann M, Kraume M, Schomäcker R, von Klitzing R (2016) Characteristics of stable Pickering emulsions under process conditions. Chem Ing Tech 88:1806–1814. doi: 10.1002/cite.201600065
[203] Stehl D, Milojević N, Stock S, Schomäcker R, von Klitzing R (2019) Synergistic effects of a rhodium catalyst on particle-stabilized Pickering emulsions for the hydroformylation of a long-chain olefin. Ind Eng Chem Res 58:2524–2536. doi: 10.1021/acs.iecr.8b04619
[204] Stehl D, Skale T, Hohl L, Lvov Y, Koetz J, Kraume M, Drews A, von Klitzing R (2020) Oil-in-water Pickering emulsions stabilized by Halloysite clay nanotubes toward efficient filterability. ACS Appl Nano Mater 3:11743–11751. doi: 10.1021/acsanm.0c02205
[205] Stieß M (2009) Mechanische Verfahrenstechnik- Partikeltechnologie 1, 3rd ed. Springer-Verlag, Berlin
[206] Sun G, Qi F, Wu J, Ma G, Ngai T (2014) Preparation of uniform particle-stabilized emulsions using SPG membrane emulsification. Langmuir 30:7052–7056. doi: 10.1021/la500701a
[207] Tadros T (2004) Application of rheology for assessment and prediction of the long-term physical stability of emulsions. Adv Colloid Interface Sci 108–109:227–258. doi: 10.1016/j.cis.2003.10.025
[208] Tadros TF (2009) Emulsion Science and Technology, 1st ed. WILEY-VCH Verlag GmbH & Co KGaA, Weinheim
[209] Tang J, Quinlan PJ, Tam KC (2015) Stimuli-responsive Pickering emulsions: recent advances and potential applications. Soft Matter 11:3512–3529. doi: 10.1039/c5sm00247h
[210] Tarimala S, Dai LL (2004) Structure of microparticles in solid-stabilized emulsions. Langmuir 20:3492–3494. doi: 10.1021/la036129e
[211] Tarleton ES, Robinson JP, Millington CR, Nijmeijer A, Taylor ML (2006) The influence of polarity on flux and rejection behaviour in solvent resistant nanofiltration - Experimental observations. J Membr Sci 278:318–327. doi: 10.1016/j.memsci.2005.11.014
[212] Teixeira ARS, Willig G, Couvreur J, Flourat AL, Peru AAM, Ferchaud P, Ducatel H, Allais F

(2017) From bench scale to kilolab production of renewable ferulic acid-based bisphenols: Optimisation and evaluation of different purification approaches towards technical feasibility and process environmental sustainability. React Chem Eng 2:406–419. doi: 10.1039/c7re00017k
[213] Thieme J, Abend S, Lagaly G (1999) Aggregation in Pickering emulsions. Colloid Polym Sci 277:257–260. doi: 10.1007/PL00013752
[214] Thiermeyer Y, Blumenschein S, Skiborowski M (2018) Solvent dependent membrane-solute sensitivity of OSN membranes. J Membr Sci 567:7–17. doi: 10.1016/j.memsci.2018.08.052
[215] Thompson KL, Armes SP, York DW (2011) Preparation of Pickering emulsions and colloidosomes with relatively narrow size distributions by stirred cell membrane emulsification. Langmuir 27:2357–2363. doi: 10.1021/la104970w
[216] Timgren A, Rayner M, Dejmek P, Marku D, Sjöö M (2013) Emulsion stabilizing capacity of intact starch granules modified by heat treatment or octenyl succinic anhydride. Food Sci Nutr 1:157–171. doi: 10.1002/fsn3.17
[217] Torres LG, Iturbe R, Snowden MJ, Chowdhry BZ, Leharne SA (2007) Preparation of o/w emulsions stabilized by solid particles and their characterization by oscillatory rheology. Colloids Surf A Physicochem Eng Asp 302:439–448. doi: 10.1016/j.colsurfa.2007.03.009
[218] Touzouirt S, Kessal F, Balaidi C, Boukhalfa D (2018) Influence of processing parameters on rheological behavior of bentonite-based Pickering emulsion. J Drug Deliv Ther 8:442–447. doi: 10.22270/jddt.v8i5.1903
[219] Trzaskus KW, Lee SL, de Vos WM, Kemperman A, Nijmeijer K (2017) Fouling behavior of silica nanoparticle-surfactant mixtures during constant flux dead-end ultrafiltration. J Colloid Interface Sci 506:308–318. doi: 10.1016/j.jcis.2017.07.043
[220] Tsabet È, Fradette L (2015) Effect of the properties of oil, particles, and water on the production of Pickering emulsions. Chem Eng Res Des 97:9–17. doi: 10.1016/j.cherd.2015.02.016
[221] Tsabet È, Fradette L (2015) Effect of processing parameters on the production of Pickering emulsions. Ind Eng Chem Res 54:2227–2236. doi: 10.1021/ie504338d
[222] Tummons EN, Tarabara VV, Chew JW, Fane AG (2016) Behavior of oil droplets at the membrane surface during crossflow microfiltration of oil-water emulsions. J Membr Sci 500:211–224. doi: 10.1016/j.memsci.2015.11.005
[223] Vafaei S, Borca-Tasciuc T, Podowski MZ, Purkayastha A, Ramanath G, Ajayan PM (2006) Effect of nanoparticles on sessile droplet contact angle. Nanotechnology 17:2523–2527. doi: 10.1088/0957-4484/17/10/014
[224] Vandezande P, Gevers LEM, Vankelecom IFJ (2008) Solvent resistant nanofiltration: Separating on a molecular level. Chem Soc Rev 37:365–405. doi: 10.1039/b610848m
[225] VDI-Gesellschaft Verfahrenstechnik und Chemieingenieurwesen VDI-Wärmeatlas. Springer-Verlag, Berlin
[226] Vignati E, Piazza R, Lockhart TP (2003) Pickering emulsions: Interfacial tension, colloidal layer morphology, and trapped-particle motion. Langmuir 19:6650–6656. doi: 10.1021/la034264l
[227] Wacker Chemie AG (2012) Perfect toners hide a secret: HDK - pyrogenic silica
[228] Wacker Chemie AG (2018) Technical data sheet HDK®H15
[229] Wacker Chemie AG (2018) Technical data sheet HDK®H18
[230] Wacker Chemie AG (2018) Technical data sheet HDK®H20
[231] Wacker Chemie AG (2018) Technical data sheet HDK®H30
[232] Wacker Chemie AG (2018) Technical data sheet HDK®H2000
[233] Wacker Chemie AG (2018) Technical data sheet HDK®N20
[234] Wacker Chemie AG (2021) Pyrogenic silica. https://www.wacker.com/cms/en-us/products/product-groups/pyrogenic-silica/pyrogenic-silica.html. Accessed 13 Jan 2021
[235] Walstra P, Smulders PEA (1998) Emulsion formation. In: Modern Aspects of Emulsion Science. The Royal Society of Chemistry, Cambridge, pp 56–99
[236] Wang K, Yiming W, Saththasivam J, Liu Z (2017) A flexible, robust and antifouling asymmetric membrane based on ultra-long ceramic/polymeric fibers for high-efficiency separation of oil/water emulsions. Nanoscale 9:9018–9025. doi: 10.1039/c7nr02364b
[237] Wei J, Helm GS, Corner-Walker N, Hou X (2006) Characterization of a non-fouling ultrafiltration membrane. Desalination 192:252–261. doi: 10.1016/j.desal.2005.06.049
[238] Wei L, Zhang M, Zhang X, Xin H, Yang H (2016) Pickering emulsion as an efficient platform for enzymatic reactions without stirring. ACS Sustain Chem Eng 4:6838–6843. doi: 10.1021/acssuschemeng.6b01776
[239] Werth K, Kaupenjohann P, Knierbein M, Skiborowski M (2017) Solvent recovery and deacidification by organic solvent nanofiltration: Experimental investigation and mass transfer modeling. J Membr Sci 528:369–380. doi: 10.1016/j.memsci.2017.01.021
[240] Whitby CP, Fischer FE, Fornasiero D, Ralston J (2011) Shear-induced coalescence of oil-in-water

Pickering emulsions. J Colloid Interface Sci 361:170–177. doi: 10.1016/j.jcis.2011.05.046
[241] Whitby CP, Garcia PC (2014) Time-dependent rheology of clay particle-stabilised emulsions. Appl Clay Sci 96:56–59. doi: 10.1016/j.clay.2014.03.005
[242] Wiese S, Spiess AC, Richtering W (2013) Microgel-stabilized smart emulsions for biocatalysis. Angew Chemie - Int Ed 52:576–579. doi: 10.1002/anie.201206931
[243] Wijmans JG, Baker RW (1995) The solution-diffusion model: a review. J Membr Sci 107:1–21. doi: 10.1016/0376-7388(95)00102-I
[244] Winsor PA (1948) Hydrotropy, solubilization and related emulsification processes. Trans Faraday Soc 44:376–398. doi: 10.1039/TF9484400376
[245] Wollny S (2010) Experimentelle und numerische Untersuchungen zur Partikelbeanspruchung in gerührten (Bio-)Reaktoren. Technische Universität Berlin
[246] Wu C, Bai S, Ansorge-Schumacher MB, Wang D (2011) Nanoparticle cages for enzyme catalysis in organic media. Adv Mater 23:5694–5699. doi: 10.1002/adma.201102693
[247] Wu J, Ma G-H (2016) Recent studies of Pickering emulsions: Particles make the difference. Small 12:4633–4648. doi: 10.1002/smll.201600877
[248] Xiao J, Wang X, Perez Gonzalez AJ, Huang Q (2016) Kafirin nanoparticles-stabilized Pickering emulsions: Microstructure and rheological behavior. Food Hydrocoll 54:30–39. doi: 10.1016/j.foodhyd.2015.09.008
[249] Xiao M, Xu A, Zhang T, Hong L (2018) Tailoring the wettability of colloidal particles for Pickering emulsions via surface modification and roughness. Front Chem 6:1–14. doi: 10.3389/fchem.2018.00225
[250] Xie L, Rielly CD, Özcan-Taşkın NG (2008) Break-up of nano-particle agglomerates by hydrodynamically limited processes. J Dispers Sci Technol 29:573–579. doi: 10.1080/01932690701729211
[251] Yang H, Nguyen QT, Ding Y, Long Y, Ping Z (2000) Investigation of poly(dimethyl siloxane) (PDMS)-solvent interactions by DSC. J Membr Sci 164:37–43. doi: 10.1016/S0376-7388(99)00187-8
[252] Yang Y, Fang Z, Chen X, Zhang W, Xie Y, Chen Y, Liu Z, Yuan W (2017) An overview of Pickering emulsions: solid-particle materials, classification, morphology, and applications. Front Pharmacol 8:287. doi: 10.3389/fphar.2017.00287
[253] Yi XS, Yu SL, Shi WX, Sun N, Jin LM, Wang S, Zhang B, Ma C, Sun LP (2011) The influence of important factors on ultrafiltration of oil/water emulsion using PVDF membrane modified by nano-sized TiO_2/Al_2O_3. Desalination 281:179–184. doi: 10.1016/j.desal.2011.07.056
[254] Yu M, Gu G, Meng W-D, Qing F-L (2007) Superhydrophobic cotton fabric coating based on a complex layer of silica nanoparticles and perfluorooctylated quaternary ammonium silane coupling agent. Appl Surf Sci 253:3669–3673. doi: 10.1016/j.apsusc.2006.07.086
[255] Yu S, Zhang D, Jiang J, Cui Z, Xia W, Binks BP, Yang H (2019) Biphasic biocatalysis using a CO_2-switchable Pickering emulsion. Green Chem 21:4062–4068. doi: 10.1039/c8gc03879a
[256] Zagajewski M, Behr A, Sasse P, Wittmann J (2014) Continuously operated miniplant for the rhodium catalyzed hydroformylation of 1-dodecene in a thermomorphic multicomponent solvent system (TMS). Chem Eng Sci 115:88–94. doi: 10.1016/j.ces.2013.09.033
[257] Zedel D, Drews A, Kraume M (2016) Retention of surfactants by organic solvent nanofiltration and influences on organic solvent flux. Sep Purif Technol 158:396–408. doi: 10.1016/j.seppur.2015.12.040
[258] Zedel D, Kraume M, Drews A (2017) Modelling and prediction of organic solvent flux and retention of surfactants by organic solvent nanofiltration. J Membr Sci 544:323–332. doi: 10.1016/j.memsci.2017.09.041
[259] Zeidler S, Kätzel U, Kreis P (2013) Systematic investigation on the influence of solutes on the separation behavior of a PDMS membrane in organic solvent nanofiltration. J Membr Sci 429:295–303. doi: 10.1016/j.memsci.2012.11.056
[260] Zhang J, Xu S, Li W (2012) High shear mixers: A review of typical applications and studies on power draw, flow pattern, energy dissipation and transfer properties. Chem Eng Process 57–58:25–41. doi: 10.1016/j.cep.2012.04.004
[261] Zhang M, Wei L, Chen H, Du Z, Binks BP, Yang H (2016) Compartmentalized droplets for continuous flow liquid-liquid interface catalysis. J Am Chem Soc 138:10173–10183. doi: 10.1021/jacs.6b04265
[262] Zhang W, Shi Z, Zhang F, Liu X, Jin J, Jiang L (2013) Superhydrophobic and superoleophilic PVDF membranes for effective separation of water-in-oil emulsions with high flux. Adv Mater 25:2071–2076. doi: 10.1002/adma.201204520
[263] Zhao H, Li J, Wang L, Li C, Zhang S (2021) Pickering emulsion stabilized by dual stabilizer: A novel reaction/separation system for methacrolein synthesis. Chem Eng Sci 229:116038. doi:

10.1016/j.ces.2020.116038
[264] Zhou T, McBride K, Linke S, Song Z, Sundmacher K (2020) Computer-aided solvent selection and design for efficient chemical processes. Curr Opin Chem Eng 27:35–44. doi: 10.1016/j.coche.2019.10.007

List of Figures

List of Tables

A. Appendix

A.1. Supplementary Information (SI)

A.1.1. SI to Materials and Methods

Table 15. Additional characteristic properties of the organic liquids used in this thesis.

component		LogP[1] [-]	solubility in water[1] (25 °C) [mg L^{-1}]	Hildebrand solubility parameter[2] [$(J\ cm^{-3})^{0.5}$]
1-dodecene	$C_{12}H_{24}$	6.1	none	16.75
dodecane	$C_{12}H_{26}$	6.1	$3.7 \cdot 10^{-3}$	16.06
decene	$C_{10}H_{20}$	5.7	0.115	16.6
octene	C_8H_{16}	4.6	4.1	16.4
heptane	C_7H_{16}	4.7	3.4	15.2

[1] Data taken from PubChem Database (online) https://pubchem.ncbi.nlm.nih.gov (retrieved: January 14, 2021).
[2] Estimated based on the molecular structure of the solvent as described in [74].

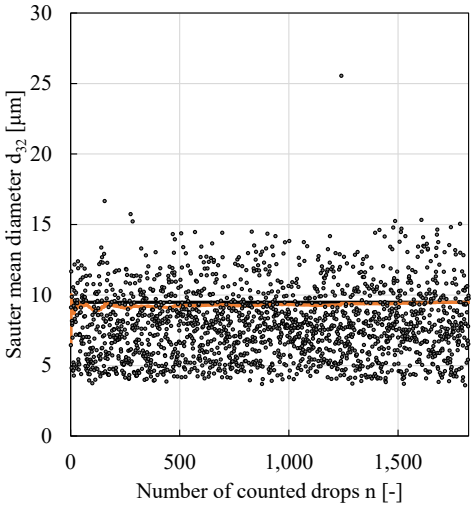

Figure 59. Example sensitivity plot for the evaluation of the drop size distribution of a "standard" w/o PE stabilized by HDK®H20 particles (20 mL, 17,500 min^{-1} / 2 min, S25N-18G). Comparison of the current and previous results for Sauter mean diameters during analysis (black symbols: single drop, orange line: d_{32}(n), black line: d_{32}(N)).

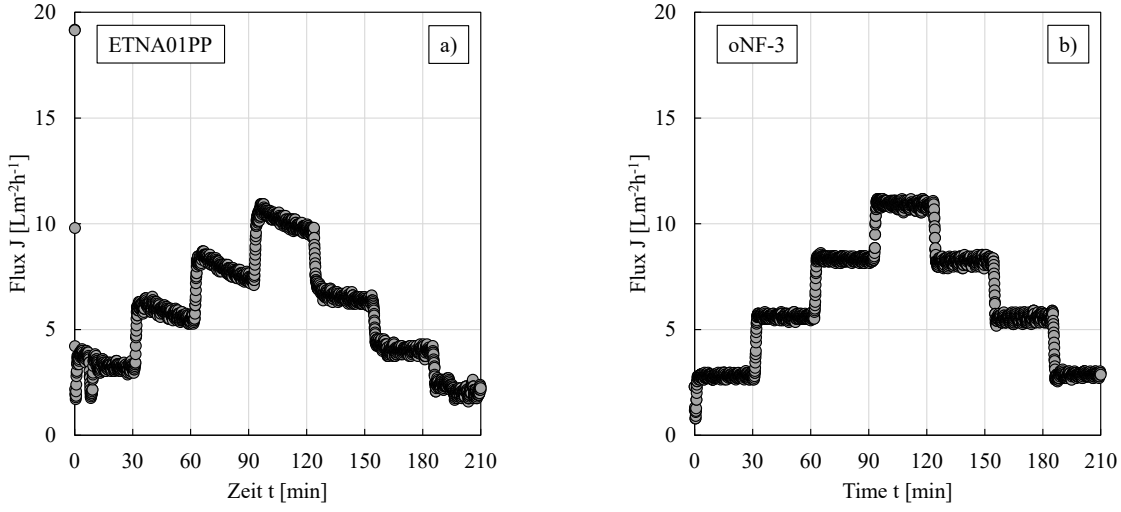

Figure 60. Pure 1-dodecene flux from pressure stepping experiments (1 - 4 - 1 bar as described in **Section 4.4.2**, after normal membrane pre-treatment) as a function of time using the **(a)** ETNA01PP and **(b)** oNF-3 membrane.

A.1.2. SI to Choice of Pickering emulsion preparation conditions

Example viscosity curves with hysteresis

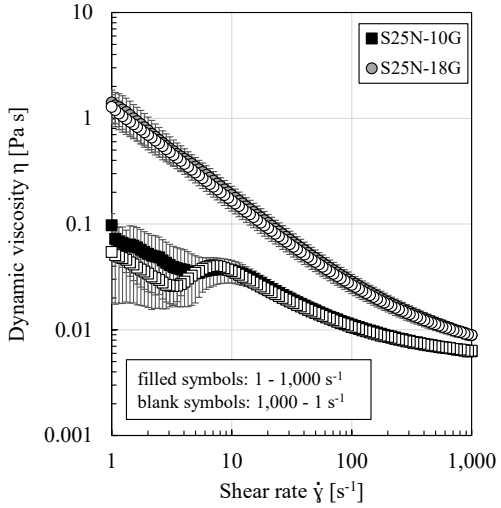

Figure 61. Emulsion viscosity against shear rate including hysteresis ("standard" w/o PEs, 17,500 min^{-1} / 2 min using the two dispersing heads). All experiments were conducted at least in triplicate and mean values are shown. Error bars represent the standard deviation. Where not visible, error bars are smaller than the symbol size.

Impact of particle mass fraction on the rheological behavior

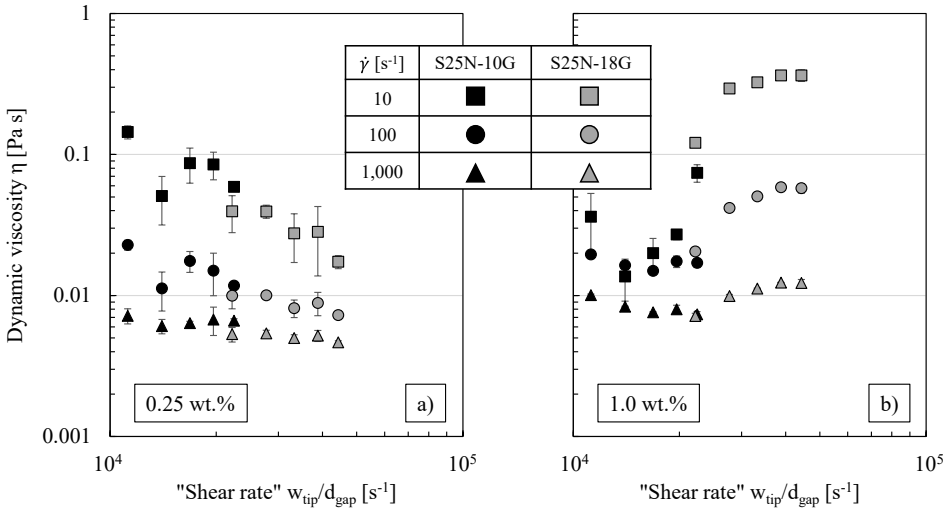

Figure 62. Emulsion viscosity at three distinct shear rates against "shear rate" during PE preparation (prepared using different dispersing speeds at a dispersing time of 2 min with the two dispersing heads). PEs were stabilized by either **(a)** 0.25 wt.% or **(b)** 1.0 wt.% HDK®H20. All experiments were conducted at least in triplicate and mean values are shown. Error bars represent the standard deviation. Where not visible, error bars are smaller than the symbol size.

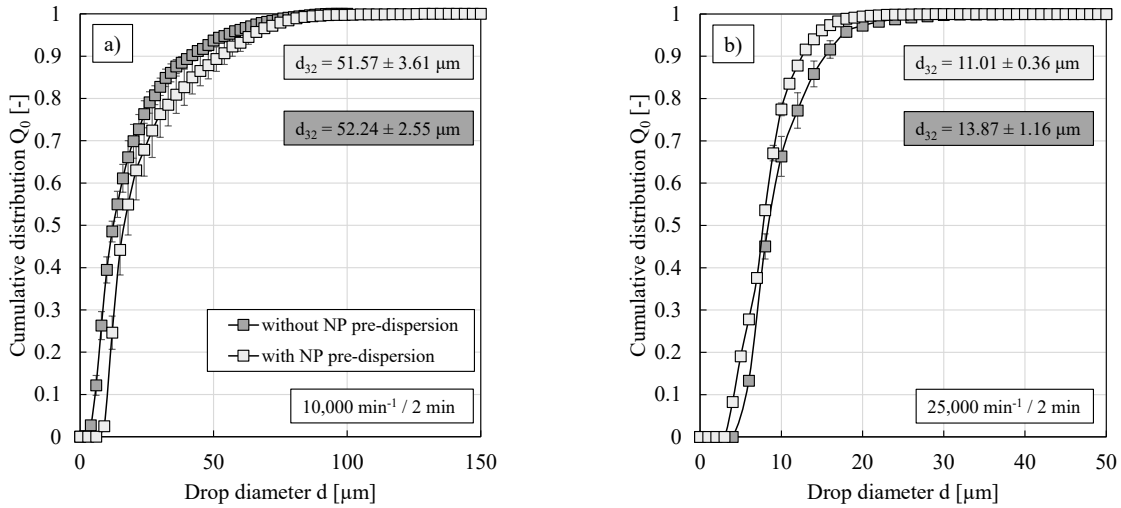

Figure 63. Cumulative number distribution against drop diameter for "standard" w/o PEs prepared without or with pre-dispersion of HDK®H20 in 1-dodecene in a sonication bath prior to PE preparation via the UT (S25N-10G) at dispersing conditions of either **(a)** 10,000 min^{-1} / 2 min or **(b)** 25,000 min^{-1} / 2 min. All experiments were conducted in triplicate and mean values are shown. Error bars represent the standard deviation. Where not visible, error bars are smaller than the symbol size.

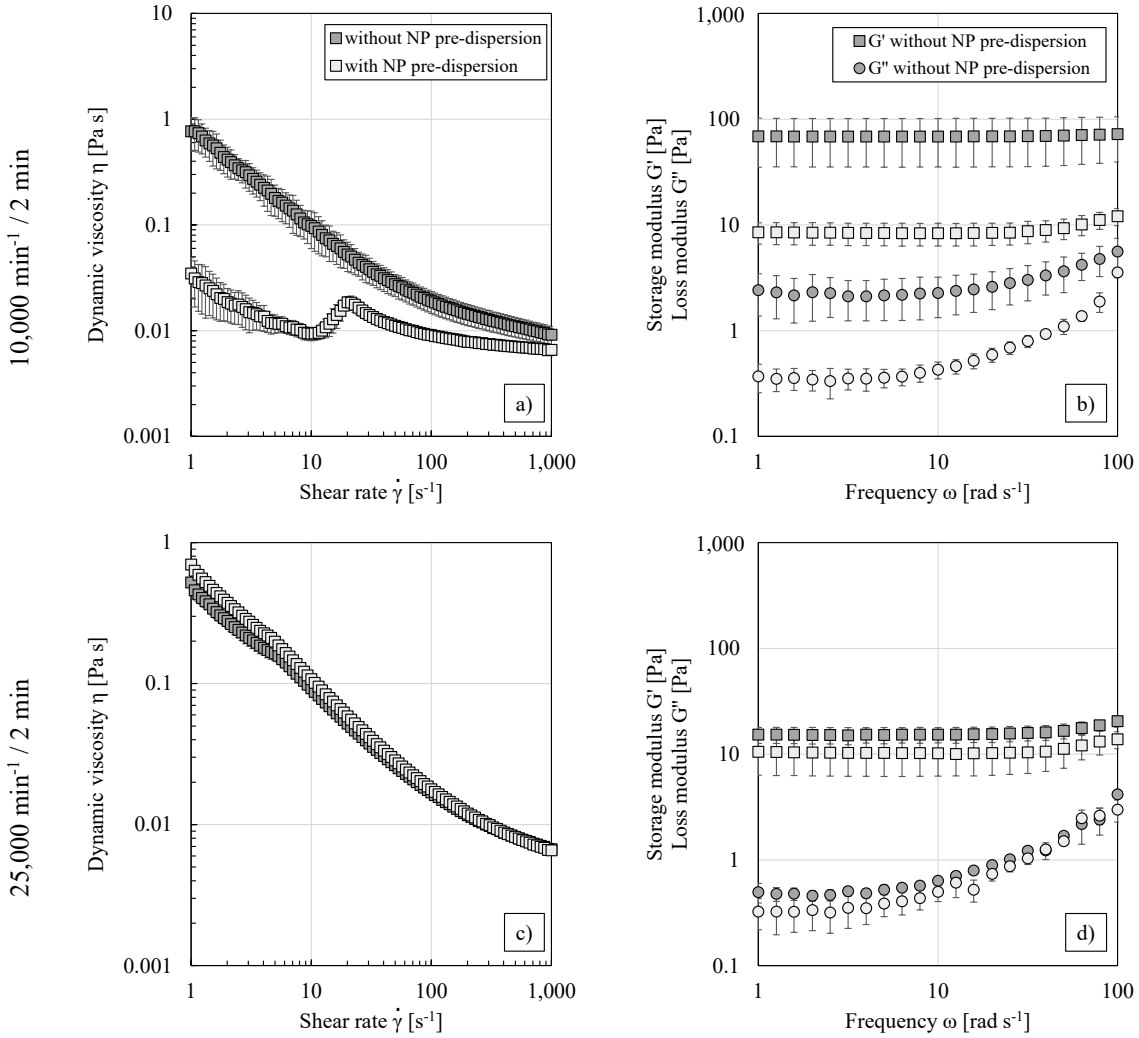

Figure 64. **(a, c)** Emulsion viscosity against shear rate and **(b, d)** frequency sweep measurements for "standard" w/o PEs prepared without or with pre-dispersion of HDK®H20 in 1-dodecene in a sonication bath prior to PE preparation via the UT (S25N-10G) at dispersing conditions of either 10,000 min^{-1} / 2 min or 25,000 min^{-1} / 2 min. All experiments were conducted in triplicate and mean values are shown. Error bars represent the standard deviation. Where not visible, error bars are smaller than the symbol size.

Impact of dispersing time and PE volume on the rheological behavior

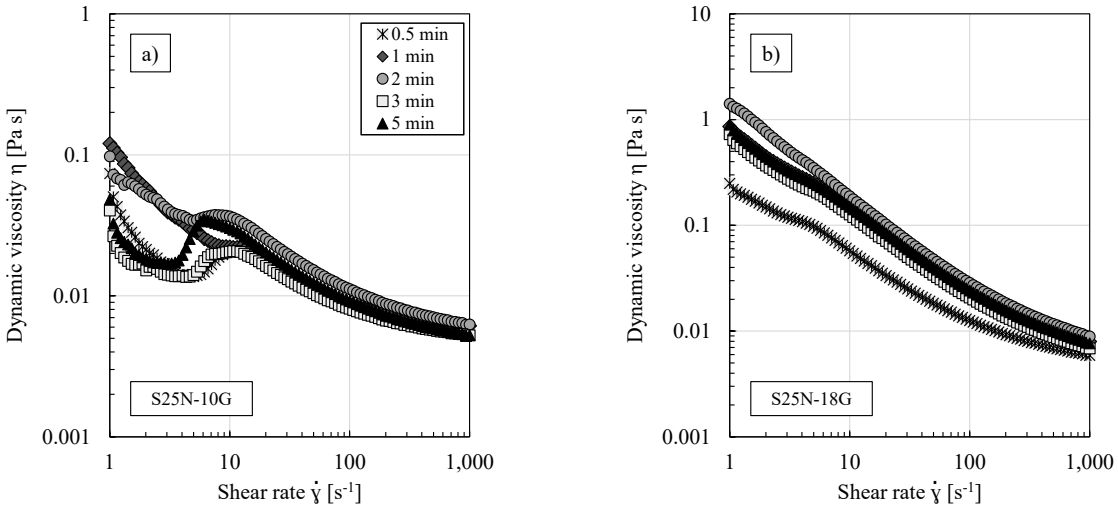

Figure 65. Emulsion viscosity against shear rate for "standard" w/o PEs prepared at 17,500 min^{-1} and different dispersing times. **(a)** S25N-10G and **(b)** S25N-18G head. All experiments were conducted in triplicate and mean values are shown. For better graph clarity, error bars are not shown.

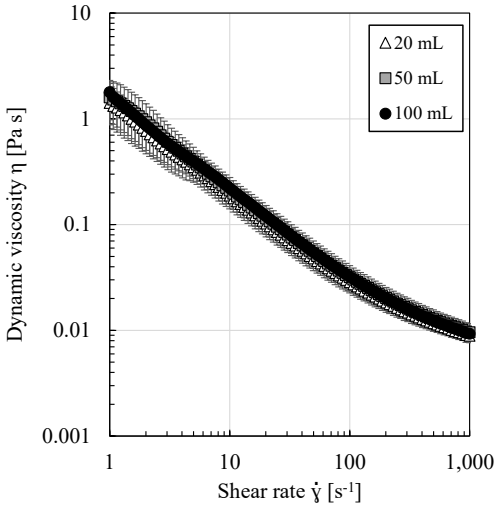

Figure 66. Emulsion viscosity against shear rate for "standard" w/o PEs with different volumes during preparation (17,500 min^{-1} / 2 min, S25N-18G). All experiments were conducted in triplicate and mean values are shown. Error bars represent the standard deviation. Where not visible, error bars are smaller than the symbol size.

Results from the membrane pre-treatment

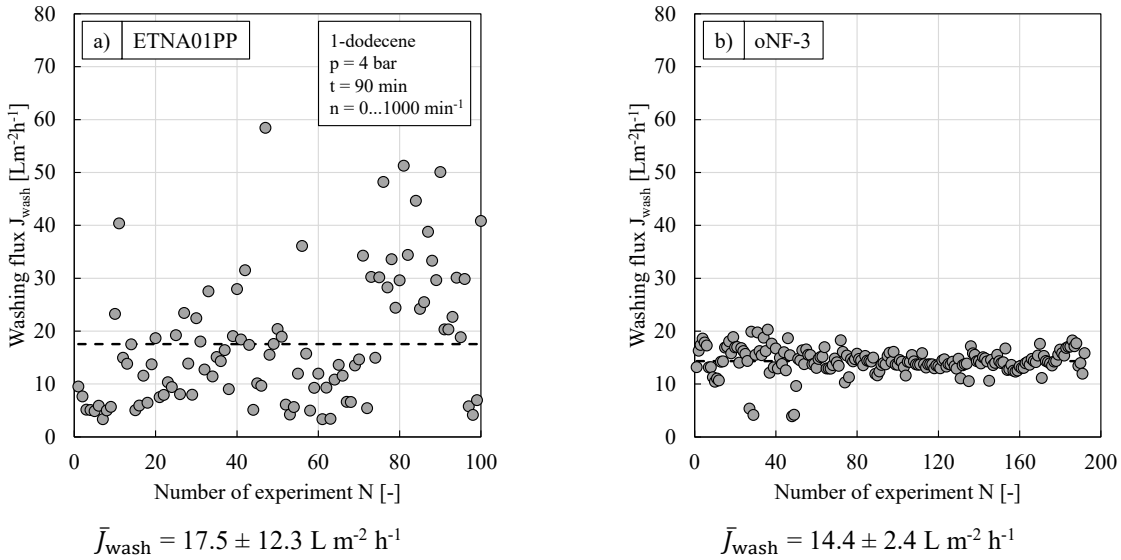

$\bar{J}_{wash}$ = 17.5 ± 12.3 L m^{-2} h^{-1} $\bar{J}_{wash}$ = 14.4 ± 2.4 L m^{-2} h^{-1}

Figure 67. Single and average 1-dodecene washing flux for the **(a)** ETNA01PP (adapted from [II]) and **(b)** oNF-3 membrane. The normal membrane pre-treatment was performed.

Impact of PE dilution on the rheological behavior

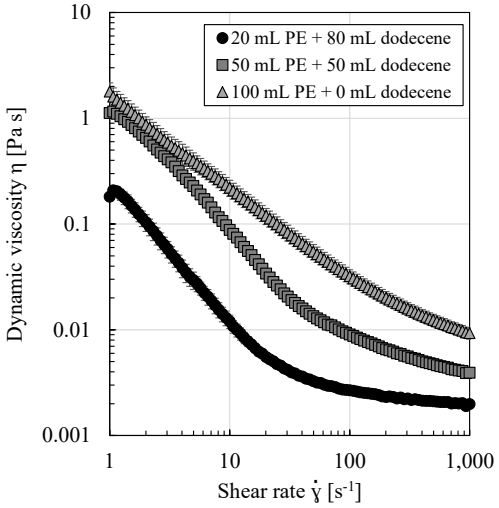

Figure 68. Emulsion viscosity against shear rate for "standard" w/o PEs with different volumes during preparation (17,500 min^{-1} / 2 min, S25N-18G) and made up to a total volume of 100 mL with 1-dodecene. All experiments were conducted in triplicate and mean values are shown. Error bars represent the standard deviation. Where not visible, error bars are smaller than the symbol size.

Self-similarity and width of drop size distributions

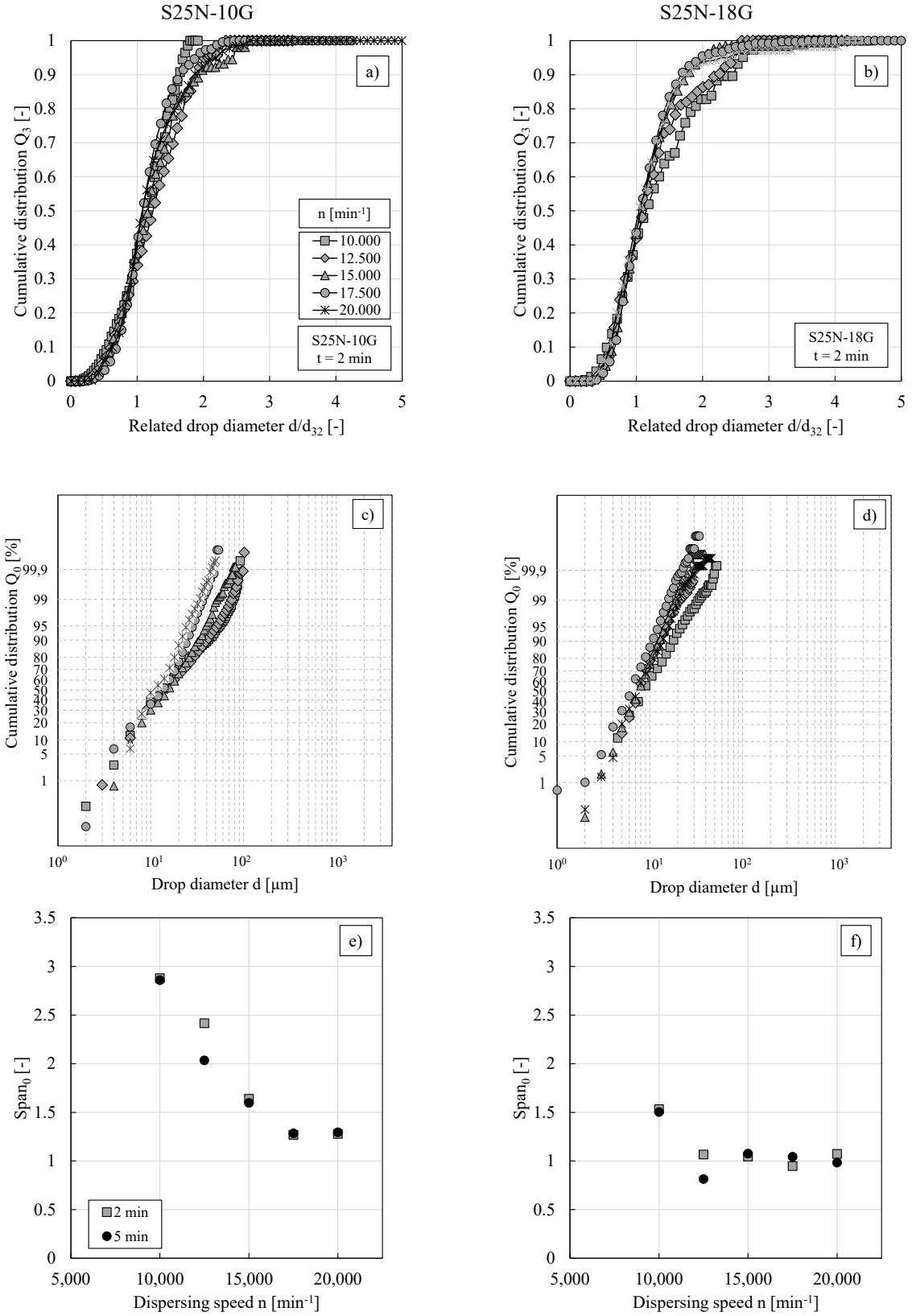

Figure 69. (a, b) Cumulative volume distribution against related drop diameter, **(c, d)** cumulative number distribution against drop diameter in a log probability plot and **(e, f)** *span*$_0$ against dispersing speed for "standard" w/o PEs prepared using different dispersing speeds using the **(left)** S25N-10G and **(right)** S25N-18G head. All experiments were conducted at least in triplicate and mean values are shown. For better graph clarity, error bars are not shown.

Filter cake characterization (investigated in collaboration with LUM GmbH)

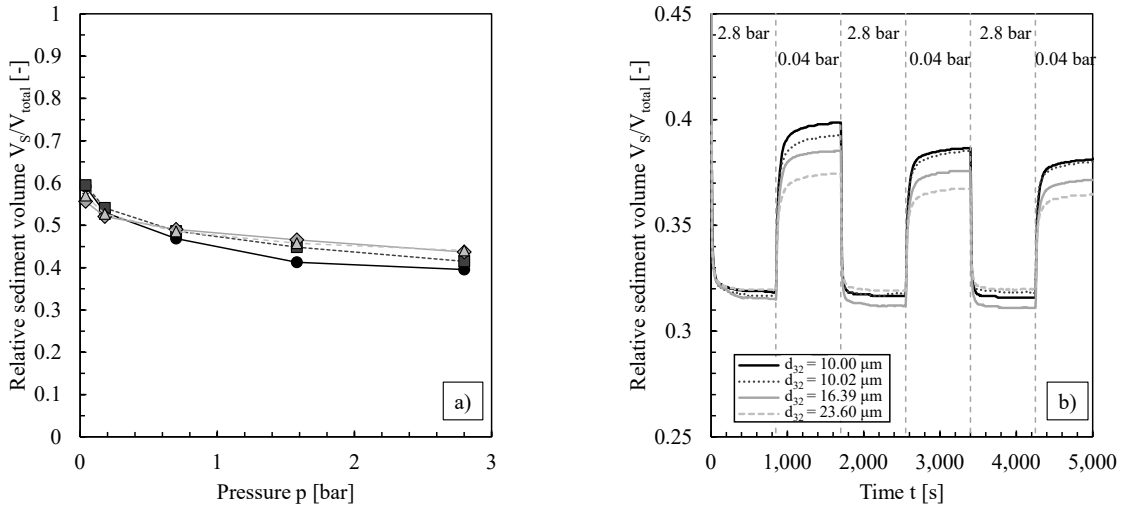

Figure 70. Relative sediment volume against **(a)** pressure and **(b)** time (applying alternating pressures) for different "standard" w/o PEs prepared using different homogenization conditions (Sauter mean diameters indicated in (b)). All experiments were conducted in duplicate and mean values are shown. Error bars presented in (a) represent the standard deviation. Where not visible, error bars are smaller than the symbol size. For better graph clarity, error bars are not shown in (b).

A.1.3. SI to PE filtration using the UF membrane ETNA01PP

Impact of particle type on the DSD and the rheological behavior

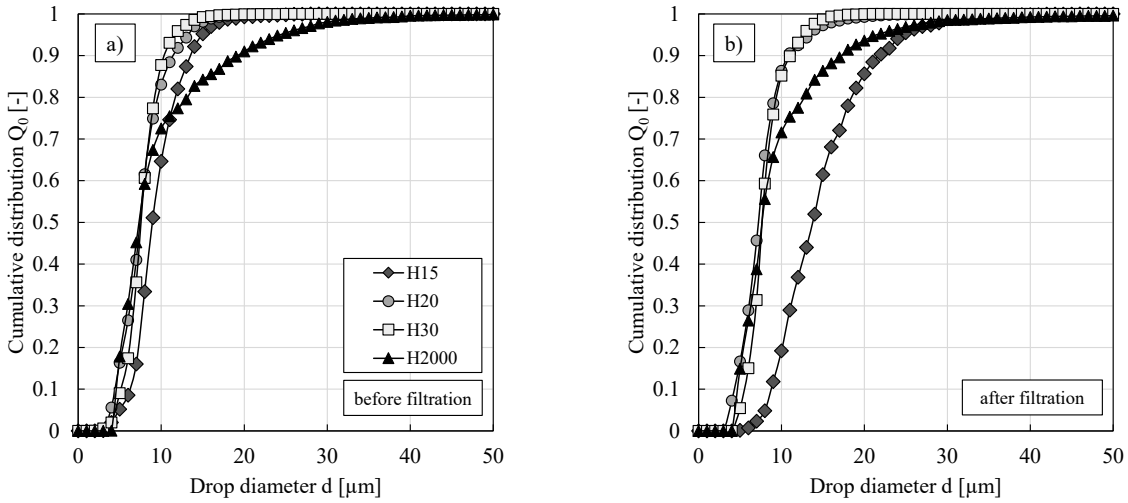

Figure 71. Cumulative number distribution **(a)** before and **(b)** after the filtration of "standard" w/o PEs stabilized by 0.5 wt.% of different particle types. All experiments were conducted at least in triplicate and mean values are shown. For better graph clarity, error bars are not shown. Adapted from [II].

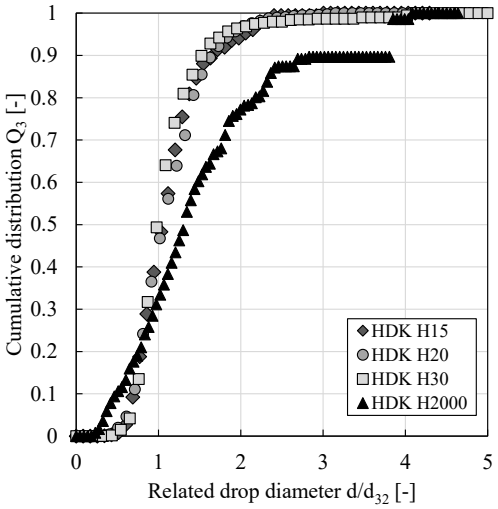

Figure 72. Cumulative volume distribution against related drop diameter for "standard" w/o PEs stabilized by 0.5 wt.% of different particle types. All experiments were conducted in triplicate and mean values are shown. For better graph clarity, error bars are not shown. Drop size distributions of HDK®H15, H20 and H30 stabilized PEs are self-similar. Drop size distributions of HDK®H2000 stabilized PEs are shifted towards larger drop sizes and are more polydisperse.

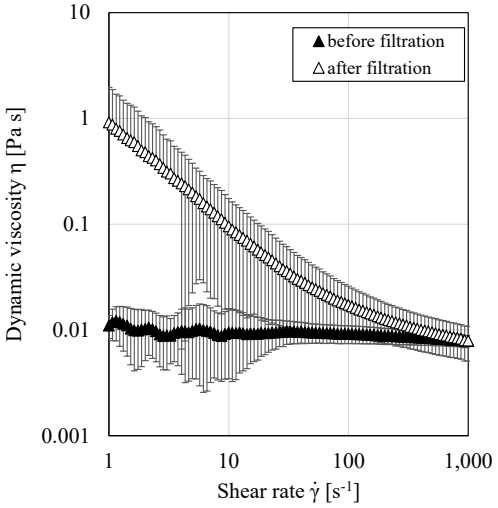

Figure 73. Emulsion viscosity against shear rate for "standard" w/o PEs stabilized by HDK®H2000 before and after the filtration. All experiments were conducted at least in triplicate and mean values are shown. Error bars represent the standard deviation.

Filtration of nanoparticle/oil suspensions

Figure 74 shows results of the filtration of HDK®H18 suspensions prepared using two different particle mass fractions. Similar to HDK®H20 suspensions (cf. **Figure 36** a)), an increase in flux compared to pure 1-dodecene and the formation of a gel layer on the membrane surface was observed. The gel layer height was 4.32 ± 0.59 mm and 8.11 ± 0.98 mm for 0.5 or 1.0 wt.% suspensions, respectively, and thus in a similar range as those observed for HDK®H20 suspensions. The slight differences in the absolute values of the gel layer thickness can possibly be explained by the difference in the tamped densities (cf. **Table 4**). Comparison of **Figure 36** a) and **Figure 74** shows no clear trend regarding the impact of particle mass fraction on the flux level. **Table 16** summarizes normalized flux values (at a pressure of 4 bar) for suspensions of three different particle mass fractions using HDK®H18 or HDK®H20 particles, respectively. It can be assumed that – depending on the particle type – a certain particle mass fraction exists above which the improvement of flux (caused by the increase of membrane wettability) is outweighed by the increasing number of particles and the flux declines.

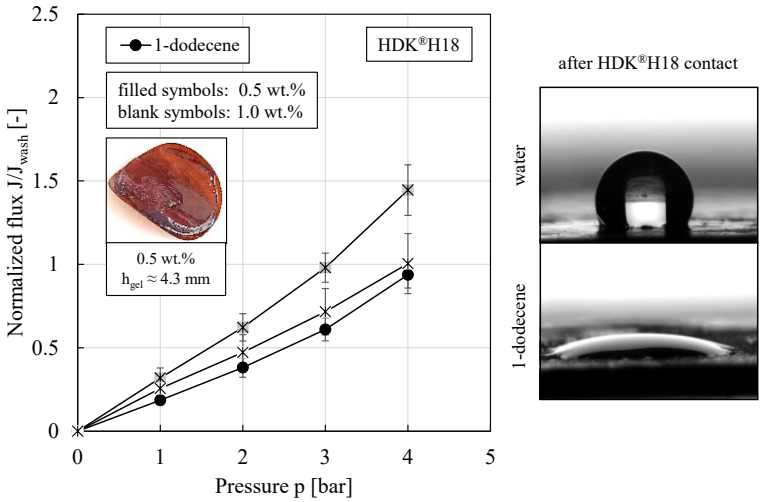

Figure 74. (Left) Normalized flux against pressure for HDK®H18 suspensions using different particle mass fractions in comparison to 1-dodecene fluxes. All experiments were conducted in triplicate and mean values are shown. Error bars represent the standard deviation. Where not visible, error bars are smaller than the symbol size. Inset shows the gel layer on the membrane surface after the filtration of a 0.5 wt.% suspension. **(Right)** Water and 1-dodecene drop on membranes after particle contact show the increased membrane hydrophobicity. Adapted from [II].

Table 16. Normalized flux at a pressure of 4 bar of suspensions prepared using different particle mass fractions of either HDK®H18 or HDK®H20, respectively. All experiments were conducted at least in duplicate and mean values as well as standard deviations are given.

particle mass fraction [wt.%]	normalized flux at p = 4 bar	
	HDK®H18	HDK®H20
0.5	1.45 ± 0.15	1.90 ± 0.19
1.0	1.00 ± 0.18	2.10 ± 0.19
1.25	0.96 ± 0.12	1.79 ± 0.07

A.1.4. SI to PE filtration using the OSN membrane oNF-3

Impact of particle mass fraction on the rheological behavior

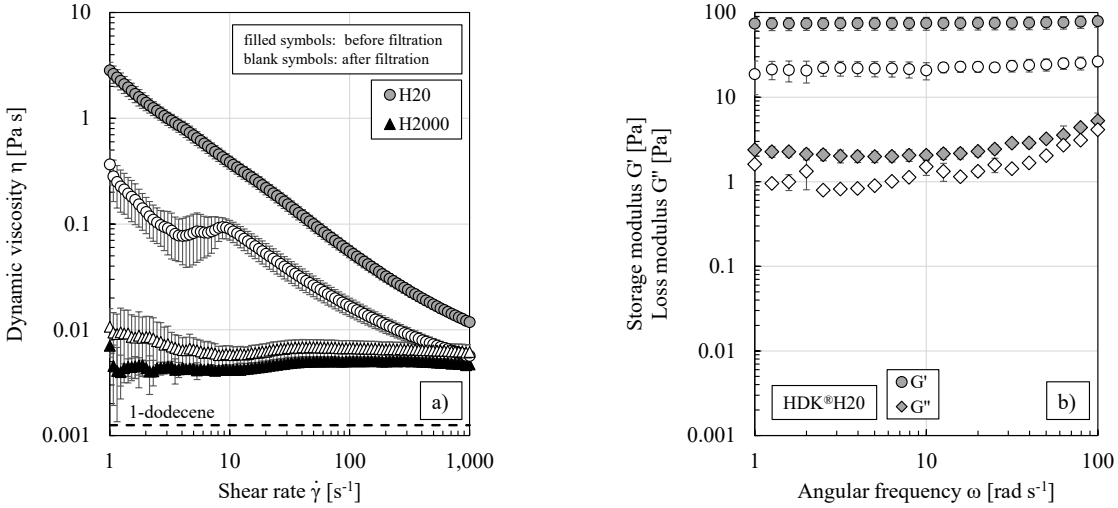

Figure 75. **(a)** Emulsion viscosity and **(b)** frequency sweep measurements before and after the filtration of w/o PEs stabilized by 1.0 wt.% of HDK®H20 or HDK®H2000. All experiments were conducted in triplicate and mean values are shown. Error bars represent the standard deviation. Where not visible, error bars are smaller than the symbol size.

Impact of dispersed phase fraction on the drop size distribution and the rheological behavior

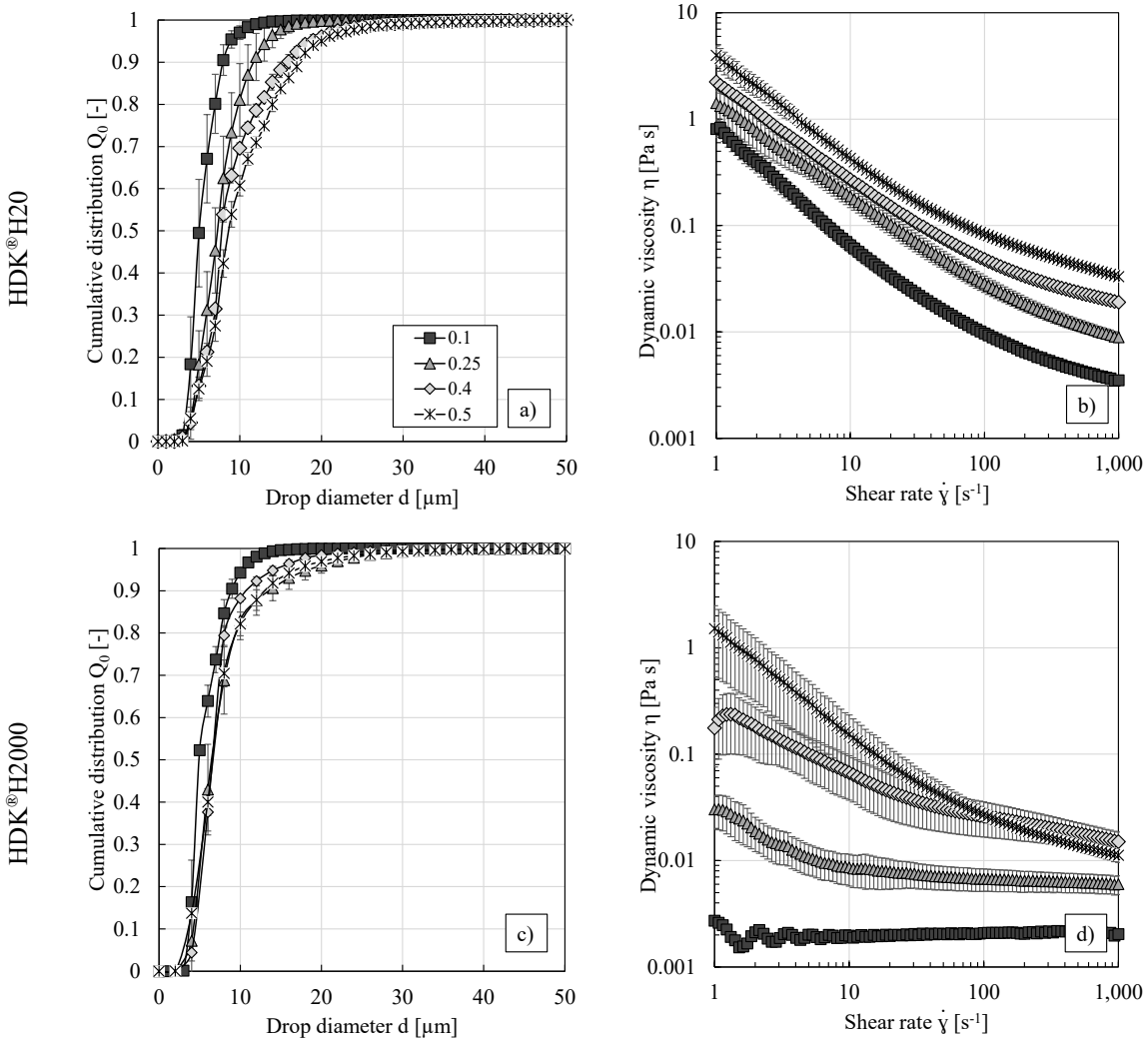

Figure 76. (a, c) Cumulative number distribution (adapted from [VI]) and **(b, d)** emulsion viscosity for w/o PEs prepared with 0.5 wt.% of HDK®H20 or HDK®H2000 and different dispersed phase fractions. All experiments were conducted in triplicate and mean values are shown. Error bars represent the standard deviation. Where not visible, error bars are smaller than the symbol size.

Impact of catalyst and reaction (by-)products on the drop size distribution

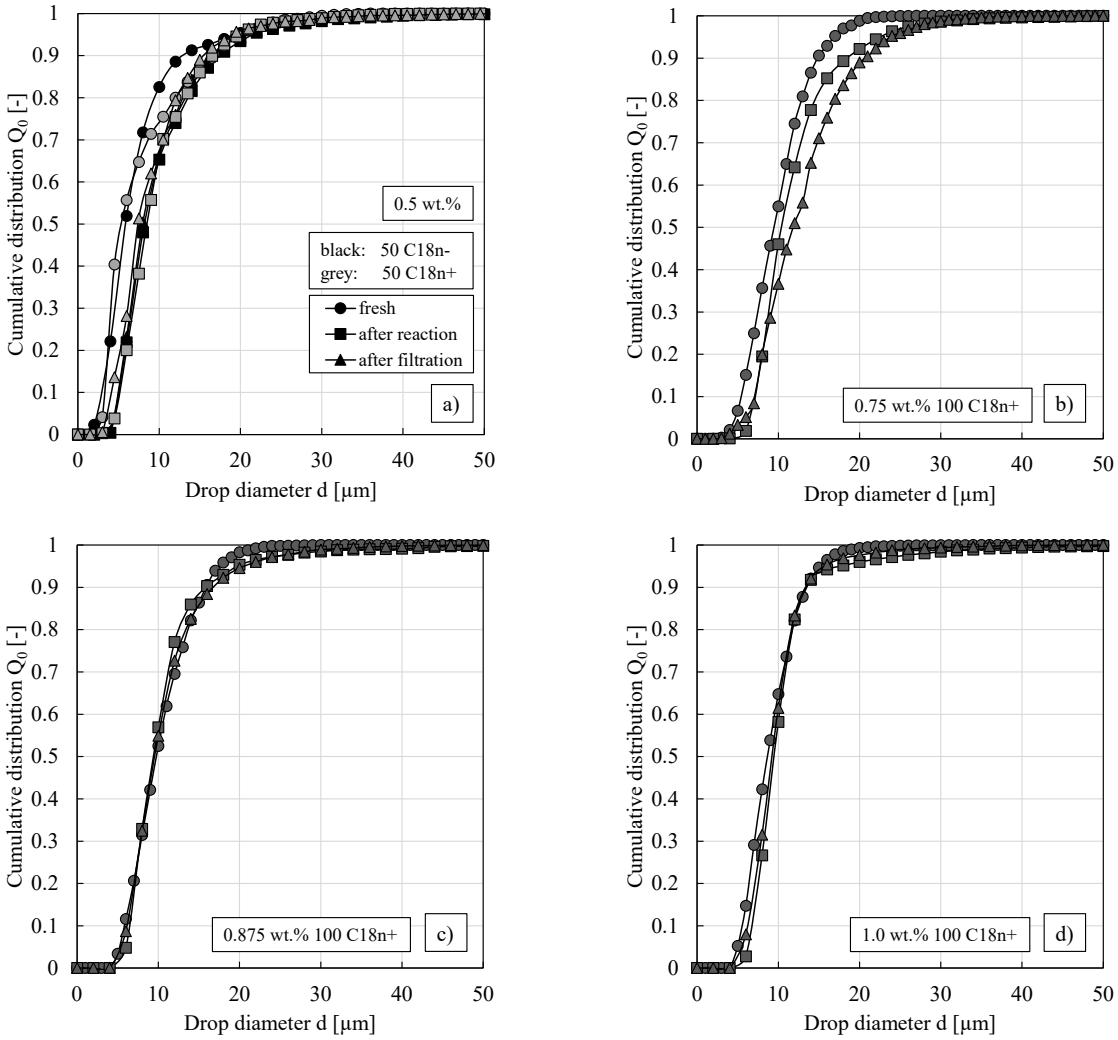

Figure 77. Cumulative number distribution against drop diameter for w/o PEs stabilized by different particle types and particle mass fractions. Drop size distributions of freshly prepared PEs, after the hydroformylation reaction and after the filtration cycle were measured and compared. All experiments were conducted once.

Impact of stirrer speed / crossflow velocity on the filtration performance

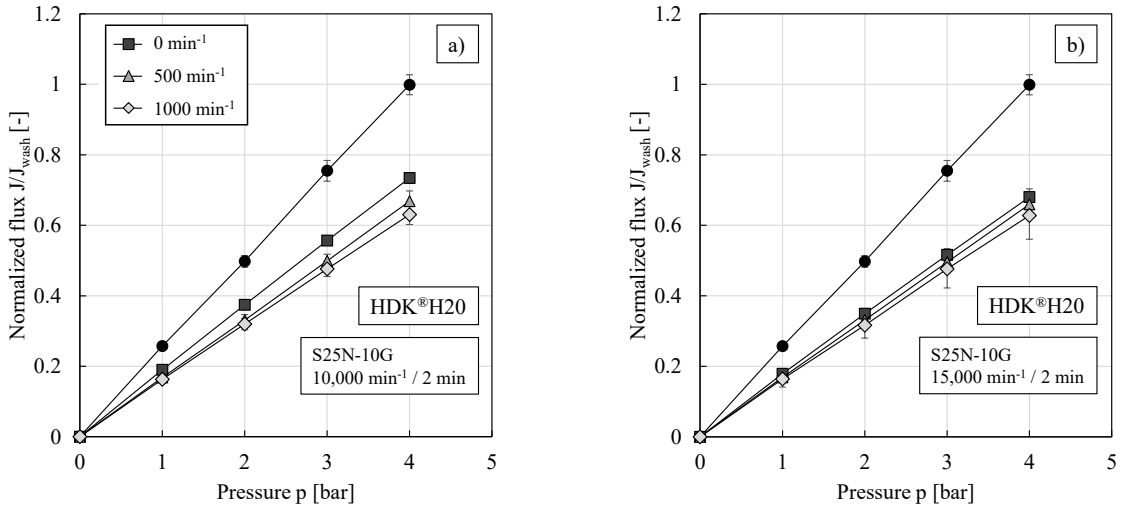

Figure 78. Normalized flux against pressure for HDK®H20 w/o PEs (prepared using different dispersing speeds (S25N-10G)) under application of different stirrer speeds within the filtration cell in comparison to pure 1-dodecene fluxes. All experiments were conducted at least in duplicate and mean values are shown. Error bars represent the standard deviation. Where not visible, error bars are smaller than the symbol size.

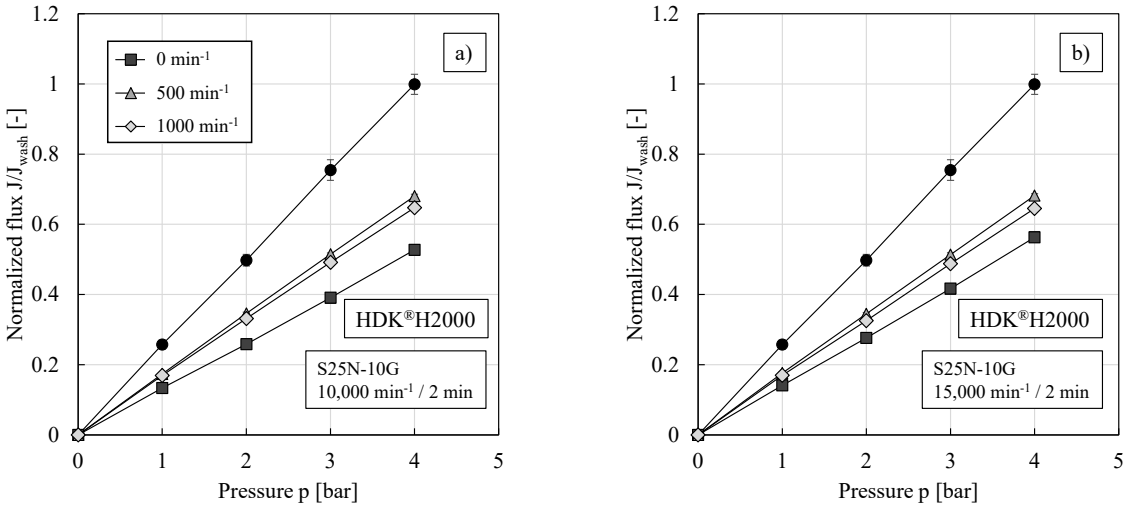

Figure 79. Normalized flux against pressure for HDK®H2000 w/o PEs (prepared using different dispersing speeds (S25N-10G)) under application of different stirrer speeds within the filtration cell in comparison to pure 1-dodecene fluxes. All experiments were conducted at least in duplicate and mean values are shown. Error bars represent the standard deviation. Where not visible, error bars are smaller than the symbol size.

Impact of stirrer speed / crossflow velocity on the DSD

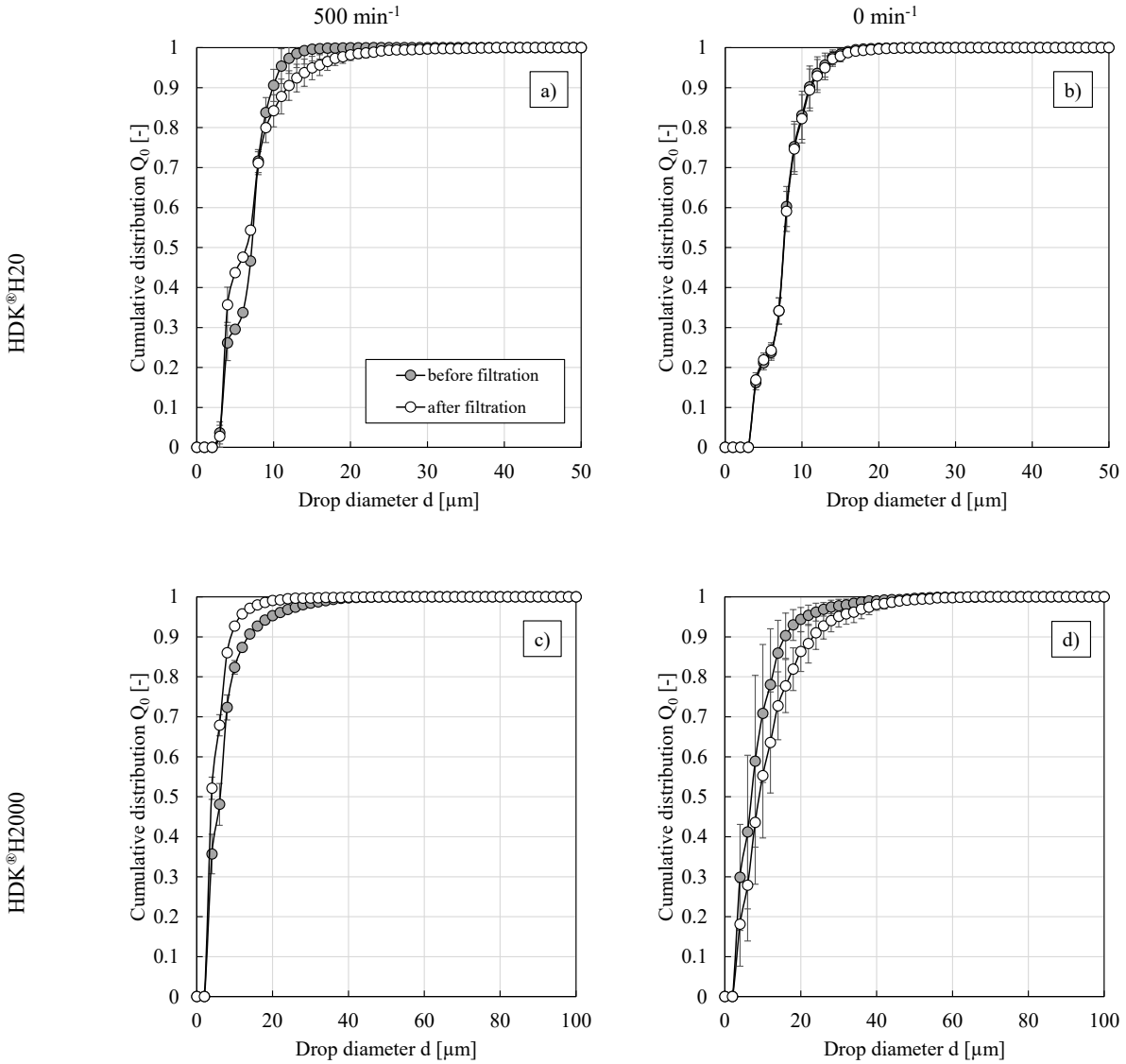

Figure 80. Cumulative number distribution against drop diameter for "standard" w/o PEs stabilized by **(a, b)** HDK®H20 or **(c, d)** HDK®H2000 before and after long-term filtration experiments (5 h at a constant pressure of 4 bar) with or without stirring within the filtration cell. All experiments were conducted at least in duplicate and mean values are shown. Error bars represent the standard deviation. Where not visible, error bars are smaller than the symbol size.

Impact of temperature on the filtration performance

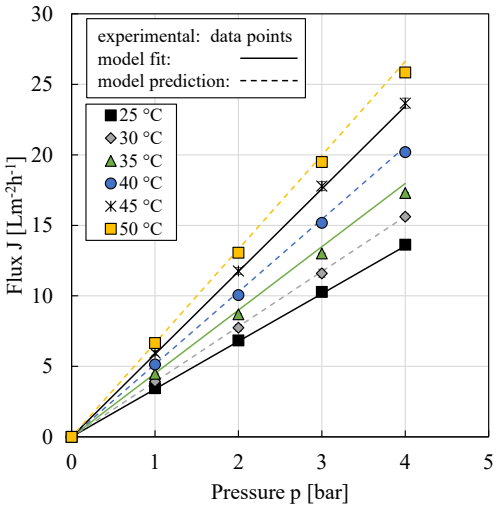

Figure 81. Experimental and modeled pure 1-dodecene flux at different temperatures against pressure. The solution-diffusion model (**Eq. (24)**) combined with an Arrhenius-type relationship to describe the temperature dependency of the diffusion coefficient (**Eq. (26)**) was used. For the model fit, the experimental results at temperatures of 25, 35 and 45 °C were used. All experiments were conducted at least in duplicate and mean values are shown. Error bars represent the standard deviation. Where not visible, error bars are smaller than the symbol size. Adapted from [V].

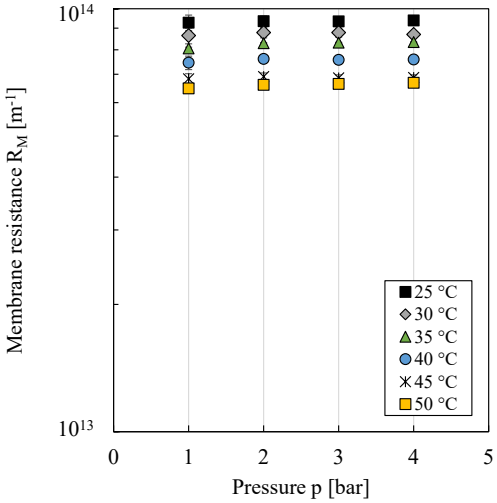

Figure 82. Membrane resistance calculated via Darcy's law (**Eq. (12)**) against pressure. For the calculation, the experimental results of pure 1-dodecene at different temperatures were used. All experiments were conducted at least in duplicate and mean values are shown. Error bars represent the standard deviation. Where not visible, error bars are smaller than the symbol size. Adapted from [V].

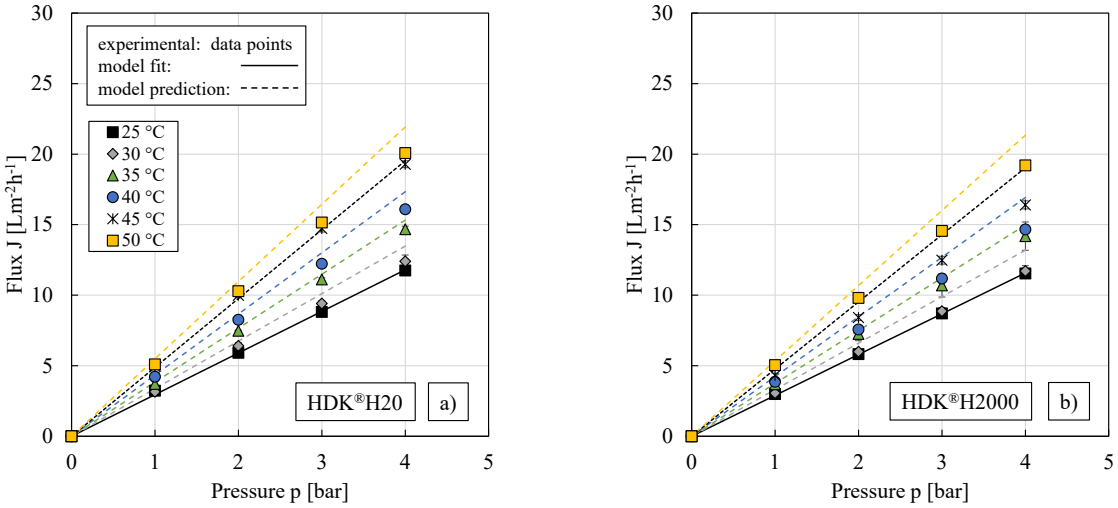

Figure 83. Experimental and modeled w/o PE flux at different temperatures against pressure. **(a)** HDK®H20 and **(b)** HDK®H2000 stabilized PEs. A combination of the solution-diffusion and the resistance in series model was used. For the model fit (**Eq. (27)**), the experimental results at a temperature of 25 °C were used. All experiments were conducted at least in duplicate and mean values are shown. Error bars represent the standard deviation. Where not visible, error bars are smaller than the symbol size. Adapted from [V].

Impact of organic solvent type on the filtration performance

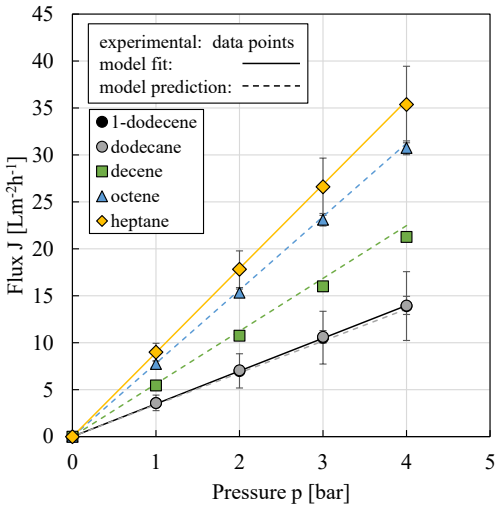

Figure 84. Experimental and modeled pure organic solvent flux against pressure. The solution-diffusion model (**Eq. (24)**) using a linear correlation between the ratio of diffusion coefficient and dry membrane thickness and the reciprocal of the molar mass of the organic solvent (**Eq. (29)**) was used. For the model fit, the experimental results using 1-dodecene and heptane were used. All experiments were conducted at least in duplicate and mean values are shown. Error bars represent the standard deviation. Where not visible, error bars are smaller than the symbol size. Experimental data points for 1-dodecene and dodecane overlap. Adapted from [VI].

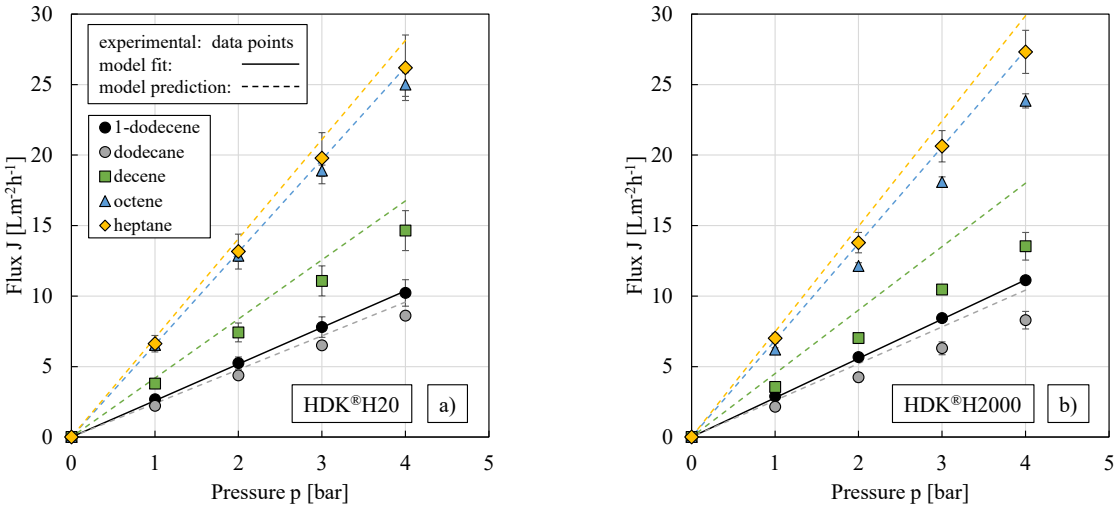

Figure 85. Experimental and modeled flux of w/o PEs prepared using different organic solvents against pressure. **(a)** HDK®H20 and **(b)** HDK®H2000 stabilized PEs. A combination of the solution-diffusion and the resistance in series model was used. For the model fit (**Eq. (27)** combined with **Eq. (29)**), the experimental results of 1-dodecene at room temperature were used. All experiments were conducted at least in duplicate and mean values are shown. Error bars represent the standard deviation. Where not visible, error bars are smaller than the symbol size.

Filtration of nanoparticle/oil suspensions using different organic solvents

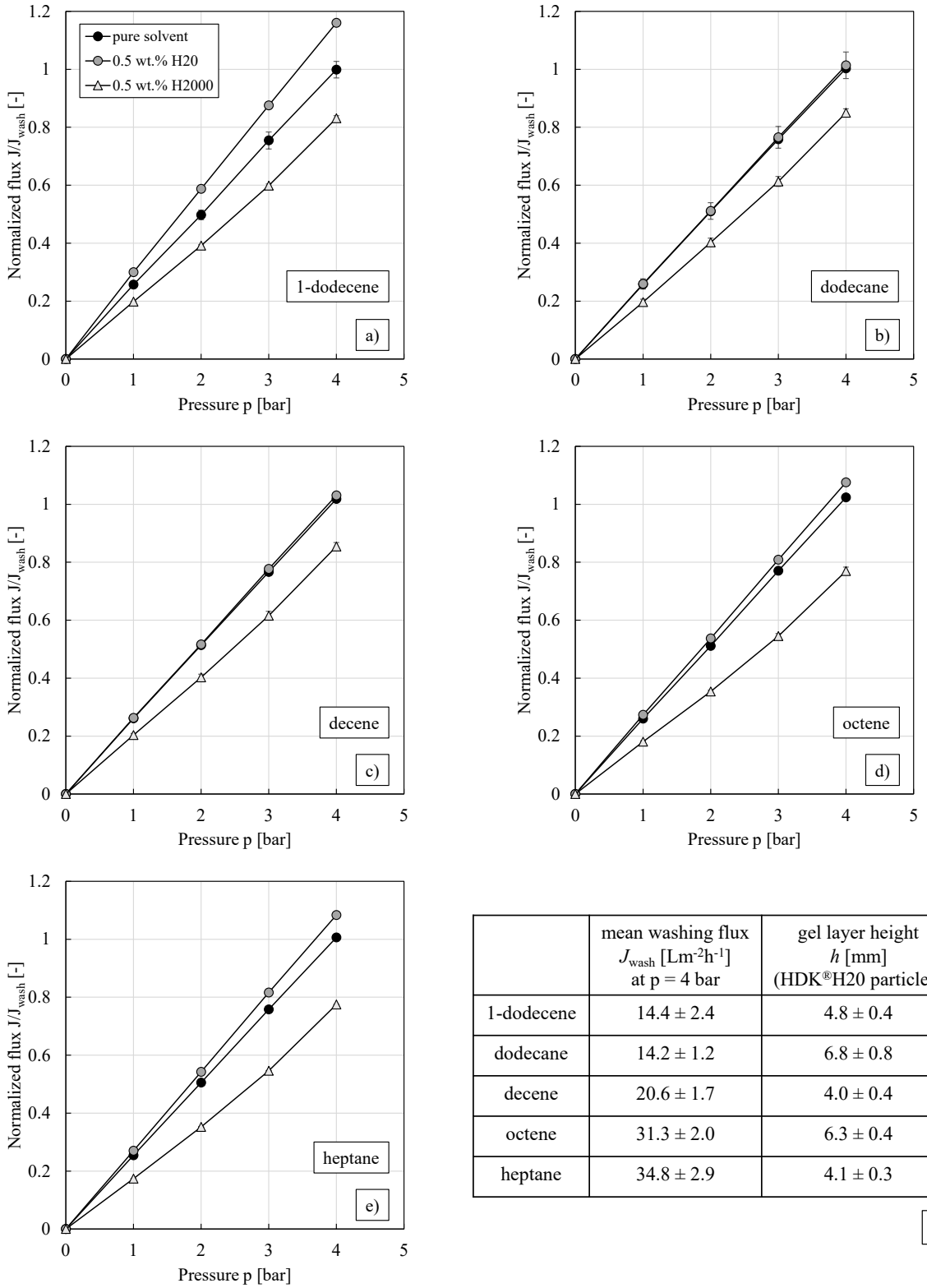

	mean washing flux J_{wash} [Lm^{-2}h^{-1}] at p = 4 bar	gel layer height h [mm] (HDK®H20 particles)
1-dodecene	14.4 ± 2.4	4.8 ± 0.4
dodecane	14.2 ± 1.2	6.8 ± 0.8
decene	20.6 ± 1.7	4.0 ± 0.4
octene	31.3 ± 2.0	6.3 ± 0.4
heptane	34.8 ± 2.9	4.1 ± 0.3

f)

Figure 86. (a)-(e) Normalized flux against pressure for "standard" suspensions prepared using different organic solvents and HDK®H20 or HDK®H2000 particles. **(f)** Average pure solvent flux from the membrane pre-treatment (at a pressure of 4 bar) and gel layer height on the membrane surface after the filtration of HDK®H20 suspensions. All experiments were conducted without stirring, at least in duplicate and mean values are shown. Error bars represent the standard deviation. Where not visible, error bars are smaller than the symbol size.

Impact of organic solvent type on the drop size distribution, the rheological behavior, the filter cake properties and the membrane resistance

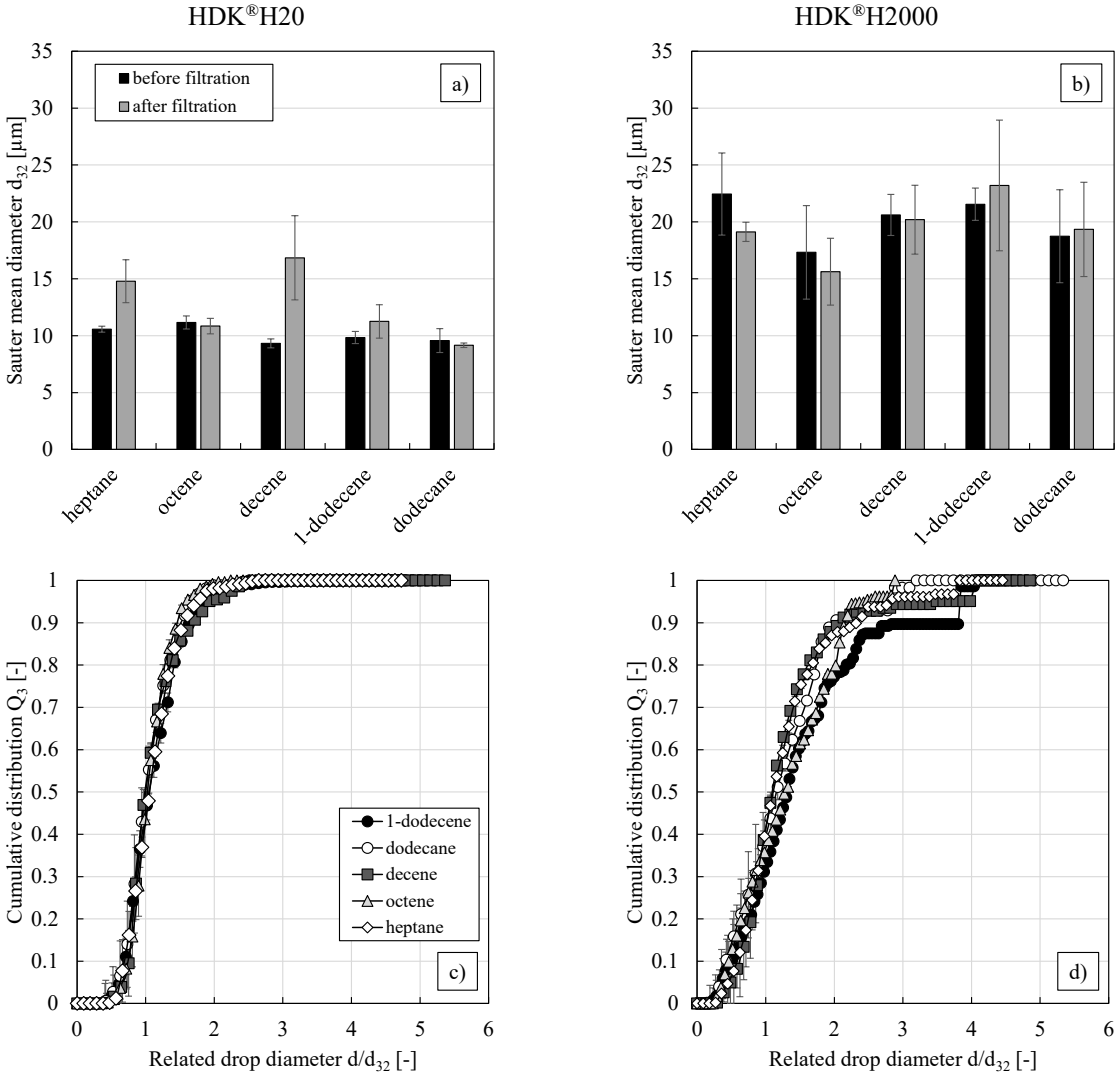

Figure 87. (a, b) Sauter mean diameter before and after the filtration of "standard" w/o PEs prepared with HDK®H20 or HDK®H2000 particles and different organic solvents. All experiments were conducted at least in triplicate and mean values are shown. Error bars represent the standard deviation. Adapted from [VI]. **(c, d)** Cumulative volume distribution (before filtration) against related drop diameter. For better graph clarity, error bars are not shown.

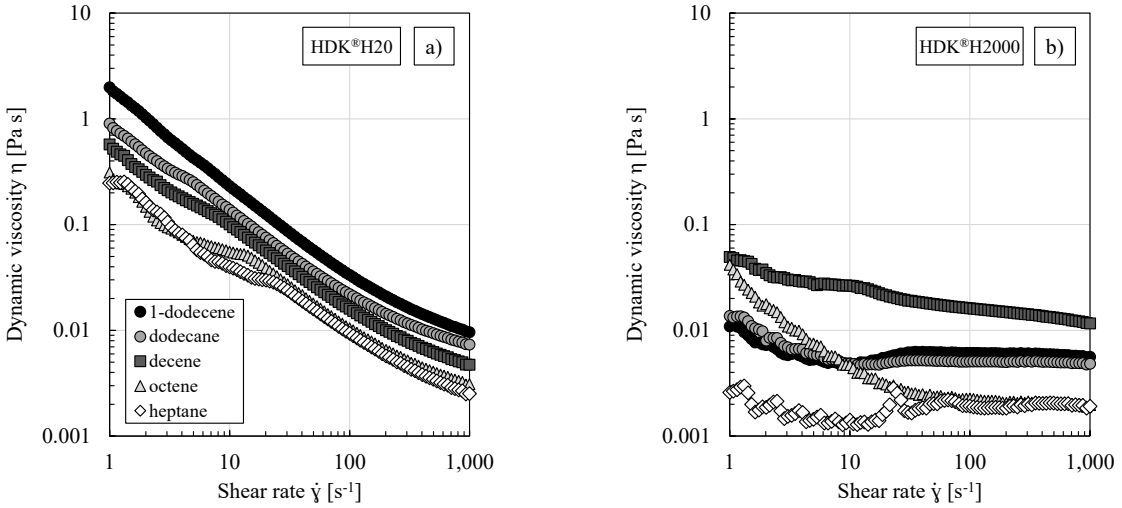

Figure 88. Emulsion viscosity against shear rate for w/o PEs prepared using different organic solvents and **(a)** HDK®H20 or **(b)** HDK®H2000 particles. All experiments were conducted at least in duplicate and mean values are shown. For better graph clarity, error bars are not shown.

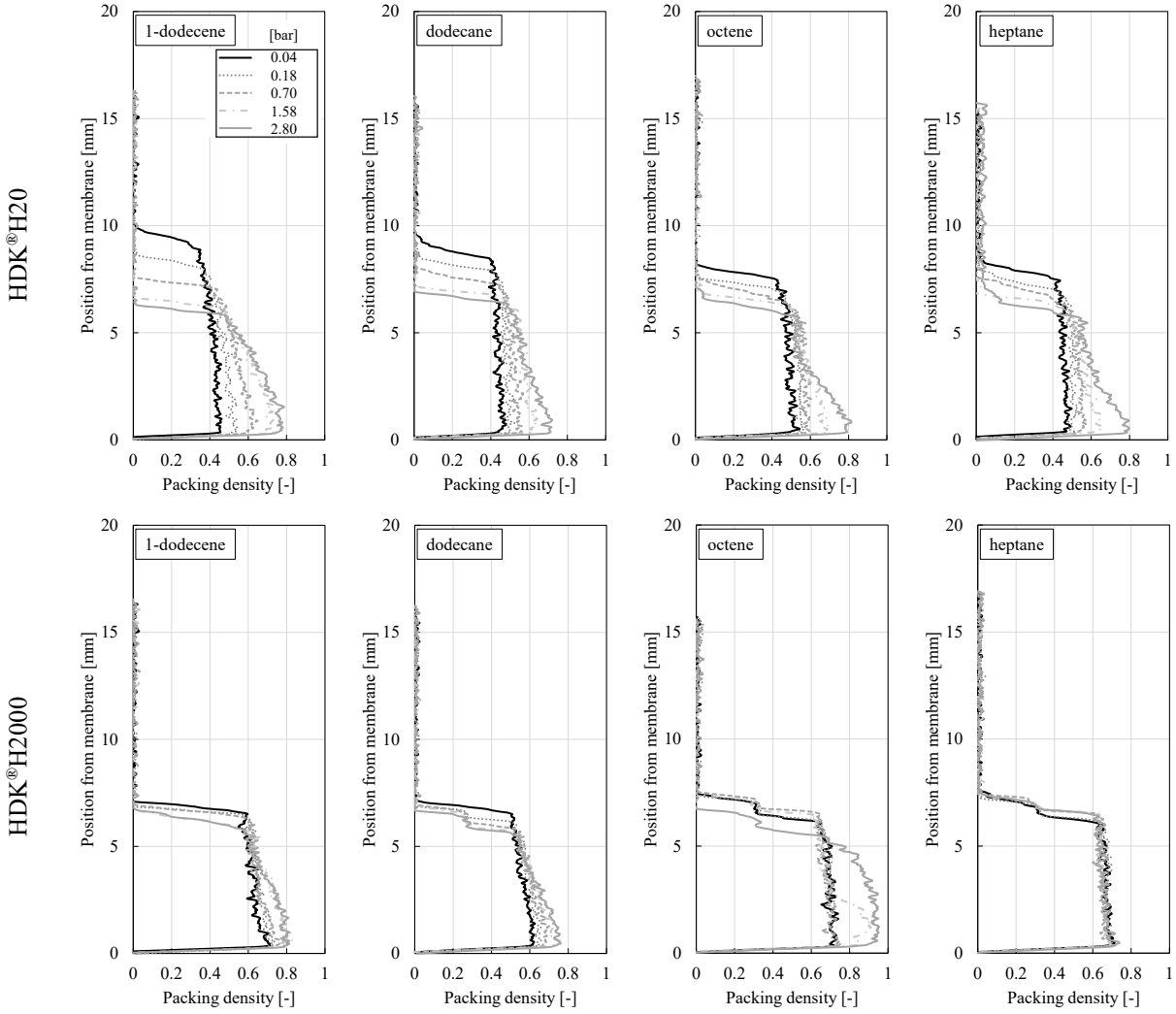

Figure 89. Packing density of different w/o PEs prepared using different organic solvents and **(top)** HDK®H20 or **(bottom)** HDK®H2000 particles against the position from the membrane surface (bottom of the sample tube, respectively). All experiments were conducted in duplicate and mean values are shown. For better graph clarity, error bars are not shown.

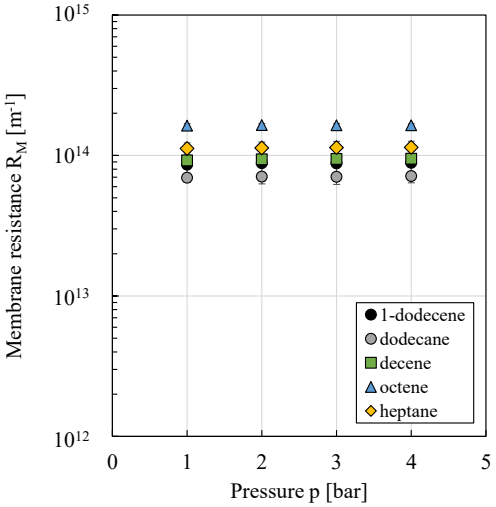

Figure 90. Membrane resistance calculated via Darcy's law (**Eq. (12)**) against pressure. For the calculation, the experimental results of pure organic solvents at room temperature were used. All experiments were conducted at least in duplicate and mean values are shown. Error bars represent the standard deviation. Where not visible, error bars are smaller than the symbol size.

A.1.5. Filtration of w/o PEs using further OSN membranes

The OSN membranes oNF-1, oNF-2, HZG PDMS and PuraMemFlux also gave relevant 1-dodecene fluxes during the membrane pre-treatment although fluxes were (except for the oNF-1 membrane) lower than those using the oNF-3 membrane (cf. **Table 5** in **Section 4.1**). By way of example, some selected filtration experiments with "standard" suspensions (0 min^{-1}) and PEs (500 min^{-1}) were conducted using these four OSN membranes (cf. **Figure 91** to **Figure 94**).

For the oNF-1 membrane (cf. **Figure 91** a)), an average pure 1-dodecene washing flux of 20.2 ± 1.0 L m^{-2} h^{-1} was obtained. When suspensions were filtered, particles with gelling properties showed the same while non-gelling particles showed lower fluxes compared to the pure solvent. PE filtration yielded lower fluxes than pure 1-dodecene and – within the experimental error – no impact of particle type was observed (cf. **Figure 91** b)). The obtained results are qualitatively consistent with those obtained using the oNF-3 membrane (cf. **Figure 41** and **Figure 86** a)). While the flux was reduced by approximately 40% when PEs were filtered using the oNF-3 membrane, the flux was reduced by only about 12% when the oNF-1 membrane was used. The extent of swelling – expressed via the amount of 1-dodecene in the membrane material – was determined via solvent uptake experiments (oNF-1: 1.61 ± 0.03 g).

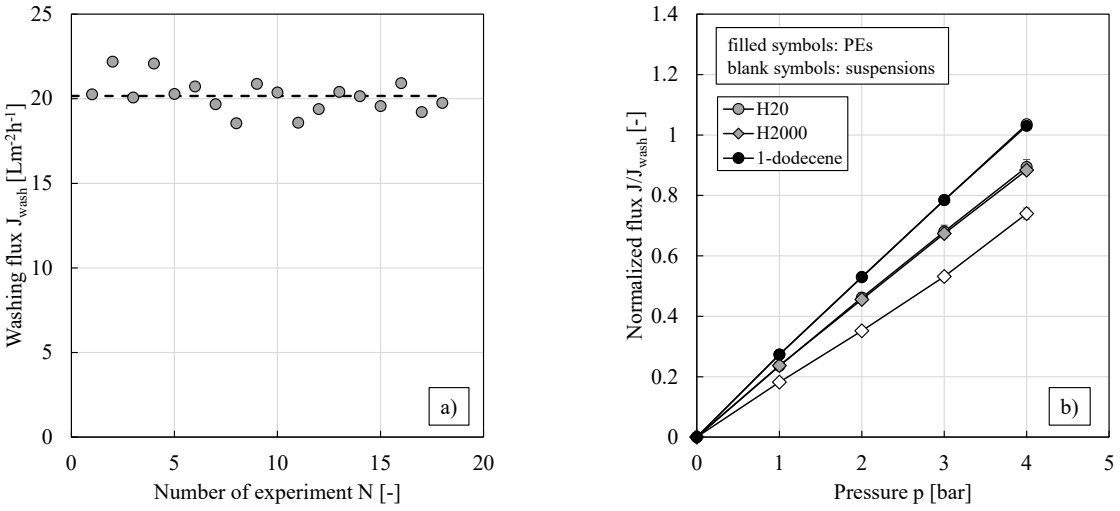

Figure 91. (a) Pure 1-dodecene flux from the membrane pre-treatment and **(b)** normalized flux against pressure for pure 1-dodecene as well as "standard" suspensions and w/o PEs stabilized by HDK®H20 or HDK®H2000 particles. All experiments were conducted at least in duplicate and mean values are shown. Error bars represent the standard deviation. Where not visible, error bars are smaller than the symbol size. The membrane oNF-1 was used.

For the oNF-2 membrane (cf. **Figure 92** a)), an average pure 1-dodecene washing flux of 12.0 ± 1.1 L m^{-2} h^{-1} was obtained. When suspensions were filtered, particles with gelling properties showed the same while non-gelling particles showed lower fluxes compared to the pure solvent. PE filtration yielded lower fluxes than pure 1-dodecene and – within the experimental error – no impact of particle type was observed (cf. **Figure 92** b)). The obtained results are qualitatively consistent with those obtained using the oNF-3 membrane (cf. **Figure 41** and **Figure 86** a)). While the flux was reduced by approximately 40% when PEs were filtered using the oNF-3 membrane, the flux was reduced by only about 15% when the oNF-2 membrane was used. The extent of swelling – expressed via the amount of 1-dodecene in the membrane material – was determined via solvent uptake experiments (oNF-2: 1.65 ± 0.01 g).

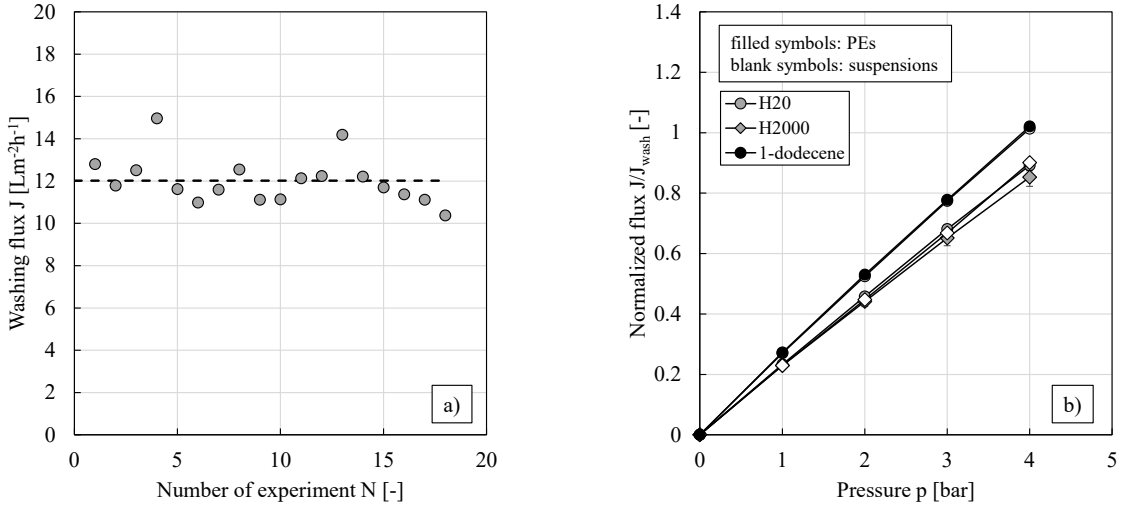

Figure 92. (a) Pure 1-dodecene flux from the membrane pre-treatment and **(b)** normalized flux against pressure for pure 1-dodecene as well as "standard" suspensions and w/o PEs stabilized by HDK®H20 or HDK®H2000 particles. All experiments were conducted at least in duplicate and mean values are shown. Error bars represent the standard deviation. Where not visible, error bars are smaller than the symbol size. The membrane oNF-2 was used.

For the HZG PDMS membrane (cf. **Figure 93** a)), an average pure 1-dodecene washing flux of 8.2 ± 3.1 L m^{-2} h^{-1} was obtained. When suspensions and PEs stabilized by two different particle types were filtered, no significant impact on the filtration behavior was observed and fluxes were – within the experimental error – comparable to those of the pure organic solvent (cf. **Figure 93** b)). These results differ from those obtained using the oNF-3 membrane (cf. **Figure 41** and **Figure 86** a)), where PEs showed significantly lower fluxes than the pure solvent and flux levels of suspensions depended on the particle type and their tendency to form network structures.

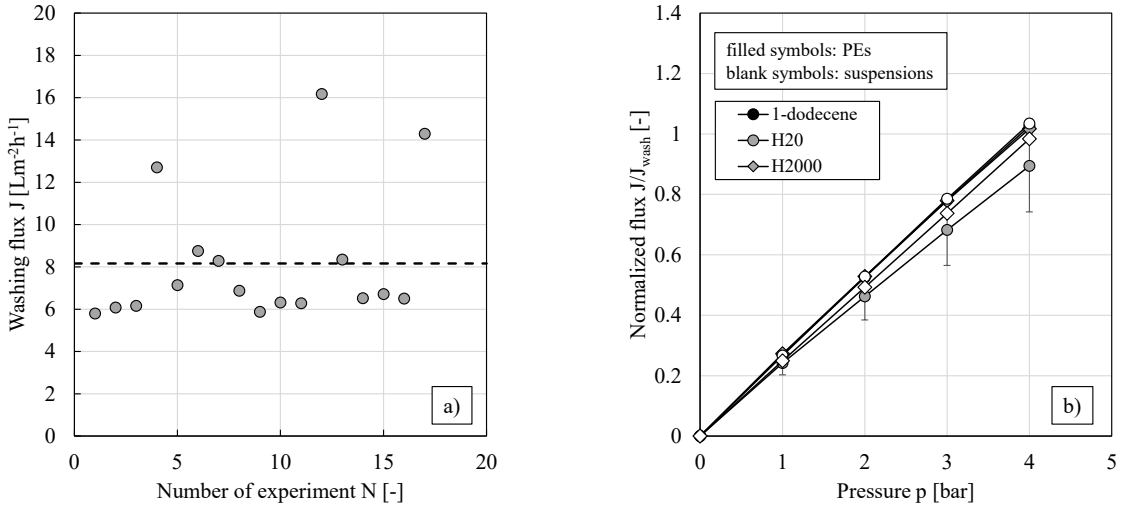

Figure 93. (a) Pure 1-dodecene flux from the membrane pre-treatment and **(b)** normalized flux against pressure for pure 1-dodecene as well as "standard" suspensions and w/o PEs stabilized by HDK®H20 or HDK®H2000 particles. All experiments were conducted at least in duplicate and mean values are shown. Error bars represent the standard deviation. Where not visible, error bars are smaller than the symbol size. The membrane HZG PDMS was used.

For the PuraMemFlux membrane (cf. **Figure 94** a)), an average pure 1-dodecene washing flux of 6.3 ± 0.5 L m^{-2} h^{-1} was obtained. When suspensions were filtered, particles with gelling properties showed slightly higher while non-gelling particles showed similar fluxes compared to the pure solvent. PE filtration yielded higher fluxes than pure 1-dodecene and – within the experimental error – no impact of particle type was observed (cf. **Figure 94** b)). The obtained results differ from those using the oNF-3 and the HZG PDMS membrane. The extent of swelling – expressed via the amount of 1-dodecene in the membrane material – could be ruled out, as solvent uptake experiments yielded similar results for all three membrane types (oNF-3: 1.58 ± 0.03 g; HZG PDMS: 1.53 ± 0.02 g and PuraMemFlux: 1.56 ± 0.03 g, respectively).

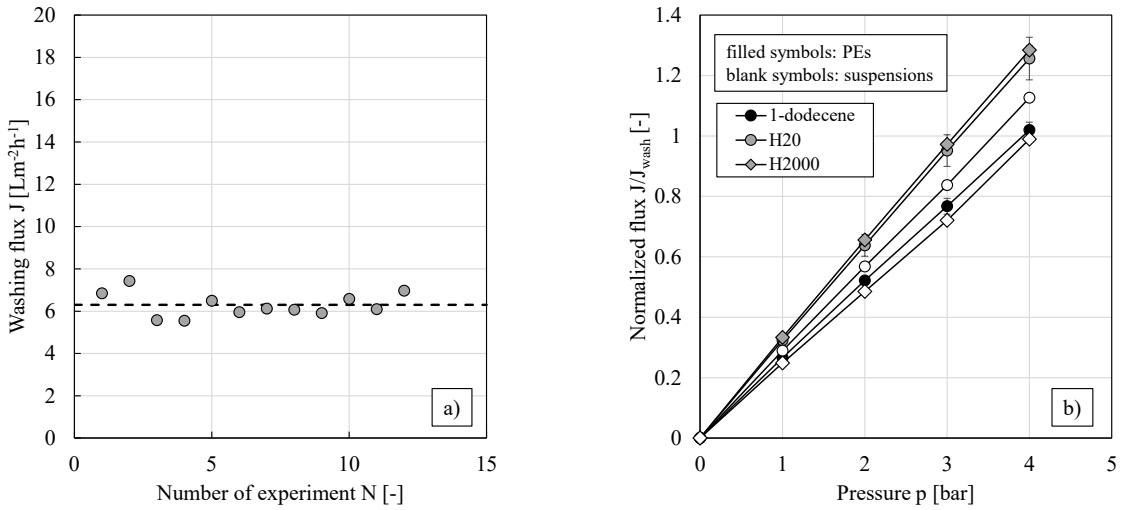

Figure 94. (a) Pure 1-dodecene flux from the membrane pre-treatment and **(b)** normalized flux against pressure for pure 1-dodecene as well as "standard" suspensions and w/o PEs stabilized by HDK®H20 or HDK®H2000 particles. All experiments were conducted at least in duplicate and mean values are shown. Error bars represent the standard deviation. Where not visible, error bars are smaller than the symbol size. The membrane PuraMemFlux was used.

As all membranes investigated in this thesis were commercially available ones, information about the membrane material, its preparation procedure and its properties are scarce. Differences in the internal free volume, the crosslinking or the thickness of the active membrane layer could have caused the differences in the observed filtration behavior. Further research on the explicit impact of membrane properties on the filtration behavior of PEs and its implementation into a mathematical model is necessary in the future.

A.2. List of supervised student projects

- Pulla, Steven: *Untersuchung der Filtrationseigenschaften sowie der Rheologie von Nanopartikelsuspensionen in organischem Lösemittel und Pickering Emulsionen – Einfluss der Partikelart*. Bachelor thesis (2018) (in German).
- Özlü, Aykut: *Einfluss der Herstellbedingungen auf die Stabilität, Rheologie, Tropfengrößenverteilung und Filtrierbarkeit von Wasser/Öl Pickering Emulsionen*. Bachelor thesis (2019) (in German).
- Schroeder, Hendrik: *Theoretische Untersuchung des Viskositäts- und Temperatureinflusses auf das Filtrationsverhalten von Pickering Emulsionen*. Bachelor thesis (2020) (in German).
- Assi, Miriam-Kousso: *Filtration von Pickering Emulsionen mittels analytischer Photozentrifugation zur Charakterisierung des Filtrationsverhaltens*. Bachelor thesis (2020) (in German).
- Masoud, Mustafa: *Aufbau und Inbetriebnahme einer in situ Visualisierung des Filterkuchens bei Crossflow-Membranfiltrationen*. Bachelor thesis (2021) (in German).

A.3. List of proceedings, posters and oral presentations

The results of this work were presented and discussed at national and international conferences in form of posters and oral presentations. The presenting author is underlined.

Proceedings

- Drews, A.; Skale, T.; Xander, N.; Kempin, M.; Heyse, A.: *Membranfiltration von Pickering Emulsionen für die kontinuierliche Mehrphasenkatalyse*. ProcessNet-Jahrestagung und 33. DECHEMA-Jahrestagung der Biotechnologen, 10.09. - 13.09.2018, Aachen, Germany (in German). Chem. Ing. Tech., 90, 1226-1226, DOI: 10.1002/cite.201855207.
- Kempin, M.; Schroeder, H.; Drews, A.; Kraume, M.: *Organic solvent nanofiltration of water-in-oil Pickering emulsions – impact of organic phase viscosity*. 10. ProcessNet-Jahrestagung und 34. DECHEMA-Jahrestagung der Biotechnologen, 21.09. - 24.09.2020, Web-Conference. Chem. Ing. Tech., 92, 1294-1295, DOI: 10.1002/cite.202055074.
- Drews, A.; Kempin, M.; Kraume, M.: *First systematic study on the impact of preparation conditions on characteristic Pickering emulsion properties*. 10. ProcessNet-Jahrestagung und 34. DECHEMA-Jahrestagung der Biotechnologen, 21.09. - 24.09.2020, Web-Conference. Chem. Ing. Tech., 92, 1295-1295, DOI: 10.1002/cite.202055073.

Posters

- Drews, A.; Kempin, M.; Skale, T.: *Membrane filtration of Pickering emulsions for continuous liquid/liquid catalysis – influence of membrane material and nanoparticle type*. 12th European Congress of Chemical Engineering, 15.09. - 19.09.2019, Florence, Italy.
- Kempin, M.; Schroeder, H.; Drews, A.; Kraume, M.: *Organic solvent nanofiltration of water-in-oil Pickering emulsions – impact of organic phase viscosity*. 10. ProcessNet-Jahrestagung und 34. DECHEMA-Jahrestagung der Biotechnologen, 21.09. - 24.09.2020, Web-Conference.
- Drews, A.; Kempin, M.; Kraume, M.: *First systematic study on the impact of preparation conditions on characteristic Pickering emulsion properties*. 10. ProcessNet-Jahrestagung und 34. DECHEMA-Jahrestagung der Biotechnologen, 21.09. - 24.09.2020, Web-Conference.

Oral presentations

- Kempin, M.; Kraume, M.; Drews, A.: *Ultrafiltration of particle stabilized Pickering emulsions: Influence of particle type and concentration*. 16th Network Young Membrains (NYM), 05.07. - 07.07.2018, Valencia, Spain.
- Drews, A.; Heyse, A.; Kempin, M.; Xander, N.; Skale, T.: *Ultrafiltration of Pickering Emulsions for Continuous Multiphase Catalysis*. Euromembrane, 09.07. - 13.07.2018, Valencia, Spain.

- Drews, A.; Skale, T.; Xander, N.; Kempin, M.; Heyse, A.: *Membranfiltration von Pickering Emulsionen für die kontinuierliche Mehrphasenkatalyse*. ProcessNet-Jahrestagung und 33. DECHEMA-Jahrestagung der Biotechnologen, 10.09. - 13.09.2018, Aachen, Germany (in German).
- Kempin, M.; Kraume, M.; Drews, A.: *Ultrafiltration of nanoparticle stabilized Pickering emulsions and suspensions*. Jahrestreffen der ProcessNet-Fachgruppen Fluidverfahrenstechnik und Membrantechnik, 27.03. - 29.03.2019, Potsdam, Germany.
- Kempin, M.; Kraume, M.; Drews, A.: *Ultrafiltration of w/o and o/w Pickering emulsions: Influence of particle type and concentration*. Engineering with Membranes Conference (EWM), 08.04. - 10.04.2019, Båstad, Sweden.
- Röhl, S.; Hohl, L.; Kempin, M.; Kraume, M.: *Impact of nanoparticles and surfactants on drop size distribution and phase separation in liquid/liquid systems*. 12th European Congress of Chemical Engineering (ECCE), 15.09. - 19.09.2019, Florence, Italy.
- Kempin, M.; Kraume, M.; Drews, A.: *Influence of filtration operating conditions on the permeability of water-in-oil Pickering emulsions*. 7th International Conference on Organic Solvent Nanofiltration (OSN), 28.10. - 30.10.2019, Enschede, The Netherlands.
- Kempin, M.; Kraume, M.; Drews, A.: *Ultrafiltration of silica stabilized water-in-oil Pickering emulsions – influence of membrane type*. Jahrestreffen der ProcessNet-Fachgruppen Hochdruckverfahrenstechnik und Membrantechnik, 17.02. - 19.02.2020, Freising, Germany.
- Drews, A.; Kempin, M.V.; Assi, M.-K.; Boldt, S.; Lerche, D.: *Membranfiltration von Pickering Emulsionen für die kontinuierliche Mehrphasenkatalyse – Lessons Learned*. Jahrestreffen der ProcessNet-Fachgruppen Extraktion und Membrantechnik, 04.02. - 05.02.2021, Web-Conference (in German).
- Kempin, M.V.; Stock, S.; von Klitzing, R.; Drews, A.; Kraume, M.: *Steps en route to the application of Pickering emulsions in L/L multiphase catalytic systems*. 13th European Congress of Chemical Engineering and 6th European Congress of Applied Biotechnology (ECCE/ECAB), 20.09. - 23.09.2021, Web-Conference.

A.4. List of own publications in peer-reviewed journals

Articles with additional information

- Röhl, S.; Hohl, L.; Kempin, M.; Enders, F.; Jurtz, N.; Kraume, M. (2019): *Influence of Different Silica Nanoparticles on Drop Size Distributions in Agitated Liquid/Liquid Systems*. Chem. Ing. Tech., 91, 1640-1655, DOI: 10.1002/cite.201900049.

Within the framework of an international cooperation with the working groups of Volodymyr V. Tarabara (Michigan State University, East Lansing, MSU) and Jia-Wei Chew (Nanyang Technological University Singapore, NTU) research on the filtration of surfactant and/or nanoparticle stabilized emulsions under non-saline and saline conditions was conducted. Crossflow experiments at constant pressure as well as DOTM tests (direct observation through the membrane) for in-situ visualization of the filter cake formed were conducted. The cooperation included a two-week stay at MSU (06.10. - 21.10.2018) and NTU (23.11. - 10.12.2018).

- Kempin, M.V.; Hejase, C.A.; Chew, J.W.; Tarabara, V.V.; Drews, A.: *Effect of emulsifying surfactant and nanoparticles on the microfiltration of oil-in-water emulsions under non-saline and saline conditions*. (in preparation).

Journal articles used for this thesis

[I] Kempin, M.V.; Kraume, M.; Drews, A. (2020): *W/O Pickering emulsion preparation using a batch rotor-stator mixer – Influence on rheology, drop size distribution and filtration behavior.* J. Colloid Interf. Sci., 573, 135-149, DOI: 10.1016/j.jcis.2020.03.103.

[II] Kempin, M.V.; Stock, S.; von Klitzing, R.; Kraume, M.; Drews, A. (2020): *Influence of particle type and concentration on the ultrafiltration behavior of nanoparticle stabilized*

Pickering emulsions and suspensions. Sep. Purif. Technol., 252, 117457, DOI: 10.1016/j.seppur.2020.117457.

[III] Kempin, M.V.; Drews, A. (2021): *What governs Pickering emulsion properties during preparation via batch rotor-stator homogenizers?* Chem. Ing. Tech., 93, 311-317, DOI: 10.1002/cite.202000130.

[IV] Stock, S.; Schlander, A.; Kempin, M.; Geisler, R.; Stehl, D.; Spanheimer, K.; Hondow, N.; Micklethwaite, S.; Weber, A.; Schomäcker, R.; Drews, A.; Gallei, M.; von Klitzing, R. (2021): *The quantitative impact of fluid vs. solid interfaces on the catalytic performance of Pickering emulsions.* Phys. Chem. Chem. Phys., 23, 2355-2367, DOI: 10.1039/D0CP06030E.

[V] Kempin, M.V.; Schroeder, H.; Hohl, L.; Kraume, M.; Drews, A. (2021): *Modeling of water-in-oil Pickering emulsion nanofiltration – influence of temperature.* J. Membr. Sci., 636, 119547, DOI: 10.1016/j.memsci.2021.119547.

[VI] Kempin, M.V.; Drews, A. (2021): *Organic solvent nanofiltration of water-in-oil Pickering emulsions – What influences permeability?* Membranes, 11, 864, DOI:10.3390/membranes11110864.

[VII] Stock, S.; Kempin, M.V.; Hohl, L.; Petzold, M.; Hecht, K.; von Klitzing, R.; Drews. A.: *Pickering Emulsions*. (Kraume M, ed.). Integrated chemical processes in liquid multiphase systems – from chemical reaction to process design. De Gruyter. (submitted)